Mechanical Activation of Secondary Processed Orally Inhaled Active Pharmaceutical Ingredients

Depasquale, Roberto

Award date:
2015

Awarding institution:
University of Bath

Mechanical Activation of Secondary Processed Orally Inhaled Active Pharmaceutical Ingredients

Roberto Depasquale

A thesis submitted for the degree of Doctor of Philosophy

University of Bath
Department of Pharmacy and Pharmacology
October 2014

ABSTRACT

The physicochemical properties and surface chemistry of orally inhaled active pharmaceutical ingredients (API) are critical to the quality attributes of dry powder inhaler (DPI) formulations. The requirement to reduce the particle size distribution of the APIs to a respirable range, largely performed through air-jet micronisation, imparts large amounts of energy to the drug particles, which together with particle fracture and size reduction, it is accompanied by the generation of structural defects and, at the limit, the formation of amorphous regions. This is known as mechanical activation, which may cause instability in the physicochemical properties and interfacial chemistry at the particle surface as it undergoes structural relaxation. During the thermodynamically driven relaxation process, differing drug properties may lead to DPI formulations with unpredictable formulation structure and product functionality. A fundamental understanding of the structural relaxation dynamics is therefore essential in the development and commercialisation of a quality-by-design led inhalation product.

This thesis investigated the structural relaxation dynamics of micronised fluticasone propionate (FP), salmeterol xinafoate (SX) and glycopyrrolate bromide (GLY). Physicochemical properties and surface interfacial chemistry, via cohesive-adhesive balance (CAB) measurements, of micronised drug are assessed as a function of environmental stressed laagering over well-defined periods of time and *in situ* conditioning in hydrofluoroalkane (HFA). The influence of these dynamics upon DPI performance was also examined in both binary (FP, SX, GLY) and tertiary formulations (FP-SX). The results indicated

how structural relaxation of hydrophobic and hydrophilic APIs trigger off different stress relaxation pathways with different sensitivities to laagering conditions. These data suggested that the introduction of a post-micronisation conditioning step may expedite structural relaxation of hydrophobic APIs. Whilst the physical properties of hydrophobic APIs are largely unaffected by mechanical activation, surface interfacial chemistry governing inter-particulate forces between API and the lactose carrier is directly affected by environmental conditions of temperature and relative humidity during structural relaxation. The study also showed the potential use of post-micronisation conditioning to tailor the surface chemistry properties of APIs. For hydrophilic APIs, data suggested that post-micronisation conditioning is essential in enabling physical and chemical stability of inhaled formulations. Furthermore, in vitro aerosolisation studies suggested that the aerodynamic particle size distribution and fine particle mass were directly affected by post-micronisation laagering conditions.

The importance of generating a well defined, understood and controlled design space throughout product development dictates the need for more robust API processing prior to DPI formulation. This work highlights how a tailored post-micronisation laagering strategy can have a significant effect on physicochemical and interfacial properties as well as product performance of binary and tertiary carrier based DPI formulations.

ACKNOWLEDGEMENTS

The first note of appreciation goes to Professor Rob Price, who throughout this period inspired me in ways which go well beyond the boundaries of academia. He not only introduced me to the top fora of our industry, but also equipped and encouraged me to get there myself.

A special token of gratitude to Dr Jag Shur, whose technical knowledge and industrial relevance are second to none. Great Western Research and Nanopharm are acknowledged for funding this PhD.

A big thank you to all my team members; Martin Rowland *in primis* for sharing this experience from the very first day to the very last, Dr Hanne Kinnunen for passing on the research group's know-how, Chris and Charlotte for sharing so many memories. A thank you goes to Dr Gabriele Kociok-Kohn and Mrs Ursula Potter for offering such highly specialised assistance with electron microscopy and X-Ray Diffraction. Thank you to all the staff in the Pharmacy & Pharmacology department whose work is vital in enabling research groups function to the best of their abilities.

Finally, eternal gratitude goes to my parents who sowed in me solid values which I have, together with my brother and sister, lived on a daily basis throughout my adolescence. It is only the resultant moral fibre which will enable me to fulfil the scope and potential of this thesis, all throughout my career.

SCIENTIFIC PUBLICATIONS

Depasquale, R., Lee, S., Saluja, B., Shur, J., Price, R. The Influence of Secondary Processing on the Structural Relaxation of Fluticasone Propionate. AAPS PharmSciTech. (Accepted 12 September 2014).

TABLE OF CONTENTS

Abstract ii

Acknowledgements iv

Scientific Publications v

Table of Contents vi

List of Figures xiv

List of Tables xx

List of Abbreviations xxiii

1 Introduction 27

1.1 Respiratory Medicine 27

1.2 Particle Deposition in the Lungs 29

1.2.1 Inertial Impaction 29

1.2.2 Sedimentation 30

1.2.3 Brownian Motion 31

1.2.4 Interception 32

1.2.5 Electrostatic Precipitation 32

1.2.6 Effect of Particle Size on Deposition in the Respiratory Tract 33

1.3 Treatment of Asthma and COPD 34

1.3.1 Bronchodilators 34

1.3.2 Anti-Inflammatory Drugs 35

1.3.3 Combination Therapy 36

1.4 Current Respiratory Drug Delivery Devices 37

1.4.1 Nebulisers 37

1.4.2 Pressurised Metered Dose Inhalers 37

1.4.3 Dry Powder Inhalers 39

1.5 Interparticulate Forces 41

1.5.1 Van der Waals Forces *42*

1.5.2 Capillary Forces *44*

1.5.3 Electrostatic Forces *45*

1.5.4 Mechanical Interlocking *47*

1.6 FACTORS AFFECTING INTERPARTICULATE FORCES 47

1.6.1 Particle Size *47*

1.6.2 Particle Shape *48*

1.6.3 Surface Roughness of Particles *49*

1.6.4 Particle Deformation *50*

1.6.5 Surface Free Energy *51*

1.6.6 Environmental Factors (Relative Humidity) *52*

1.7 ANALYTICAL TOOLS USED IN THE INVESTIGATION OF INTERFACIAL PROPERTIES VIA SURFACE CHARACTERISATION. 52

1.7.1 Centrifugal Methods *53*

1.7.2 Scanning Probe Microscopy *54*

1.7.2.1 Atomic Force Microscopy 55

1.7.2.2 Colloid Probe Atomic Force Microscopy 58

1.8 OPTIMISING PHARMACEUTICAL ENGINEERING OF DPIS 62

1.8.1 Micronisation and Mechanical Activation *63*

1.8.2 Environmental Laagering *66*

1.8.3 In-situ conditioning with supercritical fluid technologies and HFA *67*

1.9 AIMS OF THE THESIS 69

1.9.1 Thesis Structure *71*

2 The Influence of Post-Micronisation Conditioning on the Interfacial Properties and the *In Vitro* Performance of Fluticasone Propionate 72

2.1 INTRODUCTION 72

2.2 MATERIALS AND METHODS 74

2.2.1 MATERIALS *74*

2.2.2 METHODS 75

2.2.2.1 Particle Size Analysis of FP 76

2.2.2.2 Scanning Electron Microscopy of FP samples 77

2.2.2.3 X-ray powder diffraction (XRPD) analysis of FP samples 77

2.2.2.4 Differential Scanning Calorimetry of FP samples 77

2.2.2.5 Methodology of the CAB approach to colloid probe AFM 78

2.2.2.5.1 Crystallisation of substrates 78

2.2.2.5.2 Colloidal probe force measurements 79

2.2.2.6 Preparation of powder formulations 80

2.2.2.7 In vitro aerosolisation studies 81

2.2.2.8 HPLC analysis of FP and SX 81

2.2.2.9 Statistical analysis 82

2.3 RESULTS AND DISCUSSION 83

2.3.1 Physicochemical characterisation for FP sample 83

2.3.2 Surface Interfacial Properties of FP Samples 87

2.3.3 In vitro performance of FP samples in a binary formulation 91

2.3.4 In vitro performance of FP samples in a combination formulation with SX 94

2.3.5 In vitro performance of SX in a combination formulation with FP samples 97

2.3.6 Assessment of the FP sample following post-micronisation in situ conditioning using HFA-134a 101

2.3.6.1 Physicochemical Characterisation 101

2.3.6.2 Surface Interfacial Properties of FP Samples 104

2.3.6.3 In vitro performance of FP samples following *in situ* HFA conditioning 106

2.4 CONCLUSIONS 109

3 THE INFLUENCE OF SECONDARY PROCESSING ON THE STRUCTURAL RELAXATION DYNAMICS OF FLUTICASONE PROPIONATE 110

3.1 INTRODUCTION 110

3.2 MATERIALS AND METHODS 114

3.2.1 MATERIALS 114

3.2.2 METHODS 115

3.2.2.1 Conditioning of micronised FP 115

3.2.2.2 Laser Diffraction 117

3.2.2.3 Scanning Electron Microscopy (SEM) 117

3.2.2.4 X-ray powder diffraction (XRPD) 117

3.2.2.5 Differential Scanning Calorimetry (DSC) 118

3.2.2.6 Specific Surface Area by Brunauer–Emmett–Teller (BET) 118

3.2.2.7 Rugosity (R_a) 118

3.2.2.8 Thermal Activity Monitoring (TAM) 119

3.2.2.9 Cohesive-Adhesive Balance (CAB) 126

3.2.2.9.1 Preparation of crystal substrates 126

3.2.2.9.2 Interaction force measurements 127

3.2.2.10 Preparation of powder formulations 128

3.2.2.11 HPLC analysis of Fluticasone Propionate and Salmeterol Xinafoate 129

3.2.2.12 Content Uniformity 130

3.2.2.13 In Vitro Aerosolization Analysis 130

3.2.2.14 Statistical Analysis 131

3.3 RESULTS AND DISCUSSION 131

3.3.1 Physicochemical Characterization 132

3.3.2 Post-micronisation conditioning effects on amorphous content of FP samples 138

3.3.3 Post-micronisation Conditioning Effects on Interfacial Forces 138

3.3.4 Drug content uniformity 146

3.3.5 In vitro aerosolization performance of binary DPI formulations 147

3.3.6 In vitro aerosolization performance of tertiary DPI formulations 150

3.4 CONCLUSIONS 154

4 The Stress Relaxation Dynamics of Micronised Salmeterol Xinafoate 156

4.1 INTRODUCTION 156

4.2 MATERIALS AND METHODS 157

4.2.1 MATERIALS 157

4.2.2 METHODS 157

4.2.2.1 Environmental Conditioning 158

4.2.2.2 *In situ* conditioning 158

4.2.2.3 Particle Size Analysis of SX 159

4.2.2.4 Scanning Electron Microscopy of SX samples 159

4.2.2.5 X-ray powder diffraction (XRPD) analysis of SX samples 160

4.2.2.6 Differential Scanning Calorimetry of SX samples 160

4.2.2.7 Specific Surface Area by BET of SX samples 161

4.2.2.8 Rugosity Calculation 161

4.2.2.9 Cohesive-Adhesive Balance Measurements 162

4.2.2.9.1 Crystallisation of substrates 162

4.2.2.9.2 Colloidal probe force measurements 163

4.2.2.10 Preparation of powder formulations 164

4.2.2.11 In vitro aerosolisation studies 165

4.2.2.12 HPLC analysis of SX and FP 165

4.2.2.13 Statistical analysis 166

4.3 RESULTS AND DISCUSSION 167

4.3.1 Physicochemical Results for Environmentally Conditioned SX Samples 167

4.3.2 Cohesive-Adhesive Balance results for environmentally conditioned Salmeterol Xinafoate 178

4.3.3 Aerosolisation performance results for environmentally conditioned Salmeterol Xinafoate in binary formulations 183

4.3.4 Aerosolisation performance results for environmentally conditioned Salmeterol Xinafoate in ternary formulations 187

4.3.5 Physicochemical Characterisation of Post-Micronised Conditioned SX using HFA-134a 190

4.3.6 Cohesive-Adhesive Balance and Impaction results for SX conditioned in-situ with HFA post-micronisation 196

4.4 CONCLUSIONS 200

5 The Post-Micronisation Dynamics of Freshly Micronised Glycopyrrolate Bromide 202

5.1 INTRODUCTION 202

5.2 MATERIAL & METHODS 203

5.2.1 Materials 203

5.2.2 Methods 204

5.2.2.1 Micronisation of Coarse Glycopyrrolate crystals by air-jet milling 204

5.2.2.2 Particle Size Analysis 205

5.2.2.3 Scanning Electron Microscopy 206

5.2.2.4 X-ray powder diffraction (XRPD) analysis 206

5.2.2.5 Differential Scanning Calorimetry 206

5.2.2.6 Specific Surface Area by BET 207

5.2.2.7 Rugosity Calculation 207

5.2.2.8 Methodology of the CAB approach to colloid probe AFM 208

5.2.2.8.1 Crystallisation of substrates 208

5.2.2.8.2 Colloidal probe force measurements 209

5.2.2.9 Preparation of powder formulations 210

5.2.2.10 *In vitro* aerosolisation testing 210

5.2.2.10.1 Stability profile assessment for formulations via stress testing 211

5.2.2.11 HPLC Methodology for the quantification of GLY 211

5.2.2.12 Statistical analysis 212

5.3 RESULTS AND DISCUSSION 212

5.3.1 Physicochemical characterisation 212

5.3.2 Interfacial Chemistry Results 222

5.3.3 In vitro performance 226

5.3.4 Stability of Formulation Performance 230

5.3.4.1 30°C/65% RH Stability Profile Results 230

5.3.4.2 40°C/75% RH Stability Profile Results 232

5.4 CONCLUSIONS 234

6 General Conclusions 235

6.1 INTRODUCTION 235

6.2 SUMMARY 236

6.3 GENERAL CONCLUSION 238

6.4 FUTURE WORK 239

References 240

LIST OF FIGURES

FIGURE 1.1: STRUCTURE OF THE HUMAN LUNG (ADAPTED FROM GRIESENBACH *ET AL.,* 2004) 28

FIGURE 1.2: PACKING ARRANGEMENTS FOR FLAT ELONGATED PARTICLE (ZENG, MARTIN ET AL. 2001): (A) CLOSELY PACKED ORIENTATION, TYPICALLY FOUND AFTER POWDER HANDLING. (B) LOOSELY PACKED ORIENTATION..... 49

FIGURE 1.3: THE EFFECTS OF ROUGHNESS ON PARTICLE-SURFACE ADHESION. (A) SURFACE ROUGHNESS ON A SMALLER SCALE THE PARTICLE SIZE. (B) A SMOOTH SURFACE. (C) SURFACE ROUGHNESS ON A LARGER SCALE THAN PARTICLE SIZE 50

FIGURE 1.4 SCHEMATIC DIAGRAM OF AN ATOMIC FORCE MICROSCOPE 56

FIGURE 1.5 DIMENSIONS OF THE TIP AND CANTILEVER OF AN ATOMIC FORCE MICROSCOPE..... 57

FIGURE 1.6 SCHEMATIC REPRESENTATION OF THE PROCESS OF MECHANICAL ACTIVATION AND RELAXATION PROCESS OF MICRONISED PARTICLES. A = LOW SURFACE FREE ENERGY OF CRYSTALLINE UNPROCESSED MATERIAL, B = BRITTLE-DUCTILE TRANSITION, AT WHICH POINT PARTICLE FRAGMENTATION IS NOT PROBABLE, C = MECHANICALLY ACTIVATED STATED, D = RELAXATION BEHAVIOUR OF THE MECHANICALLY ACTIVATED MATERIAL OVER TIME AND E = RELAXATION OF THE MECHANICALLY ACTIVATED STATE BY POST-PROCESSING CONDITIONING..... 64

FIGURE 2.1 X-RAY POWDER DIFFRACTION PROFILES FOR THE INITIAL, HT14 AND T72 FP SAMPLES..... 84

FIGURE 2.2 DIFFERENTIAL SCANNING CALORIMETRY THERMOGRAPHS FOR THE INITIAL, HT14 AND T72 FP SAMPLES 85

FIGURE 2.3 SCANNING ELECTRON MICROGRAPHS FOR THE INITIAL FP ALIQUOT (A, B), FOR THE H2 SAMPLE (C, D), AND FOR THE T2 SAMPLE (E, F)..... 86

FIGURE 2.4 (A) COHESIVE-ADHESIVE BALANCE (CAB) PLOT OF INITIAL, T48 AND T72 FP SAMPLES WITH RESPECT TO LACTOSE, (B) CAB PLOT OF INITIAL, HT7 AND HT14 FP SAMPLES WITH RESPECT TO LACTOSE..... 89

FIGURE 2.5 (A) COHESIVE-ADHESIVE BALANCE (CAB) PLOT OF INITIAL, T48 AND T72 FP SAMPLES WITH RESPECT TO SX, (B) CAB PLOT OF INITIAL, HT7 AND HT14 FP SAMPLES WITH RESPECT TO SX..... 89

FIGURE 2.6 CAB VALUES PLOTTED AGAINST CONDITIONING PARAMETERS T72 (72 HOURS AT 60°C), T48 (48 HOURS AT 60°C), INITIAL (FRESHLY MICRONISED), HT7 (7 DAYS AT 40°C/75 % RH), AND HT14 (14 DAYS AT 40°C/75 % RH) 90

FIGURE 2.7 FINE PARTICLE FRACTION (FPF) OF FP BINARY FORMULATIONS EXPRESSED AS A PERCENTAGE OF THE RECOVERED DOSE (RD) PLOTTED AGAINST THE CAB OF FP PARTICLES WITH RESPECT TO LACTOSE 92

FIGURE 2.8 STAGE BY STAGE DEPOSITION PROFILE EXPRESSED AS THE PERCENTAGE OF DRUG DEPOSITED PER STAGE FOR FP IN BINARY FORMULATIONS; INITIAL, T48 AND T72 93

FIGURE 2.9 STAGE BY STAGE DEPOSITION PROFILE EXPRESSED AS THE PERCENTAGE OF DRUG DEPOSITED PER STAGE FOR FP IN BINARY FORMULATIONS; INITIAL, HT7 AND HT14 93

FIGURE 2.10 FINE PARTICLE FRACTION (FPF) OF FP IN COMBINATION FORMULATION WITH SX EXPRESSED AS A PERCENTAGE OF THE RECOVERED DOSE (RD) PLOTTED AGAINST THE CAB OF FP PARTICLES WITH RESPECT TO SX 95

FIGURE 2.11 STAGE BY STAGE DEPOSITION PROFILE EXPRESSED AS THE PERCENTAGE OF DRUG DEPOSITED PER STAGE FOR FP IN COMBINATION FORMULATIONS WITH SX; INITIAL, T48 AND T72 96

FIGURE 2.12 STAGE BY STAGE DEPOSITION PROFILE EXPRESSED AS THE PERCENTAGE OF DRUG DEPOSITED PER STAGE FOR FP IN COMBINATION FORMULATIONS WITH SX; INITIAL, HT7 AND HT14 97

FIGURE 2.13 FINE PARTICLE FRACTION (FPF) OF SX IN COMBINATION FORMULATION WITH FP EXPRESSED AS A PERCENTAGE OF THE RECOVERED DOSE (RD) PLOTTED AGAINST THE CAB OF FP PARTICLES WITH RESPECT TO SX 98

FIGURE 2.14 STAGE BY STAGE DEPOSITION PROFILE EXPRESSED AS THE PERCENTAGE OF DRUG DEPOSITED PER STAGE FOR SX IN COMBINATION FORMULATIONS WITH FP; INITIAL, T48 AND T72 100

FIGURE 2.15 STAGE BY STAGE DEPOSITION PROFILE EXPRESSED AS THE PERCENTAGE OF DRUG DEPOSITED PER STAGE FOR SX IN COMBINATION FORMULATIONS WITH FP; INITIAL, HT7 AND HT14 100

FIGURE 2.16 X-RAY POWDER DIFFRACTION PROFILES FOR THE INITIAL AND HFA FP SAMPLES 101

FIGURE 2.17 DIFFERENTIAL SCANNING CALORIMETRY THERMOGRAPHS FOR THE INITIAL AND HFA FP SAMPLES 102

FIGURE 2.18 SCANNING ELECTRON MICROGRAPHS FOR THE INITIAL FP ALIQUOT (A, B) AND THE HFA CONDITIONED SAMPLE (C, D) 103

FIGURE 2.19 (A) COHESIVE-ADHESIVE BALANCE (CAB) PLOT OF INITIAL AND HFA FP SAMPLES WITH RESPECT TO LACTOSE, (B) CAB PLOT OF INITIAL AND HFA FP SAMPLES WITH RESPECT TO SX 105

FIGURE 2.20 FINE PARTICLE FRACTION (FPF) OF FP IN A BINARY FORMULATION MANUFACTURED USING HFA CONDITIONED FP PARTICLES SHOWN IN CONTEXT OF SIMILAR FORMULATIONS MANUFACTURED USING FRESHLY MICRONISED FP AND *EX SITU* CONDITIONED FP AS DESCRIBED PREVIOUSLY, EXPRESSED AS A PERCENTAGE OF THE RECOVERED DOSE (RD) PLOTTED AGAINST THE CAB OF FP PARTICLES WITH RESPECT TO LACTOSE 107

FIGURE 2.21 FINE PARTICLE FRACTION (FPF) OF FP IN A COMBINATION FORMULATION WITH SX MANUFACTURED USING HFA CONDITIONED FP PARTICLES SHOWN IN CONTEXT OF SIMILAR FORMULATIONS MANUFACTURED USING

FRESHLY MICRONISED FP AND EX SITU CONDITIONED FP AS DESCRIBED PREVIOUSLY, EXPRESSED AS A PERCENTAGE OF THE RECOVERED DOSE (RD) PLOTTED AGAINST THE CAB OF FP PARTICLES WITH RESPECT TO LACTOSE 108

FIGURE 2.22 FINE PARTICLE FRACTION (FPF) OF SX IN A COMBINATION FORMULATION WITH FP MANUFACTURED USING HFA CONDITIONED FP PARTICLES SHOWN IN CONTEXT OF SIMILAR FORMULATIONS MANUFACTURED USING FRESHLY MICRONISED FP AND EX SITU CONDITIONED FP AS DESCRIBED PREVIOUSLY, EXPRESSED AS A PERCENTAGE OF THE RECOVERED DOSE (RD) PLOTTED AGAINST THE CAB OF FP PARTICLES WITH RESPECT TO LACTOSE 108

FIGURE 3.2 X-RAY POWDER DIFFRACTOGRAM OF SPRAY DRIED FP 122

FIGURE 3.3 THE WETTING AND DRYING CALORIMETRIC RESPONSE OF (A) SPRAY DRIED FP, (B) 5% SPRAY-DRIED FP WITH CRYSTALLINE FP AND (C) 3% SPRAY-DRIED FP WITH CRYSTALLINE FP 124

FIGURE 3.4 CALIBRATION CURVES FOR FP AND THE LINES SHOWN ARE LINEAR REGRESSION FITS. 125

FIGURE 3.5: X-RAY POWDER DIFFRACTION PROFILES FOR DAY 0, LH90, HH90 AND HT FP SAMPLES.....133

FIGURE 3.6: DIFFERENTIAL SCANNING CALORIMETRY (DSC) THERMOGRAPHS FOR THE DAY 0, LH90, HH90 AND HT FP SAMPLES.....134

FIGURE 3.7: SCANNING ELECTRON MICROGRAPHS FOR THE DAY 0 (A), HT (B), LH90 (C) AND HH90 (D) FP SAMPLES 136

FIGURE 3.8: (A) COHESION (F_{COH} (FP-FP)) VERSUS ADHESION (F_{COH} (FP-LAC)) PLOTS OF THE MICRONISED FP SAMPLE (DAY 0) AND SAMPLES CONDITIONED AT LOW HUMIDITY (LH30, LH60, LH90) WITH RESPECT TO LACTOSE MONOHYDRATE, (B) COHESION (F_{COH} (FP-FP)) VERSUS ADHESION (F_{COH} (FP-SX)) PLOTS OF THE MICRONISED FP SAMPLE (DAY 0) AND SAMPLES CONDITIONED AT LOW HUMIDITY (LH30, LH60, LH90) WITH RESPECT TO SX. 139

FIGURE 3.9: (A) COHESION (F_{COH} (FP-FP)) VERSUS ADHESION (F_{COH} (FP-LAC)) OF THE MICRONISED FP SAMPLE (DAY 0) AND SAMPLES CONDITIONED AT HIGH HUMIDITY (HH30, HH60, HH90) WITH RESPECT TO LACTOSE MONOHYDRATE, (B) COHESION (F_{COH} (FP-FP)) VERSUS ADHESION (F_{COH} (FP-SX)) OF THE MICRONISED FP SAMPLE (DAY 0) AND SAMPLES LAAGERED AT HIGH HUMIDITY (HH30, HH60, HH90) WITH RESPECT TO SX. 140

FIGURE 3.10: (A) COHESION (F_{COH} (FP-FP)) VERSUS ADHESION (F_{COH} (FP-LAC)) OF THE MICRONISED FP SAMPLE (DAY 0) AND SAMPLES CONDITIONED AT 60°C (HT) WITH RESPECT TO LACTOSE MONOHYDRATE, (B) COHESION (F_{COH} (FP-FP)) VERSUS ADHESION (F_{COH} (FP-SX)) OF THE MICRONISED FP SAMPLE (DAY 0) AND SAMPLES LAAGERED AT 60°C (HT) WITH RESPECT TO SX.....141

FIGURE 3.11: VARIATIONS IN THE CAB RATIOS WITH RESPECT TO LACTOSE MONOHYDRATE AND SX OF MICRONISED FP PARTICLES LAAGERED UNDER LOW AND HIGH RELATIVE HUMIDITY AT 30, 60 AND 90 DAY TIME POINTS. 142

FIGURE 3.12: IN VITRO AEROSOLIZATION PERFORMANCE OF FP IN BINARY DPI FORMULATIONS UPON LAAGERING A BATCH OF MICRONISED FP UNDER LOW AND HIGH RELATIVE HUMIDITY FOR 30, 60 AND 90 DAYS. THE CORRESPONDING CAB RATIOS WITH RESPECT TO LACTOSE MONOHYDRATE UNDER SUCH CONDITIONS ARE ALSO PLOTTED. 149

FIGURE 3.13: IN VITRO AEROSOLISATION PERFORMANCE OF SX IN COMBINATION WITH FP IN TERTIARY FORMULATIONS UPON LAAGERING A BATCH OF MICRONISED FP UNDER LOW AND HIGH RELATIVE HUMIDITY FOR 30, 60 AND 90 DAYS. THE CORRESPONDING CAB RATIOS WITH RESPECT TO SX UNDER SUCH CONDITIONS ARE ALSO PLOTTED.....152

FIGURE 4.1 X-RAY POWDER DIFFRACTION PROFILES FOR THE INITIAL, LH60, HH60 AND T60 SALMETEROL XINAFOATE SAMPLES.....168

FIGURE 4.2 DIFFERENTIAL SCANNING CALORIMETRY THERMOGRAPHS FOR THE INITIAL, LH60, HH60 AND T60 SALMETEROL XINAFOATE SAMPLES 169

FIGURE 4.3 SPECIFIC SURFACE AREA FOR SALMETEROL XINAFOATE SAMPLES DETERMINED BY BET ANALYSIS 171

FIGURE 4.4 SCANNING ELECTRON MICROGRAPHS FOR FRESHLY MICRONISED SX (A, B), AND FOR SAMPLES CONDITIONED FOR 60 DAYS AT 33%RH (C, D), 75%RH (E, F) AND AT 60°C (G, H).....173

FIGURE 4.5A DYNAMIC VAPOUR SORPTION (DVS) ISOTHERM FOR FRESHLY MICRONISED SX (INITIAL) 176

FIGURE 4.5B DYNAMIC VAPOUR SORPTION (DVS) ISOTHERM FOR SX CONDITIONED AT 33%RH FOR 60 DAYS (LH60) 176

FIGURE 4.5C DYNAMIC VAPOUR SORPTION (DVS) ISOTHERM FOR SX CONDITIONED AT 75%RH FOR 60 DAYS (HH60) 177

FIGURE 4.5D DYNAMIC VAPOUR SORPTION (DVS) ISOTHERM FOR SX CONDITIONED AT 60°C FOR 60 DAYS (T60).177

FIGURE 4.6A COHESIVE-ADHESIVE BALANCE (CAB) PLOT OF THE FRESHLY MICRONISED SX SAMPLE (INITIAL) AND SAMPLES CONDITIONED AT LOW HUMIDITY (LH30, LH60) WITH RESPECT TO LACTOSE.....180

FIGURE 4.6B COHESIVE-ADHESIVE BALANCE (CAB) PLOT OF THE FRESHLY MICRONISED SX SAMPLE (INITIAL) AND SAMPLES CONDITIONED AT LOW HUMIDITY (LH30, LH60) WITH RESPECT TO FP 180

FIGURE 4.7A COHESIVE-ADHESIVE BALANCE (CAB) PLOT OF THE FRESHLY MICRONISED SX SAMPLE (INITIAL) AND SAMPLES CONDITIONED AT HIGH HUMIDITY (HH30, HH60) WITH RESPECT TO LACTOSE.....181

FIGURE 4.7B COHESIVE-ADHESIVE BALANCE (CAB) PLOT OF THE FRESHLY MICRONISED SX SAMPLE (INITIAL) AND SAMPLES CONDITIONED AT HIGH HUMIDITY (HH30, HH60) WITH RESPECT TO FP 181

FIGURE 4.8A COHESIVE-ADHESIVE BALANCE (CAB) PLOT OF THE FRESHLY MICRONISED SX SAMPLE (INITIAL) AND SAMPLES CONDITIONED AT 60°C (T30, T60) WITH RESPECT TO LACTOSE 182

FIGURE 4.8B COHESIVE-ADHESIVE BALANCE (CAB) PLOT OF THE FRESHLY MICRONISED SX SAMPLE (INITIAL) AND SAMPLES CONDITIONED AT 60°C (T30, T60) WITH RESPECT TO FP 182

FIGURE 4.9A STAGE BY STAGE DEPOSITION PROFILE EXPRESSED AS THE PERCENTAGE OF EMITTED DOSE PER STAGE FOR SX IN BINARY FORMULATIONS MANUFACTURED USING SX CONDITIONED AT 33%RH 185

FIGURE 4.9B STAGE BY STAGE DEPOSITION PROFILE EXPRESSED AS THE PERCENTAGE OF EMITTED DOSE PER STAGE FOR SX IN BINARY FORMULATIONS MANUFACTURED USING SX CONDITIONED AT 75%RH 186

FIGURE 4.9C STAGE BY STAGE DEPOSITION PROFILE EXPRESSED AS THE PERCENTAGE OF EMITTED DOSE PER STAGE FOR SX IN BINARY FORMULATIONS MANUFACTURED USING SX CONDITIONED AT 60°C 186

FIGURE 4.10 X-RAY POWDER DIFFRACTION PROFILES FOR THE INITIAL AND HFA CONDITIONED SX SAMPLES 190

FIGURE 4.11 DIFFERENTIAL SCANNING CALORIMETRY THERMOGRAPHS FOR THE INITIAL AND HFA CONDITIONED SX SAMPLES 191

FIGURE 4.12 SPECIFIC SURFACE AREA FOR INITIAL AND HFA CONDITIONED SX DRUG SAMPLES DETERMINED BY BET ANALYSIS 193

FIGURE 4.13 SCANNING ELECTRON MICROGRAPHS FOR THE INITIAL SX SAMPLE (A) AND FOR THE HFA CONDITIONED SAMPLE (C) AT A MAGNIFICATION FACTOR OF 3,000, AND FOR THE INITIAL SX SAMPLE (B) AND THE HFA CONDITIONED SAMPLE (D) AT A MAGNIFICATION FACTOR OF 10,000 194

FIGURE 4.14A DYNAMIC VAPOUR SORPTION (DVS) ISOTHERMS FOR FRESHLY MICRONISED SX 195

FIGURE 4.14B DYNAMIC VAPOUR SORPTION (DVS) ISOTHERMS FOR SX CONDITIONED *IN-SITU* WITH HFA FOR 21 DAYS 195

FIGURE 4.15A COHESIVE-ADHESIVE BALANCE (CAB) PLOT OF THE FRESHLY MICRONISED SX SAMPLE (INITIAL) AND AND SX CONDITIONED *IN-SITU* WITH HFA WITH RESPECT TO LACTOSE 197

FIGURE 4.15B COHESIVE-ADHESIVE BALANCE (CAB) PLOT OF THE FRESHLY MICRONISED SX SAMPLE (INITIAL) AND SX CONDITIONED *IN-SITU* WITH HFA WITH RESPECT TO FP 198

FIGURE 4.16 STAGE BY STAGE DEPOSITION PROFILE EXPRESSED AS THE PERCENTAGE OF EMITTED DOSE PER STAGE FOR SX IN BINARY FORMULATIONS MANUFACTURED USING SX CONDITIONED *IN-SITU* WITH HFA 200

FIGURE 5.1 SCANNING ELECTRON MICROGRAPHS FOR GLY CRYSTALS (A), AMBIENT SAMPLE (B), T70 SAMPLE (C,D) AND HFA SAMPLE (E,F) 215

FIGURE 5.2 X-RAY POWDER DIFFRACTION PROFILES FOR GLY CRYSTALS AND THE POST-MICRONISED CONDITIONED SAMPLES 216

FIGURE 5.3 DIFFERENTIAL SCANNING CALORIMETRY THERMOGRAPHS FOR THE GLY CRYSTALS, AMBIENT, T70 AND HFA SAMPLES 217

TABLE 5.3 MELTING ENDOTHERM (J/G) FROM DSC ANALYSIS, SURFACE AREA PER UNIT VOLUME (S_v), SPECIFIC SURFACE AREA PER UNIT MASS (SSA), AND RUGOSITY VALUES (R_A) FOR GLY CRYSTALS AND THE 3 CONDITIONED MICRONISED SAMPLES 219

FIGURE 5.4 SPECIFIC SURFACE AREA THE CONDITIONED GLY SAMPLES DETERMINED BY BET ANALYSIS 219

FIGURE 5.5A DYNAMIC VAPOUR SORPTION (DVS) ISOTHERM FOR THE AMBIENT GLY CONDITIONED SAMPLE 220

FIGURE 5.5B DYNAMIC VAPOUR SORPTION (DVS) ISOTHERM FOR THE T70 GLY CONDITIONED SAMPLE 221

FIGURE 5.5C DYNAMIC VAPOUR SORPTION (DVS) ISOTHERM FOR THE HFA GLY CONDITIONED SAMPLE 221

FIGURE 5.6A PLOT FOR THE COHESION AND ADHESION FORCES FOR THE AMBIENT GLY PARTICLES WITH RESPECT TO LACTOSE 225

FIGURE 5.6B PLOT FOR THE COHESION AND ADHESION FORCES FOR THE T70 GLY PARTICLES WITH RESPECT TO LACTOSE 225

FIGURE 5.6C PLOT FOR THE COHESION AND ADHESION FORCES FOR THE HFA GLY PARTICLES WITH RESPECT TO LACTOSE 226

FIGURE 5.7 STAGE BY STAGE DEPOSITION PROFILE FOR THE 3 GLY FORMULATIONS EXPRESSED AS DRUG DEPOSITS IN µG 227

FIGURE 5.8 FINE PARTICLE FRACTION EXPRESSED AS A PERCENTAGE OF THE EMITTED DOSE FOR EACH GLY FORMULATION PLOTTED AGAINST THE RESPECTIVE CAV VALUE OF THE CONDITIONED GLY PARTICLES 229

FIGURE 5.9 FPF (%) OF AMBIENT, T70 AND HFA FORMULATIONS STORED AT 30°C/65% RELATIVE HUMIDITY FOR A 3 MONTH PERIOD 231

FIGURE 5.10 THE IMPACTOR-SIZED MASS (ISM) FOR THE AMBIENT, T70 AND HFA FORMULATIONS UPON TESTING AT THE DEFINED STABILITY TIME INTERVALS FOLLOWING STORAGE AT 30°C/65% RELATIVE HUMIDITY 232

FIGURE 5.11 FPF (%) OF AMBIENT, T70 AND HFA FORMULATIONS STORED AT 40°C/75% RELATIVE HUMIDITY FOR A 3 MONTH PERIOD 233

FIGURE 5.12 THE IMPACTOR-SIZED MASS (ISM) FOR THE AMBIENT, T70 AND HFA FORMULATIONS UPON TESTING AT THE DEFINED STABILITY TIME INTERVALS FOLLOWING STORAGE AT 40°C/75% RELATIVE HUMIDITY 233

LIST OF TABLES

TABLE 2.1 SUMMARY OF FP SAMPLES AND FORMULATIONS STUDIED THROUGHOUT THIS WORK 76

TABLE 2.2 PARTICLE SIZE DISTRIBUTION DATA FOR THE MICRONISED AND SUBSEQUENTLY CONDITIONED FP DETERMINED BY LASER DIFFRACTION 86

TABLE 2.3 COHESIVE-ADHESIVE BALANCE (CAB) VALUES WITH RESPECT TO LACTOSE AND SX FOR ALL FP SAMPLES 88

TABLE 2.4 *IN VITRO* AEROSOLISATION PERFORMANCE FOR FP FORMULATIONS PRODUCED USING INITIAL, T48, T72, HT7 AND HT14 FP. RESULTS ARE DESCRIBED BY THE RECOVERED DOSE (RD), EMITTED DOSE (ED), FINE PARTICLE MASS (FPM), FINE PARTICLE FRACTION (FPF) EXPRESSED AS A PERCENTAGE OF THE RECOVERED DOSE, MASS MEDIAN AERODYNAMIC DIAMETER (MMAD) AND GEOMETRIC STANDARD DEVIATION (GSD) 91

TABLE 2.5 *IN VITRO* AEROSOLISATION PERFORMANCE FOR FP IN COMBINATION FORMULATIONS WITH SX PRODUCED USING INITIAL, T48, T72, HT7 AND HT14 FP. RESULTS ARE DESCRIBED BY THE RECOVERED DOSE (RD), EMITTED DOSE (ED), FINE PARTICLE MASS (FPM), FINE PARTICLE FRACTION (FPF) EXPRESSED AS A PERCENTAGE OF THE RECOVERED DOSE, MASS MEDIAN AERODYNAMIC DIAMETER (MMAD) AND GEOMETRIC STANDARD DEVIATION (GSD) 94

TABLE 2.6 *IN VITRO* AEROSOLISATION PERFORMANCE FOR SX IN COMBINATION FORMULATIONS WITH FP PRODUCED USING INITIAL, T48, T72, HT7 AND HT14 FP. RESULTS ARE DESCRIBED BY THE RECOVERED DOSE (RD), EMITTED DOSE (ED), FINE PARTICLE MASS (FPM), FINE PARTICLE FRACTION (FPF) EXPRESSED AS A PERCENTAGE OF THE RECOVERED DOSE, MASS MEDIAN AERODYNAMIC DIAMETER (MMAD) AND GEOMETRIC STANDARD DEVIATION (GSD) 98

TABLE 2.7 PARTICLE SIZE DISTRIBUTION DATA FOR THE FRESHLY MICRONISED AND HFA CONDITIONED FP SAMPLES DETERMINED BY LASER DIFFRACTION 103

TABLE 2.8 COHESIVE-ADHESIVE BALANCE (CAB) VALUES WITH RESPECT TO LACTOSE AND SX FOR THE INITIAL AND HFA CONDITIONED FP SAMPLES 104

TABLE 2.9 *IN VITRO* AEROSOLISATION PERFORMANCE FOR FORMULATION MANUFACTURED USING THE INITIAL AND THE HFA CONDITIONED FP SAMPLES. RESULTS ARE DESCRIBED BY THE RECOVERED DOSE (RD), EMITTED DOSE (ED), FINE PARTICLE MASS (FPM), FINE PARTICLE FRACTION (FPF) EXPRESSED AS A PERCENTAGE OF THE RECOVERED DOSE, MASS MEDIAN AERODYNAMIC DIAMETER (MMAD) AND GEOMETRIC STANDARD DEVIATION (GSD) 106

TABLE 3.1 NOMENCLATURE OF POST-MICRONISED FP SAMPLES BASED ON THEIR CONDITIONING ENVIRONMENTS AND PERIODS 116

TABLE 3.2: PHYSICO-CHEMICAL MEASUREMENTS OF MICRONISED (DAY 0) AND LAAGERED SAMPLES OF FP 137

TABLE 3.3: IN VITRO FORMULATION PERFORMANCE, AS MEASURED BY THE MASS BALANCE (MB), IMPACTOR STAGE MASS (ISM), MASS MEDIAN AERODYNAMIC DIAMETER (MMAD), GEOMETRIC STANDARD DEVIATION (GSD) AND FINE PARTICLE MASS ($FPM_{<5\mu M}$), FROM THE AEROSOLIZATION OF BINARY AND TERTIARY DPI FORMULATIONS OF FRESHLY MICRONISED AND LAAGERED FP SAMPLES (N=3). NOTE THAT THE LARGE SDS IN SOME APSD DATA BELOW WERE RELATED TO VARIATIONS IN DEVICE LOSSES BETWEEN THE REPEATED RUNS 145

TABLE 4.1 SUMMARY OF SX SAMPLES STUDIED THROUGHOUT THIS WORK 159

TABLE 4.2 PARTICLE SIZE DISTRIBUTION OF THE MICRONISED AND SUBSEQUENTLY CONDITIONED SALMETEROL XINAFOATE DETERMINED BY LASER DIFFRACTION 170

TABLE 4.3 SURFACE AREA PER UNIT VOLUME (S_V), SPECIFIC SURFACE AREA PER UNIT MASS (SSA), AND RUGOSITY VALUES (R_A) FOR ALL SX SAMPLES.....172

TABLE 4.4 COHESIVE-ADHESIVE BALANCE (CAB) VALUES WITH RESPECT TO LACTOSE AND FLUTICASONE PROPIONATE FOR FRESHLY MICRONISED SX AND FOR SX SAMPLES CONDITIONED ENVIRONMENTALLY.....178

TABLE 4.5 IN VITRO AEROSOLISATION PERFORMANCE FOR SX FORMULATIONS MANUFACTURE WITH FRESHLY MICRONISED AND ENVIRONMENTALLY CONDITIONED SX. RESULTS ARE DESCRIBED BY THE RECOVERED DOSE (RD), EMITTED DOSE (ED), FINE PARTICLE MASS (FPM), FINE PARTICLE FRACTION (FPF) EXPRESSED AS A PERCENTAGE OF THE EMITTED DOSE, MASS MEDIAN AERODYNAMIC DIAMETER (MMAD) AND GEOMETRIC STANDARD DEVIATION (GSD)..184

TABLE 4.6 *IN VITRO* AEROSOLISATION PERFORMANCE FOR SX IN TERNARY FORMULATIONS WITH FP MANUFACTURED WITH FRESHLY MICRONISED AND ENVIRONMENTALLY CONDITIONED SX. RESULTS ARE DESCRIBED BY THE RECOVERED DOSE (RD), EMITTED DOSE (ED), FINE PARTICLE MASS (FPM), FINE PARTICLE FRACTION (FPF) EXPRESSED AS A PERCENTAGE OF THE EMITTED DOSE, MASS MEDIAN AERODYNAMIC DIAMETER (MMAD) AND GEOMETRIC STANDARD DEVIATION (GSD) 188

TABLE 4.7 *IN VITRO* AEROSOLISATION PERFORMANCE FOR FP IN TERNARY FORMULATIONS WITH SX MANUFACTURED WITH FRESHLY MICRONISED AND ENVIRONMENTALLY CONDITIONED SX. RESULTS ARE DESCRIBED BY THE RECOVERED DOSE (RD), EMITTED DOSE (ED), FINE PARTICLE MASS (FPM), FINE PARTICLE FRACTION (FPF) EXPRESSED AS A PERCENTAGE OF THE EMITTED DOSE, MASS MEDIAN AERODYNAMIC DIAMETER (MMAD) AND GEOMETRIC STANDARD DEVIATION (GSD) 189

TABLE 4.8 PARTICLE SIZE DISTRIBUTION OF THE INITIAL AND HFA CONDITIONED SX SAMPLES DETERMINED BY LASER DIFFRACTION 192

TABLE 4.9 SURFACE AREA PER UNIT VOLUME (S_v), SPECIFIC SURFACE AREA PER UNIT MASS (SSA), AND RUGOSITY VALUES (R_A) FOR THE INITIAL AND HFA CONDITIONED SX SAMPLES 193

TABLE 4.10 COHESIVE-ADHESIVE BALANCE (CAB) VALUES WITH RESPECT TO LACTOSE AND FLUTICASONE PROPIONATE FOR FRESHLY MICRONISED SX AND FOR SX SAMPLES CONDITIONED *IN-SITU* WITH HFA 197

TABLE 4.11 *IN VITRO* AEROSOLISATION PERFORMANCE DATA FOR FORMULATIONS MANUFACTURED USING SX CONDITIONED *IN-SITU* WITH HFA. RESULTS ARE DESCRIBED BY THE RECOVERED DOSE (RD), EMITTED DOSE (ED), FINE PARTICLE MASS (FPM), FINE PARTICLE FRACTION (FPF) EXPRESSED AS A PERCENTAGE OF THE EMITTED DOSE, MASS MEDIAN AERODYNAMIC DIAMETER (MMAD) AND GEOMETRIC STANDARD DEVIATION (GSD) 199

TABLE 5.1 SUMMARY OF GLY POST-MICRONISATION CONDITIONING THROUGHOUT THIS WORK 205

TABLE 5.2 PARTICLE SIZE DISTRIBUTION OF GLY SAMPLES HANDLED DURING THIS STUDY AS DETERMINED BY LASER DIFFRACTION 213

TABLE 5.4 COHESIVE-ADHESIVE BALANCE (CAB) VALUES WITH RESPECT TO LACTOSE FOR ALL 3 CONDITIONED GLY SAMPLES 223

TABLE 5.5 *IN VITRO* AEROSOLISATION PERFORMANCE FOR GLY FORMULATIONS PRODUCED USING THE CONDITIONED GLY SAMPLES; AMBIENT, T70 AND HFA. RESULTS ARE DESCRIBED BY THE RECOVERED DOSE (RD), EMITTED DOSE (ED), FINE PARTICLE MASS (FPM), FINE PARTICLE FRACTION (FPF) EXPRESSED AS A PERCENTAGE OF THE EMITTED DOSE, MASS MEDIAN AERODYNAMIC DIAMETER (MMAD) AND GEOMETRIC STANDARD DEVIATION (GSD) 226

LIST OF ABBREVIATIONS

˚C	degrees centigrade
%	percent
γ	surface tension
ΔL	change in length
ε	dielectric constant
θ	contact angle or angle between incident X-rays and crystal plane
λ	wavelength
μg	microgram (10^{-6} g)
μm	micrometre (10^{-6} m)
A	Hamaker constant or area
AFM	atomic force microscope/microscopy
ANOVA	analysis of variance
API	active pharmaceutical ingredient
CAB	cohesive adhesive balance
cm	centimeter (10^{-2} m)
d	separation distance/lattice spacing
D	diameter
D_A	amplitude
D_{ae}	aerodynamic diameter
DPI	dry powder inhaler
DSC	differential scanning calorimetry
DVS	dynamic vapour sorption
E	Young’s modulus of elasticity
ED	emitted dose

F	normal force
F_c	capillary force
F_e	Coulombic force
F_{vdw}	van der Waals interaction
FPD	fine particle dose
FPF(ED)	fine particle fraction (of the emitted dose)
FPF(RD)	fine particle fraction (of the recovered dose)
g	gramme
GSD	geometric standard deviation
GPa	gigapascal (10^9 Pa)
HOPG	highly oriented pyrolytic graphite
HPLC	high performance liquid chromatography
hr	hour
Hz	Hertz (s^{-1})
k	spring constant
K	degrees kelvin
KHz	kilohertz (10^3 Hz)
Ku	kurtosis
l	litre
L	length
LALLS	low angle laser light scattering
m	metre
mg	milligramme (10^{-3} g)
min	minute
ml	millilitre (10^{-3} l)
mm	millimeter (10^{-3} m)

MMAD	mass median aerodynamic diameter
MSLI	multi-stage liquid impinger
n	order of reflection
N	Newton
NGI	Next Generation Impactor
nm	nanometre (10^{-9} m)
nN	nanonewton (10^{-9} N)
P	probability that two populations are similar
Pa	Pascal
pK_a	acid dissociation constant
pMDI	pressurized metered dose inhaler
PSD	particle size distribution
q	charge
Q	volumetric flow
r	radius
R^2	linear correlation coefficient
RH	relative humidity
rpm	revolutions per minute
R_q	root mean square roughness
RSD	relative standard deviation
s	second
SD	standard deviation
SEM	scanning electron microscope/microscopy/micrograph
Sk	skewness
t	time
TSI	twin stage impinger

UK	United Kingdom
USA	United States of America
v	velocity
v/v	volume for volume
w/v	weight for volume
w/w	weight for weight
$\bar{x}$	mean
XRD	x-ray diffraction

1 Introduction

1.1 Respiratory Medicine

Respiratory diseases are a major concern in the medical field due to alarming statistics observed over the past decades regarding death rates and other health economic trends (Royal College of Physicians, 2014; Rea, Scragg *et al.,* 1986). Asthma and chronic obstructive pulmonary disease (COPD) cost governments billions of pounds and are one of the highest causes of death worldwide. This highlights the importance of a more efficient and effective development of aerosolised drugs as a pharmacotherapy response to evolving respiratory diseases (Harrison, Stephenson *et al.,* 2005; Anagnostou, Harrison *et al.,* 2012, Bucknall, Slack *et al.,* 1999).

The use of aerosol inhalation as a method of drug delivery to the respiratory tract has numerous advantages. Having the active drug being delivered directly to the tracheobronchial tree leads to a rapid and predictable onset of action, hence, avoiding first-pass effect and degradation within the gastrointestinal tract. This allows lower dosages to be administered as opposed to the oral route, ensuring side effects are kept to a minimum. Another major advantage of aerosol inhalation as a method of drug delivery lies in the fact that having an alternative route for delivery avoids drug-drug interaction when more than one medication is being administered concurrently (Timsina, Martin *et al.,* 2003; Patton, 1996).

Figure 1.1 illustrates the constituents of the respiratory tract as a series of branching airways. The first passageway is the trachea and assumes the respiration role of leading inspired air to the gas exchanging regions of the lung. The pharynx and larynx connect it to the oral and nasal cavities. The trachea divides into two main bronchi, which in turn bifurcate into narrower and shorter bronchi and bronchioles. These together with the trachea are known as the conducting airways (Patton, 1996). The dichotomous branching of the airways from the bronchi to the bronchioles undergoes over 32 bifurcations (Gurney, 1991). The bronchioles bifurcate further leading to the deepest part in the lung where the respiratory bronchioles and alveoli are found. This area is known as the peripheral airways.

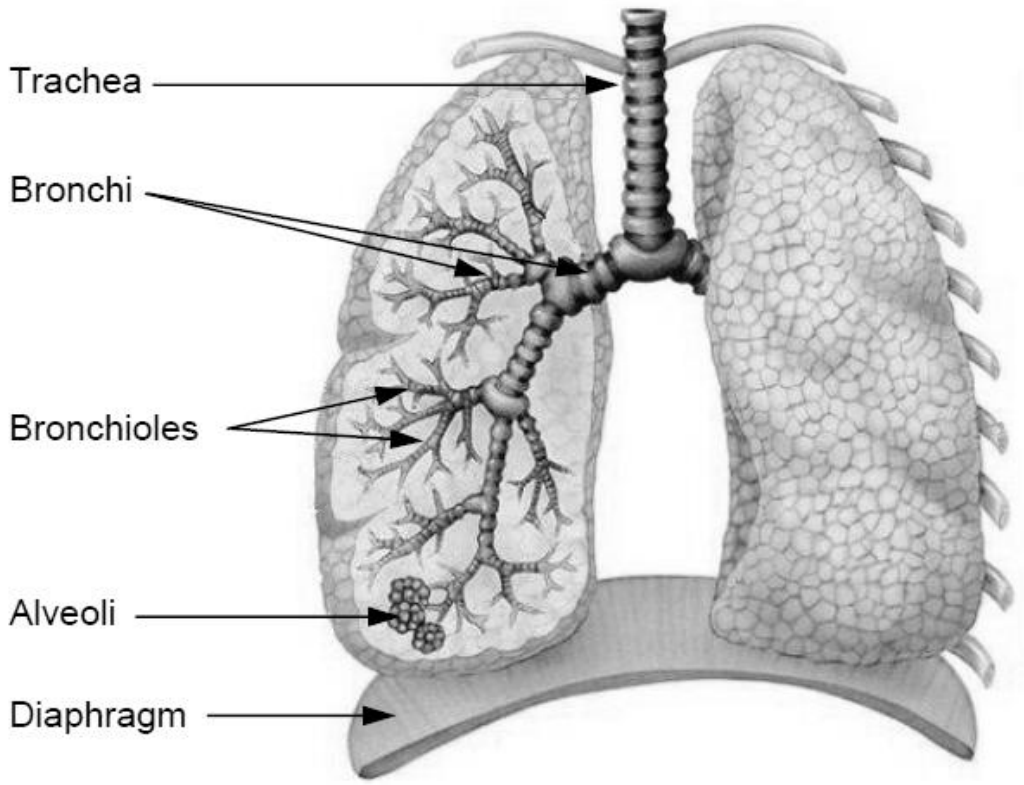

Figure 1.1: Structure of the Human Lung (adapted from Griesenbach *et al.*, 2004)

The respiratory tract offers two target sites for drugs delivered by inhalation. The conducting airways are the ideal site for drug deposits in order to cure respiratory diseases since these are generally diseases of the conducting airways themselves (Pritchard, 2006). To utilise the lung as a portal entry for systemic delivery, the peripheral airways need to be targeted with the excellent blood flow found in these regions and therefore enables a high drug absorption into the systemic circulation (Timsina, Martin *et al.,* 2003).

1.2 Particle Deposition in the Lungs

In order to achieve the desired pharmacological effect, a drug particle designed for inhalation must deposit at the site of action (Byron and Patton, 1994). The region and method with which the drug particles deposit are highly dependent on aerodynamic particle size and the three main deposition mechanisms, namely; inertial impaction, sedimentation and diffusion. Interception and electrostatic precipitation other deposition mechanism by which drug particles may deposit in the lungs (Heyder, Gebhart *et al.,* 1986; Lalor and Hickey, 1996). As described in the following sub-sections, there are a variety of variables which influence the mechanism or mechanisms by which a drug particle deposits (Martonen and Katz, 1993)).

1.2.1 Inertial Impaction

Inertial impaction is the mechanism which dominates particle deposition in the lungs, and occurs mainly in the conducting airways (Asgharian and Anjilvel, 1994). As an inhaled airstream changes direction on passing through the

repeated bifurcations and bends of the respiratory tract, a particle suspended in the airflow may not lose its inertia and relax into the new direction of the airflow, thereby impacting on the respiration surface (Martonen, Katz *et al.,* 1992). Deposition by inertial impaction is highly dependent on the material density and size of the suspended particles. The probability of impaction for a particle travelling in an airway is related to its Stokes' number (Stk), a dimensionless parameter that can be calculated using Equation 1.1.

$$Stk = \frac{\rho_p d^2 V}{18\eta R} \qquad \text{Equation 1.1}$$

where ρ_p is the particle density, d is the particle diameter, V is the air velocity, η is the air viscosity and R is the airway radius. From this equation, the higher the value of Stokes' number, the more readily particles will deposit by inertial impaction (Morrison, 1974; Martonen and Katz, 1993; Crowder, Rosati *et al.,* 2002).

1.2.2 Sedimentation

The influence of gravity of the deposition of drug particles suspended in respiratory tract is referred to as sedimentation (Clark and Egan, 1994). For particles between 1 and 40 µm diameter in a laminar airstream, the terminal velocity (V_t) at which this settling occurs is described by Stokes' law (Stokes, 1908);

$$V_t = \frac{(\rho_p - \rho_a)d^2 g}{18\eta}$$ Equation 1.2

where ρ_p is the particle density, ρ_a is the density of air, d is the particle diameter, g is acceleration due to gravity and η is the air viscosity. Particles <1 μm tend to settle with a faster terminal velocity than that predicted by Equation 1.2, whilst particles >40 μm diameter tend to settle at a slower terminal velocity (Nowak, Kakade *et al.,* 2003).

Sedimentation is a time-dependant process, as particles must have sufficient residence time in the airway to settle from their inertial position to deposit on the respiratory surface (Taulbee and Yu, 1975). It is therefore the dominant mechanism of deposition in the smaller airways and alveoli, due to the small airway dimensions and low air flow velocities found in these regions (Heyder, Gebhart *et al.,* 1986; Tsuda, Butler *et al.,* 1994a; Lalor and Hickey, 1996).

1.2.3 Brownian Motion

As the diameter of a suspended particle falls below 1 μm, the influence of gravity on its motion decreases, whilst the influence of Brownian motion caused by the random bombardment of the particle by gas molecules becomes greater (McMurry and Rader, 1985). By its very nature, Brownian motion results in particles following a random and variable path, but for those < 0.5 μm diameter, Brownian motion will tend to cause greater displacement

than sedimentation and so be the primary mechanism of deposition (McMurry and Rader, 1985; Tsuda, Butler *et al.,* 1994a). Nevertheless, due to the relative magnitudes of the displacement caused by sedimentation and Brownian motion, particles > 2 µm are more likely to deposit in the airways than those < 0.5 µm diameter (Tsuda, Butler *et al.,* 1994b).

1.2.4 Interception

Interception occurs when a particle moving within the airstream makes contact with the respiratory surface (Taulbee and Yu, 1975). Elongated particles are most likely to deposit in this manner. However, as the typical size of drug particles used in respiratory drug delivery is much smaller than that of the airways, this mechanism of deposition is relatively unimportant in most cases (Martonen and Katz, 1993).

1.2.5 Electrostatic Precipitation

Drug particles may become electrostatically charged during aerosolisation (Yeomans, Rogers *et al.,* 1949), which, in theory, might influence deposition, either through the induction of an image charge on the respiratory surface and subsequent electrostatic attraction, or via the repulsion between positively charged aerosol particles directing them towards the airway walls (Balashazy and Hofmann, 1993).

1.2.6 Effect of Particle Size on Deposition in the Respiratory Tract

Equations 1.1 and 1.2 show how aerodynamic particle size is a major variable in controlling particle deposition in the lung (Taulbee and Yu, 1975; Park and Lee, 2000). Inhalation formulations must therefore produce an aerosol of appropriately sized drug particles, to ensure an adequate dose reaches the site of action (Tismina, Martin *et al.,* 1994; Virchow, Crompton *et al.,* 2008). Even before an aerosol enters the trachea, it must negotiate a 90° bend between the oral cavity and the pharynx without impacting on the back of the throat (Taulbee and Yu, 1975). At each bifurcation, the cross-sectional area of an individual airway decreases, providing an ever more convoluted path for a particle to negotiate without impaction (Balashazy and Hofmann, 1993). Drug particles with an aerodynamic diameter larger than 10 µm will tend to impact in the throat and upper airways, whereas particles with an aerodynamic diameter less than 0.5 µm will tend to be exhaled (Hofmann, Sturm *et al.,* 2003). The majority of particles with aerodynamic diameters between 2.5 µm and 6 µm will tend to deposit in the conducting airways, whereas particles with an aerodynamic diameter less than 2.5 µm will tend to deposit in the peripheral airways (Tsuda, Butler *et al.,* 1994a; Tsuda, Butler *et al.,* 1994b). It is therefore generally accepted that the target drug aerosol aerodynamic diameter for inhalation formulations is between 1 µm and 5 µm, depending on the desired target site of action (Heyder, Gebhart *et al.,* 1986).

1.3 Treatment of Asthma and COPD

Airflow limitations and chronic inflammation are main characteristics of both asthma and Chronic Obstructive Pulmonary Diseases (COPD). The most efficacious treatment is administering of medication which acts to reduce and prevent airway constriction and inflammation. The first-line treatments in both asthma and COPD are bronchodilators (short and long acting β_2-agonists) and anti-inflammatory therapy (inhaled corticosteroids), which are employed to aid bronchodilation and reduce inflammation respectively (Greening, Ind *et al.,* 1994; Emmett *et al.,* 2001).

1.3.1 Bronchodilators

Bronchodilator drugs are used to relieve symptoms of bronchoconstriction (Barnes, 2002). These drug agents are typically β_2-agonists, which stimulate β-adrenoceptors in the smooth-muscle of the airway, producing smooth-muscle relaxation and bronchodilation (Holgate and Polosao, 2008). The short-acting β_2-agonists (SABA) include salbutamol and terbutaline, which have a duration of action of 3-4 hours with an onset of action of 15 minutes (Biddiscombe, Melchor *et al.,* 1987). In contrast, the long-acting β_2-agonists, including salmeterol xinafoate (SX) and formoterol fumarate dihydrate (FFD), have a duration of action of more than 12 hours and are helpful in controlling chronic asthma (Cazzola, Testi *et al.,* 2002).

Anticholinergic quaternary ammonium compounds are a relatively novel class of bronchodilators (Barnes, 2004). The first use of anti-muscarinic agents in

the treatment of respiratory diseases was through short-acting agents (ipratropium and oxitropium). Once-daily treatment using long-acting compounds (tiotropium and glycopyrronium) have recently been introduced (Buhl and Banerji, 2012). Anticholinergic drugs work by competitive blockage of muscarinic cholinergic receptors, inhibiting bronchoconstriction and bronchial hypersecretion leading to airway dilation (Buhl and Banerji, 2012).

1.3.2 Anti-Inflammatory Drugs

The use of inhaled corticosteroids (ICS) is widespread in the treatment of asthma and COPD. ICS such as budesonide and fluticasone propionate (FP) reduce airway inflammation which is the underlying pathophysiological process in both diseases (Barnes, 2002). The responsiveness of ICS therapy is usually high in asthma. Corticosteroids suppress inflammation by inducing the recruitment of nuclear enzyme histone deacetylase 2 (HDAC2), which suppresses the expression of genes of various inflammatory mediators (Barnes, 2004).

On the other hand, the use of ICS therapy in COPD treatment fails to suppress inflammation leading to a poor patient response. This has been reported to be related to the decrease of activity and expression of HDAC2 in the inflammatory cells and peripheral lungs of COPD patients (Barnes, 2008).

1.3.3 Combination Therapy

Several studies have shown how a long-acting β_2-agonist in combination with an ICS leads to superior results in controlling asthma (Matz, Emmett *et al.,* 2001). Data have shown that when FP and SX are combined, there is an increased clinical benefit when compared to individual drug components used separately (Nelson, Chapman *et al.,* 2003). For patients with more severe COPD, the study suggested that using a combination of budesonide and FFD improves the overall exacerbation rate when compared to β_2-agonist alone (Campbell and Szafranski, 2002). In addition, a 3-year retrospective study of COPD patients managed in primary care concluded that regular use of FP in combination with SX is associated with significantly higher rates of survival of COPD patients (Calverley, Pauwels *et al.,* 2003).

The superior clinical performance of combined therapy as opposed to the administering of individual drugs has been related to complementary efficacy of both long-acting β_2-agonists and ICS when co-administered (Zetterstrom, Buhl *et al.,* 2001). Another explanation to this superior clinical efficacy of co-administration may be the synergistic interactions if ICS and long-acting β_2-agonists are co-deposited at the receptor, molecular and cellular level (Nelson, Chapman *et al.,* 2003).

1.4 Current Respiratory Drug Delivery Devices

There are currently three main drug delivery devises used to delivery medication to the lungs; nebulisers, pressurised metered dose inhalers (pMDIs), and dry powder inhalers (DPIs) (Hickey and Dunbar, 1997). These three devices are all used to treat respiratory conditions such as asthma and COPD (Lalor and Hickey, 1996).

1.4.1 Nebulisers

Nebulisers are devices which employ either compressed gas or ultrasonic energy to aerosolise aqueous drug solutions or suspensions for patient inhalation (Clarke, 1995). Unlike other devices, they do not require the use of complex breathing manoeuvre and by extending the time of operation, they can be used to deliver large doses (up to 1g) (de Boer, Hagedoorn *et al.,* 2003). The use of nebulisers is limited, however, by the length of time taken to deliver the required dose (10-15 minutes), their bulky size and high cost, which usually limits their use to hospitals and non-ambulatory patients (Garcia-Contreras and Hickey, 2003). Recent developments in nebuliser technology are beginning to overcome some of these problems, allowing accurate metering of doses and increasing their portability (Dalby, Spallek *et al.,* 2004).

1.4.2 Pressurised Metered Dose Inhalers

Pressurised metered dose inhalers (pMDIs) have been the drug delivery device of choice for respiratory diseases since 1956, as a result of their portability, robustness and cheap to manufacture (Hickey and Dunbar, 1997). Traditionally, these devices consist of a solution or suspension of fine drug

particles in a chlorofluorocarbon (CFC) propellant sealed in a canister at high pressure (Biddiscombe, Melchor *et al.,* 1987). Actuation of the inhaler results in the release of a metered volume of this solution or suspension, which, driven by the pressure within the canister, emerges at high speed through a narrow orifice (Smyth, Hickey *et al.,* 2006). This process, combined with evaporation of the propellant, results in an aerosol of drug particles in the inhalable size range (Berry, Kline at al., 2003). Notwithstanding the fact that pMDIs are the most frequently prescribed inhalation dosage form, most patients are unable to use them correctly (Virchow, Crompton *et al.,* 2008). This is due to the high speed aerosol plume generated by the device, which requires the patient to use accurate co-ordination of inspiration and inhaler activation to ensure correct inhalation and deposition of the drug in the lungs (Virchow, Crompton *et al.,* 2008). Even with the correct inhalation technique, pMDIs are inefficient often delivering less than a third of the emitted dose to the lungs (Virchow, Crompton *et al.,* 2008). In addition to these problems, the introduction of the Montreal Protocol resulted in the phase out of CFC propellant gas in all aerosol-based products, including pMDIs. As a result, all pharmaceutical CFC-based pMDI products were re-formulated using hydrofluoroalkanes (HFA) propellant (Richards, Hirst *et al.,* 2001). The difficulties and expense incurred in re-formulating pMDI products and long term issues regarding the greenhouse gas properties of HFA-based propellants, have prevented, more recently, companies from launching new drugs as pMDI formulations (McDonald and Martin, 2000).

1.4.3 Dry Powder Inhalers

Dry powder inhalers (DPIs) allow an accurate dose of drug to be delivered to the respiratory airways as a dry powder aerosol (Tismina, Martin *et al.,* 1994). Interest in DPIs for inhalation therapy grew strongly due to their potential to offer CFC-free alternatives to pMDIs (McDonald and Martin, 2000). Currently, the spectrum of applications for DPIs has become much broader, due to the high lung deposition that can be attained and their suitability for pulmonary delivery of therapeutic peptide and proteins both for local and systemic conditions (Byron and Patton, 1994). DPIs are breath-actuated drug delivery systems, which enable a respirable cloud to be generated in response to the patient's inspiratory effort (Tismina, Martin *et al.,* 1994). DPIs may therefore have many advantages over pMDIs (Hannemann, 1999; Newman and Busse, 2002; Virchow, Cromptom *et al.,* 2008). Firstly, DPIs do not need a propellant, which has been the driving force behind the introduction of a large number of novel DPI devices in recent years (Tismina, Martin *et al.,* 1994). The second benefit is that DPIs eliminate the need for patient co-ordination of actuation and inhalation (Newman and Busse, 2002). Finally, in DPIs, the particles are travelling at a slower rate, therefore, an excessive drug loss due to impaction in the throat is avoided (Pauwels, Newman *et al.,* 1997).

Having particles with a mass median aerodynamic diameter (MMAD) less than 5 µm is critical in achieving lung deposition of the said drug particles (Heyder, Gebhart *et al.,* 1986; Tismina, Martin *et al.,* 1994; Prime, Atkins *et al.,* 1997). Controlling this variable is usually obtained by high-energy micronisation

techniques (Thibert and Tawashi, 1999), although numerous other technologies such as spray drying (Li, Seville *et al.,* 2005), and supercritical fluid technologies (Shekunov, Feeley *et al.,* 2003) have been evaluated. However, respirable sized particles exhibit high surface energies, which lead to particle aggregation, poor flow and entrainment properties, and therefore make re-dispersion of the drug a difficult process (Feeley, York *et al.,* 1998). These problems relate to the cohesive nature of the powder. To overcome particle-particle cohesion, the drug is mixed with with a coarse excipient, traditionally lactose monohydrate (Bell, Hartley, 1971). The micronised drug is blended with carrier particles of a much larger size range (20-100 µm), whereby the drug particles form an interactive mixture with the surfaces of the coarse lactose particles (Ganderton, 1992). The turbulent airflow generated within the device upon forced inspiration should be sufficient to fluidise the formulation from the device and to de-aggregate the drug particles from the carrier particles (Telko and Kickey, 2005; Shur, Harris *et al.,* 2008). The drug particles are then entrained into the airstream, which enables the drug particle to enter the lung (Shur, Harris *et al.,* 2008).

DPIs are currently available in three different types; the single-dose, the multi-dose and the reservoir-based dose (Prime, Atkins *et al.,* 1997; Malcolmson and Embleton, 1998; Smith and Parry-Billings, 2003). Every DPI device exhibits an internal resistance which determines the inhaled flow rate that a patient can achieve when using the device (Harris, 2007). As flow rate will inevitably be linked with inhaler performance, it is essential that such factors

are considered in any *in vitro* comparative testing of DPIs (Harris, 2007). Successful development of DPI systems requires development on two integrated fronts; device engineering and powder formulation engineering (Tismina, Martin *et al.,* 1994).

1.5 Interparticulate Forces

Having highlighted the importance of interparticulate interactions on the performance and behaviour of DPI formulations, the following section will look into the origins which determine these highly influential interparticulate forces. Interactions between particles forming a powder interact with each other through a composite of physical forces (Johnson, 1996). Although these forces are relatively weak, never exceeding 40 $kJ.mol^{-1}$ as opposed to the typical 300-700 $kJ.mol^{-1}$ for covalent bonds (Johnson, 1996), their influence on powder behaviour is significant on particles having a diameter below 10 µm, as the force of gravity becomes relatively insignificant (Johnson, 1996). Such interactions may be classified as being either cohesive (interactions between particles of the same chemical structure and similar particle size), or adhesive (interactions between particles with different chemical structures and size) (Johnson, 1996). The physical forces which dominate the cohesive and adhesive properties of respirable drug particles are van der Waals, capillary and electrostatic forces (Johnson, 1996).

1.5.1 Van der Waals Forces

Van der Waals forces account for the major force of interaction between uncharged particles in a dry environment (Lifshitz, 1955). These forces are the summation of the attractions between molecules that are temporarily dipolar, due to random fluctuations in their surrounding electron cloud, which may also induce the corresponding polarity in another molecule in close proximity (Lifshitz, 1955).

The van der Waals forces (F_{VDW}) between two ideally smooth spheres in a vacuum can be described by Hamaker (Hamaker, 1937) :

$$F_{VDW} = \frac{H}{12s^2}\left(\frac{d_1 d_2}{d_1 + d_2}\right) \qquad \text{Equation 1.3}$$

where H is the Hamaker constant (Equation 1.4), s is the separation distance between the spheres and d_1 and d_2 are the diameters of the two spheres. The Hamaker constant is given by:

$$H = \pi^2 v_1 v_2 \lambda_{1,2}^d \qquad \text{Equation 1.4}$$

where v_1 and v_2 are the number of atoms per unit volumes of particle 1 and 2 and $\lambda_{1,2}^d$ is the constant of dispersion:

$$\lambda_{1,2}^d = -\frac{3}{4} hFa^2 \qquad \text{Equation 1.5}$$

where h is Planck's constant, F is the vibration frequency of the interacting electronic oscillators and a is the polarisability of the molecules.

The adhesive force between a sphere (diameter d_1) and a plane composed of the same material and separated by distance s is described by:

$$F_{VDW} = \frac{H_{11} d_1}{6s^2} \qquad \text{Equation 1.6}$$

whereas the adhesion between a sphere (diameter d_1) and a plane composed of different materials and separated by distance s is expressed by:

$$F_{VDW} = \frac{\sqrt{H_{11} H_{22}}}{6s^2} d_1 \qquad \text{Equation 1.7}$$

where H_{11} and H_{22} are the Hamaker constant for the particle and the plane surface, respectively.

Equations 1.3, 1.6 and 1.7 demonstrate the importance of the separation distance, s, in determining the van der Waals forces between two solid objects. It is clear that these will retard rapidly with increasing separation distance, so it is not surprising that van der Waals forces exert their influence only over a narrow range of approximately 10 nm (Hamaker, 1937).

1.5.2 Capillary Forces

When relative humidities exceed 50 %, water may condensate onto particle surfaces and may lead to the formation of liquid bridges between contiguous particles (McFarlane and Tabor, 1950; Hiestand, 1966). Such structures will lead to an increase in adhesive forces between particles due to the surface tension of water and the formation of a meniscus creating a capillary force of interaction (McFarlane and Tabor, 1950). The magnitude of this capillary force (F_c) between two identical smooth spheres (radius r) can be calculated as:

$$F_c = 2\pi\gamma_w r\cos\alpha \qquad \text{Equation 1.8}$$

where γ_w is a surface tension of water and α is a contact angle between water and the spheres. In the case of a sphere (radius r) adhering to a surface, the capillary force resulting from the condensation of water in the interface can be calculated as:

$$F_c = 2\pi\gamma_w r(\cos\alpha + \cos\beta) \qquad \text{Equation 1.9}$$

where α and β are the contact angles of the water with the surface and particle, respectively.

When the relative humidity is in excess of 65 %, capillary forces may become the dominant force of interaction (Hiestand, 1966; Price, Young *et al.,* 2002).

1.5.3 Electrostatic Forces

Particles may become charged during powder handling by contact or friction with other particles or surfaces. This process is known as triboelectrification (Staniforth and Rees, 1982). If charged particles are brought into proximity of one another, a long-range electrostatic force (either attractive or repulsive, depending whether the particles are like or oppositely charged) will be generated which can be described by Coulomb's law (Coulomb, 1785):

$$F_{EL} = \frac{q_1 q_2}{4\pi\varepsilon s^2} \qquad \text{Equation 1.10}$$

where F_{EL} is the electrostatic force, q_1 and q_2 are the electrical charges on the two particles, ε is the permittivity and s is the separation distance between the particles.

Furthermore, an uncharged particle may become charged if an image charge is induced upon it by the approach of a charged particle (Onsager and Samaras, 1934). The resultant electrostatic force may be shown by:

$$F_{EL} = \frac{q^2\left(1 - \frac{s}{\sqrt{r^2 + s^2}}\right)}{16\pi\varepsilon s^2} \qquad \text{Equation 1.11}$$

where s is the separation distance between charged and uncharged particles. This equation may be modified to describe the adhesion of a charged particle

to a flat earthed conducting surface via the formation of an image charge by making the assumption that $r \to \infty$:

$$F_{EL} = \frac{q^2}{16\pi\varepsilon s^2} \qquad \text{Equation 1.12}$$

Contact between two uncharged particles with different work functions may also result in the flow of electrons from the particle with the lower work function to the particle with the higher work function until an equilibrium is established (Tabor, 1976). This is known as contact electrification and the resultant force of attraction (F_w) can be described as:

$$F_w = \pi\varepsilon r \frac{(\Delta U)^2}{s} \qquad \text{Equation 1.13}$$

where r is the radius of the particles and ΔU is the potential difference arising from the difference in work functions.

Electrostatic forces are largely dependent on the electrical properties of the particles involved and the separation distance between them. Under normal environmental conditions, electrostatic forces are at least ten times smaller than van der Waals forces (Tabor, 1976). This leads to the dominance of the omni-present van der Waals forces, which is largely responsible for the strength of the adhesion, especially if the build-up of electrostatic charges can be mitigated (Johnson, 1996).

1.5.4 Mechanical Interlocking

The typical micronised drug particle has a microscopically rough surface topography, which may result in the interlocking of contacting asperities and may thus increase interparticulate interactions (Jayasing, Pilpel *et al.,* 1970; Adolfsson, Olsson *et al.,* 1997). If the roughness causes particle-particle contact to only occur over a small surface area, the interparticulate forces acting on this small area will produce an extremely high pressure (Fuller and Tabor, 1975). This may exceed the yield value of the material, resulting in increased mechanical interlocking and van der Waals forces.

1.6 Factors Affecting Interparticulate Forces

Previous sections have indicated a range of factors may influence the adhesion force between particles. The following section reviews, in more detail, the specific influence of the physical and interfacial chemical characteristics of particles on interparticulate forces.

1.6.1 Particle Size

The van der Waals, capillary and electrostatic forces (shown in section 1.4), describe how these forces are directly proportional to particle diameter, with gravitational forces being proportional to diameter cubed (d^3). These relationships suggest as particle size is reduced, the physical forces experienced by a particle become more and more significant when compared to the gravitational forces (Visser, 1995). Depending on a material density, for

particles smaller than approximately 10-20 µm, the physical forces dominate gravitational forces, which explain the cohesiveness and poor flowability of very fine powders.

1.6.2 Particle Shape

The way in which particle shape influences adhesion is very difficult to quantify and control on a macroscopic scale. The equations describing particle adhesion make the assumption that particles are spherical in shape and smooth, an assumption which hardly ever mirrors reality.

The short-range van der Waals and the long-range electrostatic forces both decrease as a function of the square of the separation distance between particles (Equations 1.3, 1.6, 1.7 and 1.10 to 1.12). Hence, an increase in separation distance between contacting particles would reduce particulate interaction. The range over which the latter exerts an influence on the van der Waals force is between 10-100 nm. Thus, any effect of particle shape on interparticulate distance may significantly influence particle interactive forces (Johnson, Kendall *et al.,* 1971). For instance, small, non-interlocking surface asperities which increase the separation distance between particles will reduce the force of adhesion upon contact (Johnson, Kendall *et al.,* 1971). When the asperities are of the order of 1 µm, the separation distance will be large, thereby limiting the van der Waals attractions to almost zero (Castellanos, 2005). Alternatively, smooth, flat elongated particles which pack as shown in Figure 1.2A will experience increased interparticulate adhesion due to their reduced separation distance and increased interparticulate contact area. The packing of such particles would also depends on their process history. In the

absence of significant compaction, they tend to be loosely packed together (Figure 1.2), giving rise to higher separation distance and reduced area of contact leading to a reduction in their adhesive interactions (Valverde, Ramos *et al.,* 1998).

Figure 1.2: Packing arrangements for flat elongated particle (Zeng, Martin et al. 2001): (A) Closely packed orientation, typically found after powder handling. (B) Loosely packed orientation

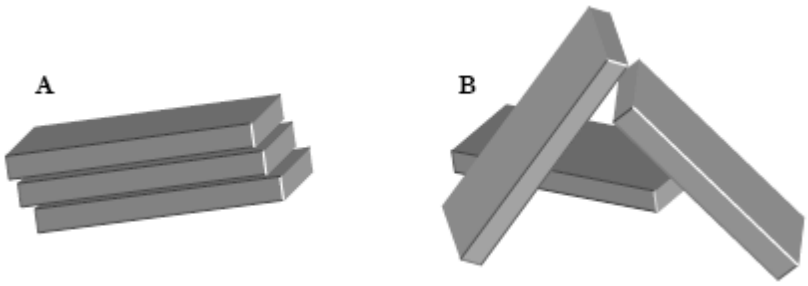

1.6.3 Surface Roughness of Particles

As with particle shape, surface roughness will directly influence contact geometry and interparticulate forces on a mesoscopic scale (Fuller and Tabor, 1975). Figure 1.3 shows how, if the roughness of a substrate is of a smaller scale than the adhering particle, the contact area between the particle and the surface will be decreased and the separation distance increased when compared to adhesion to a flat surface (Figure 1.3B), resulting in decreased interparticulate forces (Johnson, Kendall *et al.,* 1971; Fuller and Tabor, 1975; Johnson, 1996). When the roughness of substrate is on a larger scale than the adhering particle, the situation is reversed (Figure 1.3C). In addition, when

mechanical interlocking occurs between asperities, a signifcant increase in interparticulate forces can be generated.

Figure 1.3: The effects of roughness on particle-surface adhesion. (A) Surface roughness on a smaller scale the particle size. (B) A smooth surface. (C) Surface roughness on a larger scale than particle size

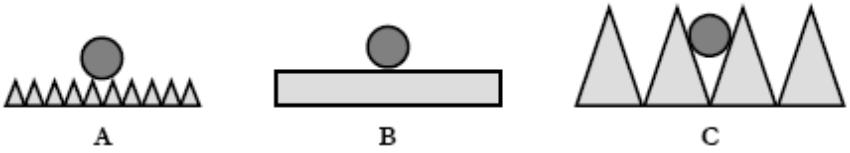

One must note that in most instances, particle adhesion in pharmaceutical powders occurs between two rough particles or a rough particle and a smooth surface, therefore the examples shown in Figure 1.3 tends to simplify the actual situation (Zeng, Martin *et al.,* 2001).

1.6.4 Particle Deformation

Local deformation of adhering particle surface may also influence interparticulate forces by decreasing particle-particle separation and increasing contact area, leading to a greater van der Waals force of interaction (Krishnan, Busnaina *et al.,* 1994). The extent of any deformation is dependent on the elastic/plastic properties of the particles, the pressure generated between two contacting asperities, the magnitude of the attractive forces and the magnitude and duration of any external forces applied to the particles (Johnson, 1996). For certain materials such as polymer-like materials, the duration of contact is

also important as deformation will increase with time resulting in increased adhesion, a phenomenon known as aging (Krupp, 1967).

1.6.5 Surface Free Energy

The surface free energy from a solid material is described as the energy required to produce a unit area of surface and is analogous to the surface tension of a liquid (Johnson, Kendall *et al.,* 1971). Unlike liquids, the molecules of a solid are not free to move, therefore, surface free energy is not uniform over a surface and depends on the history of the material (Johnson, 1998). The quantity of work required to separate two surfaces of two materials is called the work of adhesion (W_a) and is related to the surface free energy of the surfaces by the following equation:

$$W_a = A_s(\gamma^C + \gamma^D - \gamma^{CD}) \qquad \text{Equation 1.14}$$

where A_s is the area of surface produced by the separation, γ^C and γ^D are the free energies per unit surface area of solids C and D in air, respectively; and γ^{CD} is the free energy of the C-D interface per unit area. Therefore, the work of cohesion (W_c) (i.e. the work requires to separate two surfaces of the same material) is shown by:

$$W_c = 2A_s\gamma^C \qquad \text{Equation 1.15}$$

In addition to the physical contact geometry, interparticulate cohesion and adhesion will, in part, be determined by the surface free energies of the interacting particles and their work of adhesion (Johnson, Kendall *et al.,* 1971).

1.6.6 Environmental Factors (Relative Humidity)

There are two mechanisms by which relative humidity may affect interparticulate forces. Firstly, relative humidity increases particulate interaction via capillary forces when a sufficient amount of water is condensed on the surfaces of the interacting system (McFarlane and Tabor, 1950; Price, Young *et al.,* 2002). Secondly, the conductivity of both interactive particles will be increased and will accelerate the dissipation of electrostatic charges on the particles (Byron, Peart *et al.,* 1997). Hence, water at high relative humidity can condensate at the contact points between particles, resulting in the formation of the liquid bridges and the formation of a dominant capillary force (Price, Young *et al.,* 2002; Young, Price *et al.,* 2003).

1.7 Analytical Tools used in the investigation of interfacial properties via surface characterisation

The importance of interfacial chemistry on the performance of DPI formulations has led to the necessity of analytical tools that enable direct and/or indirect measurements of surface energetics and particle-particle interactions. A number of different techniques have previously been used to quantify particle-

particle or particle-surface adhesion in air, including centrifugal detachment, aerodynamic detachment, impact separation, vibration, and microbalance techniques. In addition to these techniques, a number of other tools have been recently investigated to determine the relationship between particle surface interfacial properties and dry powder inhaler (DPI) formulation performance, for example, centrifugal methods and colloid probe atomic force microscopy (AFM). The following section introduces some of these techniques and their application for investigating surface interfacial properties of pharmaceutical materials.

1.7.1 Centrifugal Methods

Centrifugal methods examine the forces between particles and flat surfaces. The equipment consists of a centrifuge, which has been modified by the introduction of specially manufactured adapters, in which disks of material, with particles added onto the top, can be placed. A typical centrifuge experiment begins with the disks being placed inside the adapters, with the particles placed facing the centre of the centrifuge rotor (Kulvanich and Stewart 1987). This allows a press-on force to be applied. Following this, the number of particles on the disk is counted and the disk is then placed in the centrifuge again, although this time the disk is facing outwards. The removal force is then applied (Podczeck and Newton, 1995). The detachment force (F_{det}) applied is directed through the centre of gravity of the particle, outwards from the centre of rotation (Kulvanich and Stewart 1987) and is described by equation 1.16:

$$F_{\mathrm{det}} = M_p.r.\omega^2 \qquad \text{Equation 1.16}$$

where M_p is the particle's mass, r is the distance from the axis of rotation to the particle and ω is the angular velocity (Booth and Newton, 1987). The centrifuge system has been used to study a number of different pharmaceutical systems. Lam and Newton (1993) used it to examine the effect of time on the press-on force of particles of PEG 4000 and Starch 1500 against a steel surface, whereas Podczeck, *et al.* (1997) used it to compare the effects of particle on compressed disk of material to particle-on-particle experiments. The centrifuge and impaction approaches to particle measurements have many advantages. They provide data regarding the bulk, integrated effects of physical and environmental variation of particle adhesion, are of low cost, and are simple and accessible. However, the main disadvantage is that due to the large-scale nature of the measurements, it provides limited information on individual particle interactions (Podczeck and Newton 1995).

1.7.2 Scanning Probe Microscopy

The ability to generate data regarding single particle events has been facilitated by the advent of the scanning probe microscope, particularly the introduction of the colloid probe atomic force microscope (AFM) technique (Ducker, *et al.,* 1991).

Scanning probe microscopy (SPM) is the name given to a range of techniques which involves the formation of images and acquisition of surface property data from a range of physical, optical and chemical interactions between a sharp proximal probe and a surface (Shao*, et al.* 1996; Vansteenkiste*, et al.* 1998). Scanning tunnelling microscopy (STM) was the first in a series of high-resolution SPM techniques (Hansma and Pietrasanta, 1998). STM relies on the use of an atomically fine tip that is brought into very close proximity to a conducting or semi-conducting surface (Yip, 2001). A bias potential is applied across the gap and a tunnelling current measured. The tip is then rastered over the surface to build a map showing the local density of states, commonly giving a topography image. Binnig and Rohrer received the Nobel Prize for Physics after inventing STM instrument in 1982, where they showed an atomically-resolved gold surface (Binnig*, et al.* 1986). A fundamental disadvantage with STM is the inability to image insulating specimens, such as biological materials and polymers. Atomic Force Microscopy (AFM) circumvented the need for conducting surfaces by measuring forces, rather than tunnelling currents, between the probe and the surface (Binnig*, et al.* 1986). AFM has quickly become a routine microscopy technique, offering many advantages, such as minimal sample preparation, the non-requirement for high-energy electron beams or high vacuum conditions.

1.7.2.1 Atomic Force Microscopy

In the AFM, a sharp, pyramidal tip mounted on a cantilever, which is brought into close contact to the surface where the intermolecular forces acting

between the tip and the surface cause the cantilever to bend (Yip 2001). Topographical images of the surface are obtained by recording the cantilever deflections, as detected by a laser beam focused on the top of the cantilever tip, as the sample is scanned beneath. The AFM can be operated in air or liquid environment, which has been made possible by the development of AFM wet cells (Traini*, et al.* 2005). The AFM has three main parts: cantilever, scanner and optical deflection system consisting of a laser diode and photodetector (Figure 1.4).

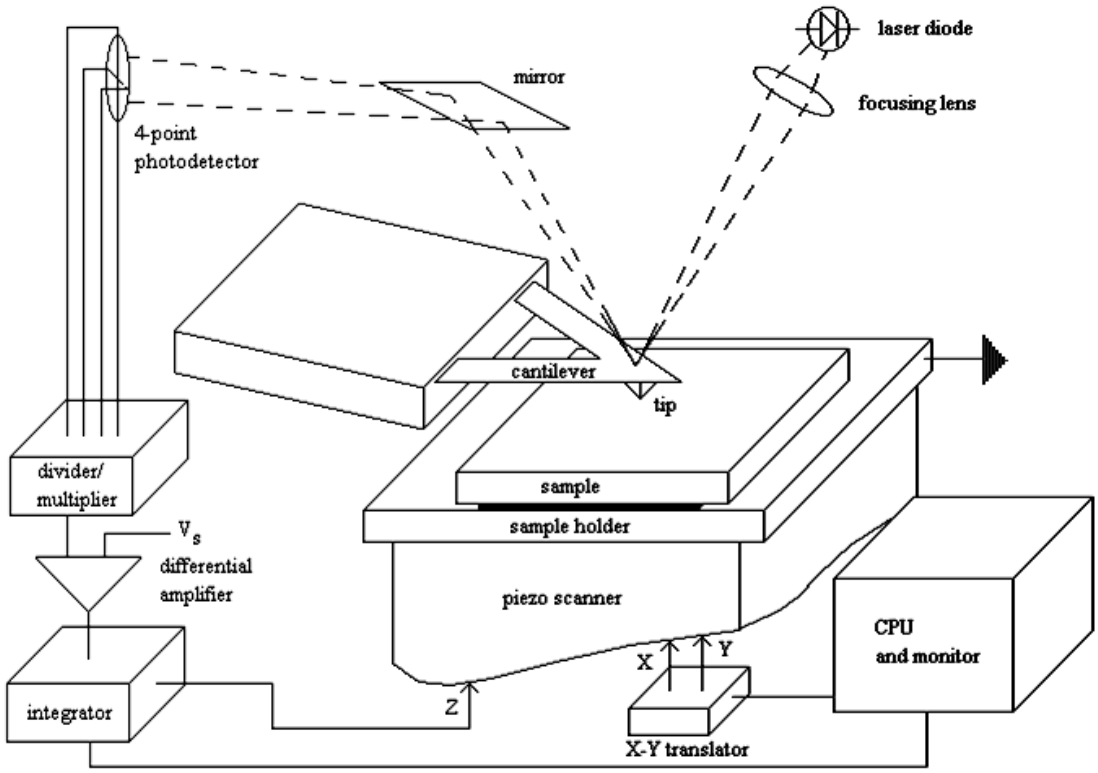

Figure 1.4 Schematic Diagram of an Atomic Force Microscope

The cantilever is microfabricated from silicon nitride (sometimes silicon, for stiffer levels) with typical dimensions that are 100 – 300 μm in length, 10 – 30 μm in width and 0.5 – 3 μm in thickness (Figure 1.5).

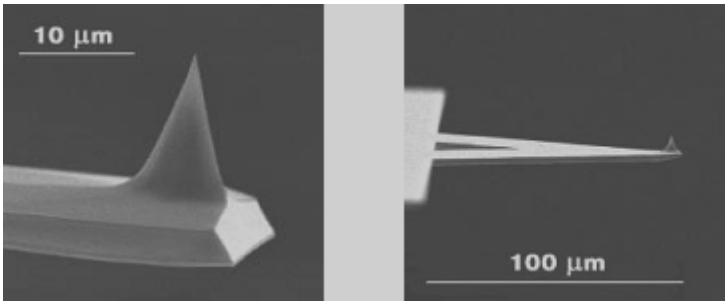

Figure 1.5 Dimensions of the Tip and Cantilever of an Atomic Force Microscope

Very small deflections of the cantilever are amplified by a laser beam that reflects off the end of the cantilever onto the photodetector, which senses the changes in the position of the laser beam (Yip 2001). A four-quadrant photodetector gives the opportunity to measure both normal bending and torsion of the cantilever, corresponding to normal and lateral forces (Young*, et al.* 2003).

The sample is mounted *via* a sample holder on to the AFM scanner, which consist of piezoelectric ceramics that move the sample relative to the cantilever in three dimensions (*x*, *y* and *z* directions). In the contact mode of operation, the tip and sample are placed in contact and the tip is rastered across the surface resulting in a topographical image of the surface. The scanning is done under feedback control where the sample is moved towards or away from the cantilever during the scan to maintain constant force on the

sample surface. Hence, the scanner retracts if the tip moves over a high feature or towards the cantilever over low features. This up and down motion of the sample is therefore a record of the sample topography (Hansma and Pietrasanta 1998).

1.7.2.2 Colloid Probe Atomic Force Microscopy

Soon after the invention of the AFM, the colloid probe technique was developed for mapping the interaction forces of colloid probes in air and liquid environments (Ducker*, et al.* 1991). Data from the force-distance curves generated have been utilised to study interfacial particle interactions and to characterise material properties such as elasticity and the coefficient of friction.

The principle of the colloid probe technique is the same as standard AFM as outlined above, except that the sharp tip is replaced with a colloid probe attached to the end of a tipless cantilever. In force measurement mode, the sample is moved up and down, by applying a voltage to the piezoelectric translator, onto which the sample is mounted, while recording the cantilever deflection. The deflection of the cantilever is normally measured using the optical lever technique. A beam from a laser diode is focused onto the end of the cantilever and the position of the reflected beam is monitored by a position sensitive detector. The backside of the cantilever is usually covered with a thin gold layer to enhance its reflectivity.

Analysis of a typical force measurement consists of the following:

1. Initially, the probe and substrate have a large separation distance and there is no interaction, so no displacement of the cantilever is recorded.

2. As the substrate approaches the probe, the presence of long-range electrostatic forces can be evaluated. In the example shown, there is an electrostatic repulsion between the probe and substrate leading to the cantilever being deflected away from the surface.

3. As the separation between the probe and substrate decreases, the short-range, attractive van der Waals forces overcome the repulsion and the probe jumps into contact with the substrate.

4. The probe and substrate are pressed together with a pre-set compressive loading.

5. The substrate is subsequently withdrawn from the probe until they are pulled apart. The point at which this happens corresponds to the adhesive force and the area between the curve and the zero interaction level can be integrated to give the energy of adhesion.

The direct result of such a force measurement is the detector signal in volts, ΔV, versus the position of the piezo Δ_{zp}, normal to the surface. To obtain a force-versus-distance curve ΔV and Δ_{zp} are converted into force and distance.

To calculate the cantilever deflection from the detector signal, the corresponding conversion factor is needed, which can be obtained from a linear fit of the constant compliance region. The tip-sample separation is then obtained by adding the cantilever deflection to the piezo position.

The force acting on the cantilever, F, is obtained by Hooke's law, which relates the stiffness of the cantilever (k, the spring constant) and deflection of the cantilever (x):

$$F = -kx \qquad \text{Equation 1.17}$$

In order to make a quantitative measurement, it is necessary to know the spring constant of the cantilever, which can either be taken from the manufacturer's literature or, more accurately, determined for individual cantilevers using a variety of methods.

Force-distance curves can be generated singly, but in order to obtain a statistically relevant set of data in a single operation, force-volume mode can be employed. In this mode, the AFM raster scans the substrate under the colloidal probe to produce a series of force-distance curves, each from a well-defined interval in the *x* and *y* direction, and a low-resolution topographical image. These data can be processed to calculate the force of adhesion from each individual force curve, which can be displayed as a force map, showing variation in adhesion over the surface.

Given the importance of inter-particle adhesion to the performance of DPI formulations, it is not surprising that the colloidal probe technique has been

applied to this area of research (Louey*, et al.* 2001; Price*, et al.* 2002; Tsukada*, et al.* 2004; Hooton*, et al.* 2008). The naturally irregular morphology of the particles in DPI formulations, however, was found to produce great variability in the results of colloid probe adhesion measurements between formulation components, as it led to significant variation in the contact area between the colloidal probe and substrate, to which adhesion is directly proportional. As a result, the use of colloidal probe AFM in the study of inhalation formulations was largely qualitative. Recently, however, a number of techniques have been developed to overcome this limitation. One such technique employs a grid of extremely sharp spikes over which the colloidal probe is scanned, resulting in an image of its interacting region from which the morphology and the contact area can be calculated. It is then possible to normalise adhesion measurements by the contact area and so calculate the work of adhesion between the substrate and particle.

Another technique that to some extent, overcomes the limitation of contact area and which has been used to explain the behaviour of DPI systems is known as the cohesive-adhesive balance (CAB) procedure (Begat*, et al.* 2004a, b). This employs specially grown molecularly smooth crystals as substrates to ensure that the contact area between a given colloidal probe and various substrates is uniform and constant.

A number of colloidal probes of each material under investigation are prepared and the adhesive force between each probe and a crystalline substrate of each material under investigation is measured in force-volume mode. This data is used to produce a CAB graph, by plotting the mean force of cohesion for each

probe (the adhesive force between a probe and a substrate of the same material) against the mean force of adhesion between that probe and a substrate of another material. When data for a number of probes of the same material interacting with the same substrate are plotted on the same axes, a straight line is formed allowing linear regression analysis of these data. Although the contact area of each probe may vary significantly, the contact area of an individual probe is the same for both the cohesive and adhesive measurements and thus the ratio between cohesion and adhesion remains consistent between different probes. This ratio, known as the CAB ratio, can be measured from the analysis of the gradient of the CAB plot.

The CAB procedure is able to produce data that are independent of the contact area between the colloidal probe and substrate and which are, therefore, quantitative. The approach has been shown to predict the force balance and behaviour and possibly the *in vitro* performance of simple powder formulations of binary DPI systems.

1.8 Optimising Pharmaceutical Engineering of DPIs

The fundamentals of DPI formulation engineering is firstly the milling (air-jet micronisation) of large, primary crystalline drug particles to produce fine particles with a median geometric diameter of 1-5 μm (Telko and Hickey, 2005). Secondly, the blending of these particles with large carrier particles,

traditionally lactose monohydrate, to improve powder fluidisation (Dunbar, Morgan *et al.,* 2000). Due to the influential interparticulate cohesive and adhesive forces noted with fine drug particles and the large carrier particles, lung delivery efficiencies of just 10-30 % of the nominal dose are typically observed (Dunbar, Morgan *et al.,* 2000). This highlights the dependence of particle entrainment and drug deposition in the airways, on the balance of interfacial forces between components of DPI formulations (Jones, Harris *et al.,* 2008). Hence, the control and understanding of the interfacial properties of DPI formulations are critical in enabling the formation of DPI products with defined quality and functionality (Edge, Muller *et al.,* 2008).

The primary design concept in drug particle manufacturing is particle size, notwithstanding the common knowledge that surface properties will drastically alter DPI product performance. However, our limited understanding of the effects of processing on drug surface properties, has limited adequate control of product performance.

1.8.1 Micronisation and Mechanical Activation

To reduce the particle size of a primary drug crystal, a destructive, highly energetic processing techniques, such as air-jet micronisation, are commonly employed (Malcolmson and Embleton, 1998). During comminution, mechanical loading of the crystalline solid is known to cause distortion and disordering of the crystal lattice leading to structural and thermodynamic modifications of the processed material. The thermodynamically activated state of the micronised

material is commonly described as “mechanical activation” (Huttenrauch, Fricke *et al.,* 1985). A graphical illustration of the relationship between mechanical activation and the free energy state of a material during micronisation and its relaxation post processing is shown in Figure 1.6.

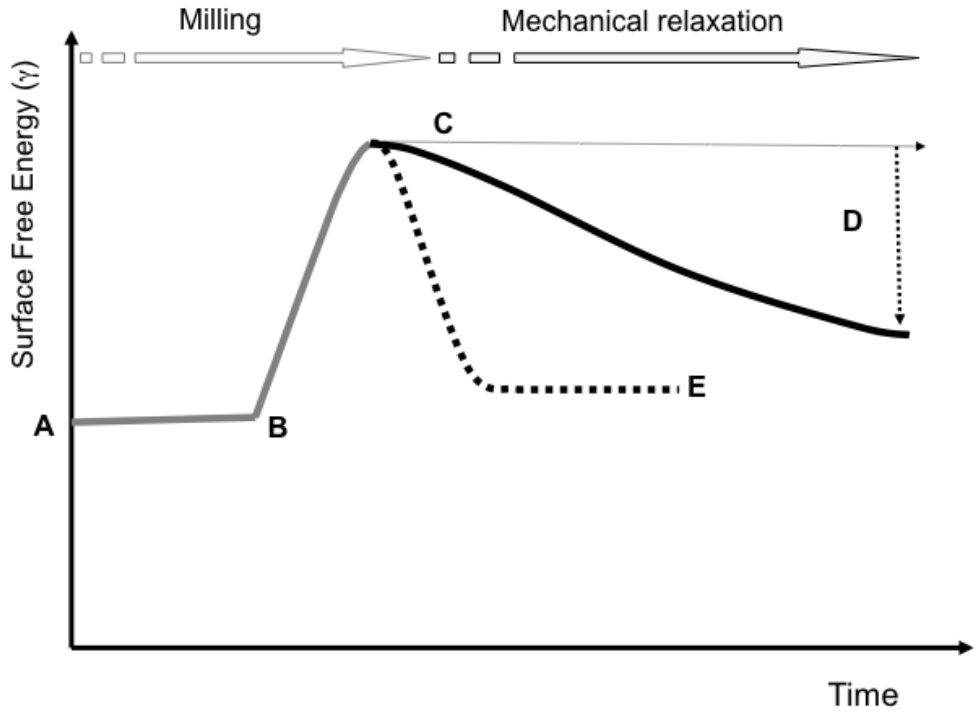

Figure 1.6 Schematic representation of the process of mechanical activation and relaxation process of micronised particles. A = Low surface free energy of crystalline unprocessed material, B = Brittle-ductile transition, at which point particle fragmentation is not probable, C = Mechanically activated stated, D = Relaxation behaviour of the mechanically activated material over time and E = Relaxation of the mechanically activated state by post-processing conditioning.

During micronisation the high degree of particle-particle collisions leads to significant crystal fracturing and particle size reduction. At a critical particle size, the material reaches its brittle-ductile transition (Figure 1.6B), at which

point the material becomes less likely to undergo fracture. At this transition, materials under mechanical loading will experience a dramatic increase in elastic strain energy as the tensile strength and boundary surface tension of the material are overcome. The loading may be sufficient to plasticise the material and the corresponding elastic strain energy within the crystalline lattice is stored in the form of structural defects, dislocations and surface amorphicity. It has been reported that lattice defects introduced upon mechanical activation is a surface led phenomena and penetrates into the lattice to depths of 10^{-6} to 10^{-8} m (Huttenrauch, Fricke *et al.,* 1985). The elastic energy that remains upon mechanical treatment is the source of excess enthalpy and Gibbs free energy. Structural changes directly influence the thermodynamic properties of a substance, for example, surface free energy, reactivity, conductivity and true density. Hence, the process of mechanical activation of micronised solids may directly influence the surface free energy of the material that will affect adhesion between the processed API and carrier particles, which in turn, will have a critical affect on DPI drug product quality and performance.

Since the mechanically activated system is thermodynamically unstable, the process is reversible, whereby there is an energy loss and energy output of the system. For mechanically activated solids, the reverse process is driven towards equilibrium but never reaches a state free of structural defects, leading to some residual activity. The rate of structural relaxation depends on

environmental conditions and material properties and is thought to range between a few milliseconds to several months. The kinetics of relaxation depends primarily on the structural nature of the material and environmental conditions (temperature and relative humidity), which may influence the degree of molecular mobility within the material. However, the relaxation of these structural modifications may never reach the initial low surface energy state of the crystalline material and thereby a residual activity will remain (Huttenrauch, Fricke *et al.,* 1985). The time dependant re-crystallisation of amorphous regions and relaxation of process induced defects may result in irreversible agglomeration (caking) of micronised materials, and thereby rendering the drug product unusable (Ahlneck and Zografi, 1990). During this process of relaxation the surface free energy of the material may also significantly change over-time as indicated in Figure 1.6D. This may have a corresponding effect on particle adhesion, which will affect the surface interfacial force balance within a DPI formulation and therefore, product performance. Hence, active ingredient processing conditions must be controlled to produce materials that have suitable physicochemical and surface energetic properties. However, as there are many difficulties associated with controlling micronisation processing of materials, this can result in variations in the surface properties of equivalent drug batches and therefore adhesion, which can lead to significant batch-to-batch variability in drug product performance (Feeley, York *et al.,* 1998).

1.8.2 Environmental Laagering

One of the methods employed to improve the physicochemical stability of micronised API and, hence, reduce or eliminate batch to batch variability, is

the introduction of a post-micronisation conditioning step (Trofast, Trofast *et al.,* 1992; Pfeiffer-Brodka, Haeusler *et al.,* 2003). During this process, the structural relaxation of a material is expedited under conditions that are controlled with respect to relative humidity and temperature (Pfeiffer-Brodka, Haeusler *et al.,* 2003). Furthermore, the conditioning of hydrophobic materials using organic vapours such as ethanol have also been investigated (Trofast, Trofast *et al.,* 1992; Jones, Young *et al.,* 2008). Since the activated state of the micronised material is thermodynamically unstable (Huttenrauch, Fricke *et al.,* 1985), accelerated conditioning aims at dissipating much of the stored mechanical energy, induce re-crystallisation of amorphous domains in reducing the free energy of the material, as indicated in Figure 1.6. Previous studies have shown that conditioning of micronised drug actives results in significant reduction in surface amorphous content, allowing greater control of batch-to-batch variations of material physicochemical properties (Pfeiffer-Brodka, Haeusler *et al.,* 2003). The importance of post-micronisation conditioning within the industry is indicated through the registration of a number of patents documenting the use of several conditioning steps involving humidity and temperature (Morton, Shott *et al.,* 2008; Jakupovic and Trofast, 1998; Brodka-Pfeiffer, Grass *et al.,* 2004; Trofast, 2000).

1.8.3 In-situ conditioning with supercritical fluid technologies and HFA

The requirement for consistent and reliable manufacture of drug compounds with controlled and stable physical properties has driven the advance of supercritical fluid (SCF) technology to make giant leaps over the past decade

(Muhammad *et al.,* 2010; Pathak, Meziani *et al.,* 2005). A widely published use of SCFs in the manufacture of particles for inhalation via the solution enhanced dispersion by supercritical fluids (York, Hanna *et al.,* 1998). This process uses CO_2 to extract the solvent within which the drug crystals are dissolved, using temperature and pressure to control the properties of the drug particles (York, Hanna *et al.,* 1998). The use of similar technologies have shown the potential of controlled key particle parameters such as particle size, shape and morphology, rendering the application desirable for use in pulmonary delivery (Muhammad *et al.,* 2010). Whilst the use of CO_2 as a SCF in the manufacture or particles intended for delivery to the lungs consistently yields particles with desirable properties, the delivery of particles to the lungs once formulated have generally shown an inferior efficiency to other more traditional manufacturing processes (Vervaet and Byron, 1999).

In recent years, the use of 1,1,1,2-tetrafluoroethane (HFA 134a) has been investigated as a replacement for CO_2 in organic chemistry. It has been shown to be effective as a reaction medium for a variety of reaction mechanisms (Tallon and Catchpole, 2008). HFA is a gas at atmospheric pressure with a boiling point of -26.3°C and a molecular formula of CH_2FCF_3. HFA is widely used as a liquefied propellant, including MDIs as discussed previously. It has a distinctively low interfacial tension value (Vervaet and Byron, 1999) giving HFA good dispersive properties.

1.9 Thesis Overview

Structural relaxation kinetics has been shown to be strongly dependent on environmental conditions (temperature and relative humidity), which may influence the degree of molecular mobility within the material, and the period of exposure to such conditions. The laagering or quarantine period required for materials to undergo structural relaxation may vary significantly from minutes, hours to months and appears to be highly dependent on their hydrophilic/hydrophobic nature. However, there remain lapses in published knowledge relating to the influence of processing history on the dynamics of particles' properties and their subsequent *in vitro* performance.

1.9.1 Aims of this Thesis

This study aims at enhancing the knowledge of how processing histories relate to critical drug surface properties including interfacial behavior. A number of studies will be undertaken to study trends in the post-micronisation behaviour of various drug compounds through physicochemical and interfacial properties, together with their corresponding *in vitro* performance. This study will also evaluate the potential of HFA as a post-micronisation process for *in situ* conditioning of a mechanically activated drug. The studies will seek to gain a better understanding of the dynamics through which micronised particles regain stable properties and will also assess the potential of stress conditions in accelerating the mechanical relaxation profile of a drug. This work aims at increasing the understanding in the relation between manufacturing cycle times and drug product critical quality attributes. The outcome of this work will

assist in the complex interaction between technical requirements driven by the nature of the active pharmaceutical ingredient and the needs of quality attributes specifically fine particle mass of the aerosolised dose to be within registered specification. This work will potentially allow for the shortening/removal of post-micronisation ‘waiting’ periods by introducing conditioning steps which expedite the stress relaxation of micronized drug ensuring the physicochemical properties leading to robust and stable critical quality attributes of the drug product.

1.9.2 Thesis Structure

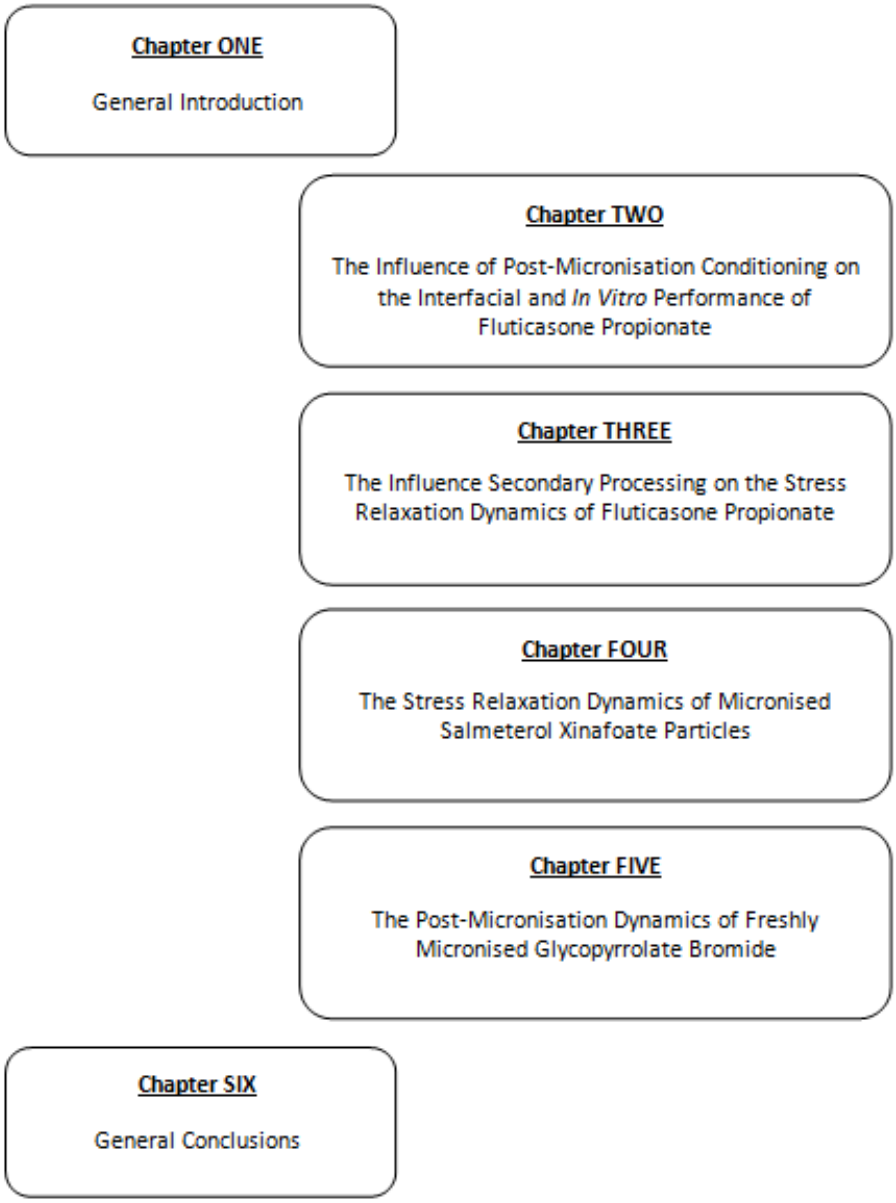

2 The Influence of Post-Micronisation Conditioning on the Interfacial Properties and the *In Vitro* Performance of Fluticasone Propionate

2.1 INTRODUCTION

Tailoring an active pharmaceutical ingredient (API) to respirable sized particles through jet-milling micronisation is a highly energetic, poorly controlled process (Malcolmson and Embleton, 1998). The lack of control throughout this process leads to energy levels exceeding the particle fracture energy threshold, hence inducing an increased Gibbs free energy to the drug surfaces, which may cause plastic deformation (Colombo, Grassi *et al.,* 2009). The altered chemical and physical properties of the newly created surfaces are highly unstable and require an undetermined period of stress relaxation during which surface properties can shift towards their more stable, lower energy, state (Florence and Salole, 1976; Sekiguchi, Shirotani *et al.,* 1980; Buckton, Choulorton *et al.,* 1988; Otsuka and Kaneniwa, 1990; Saleki-Gerhardt, Ahlneck *et al.,* 1994; Briggner, Buckton *et al.,* 1994). This process induced structural disorder (PISD) may directly influence the physicochemical properties of a substance, including surface free energy, reactivity, conductivity and true density. For respirable drug particles, mechanically activated particles directly influence the interfacial free energy, which may directly affect particle interactions between the processed API and carrier particles. This instability may translate into an unacceptable degree of variability in the drug/formulation stability and *in vitro* performance as interfacial forces are instrumental to the aerosolisation of

powders (Frijlink and de Boer, 2004; Ganderton and Kassem, 1992). One of the approaches utilised to circumvent this problem is the introduction of post-micronisation conditioning (Trofast *et al.,* 1992; Brodka-Pfeiffer, Haeusler *et al.,* 2003). During this conditioning step, the rate of structural relaxation is critically dependant on the relative humidity and temperature during laagering (Brodka-Pfeiffer, Haeusler *et al.,* 2003). This process aims to dissipate the stored structural elastic strain energy and thereby aid relaxation of the micronised material. Accelerated stability conditions (temperature and relative humidity) have also been shown to expedite the dissipation of much of the stored mechanical energy and to stabilize particulate surfaces upon secondary processing (Liu, Rigsbee *et al.,* 2002). Studies have shown that conditioning of micronised drug actives results in significant reduction in surface amorphous content, allowing greater control of batch-to-batch variations of material physicochemical properties (Brodka-Pfeiffer, Haeusler *et al.,* 2003). The importance of post-micronisation conditioning is evidenced in the registration of a number of patents documenting the use of several conditioning steps involving humidity and temperature (Morton, Shott *et al.,* 2008; Jakupovic and Trofast, 1998; Brodka-Pfeiffer, Grass *et al.,* 2004; Trofast, 2000).

Fluticasone propionate (FP) has an extremely low aqueous solubility (>100ng mL^{-1}) (Davies and Feddah, 2003) due to its hydrophobic molecular nature (Magee, French *et al.,* 2003). The hydrophobic nature of FP may hinder the re-crystallisation of amorphous regions created upon micronisation. The aims of this study are therefore to study the dynamics by which FP undergoes stress relaxation as a function of elevated temperature and humidity. This study

investigates the changes in the cohesion and adhesion balance (CAB) of micronised FP particles and the impact that the new interfacial chemistry has on the *in vitro* performance. This work also assesses the use of a liquefied propellant, hydrofluoroalkane-134a (HFA), as a novel method of *in situ* post-micronisation conditioning by suspending the drug particles in HFA in an attempt to expedite the stress relaxation for micronised FP particles.

2.2 MATERIALS AND METHODS

2.2.1 MATERIALS

Freshly micronised FP (FP) was supplied by Chemagis (Bnei Brak, India). FP is a synthetic corticosteroid. It is chemically described as S-(fluoromethyl)6a,9-difluoro-11b,17-dihydroxy-16a-methyl-3-oxoandrosta-1,4-diene-17b-carbothioate,17-Propionate. FP has a molecular mass of 500.57 and a molecular formula of $C_{25}H_{31}F_3O_5S$. A milled grade of lactose, ML001, was used throughout this study, supplied by DFE Pharma (Vehgel, Netherlands). All solvents used were of HPLC grade (Fisher Chemicals, Loughborough, UK). Ultra pure water was produced by reverse osmosis (MilliQ, Millipore, Molsheim, France).

Hydrofluoroalkane 134a (HFA 134a) is an inert gas with a chemical name of 1,1,1,2-Tetrafluoroethane. It has a molecular mass of 102.03 and a molecular formula of CH_2FCF_3. HFA 134a is a non-polar propellant widely used in aerosol products. HFA 134a was purchased from Mexichem, Cheshire, UK (Batch number 003215).

2.2.2 METHODS

An initial 2 gram aliquot was taken from the freshly micronised FP for full physicochemical characterisation, formulation and testing for *in vitro* performance. In parallel to this, the remaining micronised FP was split into two *ex situ* post-micronisation conditioning arms. In one arm, the micronised FP was conditioned at a relative humidity of 75 % relative humidity and a temperature of 40°C. At day 7 and 14, drug aliquots of 2 grams each, referred to hereunder as HT7 and HT14 were removed for characterisation, formulation and testing. In another conditioning arm, FP was conditioned at 60°C and ambient relative humidity (33 %). After 48 and 72 hours, 2 gram drug samples, referred to as T48 and T72 were once again taken for characterisation, formulation and testing.

In situ conditioning of the freshly micronised FP was conducted in parallel by placing 3 grams of FP in 90 grams of HFA 134a (Mexichem Fluor, Cheshire, UK). The HFA was controllably filled into a pressurised vessel and kept under pressure for 7 days. The vessel was subsequently de-pressurised at a rate of 0.1 bar per minute. The HFA conditioned FP was dried in controlled ambient conditions (25°C, 33 % RH) for 12 hours. All FP samples were sieved through a 500 µm mesh sieve prior to use. The study protocol for this study is tabulated in table 2.1.

Table 2.1 Summary of FP samples and formulations studied throughout this work

Conditioning Environment	Conditioning Period	Sample Reference	Formulations
Freshly Micronised	Day 0	Initial	FP Binary FP/SX Combination
40˚C/75 % RH	7 Days	HT7	FP Binary & FP/SX
	14 Days	HT14	FP Binary & FP/SX
60˚C, 44 % RH	48 Hours	T48	FP Binary & FP/SX
	72 Hours	T72	FP Binary & FP/SX
HFA	7 Days	HFA	FP Binary & FP/SX

2.2.2.1 Particle Size Analysis of FP

Particle size distributions of all FP samples were measured in the wet state using a Sympatec HELOS and CUVETTE (Sympatec GmbH, Clausthal-Zellerfeld, Germany) laser diffraction system using an R3 lens (0.5-175 µm). Approximately 10 mg of FP was suspended in HPLC grade cyclohexane containing 0.5 % w/v lecithin (Acros Organics, Geel, Belgium) and sonicated for 5 minutes and immediately transferred into a 50 mL cuvette to produce an appropriate optical concentration (8-12 %). Each measurement was performed in triplicate and particle size analysis was performed using WINDOX 5.0 software (Sympatec GmbH, Clausthal-Zellerfeld, Germany).

2.2.2.2 Scanning Electron Microscopy of FP samples

Particle morphology of all FP samples was investigated using scanning electron microscopy (SEM). Sample aliquots were fixed onto sticky carbon tabs (Agar Scientific, Cambridge, UK) followed by removal of excess powder using pressurised air. Samples were subsequently sputter coated with gold (Edwards Sputter Coater S150B, Edwards High Vacuum, Sussex, UK) to achieve a thickness of approximately 20 nm. Imaging was performed using a scanning electron microscope (JEOL JSM6480LV, Tokyo, Japan) using 15 kV accelerating voltage.

2.2.2.3 X-ray powder diffraction (XRPD) analysis of FP samples

The X-ray powder diffraction (XRPD) patterns of FP samples were analysed on a Bruker Powder Diffractometer (D8; Bruker AXS Inc., Madison, USA) using CuKα radiation (λ=1.54 Å). The data were collected over a single 2θ sweep with range 2θ = 5 - 30° and a step size of 0.025°/step with a step time of 1.5 s.

2.2.2.4 Differential Scanning Calorimetry of FP samples

The thermal properties of all samples were investigated using a differential scanning calorimeter (DSC 2920, TA Instruments, Surrey, UK), calibrated with an indium standard. Approximately 3 mg of sample were accurately weighted into an aluminium pan and crimped with a lid to form a hermetic seal. The sample and reference pan were heated at a rate of 10°C/min from 30°C to

350°C. The calorimeter head was continuously flushed with dry nitrogen gas at 0.2 L/min during all measurements.

2.2.2.5 Methodology of the CAB approach to colloid probe AFM

2.2.2.5.1 Crystallisation of substrates

To perform quantitative binary and combination AFM-CAB analysis of secondary processed FP samples, smooth single crystal surfaces of FP, salmeterol xinafoate (SX) and lactose monohydrate were produced. Briefly, saturated solutions of FP in 2 ml of acetone were prepared and sonicated prior to filtration via a 0.22-µm PTFE membrane filter (Whatman Inc., Clifton, NJ, USA). FP was crystallised using water as the anti-solvent. Briefly, a microscope cover slip (12 mm x 12 mm) was supported on a vertical post in a crystallisation dish that contained the anti-solvent. A droplet of the saturated solution of the API was then placed on the coverslip using a syringe attached to the 0.22-µm-membrane filter. The system was sealed by inverting a glass lid in the crystallisation dish to allow vapour phases of the miscible solvents to come into equilibrium resulting in heterogeneous nucleation and crystal growth within the droplet. The glass cover slip was then attached to a magnetic AFM stub.

Lactose and SX were crystallized upon introduction of saturated droplets between two glass cover slips. Smooth lactose crystals were generated upon preparing a solution of lactose (1 gm^{-1}) in double-distilled water, which was heated to 100 °C with constant stirring. The heated saturated droplet of the

solution was filtered through a 0.2 µm PTFE membrane filter (Whatman Inc., Clifton, NJ, USA) and placed on to the centre of a clean cover slip, which was then sandwiched by placing another cover slip over the droplet. Similarly, a solution of SX (0.75 gm^{-1}) was prepared in methanol following sonication for 30 mins, following which the solution was filtered through a 0.2 µm PTFE membrane filter and a droplet of this solution was then sandwiched between two coverslips. The resulting crystals of lactose or SX were then isolated upon cleaving the coverslips apart and attaching each coverslip to a magnetic AFM stub.

2.2.2.5.2 Colloidal probe force measurements

Prior to colloidal force measurements, individual particles from each sample of FP were attached onto standard V-shaped tipless cantilevers with pre-defined spring constants (DNP-020, DI, CA, USA) using an epoxy resin glue (Araldite, Cambridge, UK). Five probes were prepared for the as received, LH, HH and HT conditioned FP samples at each pre-defined laagering stage. All probes were examined with an optical microscope (magnification 50x) to ensure the integrity of the attached particle, before allowing the thin layer of glue to cure and dry.

Single crystal substrates were loaded onto an AFM scanner stage, which was enclosed in a custom-built environmental chamber, in which the ambient conditions were maintained at a constant temperature of 25 °C (± 1.5 °C) and relative humidity of 35 % RH (± 3 %). The interaction forces were measured by recording the deflection of the AFM cantilever as a function of the substrate displacement (z) by applying Hooke's Law. Individual force curves (n = 1024)

were conducted over a 10 µm x 10 µm area at a scan rate of 4 Hz and a compressive load of 40 nN.

A custom-built software was developed to extract data contained within each force-volume dataset. These data was analyzed to ensure normal distribution, indicating uniform contact area between the drug probe and the smooth substrate surfaces. Arithmetic mean and standard deviation were measured to produce CAB plots for the interactions of the different batches of FP with both lactose monohydrate and SX.

2.2.2.6 Preparation of powder formulations

Binary formulation blends (1.0 % $^{w}/_{w}$) were manufactured using the initial FP aliquot and each of the conditioned FP samples (HT7, HT14, T48 and T72). These blends were manufactured by the sequential addition of the drug to the milled lactose (ML001) followed by low shear blending using a T2F Turbula® mixer (Wily A Bachofen AG, Basel, Switzerland) for 45 minutes at 46 rpm.

Combination formulations containing FP (1.0 % $^{w}/_{w}$) and SX (0.2 % $^{w}/_{w}$) (Merck Generics, Potters Bar, UK) were also manufactured using the same method for each of the FP samples; Initial, HT7, HT14, T48 and T72.

A fill weight of 25 ± 1 mg of each blend was loaded into size 3 hydroxypropylmethyl cellulose (HPMC, Shionogi Qualicaps, Madrid, Spain) capsules. The loaded dose for the FP binary formulations was 250µg of FP per 25 mg fill weight. For the FP SX combination formulations, the loaded doses were 250 µg of FP and 50 µg of SX per 25 mg fill weight. The capsules were

stored at 44 % RH for 24 hours prior to in vitro testing to ensure the dissipation of any electrostatic charges introduced during processing.

2.2.2.7 In vitro aerosolisation studies

In vitro testing was performed using a Next Generation Impactor (NGI, Copley Scientific, Nottingham, UK) with a pre-separator, connected to two vacuum pumps to create sonic flow (GE Motors). The pre-separator contained 15 ml of mobile phase. The NGI cups were coated with 1 % $^{v}/_{v}$ silicone oil in hexane to eliminate any particle bounce. For each experiment, two individual 25 mg capsules of the same blend were discharged into the NGI at 55 L/min for 4.4 s, equivalent to a total volume of 4 L, from a Rotahaler® DPI device (Cipla, Mumbai, India). Before each test, the flow rate was verified with a flow meter (DFM 2000, Copley Scientific, Nottingham, UK). The amount of API deposited on each part of the NGI was determined by high pressure liquid chromatography (HPLC). This testing protocol was repeated three times for each blend, following which, the mass median aerodynamic diameter (MMAD) geometric standard deviation (GSD), fine particle dose less than 5.0 μm (FPD) and fine particle fraction (FPF) were determined.

2.2.2.8 HPLC analysis of FP and SX

The drug content was detected and quantified using HPLC. For the determination of drug content in FP binary formulations, the HPLC method consisted of a pump coupled to an auto-sampler and multi-wavelength UV detector (Agilent 1200, Wokingham, UK) set at 235 nm. The pump flow rate

was set to 1.5 mL/min through a Hypersil ODS-C_{18} column (Fisher Scientific, Loughborough, UK, column length 250 mm, internal diameter 4.6 mm, and particle size of the packing material 5 μm), which was placed in a column oven (Agilent, Wokingham, UK) set to 40°C. The mobile phase consisted of methanol, acetonitrile and water (45:35:20 % $^{v}/_{v}$). The elution time for the FP peak using this method was 3.4 minutes. For the drug content determination of FP SX combination formulations, the HPLC method used a flow rate of 1.0 mL/min through a Hypersil BDS-C_{18} column (Fisher Scientific, Loughborough, UK, column length 250 mm, internal diameter 4.0 mm, and particle size of the packing material 5 μm) placed in a column oven set at 40°C. The mobile phase consisted of 75:25 % $^{v}/_{v}$ methanol:0.6 % aqueous ammonium acetate.

For both methods, linear regression analysis was used for the assessment of the HPLC calibration. Quantification was carried out by an external standard method, and linearity was verified between 0.05 and 50 μg/mL. The limit of detection was 0.02 μg/mL and 0.03 μg/mL for both FP and SX respectively.

2.2.2.9 Statistical analysis

Linear regression analysis was used for the assessment of HPLC calibration. Statistical analysis between different populations carried out using one-way analysis of variance. Comparison of the mean values was performed by Tukey's multiple comparison. All statistical analyses were performed using GraphPad Prism software (GraphPad Software Inc, California, USA). Error bars in graphical representations of data show ± standard deviation (s.d.) in all

cases.

2.3 RESULTS AND DISCUSSION

In order to investigate the influence of post-micronisation conditioning on the dynamics of the mechanical stress relaxation of micronised FP, conditioned samples were analysed for physicochemical changes. Measurements of the functional influence of conditioning on the surface interfacial properties of conditioned FP samples with both lactose and SX substrate surfaces were recorded by colloidal probe CAB-AFM. The *in vitro* performance of formulations manufactured using the different FP samples was studied in relation to the CAB values.

2.3.1 Physicochemical characterisation for FP sample

The XRPD profiles for the initial, HT14 and T72 FP samples are shown in Figure 2.1. The comparison of these patterns shows the presence of distinct peaks throughout the diffractograms, suggesting that all FP samples were of the same polymorphic form. This suggests that the polymorphic form for FP samples is not affected by the post-micronisation conditioning used within this study.

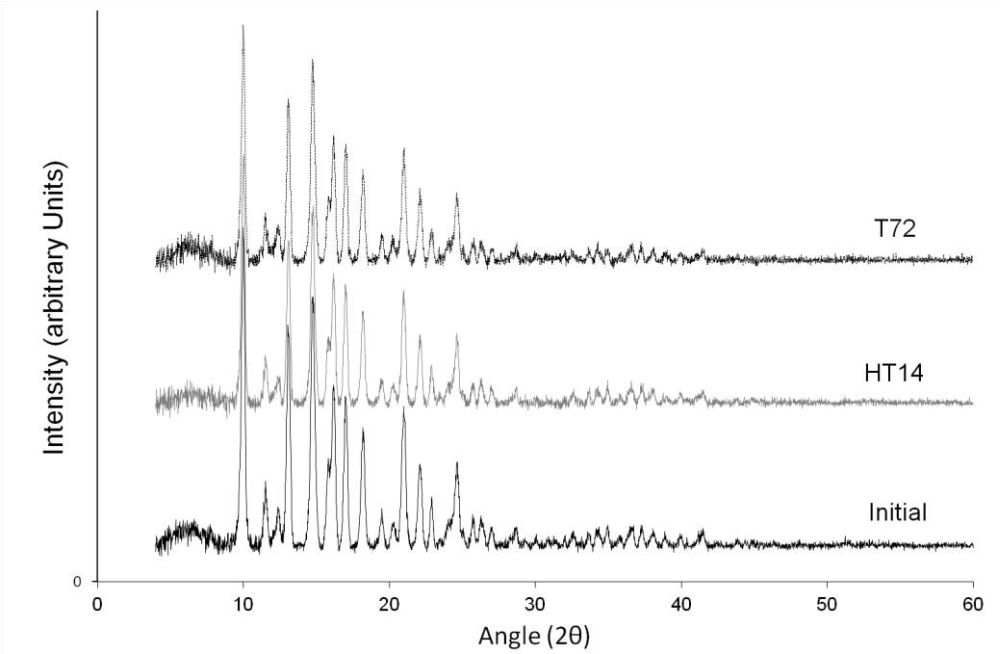

Figure 2.1 X-ray powder diffraction profiles for the Initial, HT14 and T72 FP samples

Representative DSC thermographs of the initial, HT14 and T72 FP, shown in Figure 2.2, also suggested the insensitivity of polymorphic form to conditioning. Thermal analysis of all conditioned samples (intermediate time points data not shown) indicated that all samples had an onset of melt at approximately 295 °C, which was related to the melting of polymorphic form I of FP (Pitchayajittipong, Shur et al.). The initial FP sample does exhibits an exothermic response in a region preceding the melting phase, which may suggest the presence of amorphous content in the FP sample. This response is visibly reduced in the HT14 and T72 samples, suggesting that both *ex situ* post-micronisation conditioning may reduce the amorphous content present in the FP sample to some degree.

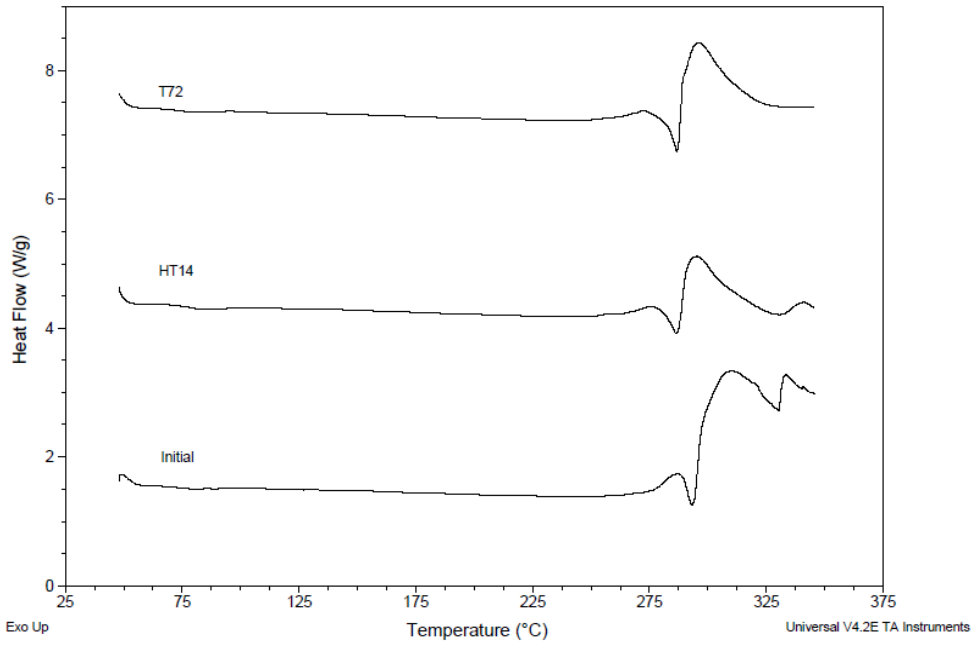

Figure 2.2 Differential Scanning Calorimetry thermographs for the Initial, HT14 and T72 FP samples

Particle size distribution analyses of all the FP samples handled throughout this study are tabulated in Table 2.2. The d_{10}, d_{50} and d_{90} values show a high degree of physical stability upon post-micronisation conditioning. All particle size results suggest suitability for DPI formulations (Frijlink and de Boer, 2004). Inspection of SEM images shown in Figure 2.3 confirms that all FP samples shared a common morphology with similar particle size distributions.

	d_{10} (µm)	d_{50} (µm)	d_{90} (µm)
Initial	0.74 ±0.02	1.79 ±0.03	3.67 ±0.01
T48	0.74 ±0.01	1.81 ±0.02	3.68 ±0.01
T72	0.73 ±0.03	1.81 ±0.01	3.66 ±0.02
HT7	0.74 ±0.01	1.79 ±0.01	3.64 ±0.02
HT14	0.73 ±0.02	1.77 ±0.03	3.61 ±0.02

Table 2.2 Particle Size Distribution data for the micronised and subsequently conditioned FP determined by laser diffraction

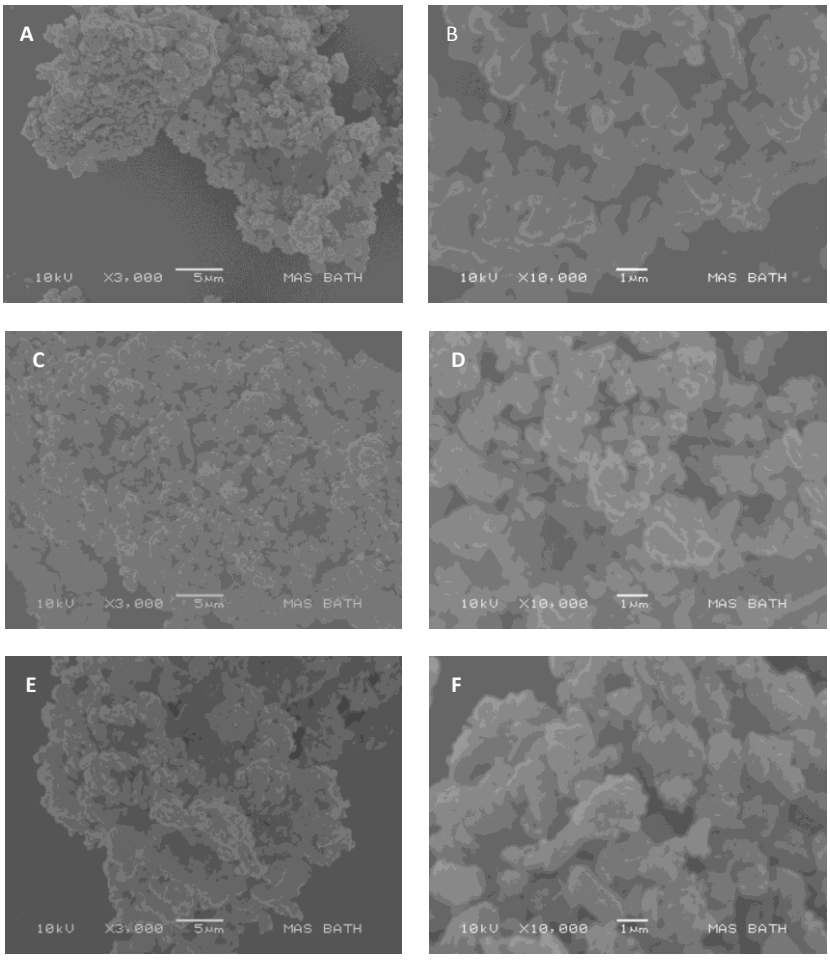

Figure 2.3 Scanning Electron Micrographs for the initial FP aliquot (A, B), for the H2 sample (C, D), and for the T2 sample (E, F)

2.3.2 Surface Interfacial Properties of FP Samples

Table 2.3 tabulates the influence that post-micronisation conditioning has on the surface interfacial chemistry of the FP samples. Figures 2.4 and 2.5 show the linear regression analysis of the CAB plots with respect to lactose and SX respectively. The CAB ratios were determined from the gradient of each plot.

The balance of the interaction forces between FP and lactose particles are described in Table 2.3 as the CAB values with respect to lactose. The initial FP sample shows a slightly cohesive nature, indicating a preference for the FP particles to adhere to themselves rather than to the lactose particles. The conditioning of this sample failed to impose highly significant shifts to the nature of its interfacial chemistry, however, an opposing trend emerged from the different conditioning environments. Whilst the post-micronisation conditioning of FP samples in an environment set at 40°C and 75 % RH showed no significant changes in terms of interfacial chemistry, conditioning at 60°C provoked a significant (p<0.05) trend towards a less cohesive behaviour of the FP particles. There was no significant difference after conditioning for 48 hours (T48), however the T72 sample exhibited a significantly less cohesive behaviour than all the other samples. Figure 2.4A and 2.4B show the CAB plots with respect to lactose for the HT(7, 14) and T(48, 72) FP samples. These figures show how besides the adhesive-driven trend described previously, the samples conditioned at 60°C seem to exhibit higher adhesive and cohesive forces.

The CAB values for FP particles with respect to SX (Table 2.3) show a higher sensitivity to conditioning. The initial FP sample exhibited a slightly adhesive

nature, suggesting that the FP particles are slightly more inclined to interact with the SX particles. Conditioning at 60°C magnified this adhesive nature by imposing a very significant (p<0.02) adhesive-driven trend. After 72 hours of conditioning the FP samples at 60°C, the possibilities of FP particles interacting with SX particles are 1.54 times higher than that of an FP-FP interaction occurring. The HT samples on the other hand demonstrate a slight cohesive-driven trend. Both HT7 and HT14 exhibit a predominantly cohesive behaviour. This significant (p<0.02) shift suggests that the FP particles were more likely to interact with themselves rather than with SX particles. The linear regression CAB plots (Figure 2.5A and 2.5B) with respect to SX for the conditioned FP particles illustrate the significantly (p<0.001) higher forces of adhesion for the T48 and T72 samples. Over a period of 72 hours, the forces of adhesion between the Initial and T72 FP samples have tripled. These drastic changes in adhesion forces are possibly due to surface changes to the FP particles which, in turn, influence the manner in which the FP particles interact with surrounding particles.

Table 2.3 Cohesive-Adhesive Balance (CAB) values with respect to Lactose and SX for all FP samples

		CAB w.r.t Lactose	CAB w.r.t SX
Freshly Micronised	Initial	1.18 ±0.02	0.95 ±0.02
60°C	T48	1.15 ±0.03	0.82 ±0.02
	T72	1.05 ±0.04	0.65 ±0.03
40°C / 75 % RH	HT7	1.21 ±0.02	1.05 ±0.01
	HT14	1.20 ±0.03	1.10 ±0.04

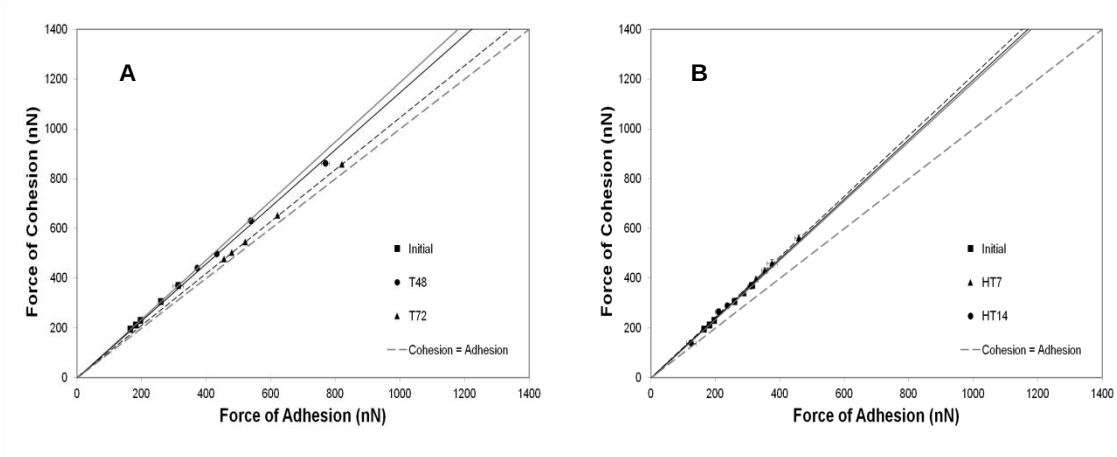

Figure 2.4 (A) Cohesive-Adhesive Balance (CAB) plot of initial, T48 and T72 FP samples with respect to lactose, (B) CAB plot of initial, HT7 and HT14 FP samples with respect to lactose

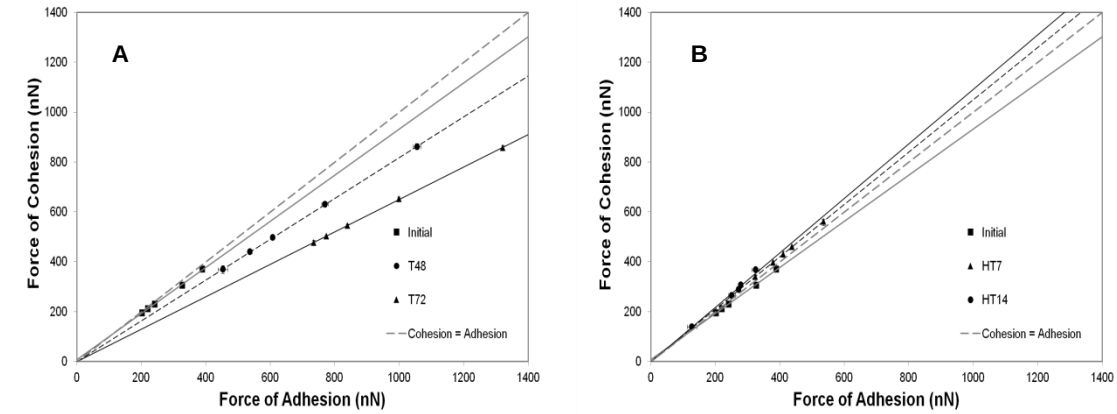

Figure 2.5 (A) Cohesive-Adhesive Balance (CAB) plot of initial, T48 and T72 FP samples with respect to SX, (B) CAB plot of initial, HT7 and HT14 FP samples with respect to SX

The sensitivity of the interfacial chemistry to post-micronisation conditioning is illustrated in Figure 2.6 both in terms of both FP-SX and FP-lactose

interactions. Whilst particulate interactions between FP and SX particles varies between a slightly cohesively-led system (1.10 ±0.04) and a highly dominant adhesive one (0.65 ±0.03), the interfacial chemistry describing the interactions between FP and lactose suggests a very low sensitivity towards conditioning. The lower sensitivity of FP-lactose interactions towards conditioning is probably due to the size difference between the particles in question. This suggests that surface chemistry changes to the FP particles materialise into functional changes more readily when present in a system containing particles of similar size.

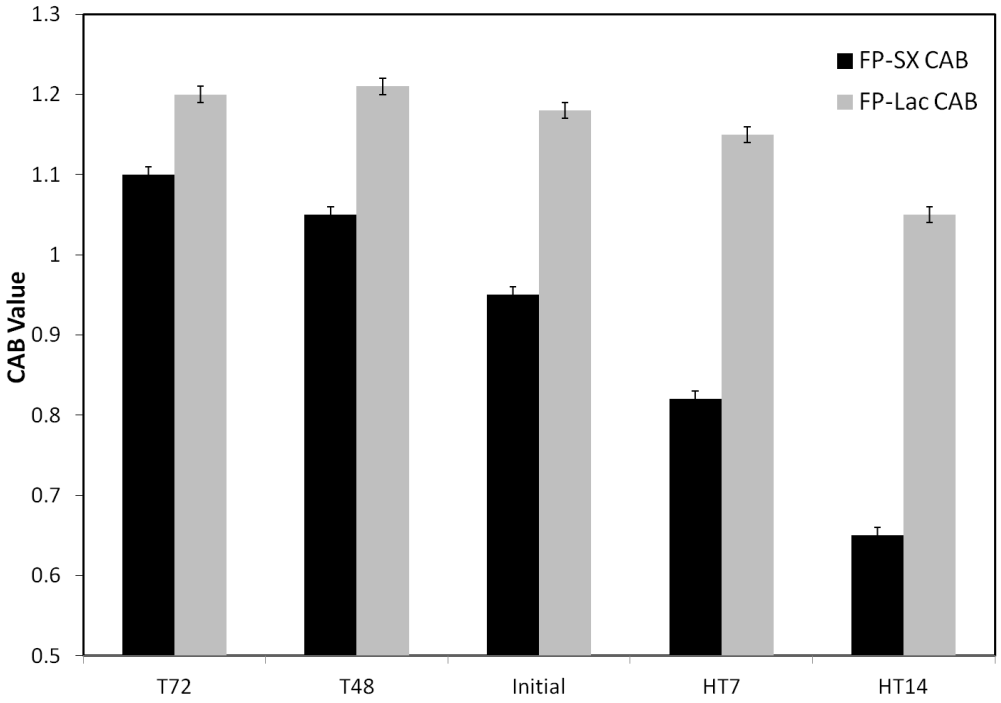

Figure 2.6 CAB values plotted against conditioning parameters T72 (72 hours at 60°C), T48 (48 hours at 60°C), Initial (freshly micronised), HT7 (7 days at 40°C/75 % RH), and HT14 (14 days at 40°C/75 % RH)

2.3.3 In vitro performance of FP samples in a binary formulation

The *in vitro* performance of the FP samples in a binary formulation is summarised in Table 2.4. There is a significant (p<0.02) and constant drop in the FPF for the T48 and T72 formulations. This dip in performance is consistent with the adhesive-driven trend seen in the CAB results for these samples with respect to lactose. The increasing affinity of the FP particles to adhere to the lactose carrier impedes the aerosolisation efficiency of the FP particles. The overall FPF increase in the HT formulation is statistically insignificant. However, qualitatively, these increases can be attributed to an increase in the cohesive nature of the FP particles, a cohesive-driven trend which although statistically insignificant, has been observed previously in CAB values.

	RD (µg)	ED (µg)	FPM (µg)	FPF (%RD)	MMAD (µm)	GSD (µm)
Initial	224.27 ±6.04	133.47 ±3.90	34.58 ±0.62	15.42 ±0.14	3.9 ±0.00	2.1 ±0.00
T48	230.18 ±12.99	147.2 ±17.69	30.56 ±1.09	13.28 ±0.12	4.43 ±0.06	2.1 ±0.00
T72	256.55 ±16.47	136.58 ±19.49	31.76 ±0.97	12.38 ±0.16	4.3 ±0.17	2.27 ±0.06
HT7	241.19 ±6.53	168.04 ±3.98	41.16 ±2.68	17.06 ±0.24	4.2 ±0.00	2.0 ±0.00
HT14	223.47 ±5.54	156.3 ±3.35	36.43 ±7.99	16.19 ±2.50	4.27 ±0.06	2.1 ±0.00

Table 2.4 *In vitro* aerosolisation performance for FP formulations produced using initial, T48, T72, HT7 and HT14 FP. Results are described by the recovered dose (RD), emitted dose (ED), fine particle mass (FPM), fine particle fraction (FPF) expressed as a percentage of the recovered dose, mass median aerodynamic diameter (MMAD) and geometric standard deviation (GSD)

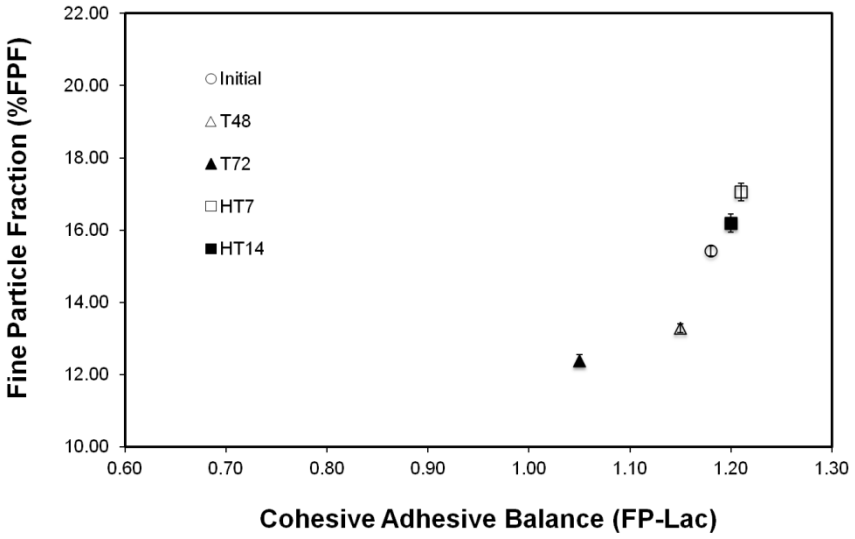

Figure 2.7 Fine Particle Fraction (FPF) of FP binary formulations expressed as a percentage of the Recovered Dose (RD) plotted against the CAB of FP particles with respect to lactose

Figure 2.7 illustrates the relationship between drug-carrier CAB ratios and the performance of the FP formulations. The opposite trends that the T and HT formulations follow have been discussed previously. What emerges from Figure 2.7 is that notwithstanding the significant (p<0.02) trend seen in the FPF of the FP formulations, the extent to which the *in vitro* performance of the FP relates to the changes in the forces of interactions between the FP particles and the carrier is limited. This clustered data set may suggest the presence of a buffer zone when the balance of cohesive and adhesive forces for FP and lactose is one that indicates a slightly cohesive nature.

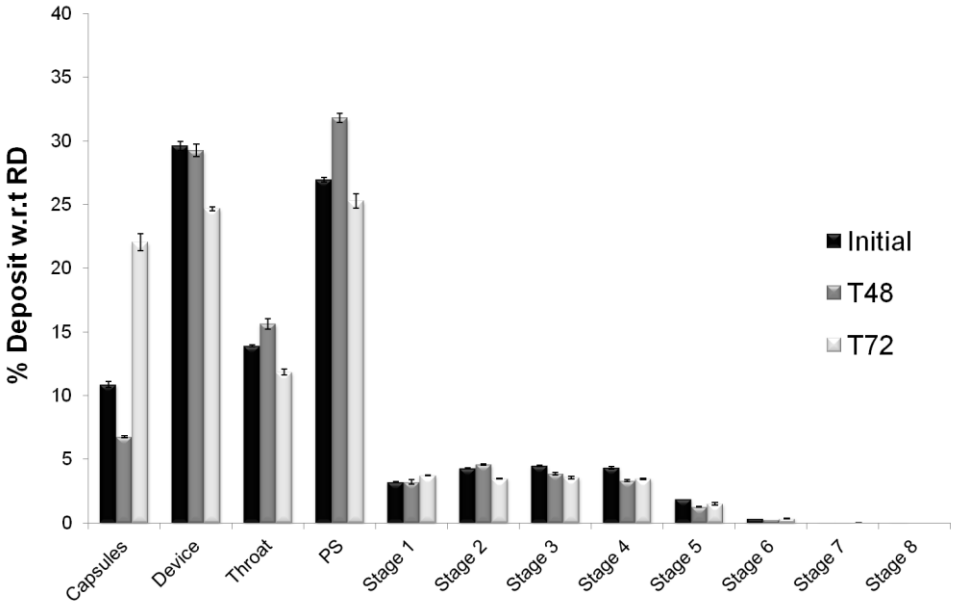

Figure 2.8 Stage by stage deposition profile expressed as the percentage of drug deposited per stage for FP in binary formulations; initial, T48 and T72

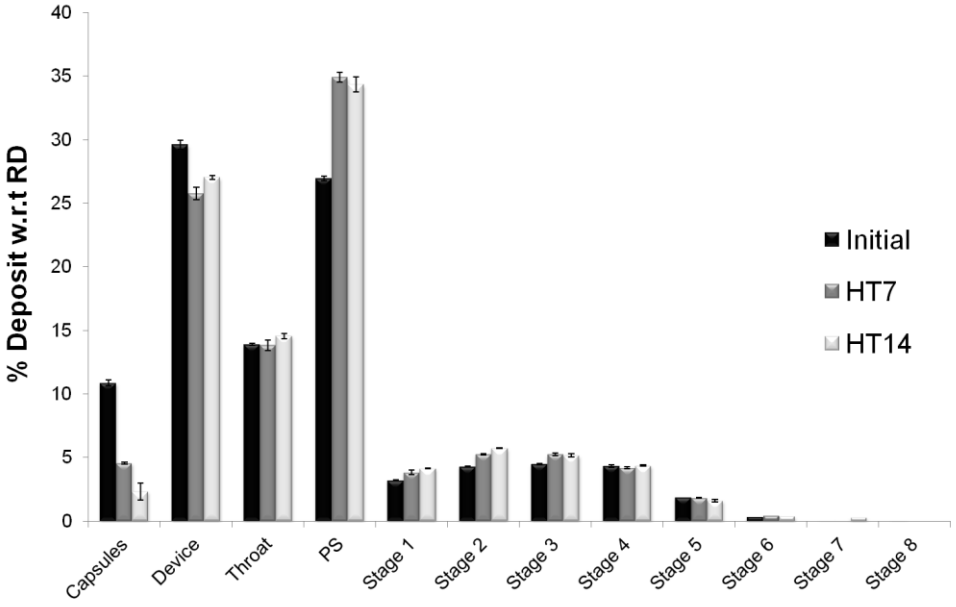

Figure 2.9 Stage by stage deposition profile expressed as the percentage of drug deposited per stage for FP in binary formulations; initial, HT7 and HT14

2.3.4 In vitro performance of FP samples in a combination formulation with SX

Table 2.5 tabulates the *in vitro* performance results for the FP samples in combination based formulations with SX. For all conditioning samples there is a significant (p<0.02) drop in FPF with respect to the Initial formulation. Furthermore, the significant (p<0.02) increase in MMAD values suggests that drug-drug agglomeration is taking place. The possible presence of these agglomerates together with the drop in the FPF for the formulations manufactured using conditioned FP samples could be interpreted in context of the balance between the cohesive and adhesive forces governing the interactions between the FP and SX particles.

	RD (µg)	ED (µg)	FPM (µg)	FPF (%RD)	MMAD (µm)	GSD (µm)
Initial	236.02 ±8.48	160.17 ±5.29	42.3 ±0.37	17.94 ±0.74	3.93 ±0.15	2.03 ±0.12
T48	276.11 ±16.14	192.14 ±5.84	41.98 ±0.76	15.2 ±0.23	4.5 ±0.10	2.17 ±0.06
T72	326.12 ±14.01	183.42 ±4.14	43.78 ±1.51	13.43 ±0.53	4.23 ±0.12	1.97 ±0.06
HT7	305.76 ±1.13	169.47 ±1.13	45.04 ±1.05	14.73 ±0.18	4.07 ±0.12	2.07 ±0.06
HT14	326.8 ±1.03	179.87 ±0.60	41.99 ±1.44	12.85 ±0.53	4.43 ±0.06	1.93 ±0.06

Table 2.5 *In vitro* aerosolisation performance for FP in combination formulations with SX produced using initial, T48, T72, HT7 and HT14 FP. Results are described by the recovered dose (RD), emitted dose (ED), fine particle mass (FPM), fine particle fraction (FPF) expressed as a percentage of the recovered dose, mass median aerodynamic diameter (MMAD) and geometric standard deviation (GSD)

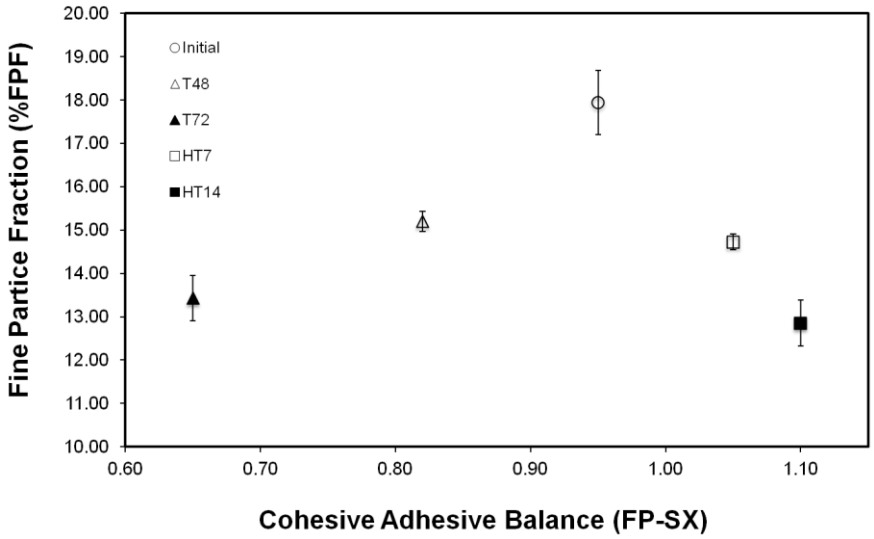

Figure 2.10 Fine Particle Fraction (FPF) of FP in combination formulation with SX expressed as a percentage of the Recovered Dose (RD) plotted against the CAB of FP particles with respect to SX

Figure 2.10 illustrates the correlation between the drop in FPF for FP and the CAB values for the conditioned FP particles and their corresponding formulations. The steady increase in the adhesive nature of the FP particles conditioned in an environment set at 60˚C points towards an increasing affinity between the FP and SX particles. This increase may lead to the formation of FP-SX agglomerates, resulting in drug agglomerates which are unable to gather the required inertial force to leave the capsule and device. This is evidenced by the significant (p<0.001) increase in the percentage of drug deposits seen for the T72 formulation on these very stages (figure 2.11). The HT FP particles on the other hand, exhibited a cohesive-driven trend in their interfacial chemistry, suggesting an increase in the FP-FP interactions over FP-SX. The shift, from an overall adhesive system to a system dominated by cohesive forces, suggested the presence of an increased amount of FP-FP

agglomerates. These agglomerates once again contributed to a drop in the FPF. This drop is evidenced in the significant increase of drug deposits in the capsule-holding device for both HT7 and HT14 formulations seen in the stage by stage analysis (figure 2.12).

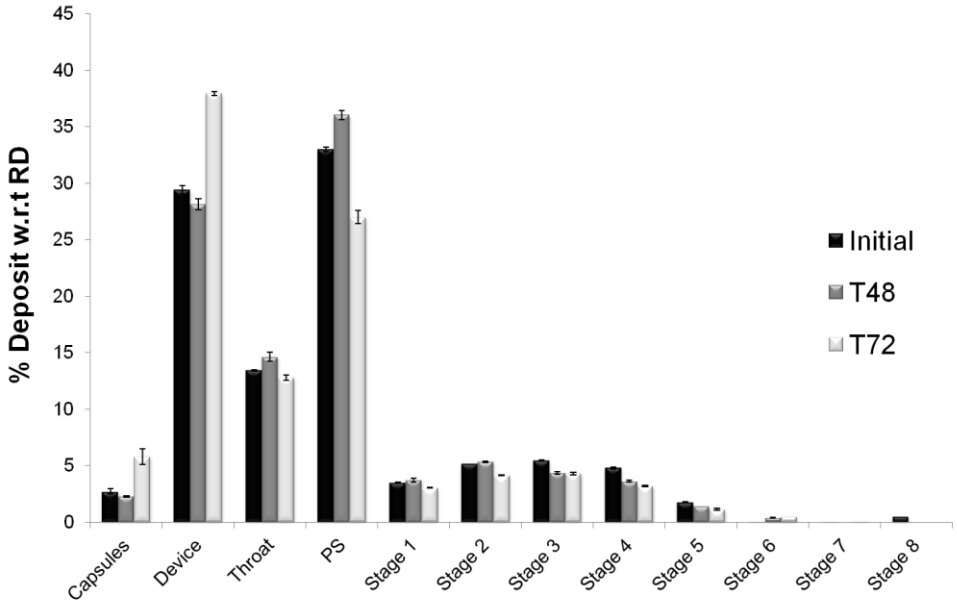

Figure 2.11 Stage by stage deposition profile expressed as the percentage of drug deposited per stage for FP in combination formulations with SX; initial, T48 and T72

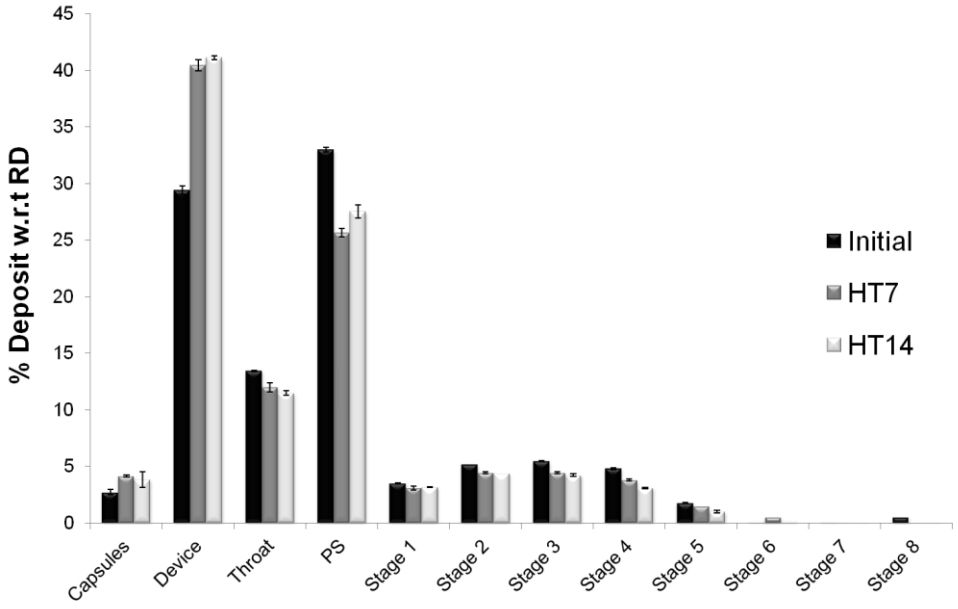

Figure 2.12 Stage by stage deposition profile expressed as the percentage of drug deposited per stage for FP in combination formulations with SX; initial, HT7 and HT14

2.3.5 In vitro performance of SX in a combination formulation with FP samples

The aerosolisation performance results for a single sourced batch of SX in combination formulations with the FP samples used throughout this study are tabulated in table 2.6. Figure 2.13 shows the correlation of the FPF for SX with the CAB values of the FP particles used in the manufacture of these formulations with respect to SX. The FPF for SX in these combination formulations with the FP samples follow opposing trends for the two different environments used to condition the FP samples following micronisation. T48 and T72 formulations aerosolise significantly (p<0.02) more efficiently than the initial FP sample formulation. Interestingly, there is no significant difference between the FPF for T48 and T72. The HT samples on the other hand

followed an inverted trend, with the FPF for SX dropping significantly for both HT7 and HT14.

	RD (µg)	ED (µg)	FPM (µg)	FPF (%RD)	MMAD (µm)	GSD (µm)
Initial	97.53 ±3.99	81.21 ±5.04	16.92 ±0.58	17.36 ±0.39	2.27 ±0.06	2.0 ±0.17
T48	93.44 ±10.38	73.43 ±10.69	17.99 ±0.81	19.24 ±0.56	2.6 ±0.00	2.2 ±0.10
T72	85.96 ±10.08	56.91 ±12.09	17.06 ±0.15	19.88 ±1.02	2.43 ±0.06	2.07 ±0.06
HT7	103.91 ±2.50	55.49 ±1.32	14.4 ±0.35	13.87 ±0.28	2.5 ±0.17	2.37 ±0.06
HT14	112.76 ±2.49	64.33 ±0.80	14.47 ±1.92	12.79 ±0.94	2.7 ±0.10	2.1 ±0.00

Table 2.6 *In vitro* aerosolisation performance for SX in combination formulations with FP produced using initial, T48, T72, HT7 and HT14 FP. Results are described by the recovered dose (RD), emitted dose (ED), fine particle mass (FPM), fine particle fraction (FPF) expressed as a percentage of the recovered dose, mass median aerodynamic diameter (MMAD) and geometric standard deviation (GSD)

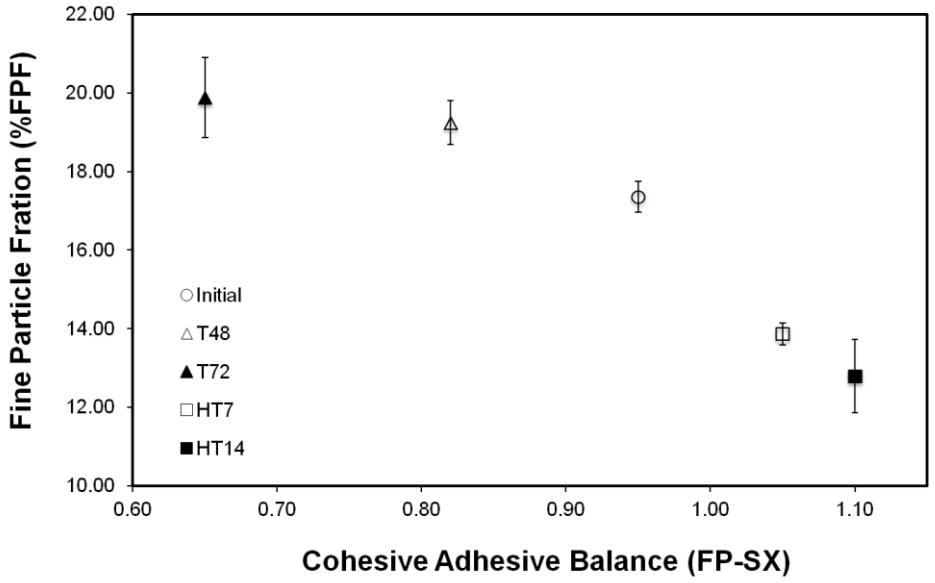

Figure 2.13 Fine Particle Fraction (FPF) of SX in combination formulation with FP expressed as a percentage of the Recovered Dose (RD) plotted against the CAB of FP particles with respect to SX

Figure 2.13 illustrates these opposing FPF trends for SX with the CAB values for FP with respect to SX. The relation between the HT samples and the CAB values is consistent with the agglomeration theory discussed previously for the performance of FP in combination with SX. The FPF for SX drops as the interfacial chemistry of the formulation becomes cohesive, suggesting that SX may prefer an adhesive tendency to the FP, as suggested by Jones et al. (2008).

The increasing adhesive nature of the FP particles conditioned at 60˚C with SX suggests the formation of stable FP-SX agglomerates. Whilst these agglomerates can impede capsule and device emptying as evidenced by the increasing amount of SX deposits in the device (figure 2.14), an increase in the affinity of the two APIs significantly improved the aerosolisation of the lower dose of SX from the lactose carrier significantly (p<0.02) as evidenced by the significant decrease in the amount of SX deposited in the pre-separator (figure 2.14).

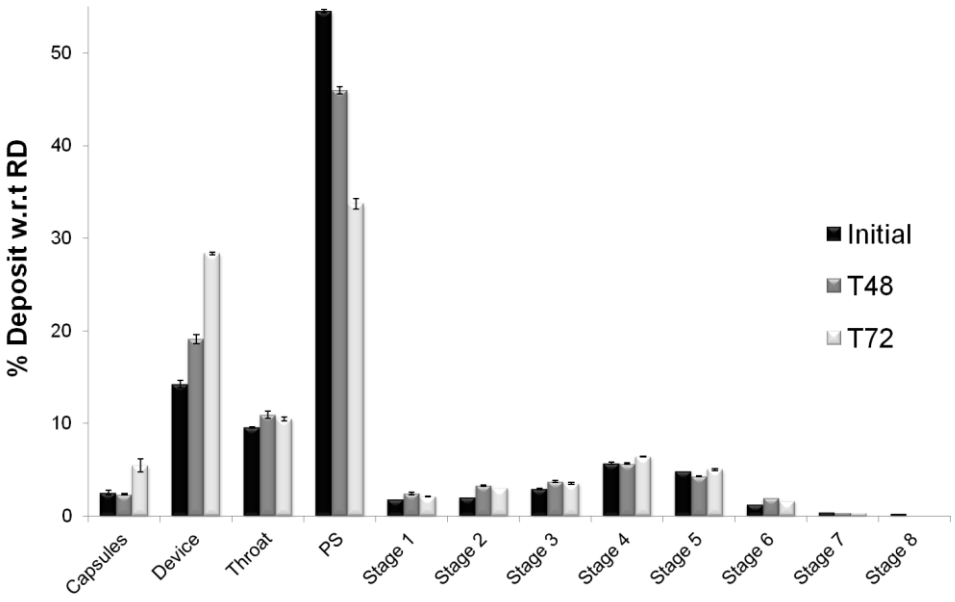

Figure 2.14 Stage by stage deposition profile expressed as the percentage of drug deposited per stage for SX in combination formulations with FP; initial, T48 and T72

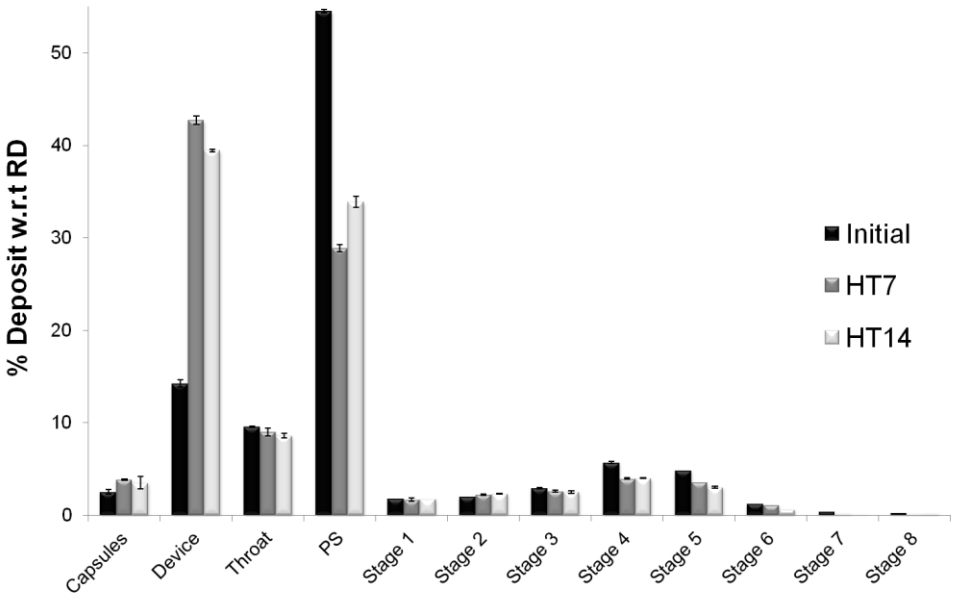

Figure 2.15 Stage by stage deposition profile expressed as the percentage of drug deposited per stage for SX in combination formulations with FP; initial, HT7 and HT14

2.3.6 Assessment of the FP sample following post-micronisation in situ conditioning using HFA-134a

2.3.6.1 Physicochemical Characterisation

Figure 2.16 shows the XRPD profiles for the initial and HFA-conditioned FP samples. The distnctive peaks present suggested that the polymorphic form for the FP sample conditioned *in situ* with HFA-134a remained unchanged.

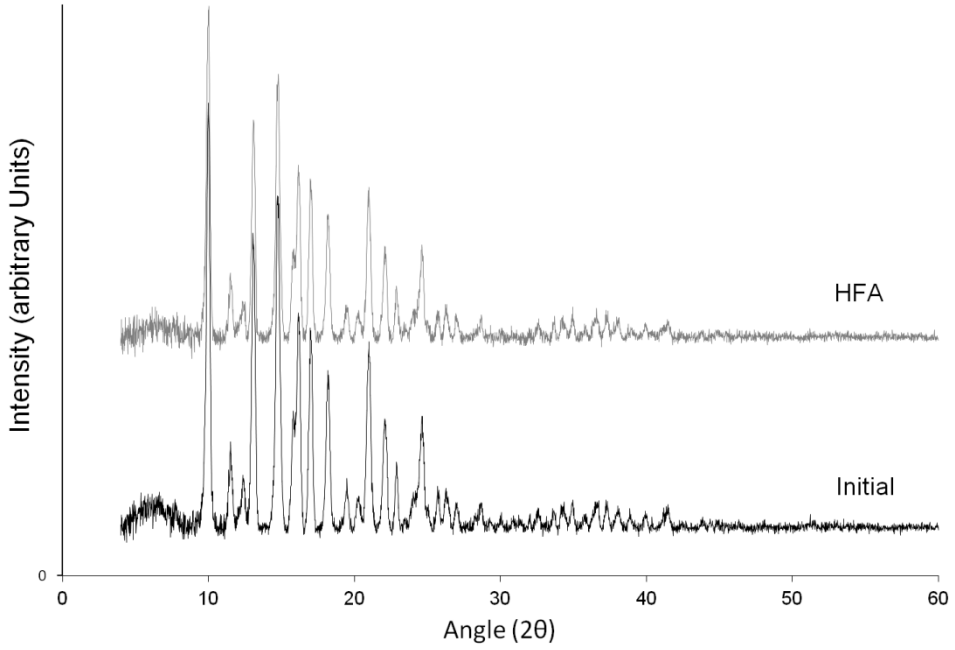

Figure 2.16 X-ray powder diffraction profiles for the Initial and HFA FP samples

The representative DSC thermographs for the initial and HFA-conditioned samples are shown in figure 2.17. The thermal analysis showed both FP samples having a melting onset of 295 °C, which was related to the melting of polymorphic form I of FP (Pitchayajittipong, Shur et al.). The isotherm for the initial FP sample shows an endotherm in the crystallisation region preceding

the melting phase, which suggests the presence of amorphous content in the FP sample. The absence of this endotherm in the thermal analysis of the HFA sample suggests that the *in situ* conditioning may have re-crystallised any process induced structural disorder in the initial FP sample.

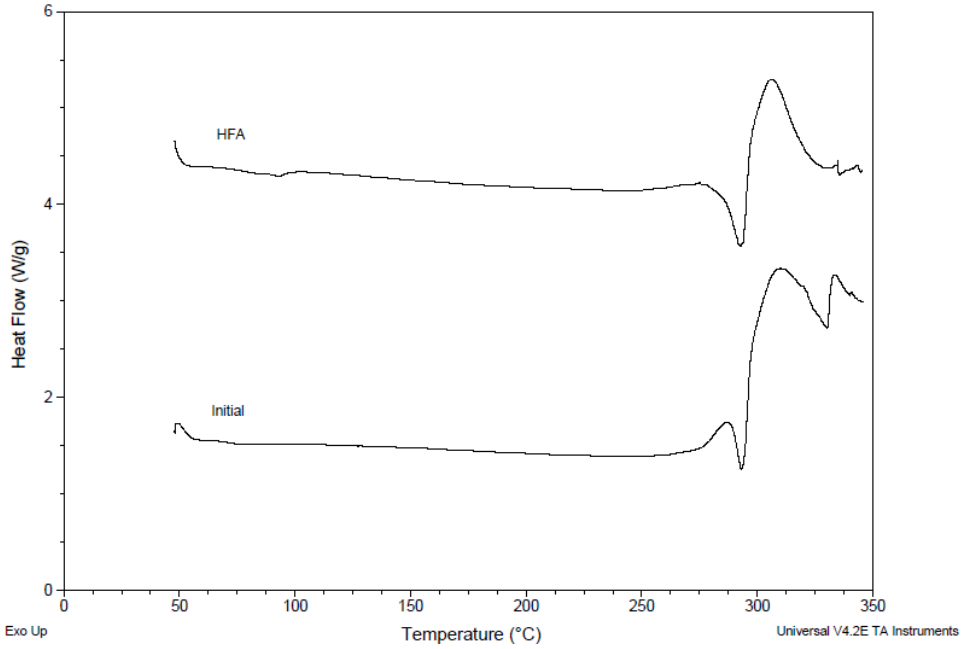

Figure 2.17 Differential Scanning Calorimetry thermographs for the Initial and HFA FP samples

Table 2.7 shows the particle size distribution for the initial and the HFA conditioned FP samples. The d_{10}, d_{50} and d_{90} values suggest a significant (p<0.02) increase in the particle size of the FP particles upon *in situ conditioning* with HFA. This increase may relate to the low solubility of FP within HFA-134a (approx. 9.6 µg/ml) which may cause the fine fraction of FP particles to dissolve. However, with a d_{90} value of 4.45 µm, the FP drug particles conditioned using HFA are nonetheless suitable for DPI formulations (Frijlink and de Boer, 2004). The SEM images shown in Figure 2.18 suggest

similar shape and sized particles between initial and HFA samples. However, in situ conditioning appeared to reduce the degree of surface roughness of the micronised particles, which may relate to the slight dissolution of FP in HFA-134a.

	d_{10} (µm)	d_{50} (µm)	d_{90} (µm)
Initial	0.74 ±0.02	1.79 ±0.03	3.67 ±0.01
HFA	0.92 ±0.02	2.24 ±0.04	4.45 ±0.03

Table 2.7 Particle Size Distribution data for the freshly micronised and HFA conditioned FP samples determined by laser diffraction

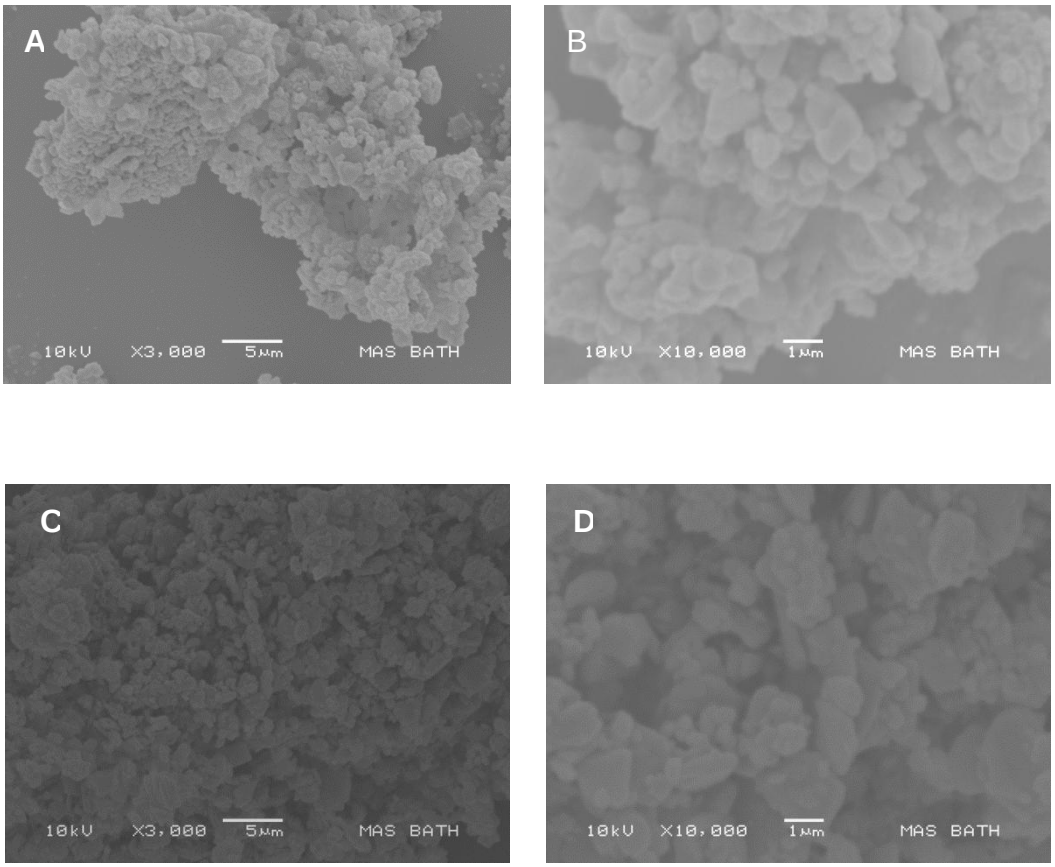

Figure 2.18 Scanning Electron Micrographs for the initial FP aliquot (A, B) and the HFA conditioned sample (C, D)

2.3.6.2 Surface Interfacial Properties of FP Samples

Table 2.8 tabulates the cohesive and adhesive balance following *in situ* conditioning of FP with HFA. Figures 2.19A and 2.19B show the linear regression analysis of the CAB plots with respect to lactose and SX respectively. The CAB ratios were determined from the gradient of each plot. The CAB values shown in table 2.8 suggest that HFA conditioning did not alter the interfacial properties of the FP particles. The CAB results for the initial FP sample with respect to lactose suggest an interfacial chemistry with a slightly cohesive nature (1.18 ±0.02). Following *in situ* conditioning with HFA for 7 days, the FP particles seem to maintain an unchanged balance between the cohesive and adhesive forces (1.15 ±0.04), showing no statistical difference from the initial FP sample. Figure 2.19A however, shows a significant (p<0.05) decrease in the forces constituting these CAB values. This decrease in the magnitude of forces, whilst maintaining a cohesive balance, suggests physical changes to the particle surfaces may occur.

		CAB w.r.t Lactose	CAB w.r.t SX
Freshly Micronised	Initial	1.18 ±0.02	0.95 ±0.02
HFA	HFA	1.15 ±0.04	0.90 ±0.04

Table 2.8 Cohesive-Adhesive Balance (CAB) values with respect to Lactose and SX for the initial and HFA conditioned FP samples

The CAB values for the initial FP particles with respect to SX suggested an interfacial chemistry dominated by adhesive forces (0.95 ±0.02). Once again, the HFA FP sample showed no significant differences from the initial sample

(0.90 ±0.04), retaining a slight adhesively-led interfacial system. Figure 2.19B also shows a significant (p<0.05) decrease in the adhesive and cohesive forces.

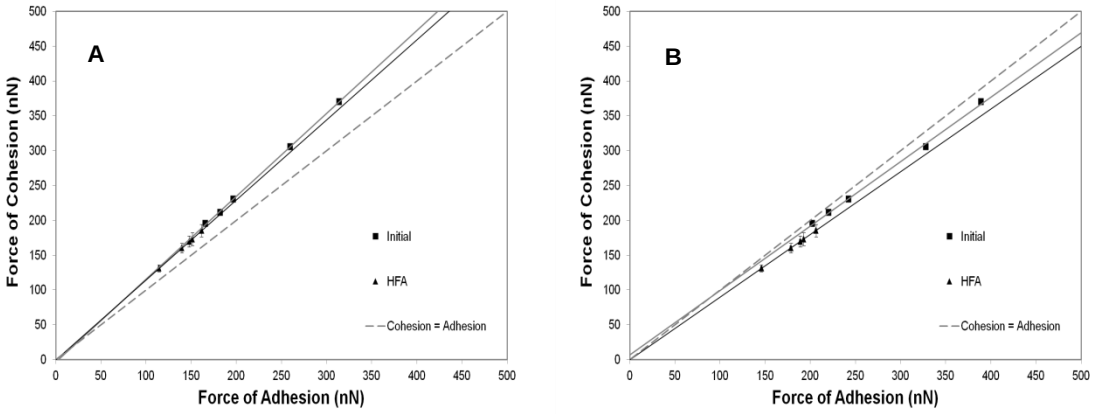

Figure 2.19 (A) Cohesive-Adhesive Balance (CAB) plot of initial and HFA FP samples with respect to lactose, (B) CAB plot of initial and HFA FP samples with respect to SX

2.3.6.3 In vitro performance of FP samples following *in situ* HFA conditioning

	RD (µg)	ED (µg)	FPM (µg)	FPF (%RD)	MMAD (µm)	GSD (µm)
FP Binary						
Initial	224.27 ±6.04	133.47 ±3.90	34.58 ±0.62	15.42 ±0.14	3.9 ±0.00	2.1 ±0.00
HFA	319.92 ±11.45	199.79 ±10.68	49.67 ±2.43	15.44 ±0.93	4.03 ±0.31	2.07 ±0.15
FP in Combination with SX						
Initial	236.02 ±8.48	160.17 ±5.29	42.3 ±0.37	17.94 ±0.74	3.93 ±0.15	2.03 ±0.12
HFA	230.59 ±10.16	187.3 ±14.18	40.42 ±2.78	17.56 ±1.35	4.43 ±0.21	2.0 ±0.17
SX in Combination with FP						
Initial	97.53 ±3.99	81.21 ±5.04	16.92 ±0.58	17.36 ±0.39	2.27 ±0.06	2.0 ±0.17
HFA	86.34 ±9.01	73.65 ±9.17	15.6 ±0.91	18.08 ±0.31	2.63 ±0.25	2.1 ±0.20

Table 2.9 *In vitro* aerosolisation performance for formulation manufactured using the initial and the HFA conditioned FP samples. Results are described by the recovered dose (RD), emitted dose (ED), fine particle mass (FPM), fine particle fraction (FPF) expressed as a percentage of the recovered dose, mass median aerodynamic diameter (MMAD) and geometric standard deviation (GSD)

Table 2.9 shows the *in vitro* performance of binary and combination based formulations manufactured using FP particles conditioned using HFA. Results suggest that there are no statistically significant differences between the performances of formulations manufactured using freshly micronised FP (Initial) and those manufactured using HFA-conditioned FP. These data are consistent with the CAB results which suggest that the way in which the FP particles interact with the lactose and the SX particles is unchanged between the initial and the HFA-conditioned FP sample. Figures 2.20-2.22 show the FPF of the formulations manufactured using the HFA conditioned FP in relation to the other FP samples used in this study, showing a very close relation between the interfacial chemistry and the *in vitro* performance.

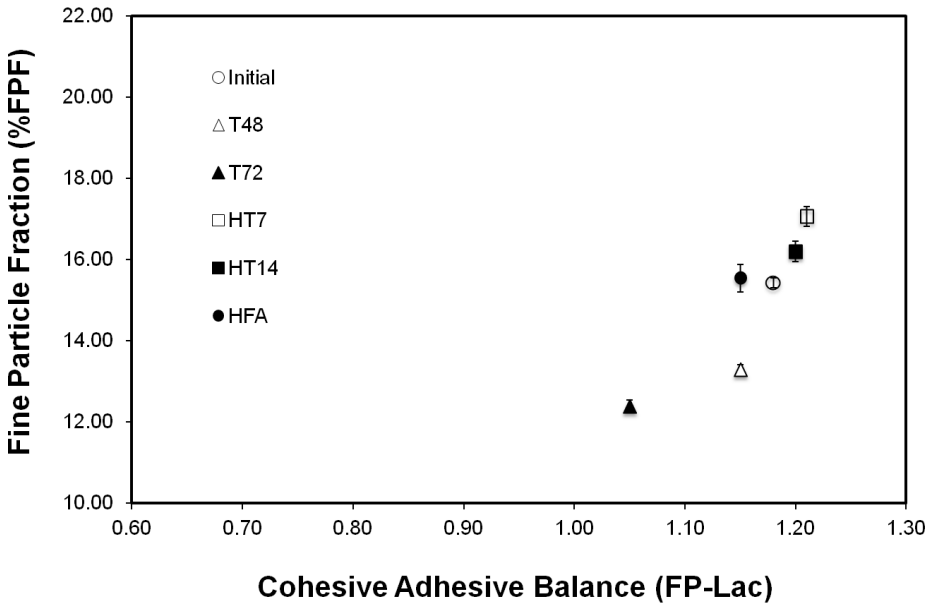

Figure 2.20 Fine Particle Fraction (FPF) of FP in a binary formulation manufactured using HFA conditioned FP particles shown in context of similar formulations manufactured using freshly micronised FP and *ex situ* conditioned FP as described previously, expressed as a percentage of the Recovered Dose (RD) plotted against the CAB of FP particles with respect to lactose

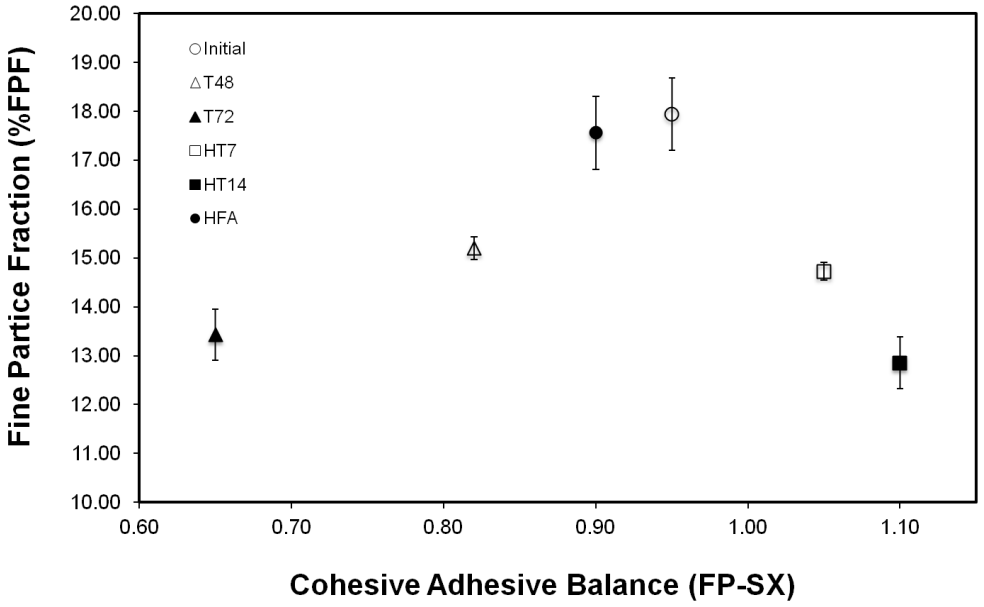

Figure 2.21 Fine Particle Fraction (FPF) of FP in a combination formulation with SX manufactured using HFA conditioned FP particles shown in context of similar formulations manufactured using freshly micronised FP and ex situ conditioned FP as described previously, expressed as a percentage of the Recovered Dose (RD) plotted against the CAB of FP particles with respect to lactose

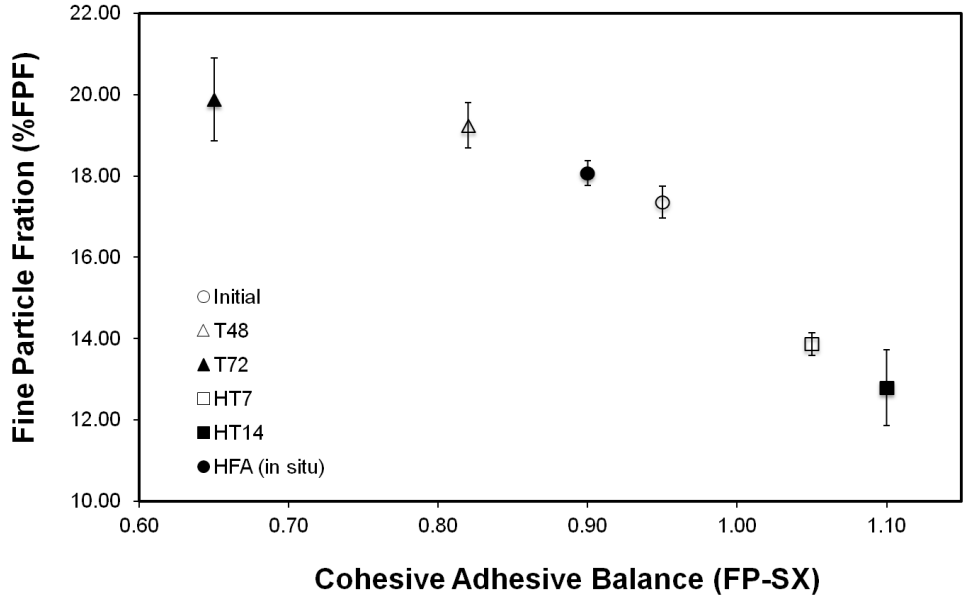

Figure 2.22 Fine Particle Fraction (FPF) of SX in a combination formulation with FP manufactured using HFA conditioned FP particles shown in context of similar formulations manufactured using freshly micronised FP and ex situ conditioned FP as described previously, expressed as a percentage of the Recovered Dose (RD) plotted against the CAB of FP particles with respect to lactose

2.4 CONCLUSIONS

The results shown in this study suggest that whilst *ex situ* and *in situ* post-micronisation conditioning does not alter the polymorphic form of FP, conditioning appears to directly influence the physical and interfacial chemistry of micronised FP. It was shown that the interfacial chemistry of the FP particles with respect to SX changes significantly upon post-micronisation conditioning, with temperature imposing an adhesive-driven trend whilst humidity shifts the adhesive FP particles to a cohesively-led system. The *in vitro* performance of the formulations followed the relevant changes to the interfacial properties of FP, with the FPF of SX also being affected by the changing properties of the FP particles. The similarity in the *in vitro* results seen between the initial and HFA-conditioned sample suggests that the stress relaxation pathway taken during *in situ* conditioning with HFA promotes interfacial stability. The differences seen in both the interfacial properties of FP and the FPF of all the formulations highlight the importance for a better understanding and control on the stress relaxation of FP particles following micronisation.

3 THE INFLUENCE OF SECONDARY PROCESSING ON THE STRUCTURAL RELAXATION DYNAMICS OF FLUTICASONE PROPIONATE

3.1 INTRODUCTION

Particle size reduction of active pharmaceutical ingredients (APIs) for delivery to the lungs requires secondary processing of primary crystals using highly energetic comminution techniques, such as air-jet micronisation (Kubavat *et al.,* 2012). For brittle materials, particle-particle and particle-wall collisions within a micronizer often leads to the formation of short-lived defects formed along existing flaws within a crystalline lattice that can lead to crystal fracture (Ward and Schultz, 1995; Joshi *et al.,* 2002). However, at the brittle-ductile transition, the material absorbs a significant amount of impact energy before undergoing any further particle reduction (Huttenrauch *et al.,* 1985). This impact energy is stored as strain energy within the crystalline lattice in the form of structural defects, dislocations and, at the limit, can lead to localized amorphous regions on a particle surface (Huttenrauch *et al.,* 1985; Brodka-Pfeiffer *et al.,* 2003a; Shur *et al.,* 2013).

Process induced structural disorder can lead to uncontrolled thermodynamic changes to the materials, and is commonly described as “mechanical activation” (Wildfong *et al.,* 2006; Huttenrauch *et al.,* 1985; Brodka-Pfeiffer *et al.,* 2003a; Shur *et al.,* 2013). Mechanical activation may directly influence the physicochemical properties of a substance, for example, surface free energy,

reactivity, conductivity and true density (Shur *et al.,* 2013; Colombo *et al.,* 2009). For carrier-based dry powder inhaler (DPIs) formulations, mechanical activation can directly influence the interfacial free energy of the respirable drug particles (e.g. < 5 µm), which may increase the tendency for agglomeration. This may also affect the relative magnitude of the cohesive (drug-drug) and adhesive (drug-excipient) inter-particulate forces. Since the performance of adhesive mixtures is a function of the relative magnitude of these forces, the interfacial properties of secondary processed APIs can dominate blending dynamics, formulation microstructure and ultimately drug product quality and performance of carrier-based DPI formulations (Shur *et al.,* 2013).

Mechanically activated particles are thermodynamically unstable and are driven to undergo structural relaxation to a more stable state (Huttenrauch *et al.,* 1985; Brodka-Pfeiffer *et al.,* 2003a). Structural relaxation kinetics has been shown to be strongly dependent on environmental conditions (temperature and relative humidity), which may influence the degree of molecular mobility within the material, and the period of exposure to such conditions (Brodka-Pfeiffer *et al.,* 2003a; Shur *et al.,* 2013). The laagering or quarantine period required for materials to undergo structural relaxation may vary significantly from minutes, hours to months and appears to be highly dependent on their hydrophilic/hydrophobic nature (Huttenrauch *et al.,* 1985; Shur *et al.,* 2013).

Accelerated stability conditions of both temperature and relative humidity have been shown to expedite the rate of structural relaxation and may aid in stabilization of particulate surfaces upon secondary processing (Shur *et al.,* 2013; Brodka-Pfeiffer *et al.,* 2003b). Studies have also shown that post-micronisation relaxation may significantly reduce the levels of localized amorphous disorder, and the tendency for micronised particles to aggregate (Brodka-Pfeiffer *et al.,* 2003b). The use of post-micronisation environmental conditioning appears to be widely applied to hydrophilic compounds (Bender *et al.,* 2004; Riebe *et al.,* 2003; Muhrer *et al.,* 2012). For example, micronised tiotropium bromide monohydrate was exposed to the conditions of 70-80 % RH and 25-30 °C for up to 28 hours on sheet metal racks prior to formulating as a DPI product (Bender *et al.,* 2004). The structural relaxation of the conditioned tiotropium bromide monohydrate is characterized by measuring the change in specific enthalpy of solution. Micronised salbutamol sulphate was mechanically relaxed to a low energy, crystalline form for use in suspension-based metered dose inhalers (MDIs) by exposing a shallow bed of powder to the conditions of 60 % RH and 25 °C for 65 hours (Riebe *et al.,* 2003). Micronised glycopyrrolate bromide could be exposed to a dry environment at an elevated temperature between 60 and 90°C for at least six hours, but preferably between 24 and 50 hours, to limit the tendency of the particles to aggregate and/or agglomerate upon storage of the DPI formulation (Muhrer *et al.,* 2012).

For hydrophobic drugs, there is limited literature regarding the use of environmental conditions for post-micronisation surface conditioning of materials. Among these, Joshi et al. showed an interesting observation on temperature-dependent stress relaxation of budesonide that led to an anomalous increase in specific surface area during post-micronisation storage (Joshi *et al.,* 2002). The significant increase in surface area of budesonide upon storage was hypothesized to be related to the residual stress stored in the form of defects and dislocation upon micronisation, which may lead to crack propagation and induce secondary particle fracture with the creation of new surface (Joshi *et al.,* 2002).

Based on the above information, the properties of carrier-based DPI formulation prepared with the freshly micronised or laagered (post-micronisation and conditioned) drug are likely to be different, particularly as its performance is strongly dependent on the particle size, morphology and interfacial chemistry of the particle surface (Shur *et al.,* 2013). Any processing or storage conditions that may affect such properties need to be monitored and controlled to ensure formulation consistency during processing and over the product shelf life. Therefore, the aim of this study is to investigate the structural relaxation of micronised fluticasone propionate (FP) stored under different conditions of temperature and relative humidity and their possible influence on the FP physicochemical and interfacial properties. FP was chosen due to its hydrophobic nature and our limited understanding of the structural relaxation kinetics of such hydrophobic materials. The results of this

study are expected to provide a valuable insight into how changes to these material properties during relaxation affect cohesive forces (FP-FP), adhesive forces with another drug component such as salmeterol xinafoate (SX) and lactose monohydrate, and consequently the in vitro performance of carrier-based DPI formulations.

3.2 MATERIALS AND METHODS

3.2.1 MATERIALS

Micronised FP ($C_{25}H_{31}F_3O_5S$, Molecular weight = 500.571) was purchased from Chemagis (Lot no. 104364, 100 grams, Bnei Brak, Israel). The FP sample was shipped directly upon micronisation and supplied in very tight packaging and held under 10 % RH during transport. Salmeterol Xinafoate ($C_{36}H_{45}NO_7$, molecular weight = 603.745) was sourced from Neuland Pharmaceuticals (Lot no. 12004, 20 grams, Mumbai, India). A milled grade (ML001) of lactose monohydrate ($C_{12}H_{24}O_{12}$, molecular weight = 360.312) was sourced from DFE Pharma (Lot no. 10474128, Borculo, Netherlands). In vitro aerosolization testing of the binary and combination DPI formulations was performed using a Cipla Rotahaler® DPI capsule device (Cipla, Mumbai, India). Water used during the studies was Milli-Q reverse osmosis purified

(Merck Millipore, Darmstadt, Germany). Methanol and acetonitrile were of HPLC grade and purchased from Sigma (Gillingham, UK).

3.2.2 METHODS

A 2g sample of FP was taken from a micronised batch for full physicochemical characterization. The remaining drug sample was separated into three 6g batches and conditioned under three different environmental conditions of temperature and relative humidity for well-defined periods. An aged batch of micronised SX (>12 months) was used for tertiary DPI formulation preparations, and was kept under ambient conditions during the period of the study. The use of such aged SX batch allowed the investigation to focus on examining the effect of FP relaxation behavior under different storage conditions on the in vitro performance of the tertiary DPI formulation, as its physicochemical and interfacial properties were not expected to change. The particle size distribution of the coarse lactose monohydrate was monitored during the study to ensure that there was no change to particle size, since any change to the fine or coarse end of the particle size distribution may influence drug product performance.

3.2.2.1 Conditioning of micronised FP

The three conditioning environments chosen for this investigation were (1) ambient temperature and low humidity (LH) (25 °C, 33 % RH), (2) ambient temperature and high humidity (HH) (25 °C, 75 % RH), and (3) high

temperature and ambient humidity (HT) (60 °C, 44 % RH). An aliquot of each conditioned FP sample (2 g) was taken from the LH and HH conditions upon being laagered for 30, 60 and 90 days. The HT sample was quarantined at a single time point of 14 days. All samples were sieved through a 500 µm mesh sieve prior to physicochemical characterization. Table 3.1 provides a summary of the conditioning environments and periods for micronised FP samples as well as their corresponding nomenclatures.

Table 3.1 Nomenclature of post-micronised FP samples based on their conditioning environments and periods

Conditioning Environment	Conditioning Period	Sample Reference
Micronised (used as received)	0 Days	Day 0
25 °C, 33 %RH	30 Days	LH30
	60 Days	LH60
	90 Days	LH90
25 °C, 75 %RH	30 Days	HH30
	60 Days	HH60
	90 Days	HH90
60 °C, 44 %RH	14 Days	HT

3.2.2.2 Laser Diffraction

Particle size distributions (PSDs) of all FP samples were measured in the wet state. Approximately 10 mg of FP was suspended in HPLC grade cyclohexane containing 0.5 % w/v lecithin (Acros Organics, Geel, Belgium) and sonicated for 5 minutes and then immediately transferred into a 50 mL cuvette to produce an appropriate optical concentration (8-12 %). Each measurement was performed in triplicate. Particle size analysis was performed using WINDOX 5.0 software (Sympatec GmbH, Clausthal-Zellerfeld, Germany).

3.2.2.3 Scanning Electron Microscopy (SEM)

Particle morphology of all FP samples was investigated using scanning electron microscopy (SEM). Sample aliquots were fixed onto sticky carbon tabs (Agar Scientific, Cambridge, UK), followed by removal of excess powder using pressurized air. Samples were subsequently sputter coated with gold (Edwards Sputter Coater S150B, Edwards High Vacuum, Sussex, UK) to achieve a thickness of approximately 20 nm. Imaging was performed using a scanning electron microscope (JEOL JSM6480LV, Tokyo, Japan) using 15 kV accelerating voltage.

3.2.2.4 X-ray powder diffraction (XRPD)

The X-ray powder diffraction (XRPD) patterns of FP samples were analyzed by a Bruker Powder Diffractometer (D8; Bruker AXS Inc., Madison, USA) using CuKα radiation (λ=1.54 Å). The data were collected over a single 2θ

sweep with range 2θ = 5 - 30° and a step size of 0.025°/step with a step time of 1.5 s.

3.2.2.5 Differential Scanning Calorimetry (DSC)

The thermal properties of all samples were investigated using a differential scanning calorimeter (DSC 2920, TA Instruments, Surrey, UK).

3.2.2.6 Specific Surface Area by Brunauer–Emmett–Teller (BET)

The specific surface area (SSA) of FP samples was measured using a Gemini 2360 surface area analyser (Micromeritics Instrument Corporation, Norcross, USA). A five-point BET nitrogen adsorption analysis was carried out in triplicate after degassing the samples for 24 hours in a FlowPrep 060 degasser (Micromeritics Instrument Corporation, Norcross, USA).

3.2.2.7 Rugosity (R_a)

Rugosity (R_a) is a semi-quantitative measure of shape and surface texture of particles and can be calculated based on the ratio of the surface area calculated by BET (SSA) to a product of the drug density and the surface area by laser diffraction (S_v) (Joshi *et al.,* 2002). As described above, the laser diffraction measurement assumes that particles are smooth and spherical, and does not account for the surface roughness or shape of particles in its theoretically calculated surface area. Thus, R_a can provide an estimate of changes that could be attributed to surface texture and smoothness.

3.2.2.8 Thermal Activity Monitoring (TAM)

3.2.2.8.1 Preparation of Amorphous Form

A small-scale spray dryer with inert loop (model B-295, Büchi, Labortechnik AG, Flawil, Switzerland) was used for spray drying FP. The system incorporated a high-efficiency cyclone and was fitted with a co-axial two-fluid atomizer with an orifice of 0.7 mm. The nozzle was also equipped with automated cooling and cleaning systems. The relative humidity (RH) of the drying air before heating was 0 % and both the inlet and outlet air temperatures were monitored. Spray drying of FP was conducted upon spraying a 0.5 w/v solution of the drug in acetone. The resultant droplets were dried at 110°C inlet temperature, outlet temperature ranged between 50 – 60°C, spray flow rate of 500 dm^3. h^{-1} and solution feed rate of 8 $cm^3.min^{-1}$. Once the material was produced it was immediately transferred into a container and stored at -90°C. In doing this, the materials remained amorphous for up to 1 month.

3.2.2.8.2 Preparation of Calibration Curve

The amorphous samples used to construct the calibration plots were prepared by directly weighing proportional masses of the appropriate crystalline and amorphous materials into the calorimetric ampoule. Saturated solutions of fluticasone propionate were prepared in acetone at 21°C under continual stirring. The solutions were then filtered in heated labware using a 0.45 µm

nylon membrane filter (Whatman, Brentford, UK) and introduced to a sealed glass crystallisation vessel continually stirred by an overhead stainless steel three blade stirrer with a water-jacket temperature control maintained at 21°C (K20; Haake, Karlsruhe, Germany). The FP was crystallised by the addition of an excess amount of n-hexane to a saturated solution of FP in acetone. The mass of the crystalline component was kept constant in all the mixtures (50 ± 0.01 mg) and an appropriate amount of spray-dried material was added to make 1, 3, 5 and 10 % amorphous samples. The mixtures were made homogenous in the calorimetric ampoule by geometric mixing of the spray dried and amorphous forms of the drug in the ampoule before loading onto the perfusion apparatus. The mixing was conducted at low humidity to prevent physicochemical changes occurring in the bulk. Calibration curves were then constructed for each of the drug samples by plotting the measured heat of crystallization versus the known amorphous content.

3.2.2.8.3 Isothermal Microcalorimetry (TAM)

Calorimetric data were recorded using a 2277 Thermal Activity Monitor (TAM, Thermometric AB, Jarfalla, Sweden) at 25 °C equipped with a gas perfusion unit. Briefly, the unit controls the relative humidity (RH) of a carrier gas flowing over the sample by proportional mixing of two gas lines (0 and 100 % RH) using mass-flow controllers. In addition, the unit enables the introduction of 0.9 partial pressure of ethanol vapour pressure when used as a plasticizer. Similarly, to the humidity set-up, partial pressure of solvent can be returned to

0. This allows freshly loaded samples to be held under a dry atmosphere, preventing the onset of crystallisation and allowing the apparatus to reach thermal equilibrium before the commencement of data capture. Data were recorded every 10 s with an amplifier range of 3000 μW using the dedicated software package Digitam 4.1. Data were recorded in triplicate. Peak analysis was performed using Origin (Microcal Software Inc., USA). In the analysis of fluticasone propionate ethanol vapour was used to aid re-crystallization. For this the programme started under dry nitrogen, switched to 0.9 partial pressure and returned to 0. In both cases, upon returning the system to the dry state after crystallization, the drying response was subtracted from the wetting response.

3.2.2.8.4 Physicochemical Analysis of Spray Dried FP

The scanning electron micrographs of spray dried FP are shown in Figure 3.1. The particle of spray dried FP appeared spherical and possessed a smooth morphology. Furthermore, the particles of the material were extensively agglomerated. The X-ray powder diffractogram of spray dried FP is shown in Figure 3.2. The absence of any distinct peaks in the diffraction pattern suggests that the material was amorphous with very little crystallinity. Hence, these data suggest that the spray drying process was successful in generating an amorphous sample of FP for this study.

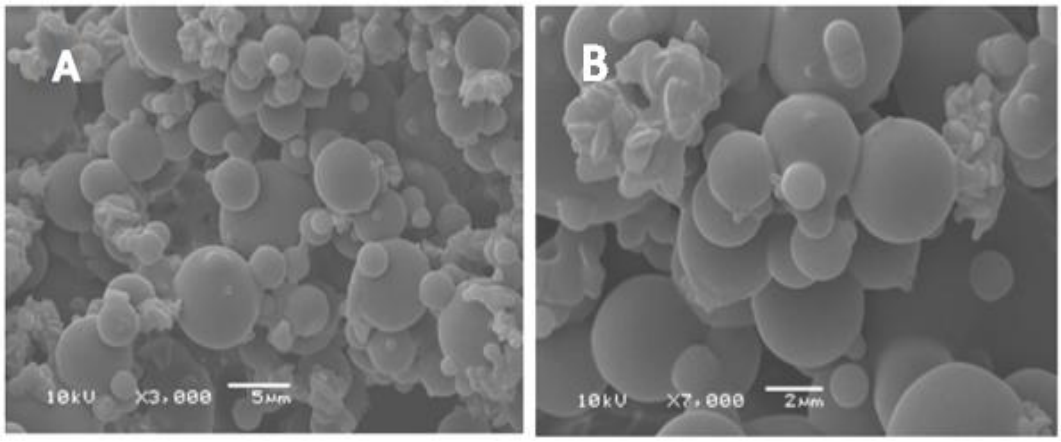

Figure 3.1 Scanning Electron Micrographs of spray dried FP at a magnification factor of (A) at 3,000 and (B) 7,000

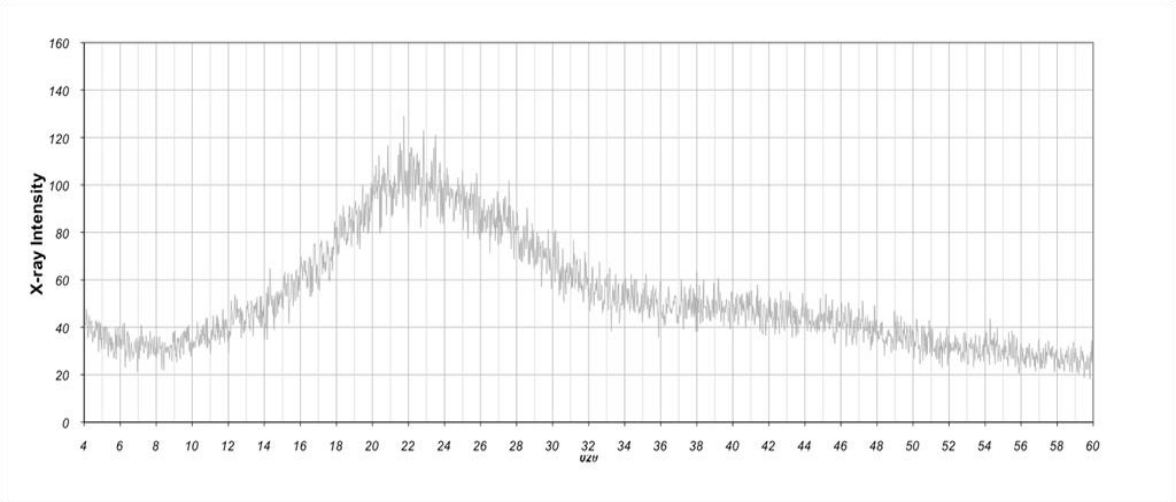

Figure 3.2 X-ray powder diffractogram of spray dried FP

3.2.2.8.5 Isothermal Calorific Responses for FP

A common approach to crystallise amorphous samples in an isothermal calorimeter is to use either elevated RH or organic vapour (maintained through the use of a mini hygrostat located in the sample ampoule). The sample absorbs humidity or vapour, which plasticises the material and, after a

time period that varies in proportion to the amorphous content, results in the crystallization of the material. While such experiments are relatively is simple to run, it is very difficult to de-convolute the many events that occur during crystallization. Two of the principal problems of the mini-hygrostat method are that hydration is initiated externally from the calorimeter, therefore, the initial wetting, and possibly some crystallisation, data are lost and that there are imbalances in the rate of solvent evaporation and condensation. The use of a perfusion unit to initiate crystallisation circumvents this problem. However, a different approach to data analysis is required. This is required, because as the humidity or vapour are elevated, all the internal surfaces of the ampoule, as well as the sample, are wetted, which produces a large exothermic heat signal that often occurs over a time-period that is longer than the time required for the sample to crystallise. In effect, the crystallisation signal is obscured by the wetting response. Hence, in order to determine the enthalpy of re-crystallization from these data it is imperative to return the system to 0 % RH after crystallisation and subtract the drying response from the wetting response. The responses of spray dried FP and mixtures of crystalline/amorphous samples are shown in Figure 3.3. The spray dried FP had a greater response than the mixtures containing either 3 % or 5 % spray dried material mixed with crystalline samples of the respective materials.

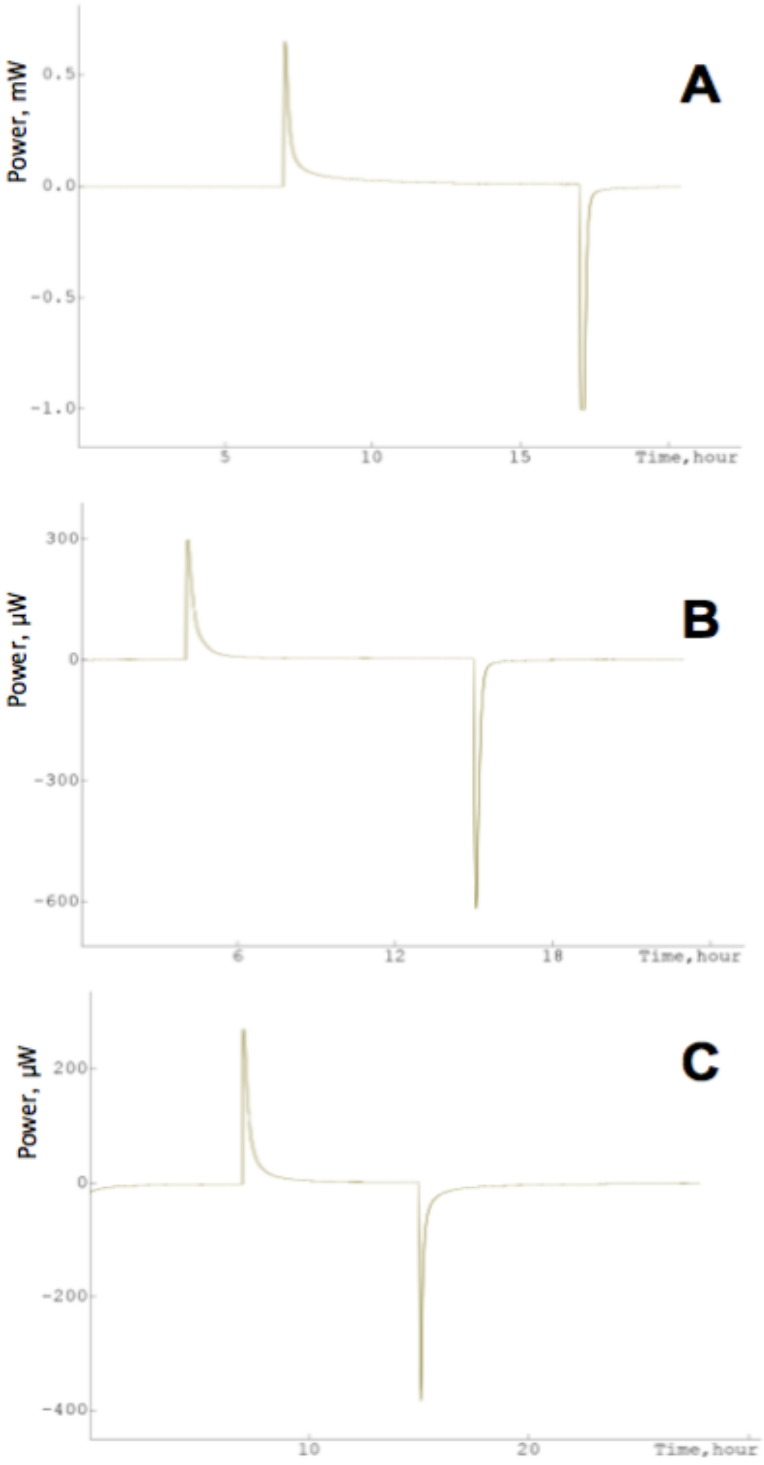

Figure 3.3 The wetting and drying calorimetric response of (A) spray dried FP, (B) 5% spray-dried FP with crystalline FP and (C) 3% spray-dried FP with crystalline FP

3.2.2.8.6 Construction of a Calibration Curve for the Amorphous Quantification of FP

The enthalpy of re-crystallization of the calibration standards of FP from the calorimetric data was calculated by subtracting the drying response from the wetting response. These data are shown in Figure 3.4. The LOD of this calibration curve was 0.16 % and the LOQ was 0.50 %.

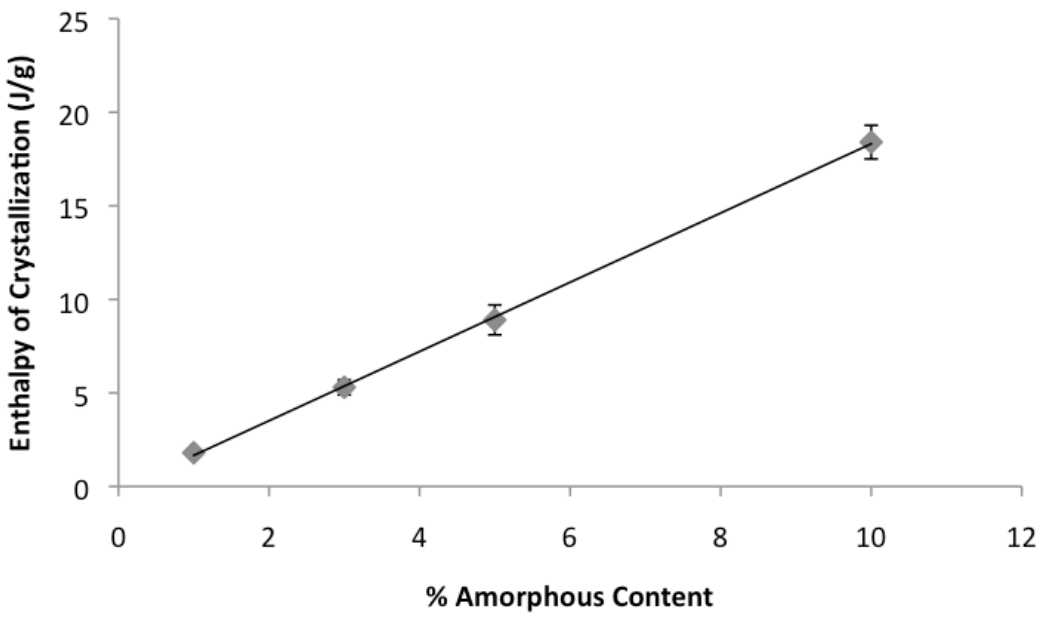

Figure 3.4 Calibration curves for FP and the lines shown are linear regression fits. Equation of line: y=1.85x – 0.16, R^2=0.99.

The amorphous content of micronised FP samples was determined using the TAM and the constructed calibration curves.

3.2.2.9 Cohesive-Adhesive Balance (CAB)

3.2.2.9.1 Preparation of crystal substrates

To perform quantitative scanning probe microscopy (SPM) measurements of the cohesive-adhesive balance (CAB) of the FP samples, smooth single crystal surfaces of FP, SX and lactose monohydrate were prepared (Begat *et al.,* 2004; Kubavat *et al.,* 2012). The procedure for these preparations is briefly summarized below.

A saturated solution of FP in 2 mL of acetone was prepared and sonicated prior to filtration via a 0.22 µm polytetrafluoroethylene (PTFE) membrane filter (Whatman Inc., Clifton, NJ, USA). FP was crystallized using water as an anti-solvent. Specifically, a microscope cover slip (12 mm x 12 mm) was supported on a vertical post in a crystallization dish that contained the anti-solvent. A droplet of the FP saturated solution was placed on the coverslip using a syringe attached to the 0.22-µm-membrane filter. The system was sealed by inverting a glass lid in the crystallisation dish to allow vapor phases of the miscible solvents to come into equilibrium, resulting in heterogeneous nucleation and crystal growth within the solution droplet. A similar approach was used for the preparation of smooth crystal substrates of lactose monohydrate and SX and a detailed method is published elsewhere (Kubavat *et al.,* 2012).

3.2.2.9.2 Interaction force measurements

Prior to force measurements, individual particles from each sample of FP were attached onto standard V-shaped tipless cantilevers with pre-defined spring constants (DNP-020, DI, CA, USA) using an epoxy resin glue (Araldite, Cambridge, UK). Five probes were prepared for the initial, LH, HH and HT conditioned FP samples at each pre-defined laagering period. All probes were examined with an optical microscope (magnification 50x) to ensure the integrity of the attached particle, before allowing the thin layer of glue to cure and dry.

Single crystal substrates were loaded onto the scanner stage of a multi-mode scanning probe microscope (SPM) (Bruker, Santa Babara, CA, USA), which was enclosed in a custom-built environmental chamber, in which the ambient conditions were maintained at a constant temperature of 25 °C (± 1.5 °C) and relative humidity of 44 % RH (± 3 %). The interaction forces were measured by recording the deflection of a cantilever as a function of the substrate displacement (z) by applying Hooke's Law. Individual force curves (n = 1024) were conducted over a 10 µm x 10 µm area at a scan rate of 4 Hz and a compressive load of 40 nN.

A custom-built software was developed to extract data contained within each force-volume dataset. These data were analyzed to ensure normal distribution, indicating uniform contact area between the drug probe and the smooth substrate surfaces. Arithmetic mean and standard deviation were

measured to produce CAB plots for the interactions of the different batches of FP with both lactose monohydrate and SX.

3.2.2.10 Preparation of powder formulations

Binary powder blends (4 g) were manufactured using lactose monohydrate and 1.0 % w/w FP (day 0, LH, HH, or HT). A pre-weighed amount of lactose monohydrate (3.96 g) was initially passed through an 850 µm aperture sieve to break any large agglomerates which may have formed during storage. A quarter of the mass of the lactose monohydrate required was transferred to a stainless steel cylindrical vessel with an internal diameter of 100 mm and a height of 150 mm, and all the FP (40 mg) was sandwiched with another quarter of the sieved lactose monohydrate. This was mixed in a T2F Turbula® mixer (Wily A Bachofen AG, Basel, Switzerland) for 10 minutes at 46 rpm. The remaining half of the lactose monohydrate was then added and mixed for a further 45 minutes at 46 rpm. Upon blending, formulations were passed through a 250 µm sieve and stored at 20 ± 2 °C and 44 % RH for at least 48 hours before the content uniformity of the blends was assayed. Tertiary powder blends containing FP (1.0 % w/w), SX (0.2 % w/w SX base) and lactose monohydrate were similarly prepared by sandwiching 40 mg of FP and 8 mg of SX between ½ of the lactose monohydrate then mixed for 10 min at 46 rpm and then the remaining ½ of the lactose added and mixed for a further 45 minutes at 46 rpm.

Following content uniformity testing, 25 ± 1 mg of the formulated blend was loaded into size 3 hydroxypropylmethyl cellulose (HPMC, Shionogi Qualicaps, Madrid, Spain) capsules. The targeted dose of the binary formulations was 250 µg of FP per 25 mg fill weight. For the tertiary formulations, the targeted dose of FP and SX were 250 µg and 50 µg, respectively, per 25 mg fill weight. The filled capsules were stored at 20 ± 2 °C and 44 %RH for 24 hours prior to in vitro testing to ensure dissipation of any electrostatic charges that may have been introduced during processing.

3.2.2.11 HPLC analysis of Fluticasone Propionate and Salmeterol Xinafoate

The drug content was quantified using HPLC. For the determination of drug content in FP binary formulations, the HPLC method consisted of a pump coupled to an auto-sampler and multi-wavelength UV detector (Agilent 1200, Wokingham, UK) with a wavelength set at 235 nm. The pump flow rate was set to 1.5 mL/min through a Hypersil ODS-C_{18} column (Fisher Scientific, Loughborough, UK, column length of 250 mm, internal diameter of 4.6 mm, and particle size of the packing material of 5 µm), which was placed in a column oven (Agilent, Wokingham, UK) set to 40°C. The mobile phase consisted of methanol, acetonitrile and water (45:35:20 % v/v). The elution time for the FP peak using this method was 3.4 mins. For the drug content determination of FP and SX in combination formulations, the HPLC method used a flow rate of 1.0 mL/min through a Hypersil BDS-C_{18} column (Fisher

Scientific, Loughborough, UK, column length of 250 mm, internal diameter of 4.0 mm, and particle size of the packing material of 5 μm) placed in a column oven at 40 °C. The mobile phase consisted of 75:25 % v/v methanol: 0.6 % w/v aqueous ammonium acetate.

For both methods, a linear regression analysis was used for the assessment of the HPLC calibration. Quantification was carried out by an external standard method, and linearity was verified between 0.05 and 50 μg/mL. The limit of detection was 0.02 μg/mL and 0.03 μg/mL for both FP and SX respectively.

3.2.2.12 Content Uniformity

Ten random samples of 25 ± 1 mg, from different areas of the powder bed were weighed and dissolved in 50 mL of mobile phase. The amount of drug in each sample was obtained from HPLC assay and the content uniformity was expressed as a relative standard deviation (%RSD).

3.2.2.13 In Vitro Aerosolization Analysis

Analysis was performed using a Next Generation Impactor (NGI, Copley Scientific, Nottingham, UK) with a pre-separator, which was connected to two vacuum pumps (Copley Scientific, Nottingham, UK) to create critical (sonic) flow. The pre-separator contained 15 mL of mobile phase. The NGI cups were coated with 1 % v/v silicone oil in hexane to eliminate any particle bounce. For each experiment, two capsules of the same blend were discharged into the NGI at 55 L/min for 4.4 s, equivalent to a total volume of 4 L. Prior to each

test, the flow rate was verified using a digital flow meter (DFM 2000, Copley Scientific, Nottingham, UK). The amount of API deposited on each part of the NGI was determined by HPLC. This protocol was repeated three times for each formulation. The mass median aerodynamic diameter (MMAD), geometric standard deviation (GSD), fine particle dose (FPD) and impactor stage mass (ISM) were determined for each case. In all cascade impactor tests conducted, the mass balance was within ±15 % of the total recovered dose.

3.2.2.14 Statistical Analysis

Statistical analysis between different populations carried out using one-way analysis of variance. Comparison of the mean values was performed by Tukey's multiple comparison. All statistical analyses were performed using GraphPad Prism software (GraphPad Software Inc, California, USA). Error bars in graphical representations of data show ± standard deviation (SD) in all cases.

3.3 Results and Discussion

To investigate the effect of controlled environmental laagering on the structural relaxation behavior of micronised FP, a range of physicochemical properties were systematically evaluated under different storage conditions and over pre-defined time periods. Colloidal probe CAB-SPM was then utilized to provide a more functional measurement of the influence of these

physicochemical properties on the surface interfacial interaction of conditioned FP samples with FP, SX and lactose monohydrate substrate surfaces. These data were further compared to the in vitro performance of binary and tertiary DPI formulations containing the micronised (used as received) and laagered FP samples.

3.3.1 Physicochemical Characterization

Representative XRPD profiles of the Day 0, LH90, HH90 and HT FP samples are shown in Figure 3.5 (other time point traces are not shown). The presence of distinct peaks in the XRPD profiles between 10° and 40° angle 2θ for all samples suggested that all FP samples were of the same polymorphic form and that conditioning of FP samples under the environments and periods chosen in this study did not alter the crystalline form (Kubavat *et al.,* 2012). There was, however, a broad diffuse peak below 10° angle 2θ for both the LH90 and HH90 samples. The origin of this peak was not fully understood but might suggest either incorporation of greater randomness within the crystalline structure or possible changes in preferred orientation of the crystallites upon packing into the instrument caused by extended exposure to low and high relative humidity.

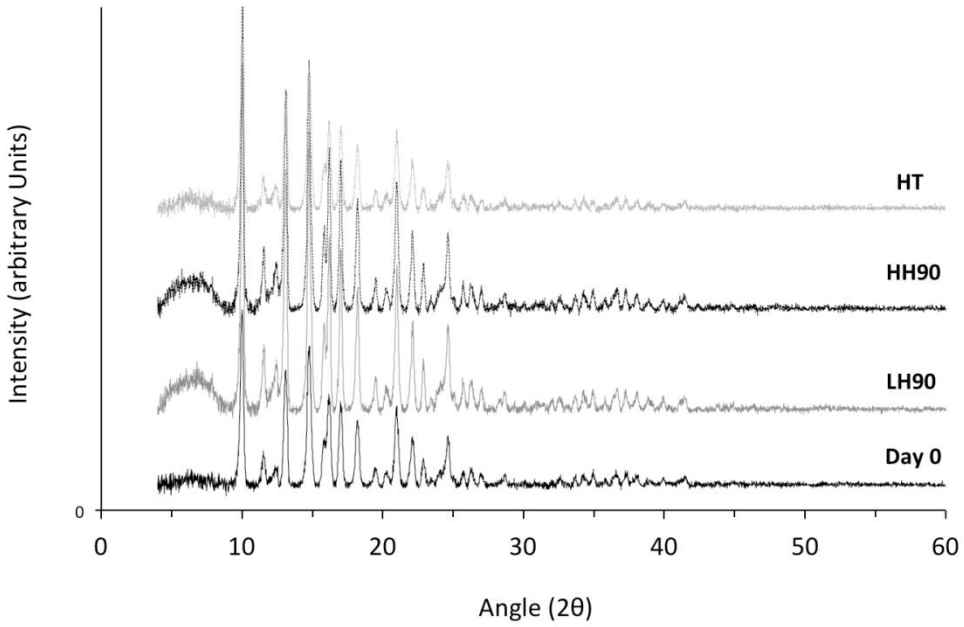

Figure 3.5: X-ray powder diffraction profiles for Day 0, LH90, HH90 and HT FP samples

Representative DSC thermographs of the Day 0, LH90, HH90 and HT FP samples are shown in Figure 3.6. Thermal analysis of all samples (other time point traces not shown) indicated that all materials had an onset of melting at approximately 295 °C, which was related to the melting point for form I of FP (Pitchayajittipont *et al.,* 2009). Again, the DSC data further supported the same polymorphic form of all FP samples.

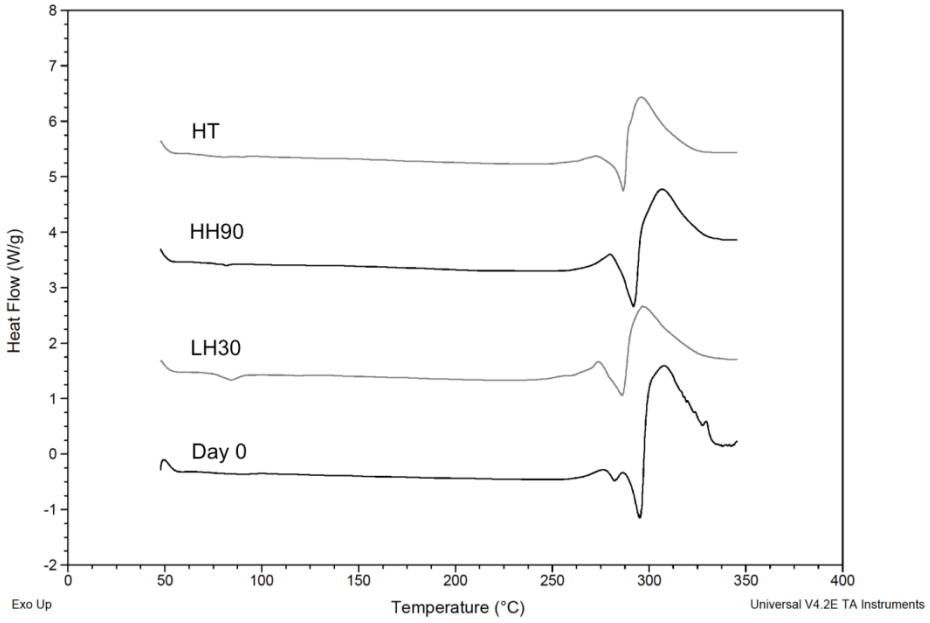

Figure 3.6: Differential scanning calorimetry (DSC) thermographs for the Day 0, LH90, HH90 and HT FP samples

PSD of Day 0 and all laagered FP samples are summarized in Table 3.2. These data showed that while the PSD was relatively insensitive to laagering at HT, laagering of FP under controlled humidity conditions led to some observable changes in the PSD of laagered FP samples. For example, upon exposure to LH, the d_{50} of FP showed an increase at 30 days (2.74 µm), followed by a decrease at 60 days (2.18 µm) and an increase at 90 day (2.68 µm) where the d_{50} remained below the initial value (2.41 µm). A similar qualitative trend was observed for HH samples.

The corresponding surface areas measured by laser diffraction and BET, as well as the R_a of the FP samples are tabulated in Table 3.2. The SSA

measurements followed, in most cases, a similar qualitative trend to that observed in the particle size and S_v measurements by laser diffraction. For example, upon exposure to 33 % RH, there were noticeable increase and subsequent decrease in the SSA at 60 and 90 days, respectively, with respect to SSA at 30 days.

However, an anomalous finding was observed for the HH90 FP sample. Unlike the particle size and S_v data of HH 30 and HH 60, the HH90 FP sample showed a significant decrease in the SSA accompanied by a noticeably smaller value of R_a with respect to all other FP samples. This observation indicated a marked reduction in the surface roughness of the HH90 FP sample. These data suggested that the morphology of the HH90 FP sample differed considerable from the other laagered FP samples.

Representative SEM images of the Day 0, HT, LH90 and HH90 FP samples are shown in Figure 3.7. With the limited spatial resolution of the SEM, it is difficult to quantitatively discern morphological and surface roughness differences of the Day 0 FP sample from the HT and LH90 FP samples. However, it appeared that laagering under high humidity conditions (HH90) created a noticeable change in morphology, resulting in increased surface smoothening (Figure 3.7) consistent with the decrease observed in the SSA and R_a measurements. However, these topographical changes were not apparent for HH30 and HH60 FP samples (data not shown). The surface transformation of the HH90 FP samples suggested that laagering at high

humidity (>75 % RH) for an extended period of time (60 < t < 90 days) may provide the conditions to overcome the activation energy required for the molecular mobility in the disordered regions to undergo surface reconstruction.

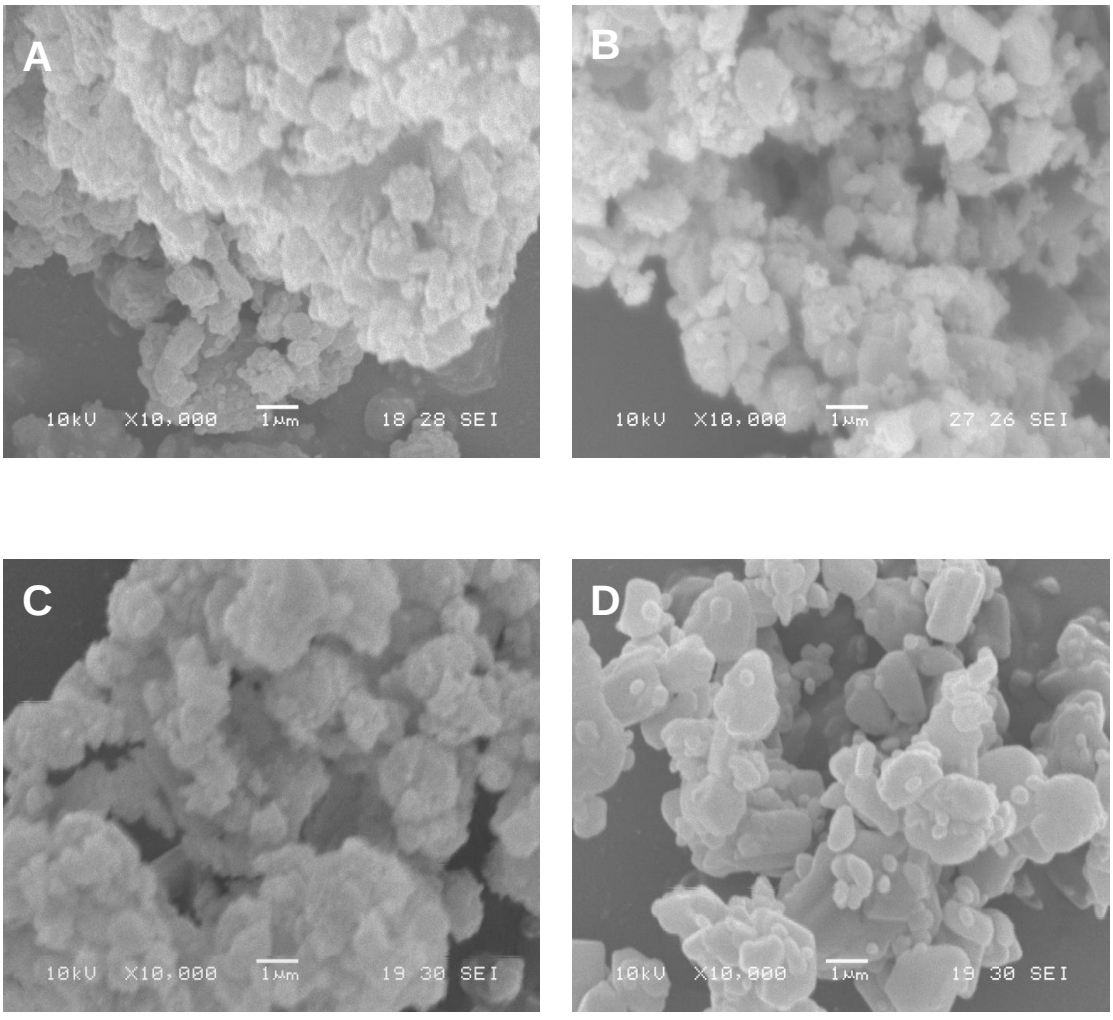

Figure 3.7: Scanning Electron Micrographs for the Day 0 (A), HT (B), LH90 (C) and HH90 (D) FP samples

Table 3.2: Physico-chemical measurements of micronised (Day 0) and laagered samples of FP

FP sample	d_{10} (µm)	d_{50} (µm)	d_{90} (µm)	S_v (m^2/cm^3)	SSA (m^2/g)	R_a	AC (%)[a]	CAB Ratio wrt Lactose	CAB Ratio wrt SX
Day 0	1.12 ±0.01	2.41 ±0.02	4.37 ±0.02	2.29	7.54 ±0.27	3.30	5.05 ±0.20	1.09 ±0.01	2.00 ±0.03
LH30	1.28 ±0.02	2.74 ±0.01	4.99 ±0.03	2.01	7.43 ±0.31	3.70	4.89 ±0.18	1.04 ±0.02	1.83 ±0.01
LH60	0.96 ±0.01	2.18 ±0.01	4.03 ±0.01	2.55	7.98 ±0.18	3.13	4.34 ±0.21	0.92 ±0.01	0.80 ±0.02
LH90	1.29 ±0.01	2.68 ±0.03	4.86 ±0.01	2.02	7.40 ±0.22	3.66	1.12 ±0.20	0.88 ±0.02	0.52 ±0.02
HH30	1.19 ±0.03	2.57 ±0.01	4.72 ±0.02	2.14	7.88 ±0.11	3.68	2.77 ±0.18	0.76 ±0.03	1.44 ±0.02
HH60	0.99 ±0.03	2.22 ±0.02	4.09 ±0.02	2.49	7.49 ±0.21	3.01	1.88 ±0.21	0.93 ±0.02	0.85 ±0.03
HH90	1.08 ±0.01	2.33 ±0.02	4.22 ±0.02	2.36	4.90 ±0.17	2.07	1.29 ±0.20	1.15 ±0.02	0.64 ±0.01
HT	1.14 ±0.02	2.40 ±0.01	4.28 ±0.03	2.27	7.01 ±0.33	3.08	<LOQ	0.74 ±0.01	1.17 ±0.02

[a]AC = amorphous content

3.3.2 Post-micronisation conditioning effects on amorphous content of FP samples

The amorphous contents by TAM for the FP samples are summarized in Table 3.2. These data indicated that all laagering conditions led to a lowering in the amorphous content. Laagering under high temperature (i.e., HT FP sample) reduced the amorphous content to below the limit of quantification (LOQ) of the analytical method. Under ambient temperatures, the partial water vapour pressure surrounding the FP powder and the period of exposure also had a direct effect on the amorphous content. Under high humidity conditions, there was a sharp decrease in the amorphous content of the HH30 and HH60 FP samples. In contrast, under low humidity, there was only a minor decrease in the amorphous content of the LH30 and LH60 FP samples. However, the amorphous contents of the LH90 and HH90 samples were low. Interestingly, while the relaxation pathway of the amorphous disorder was different for FP conditioning under 33 % RH and 75 % RH, as suggested in the previous physiochemical and SEM data, the amorphous content at 90 days was similar for the both conditions, which was around 1.0 %.

3.3.3 Post-micronisation Conditioning Effects on Interfacial Forces

The influence of different laagering conditions on the surface interfacial forces of the micronised and laagered FP samples was investigated by CAB analysis. The individual CAB plots of the FP samples with respect to both lactose monohydrate and SX are shown in figures 3.8-3.10. A summary plot of the

CAB values versus low and high humidity laagering conditions are plotted in Figure 3.11.

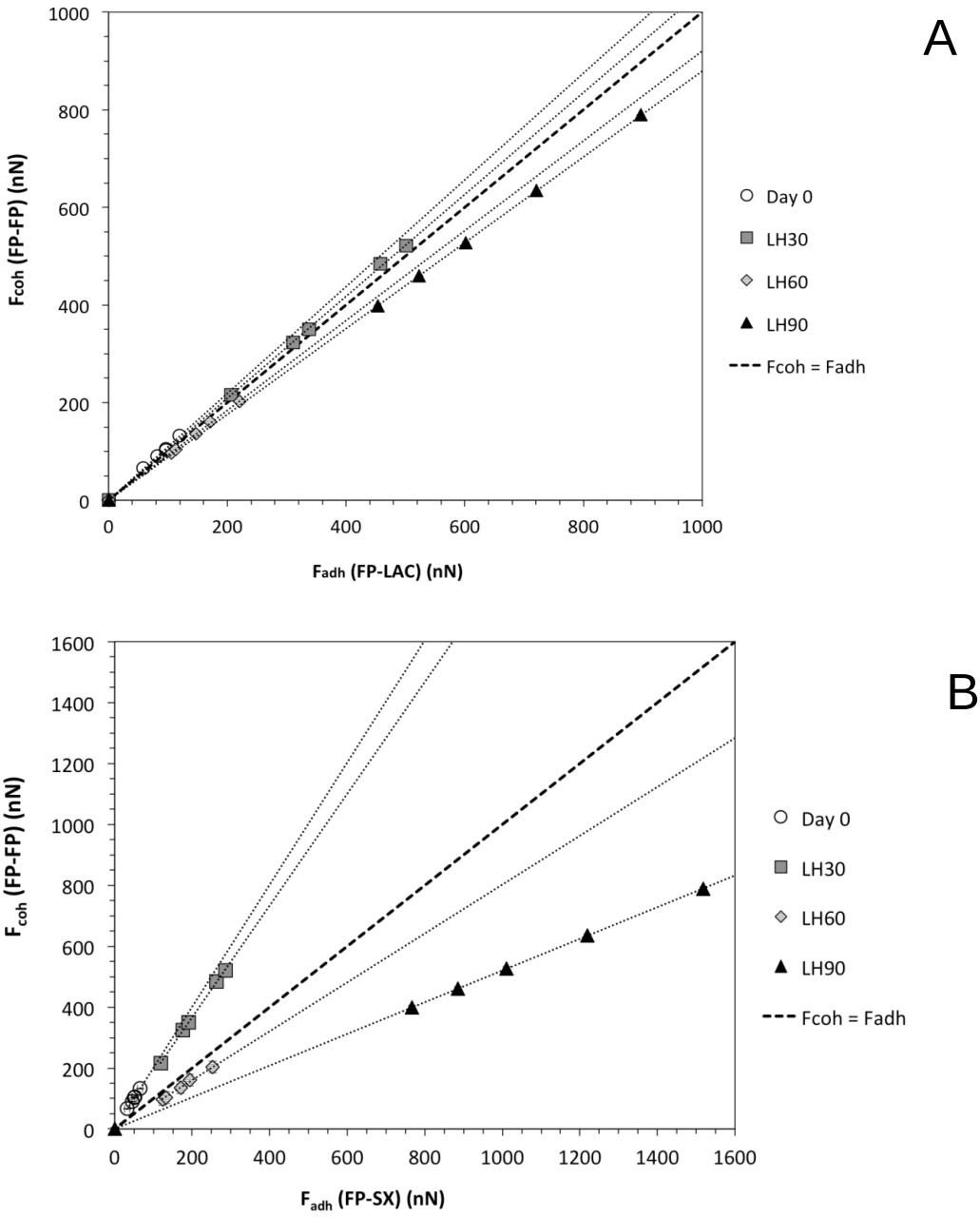

Figure 3.8: (A) Cohesion (F_{coh} (FP-FP)) versus adhesion (F_{coh} (FP-LAC)) plots of the micronised FP sample (Day 0) and samples conditioned at low humidity (LH30, LH60, LH90) with respect to lactose monohydrate, (B) Cohesion (F_{coh} (FP-FP)) versus adhesion (F_{coh} (FP-SX)) plots of the micronised FP sample (Day 0) and samples conditioned at low humidity (LH30, LH60, LH90) with respect to SX.

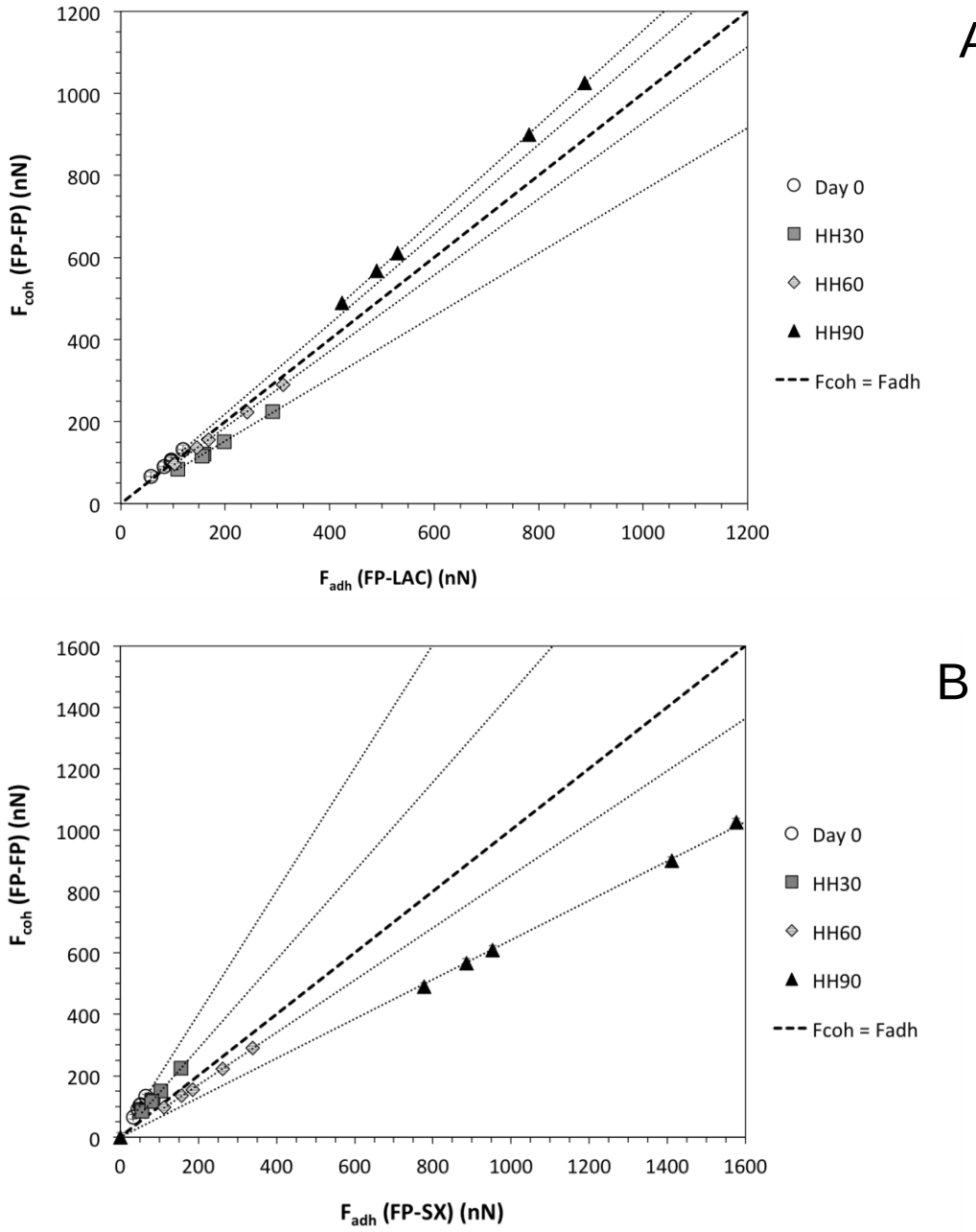

Figure 3.9: (A) Cohesion (F_{coh} (FP-FP)) versus adhesion (F_{coh} (FP-LAC)) of the micronised FP sample (Day 0) and samples conditioned at high humidity (HH30, HH60, HH90) with respect to lactose monohydrate, (B) Cohesion (F_{coh} (FP-FP)) versus adhesion (F_{coh} (FP-SX)) of the micronised FP sample (Day 0) and samples laagered at high humidity (HH30, HH60, HH90) with respect to SX.

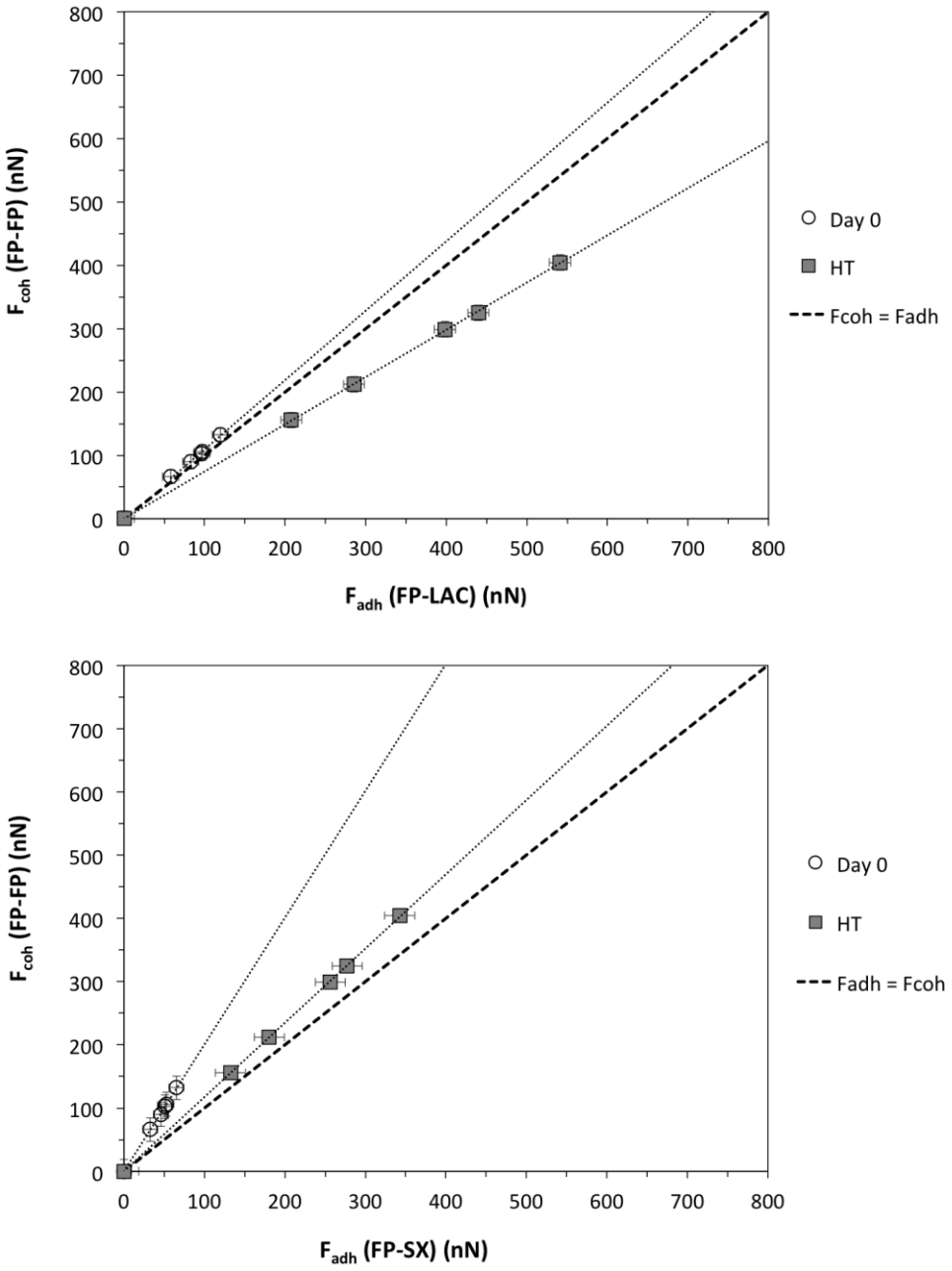

Figure 3.10: (A) Cohesion (F_{coh} (FP-FP)) versus adhesion (F_{coh} (FP-LAC)) of the micronised FP sample (Day 0) and samples conditioned at 60°C (HT) with respect to lactose monohydrate, (B) Cohesion (F_{coh} (FP-FP)) versus adhesion (F_{coh} (FP-SX)) of the micronised FP sample (Day 0) and samples laagered at 60°C (HT) with respect to SX.

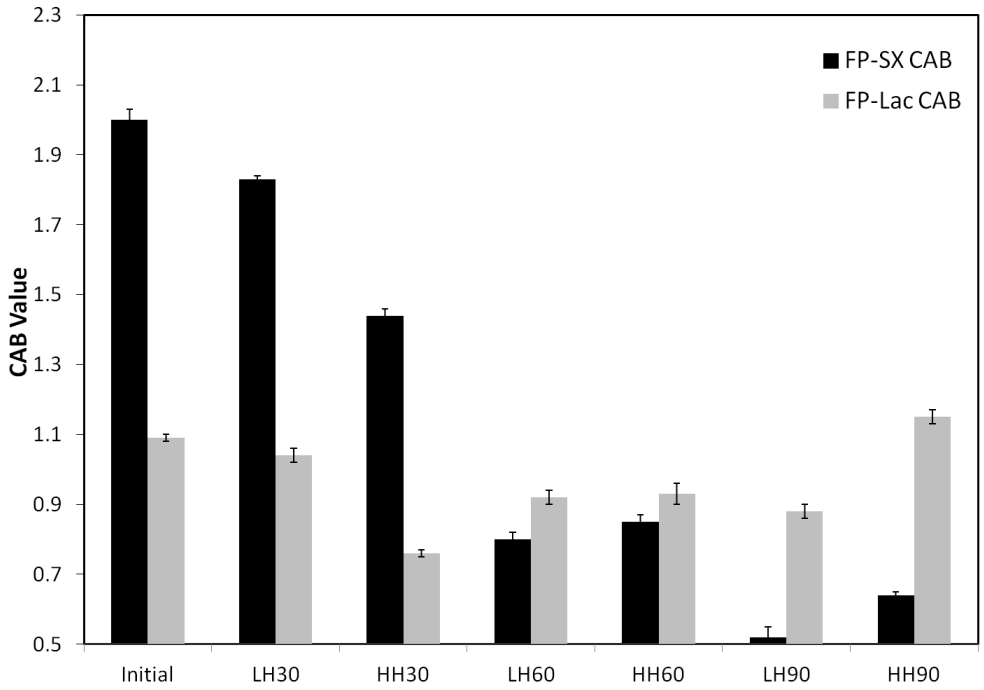

Figure 3.11: Variations in the CAB ratios with respect to lactose monohydrate and SX of micronised FP particles laagered under low and high relative humidity at 30, 60 and 90 day time points.

The CAB ratios with respect to lactose monohydrate for the low humidity laagering conditions indicated a shift from a slightly cohesive-led interaction (FP-FP, CAB ratio > 1.0) for the micronised FP to an adhesive-led system (FP-Lactose, CAB ratio < 1.0) In other words, these data suggested that the adhesion of FP to lactose monohydrate increased upon extended exposure of FP to low humidity conditions. The CAB ratios of the low humidity laagered FP samples with SX (Table 3.2), also indicated that a significant change in the interfacial forces between FP and SX substrates occurred upon laagering. The cohesive nature of the Day 0 FP sample, which was two-fold greater than its affinity to SX, only slightly decreased for the LH30 sample. However, upon laagering at low humidity for 60 days the CAB measurements demonstrated a

significant (p<0.02) shift from a highly cohesive-led system to an adhesive-led (FP-SX > FP-FP) system. This shift to an adhesive (FP-SX)-led system continued for the LH90 FP sample, with the 90 day laagered FP sample shifting the balance of forces to an approximately two-fold greater adhesive (FP-SX) interaction than its cohesive (FP-FP) interaction. These data indicated that laagering micronised FP sample for 90 days at 33 % RH, increased the adhesive interaction to the SX by about four-fold with respect to the as received micronised FP.

The low sensitivity of the FP-lactose CAB interactions and the highly sensitive nature of the FP-SX CAB to surface chemistry of the secondary processed FP have been observed previously by Kubavat et. al. (2012). They also showed that different solvent and anti-solvent conditions during primary crystallization conditions could directly affect the interfacial surface chemistry of the secondary processed FP.

A similar trend in the FP-SX CAB measurements was observed upon laagering under high humidity conditions. However, the FP-lactose CAB measurements did not follow a similar trend as the low humidity laagered FP samples. As reflected in the CAB ratios relisted in Table 3.2, initial exposure to elevated humidity increased the adhesive tendency of FP to lactose monohydrate (HH30), to a greater extent than 90-day exposure at 33 % RH (i.e., LH90 FP sample). However, both 60 and 90 day exposure to 75 % RH subsequently reduced the adhesive tendency of the laagered FP samples to lactose

monohydrate. As a result, the HH90 sample exhibited a greater cohesive tendency than its interaction with lactose monohydrate. Such findings have been previously seen between a partially and fully mechanically relaxed new chemical entity (Shur *et al.,* 2007). It should also be noted that in Table 3.2 the HH90 FP sample showed both the greatest cohesive tendency with respect to lactose monohydrate and a relatively high adhesive tendency to SX. This unique combination of changes in the interactive force measurements is most likely due to the structural reconstruction of the FP surface as indicated by the marked decrease in SSA and rugosity values of the HH90 FP.

High temperature conditioning of FP at 60°C led to the greatest increase in the adhesive tendency of the FP to lactose monohydrate, with respect to the cohesive interaction (Table 3.2). However, for the FP-SX CAB measurements, while exhibiting a significant (p<0.05) decrease in cohesiveness (Fig. 6B), the HT sample failed to shift the dominant force to an adhesive led system that was observed with laagered FP samples under high and low humidity conditions.

Table 3.3: In vitro formulation performance, as measured by the mass balance (MB), impactor stage mass (ISM), mass median aerodynamic diameter (MMAD), geometric standard deviation (GSD) and fine particle mass ($FPM_{<5\mu m}$), from the aerosolization of binary and tertiary DPI formulations of freshly micronised and laagered FP samples (n=3). Note that the large SDs in some APSD data below were related to variations in device losses between the repeated runs

Sample Binary wrt FP	%RSD (%)	MB (%)	ISM (µg ± S.D)	MMAD (µm ± S.D)	GSD (µm ± S.D)	FPM (µg ± S.D)
Day 0	1.3	92.6	32.07 ± 0.90	3.80 ± 0.03	2.01 ± 0.00	29.02 ± 0.80
LH30	0.9	103.8	35.39 ± 8.14	3.65 ± 0.04	2.04 ± 0.02	31.60 ± 7.57
LH60	1.0	91.1	48.58 ± 0.73	4.22 ± 0.01	2.03 ± 0.00	46.74 ± 0.40
LH90	1.8	105.4	57.68 ± 0.50	4.24 ± 0.01	2.05 ± 0.01	55.67 ± 0.37
HH30	1.0	97.0	29.01 ± 0.39	4.28 ± 0.01	2.15 ± 0.02	28.82 ± 0.34
HH60	1.6	92.4	36.50 ± 1.38	4.08 ± 0.13	2.00 ± 0.02	34.06 ± 0.58
HH90	2.2	98.8	47.16 ± 0.67	3.92 ± 0.01	2.01 ± 0.00	43.27 ± 0.57
HT	1.4	93.4	37.26 ± 1.06	4.06 ± 0.05	1.99 ± 0.02	34.88 ± 1.11
Tertiary wrt FP	**%RSD** **(%)**	**MB** **(%)**	**ISM** **(µg ± S.D)**	**MMAD** **(µm ± S.D)**	**GSD** **(µm ± S.D)**	**FPM** **(µg ± S.D)**
Day 0	3.0	90.6	36.18 ± 3.77	4.76 ± 0.26	2.04 ± 0.01	37.19 ± 2.57
LH30	1.6	98.4	46.03 ± 8.13	4.37 ± 0.32	2.01 ± 0.07	43.89 ± 9.86
LH60	1.4	92.0	40.61 ± 2.17	4.54 ± 0.09	1.93 ± 0.04	39.59 ± 1.02
LH90	2.2	93.2	60.48 ± 0.30	3.90 ± 0.02	2.01 ± 0.02	55.50 ± 0.04
HH30	1.0	99.1	32.75 ± 0.36	4.28 ± 0.02	1.91 ± 0.02	30.84 ± 0.16

HH60	1.3	90.6	43.70 ± 6.20	3.62 ± 0.03	1.91 ± 0.02	37.70 ± 5.29
HH90	1.9	97.0	52.79 ± 0.65	3.53 ± 0.01	1.94 ± 0.00	45.44 ± 0.57
HT	2.1	91.5	29.78 ± 1.71	4.08 ± 0.26	1.87 ± 0.12	27.14 ± 3.42

Tertiary wrt SX	**%RSD (%)**	**MB (%)**	**ISM (µg ± S.D)**	**MMAD (µm ± S.D)**	**GSD (µm ± S.D)**	**FPM (µg ± S.D)**
Day 0	5.5	91.3	8.09 ± 0.57	3.77 ± 0.05	2.18 ± 0.06	7.60 ± 0.38
LH30	2.8	97.1	11.02 ± 1.66	3.24 ± 0.17	2.15 ± 0.01	9.64 ± 1.60
LH60	1.9	95.2	11.43 ± 0.11	3.00 ± 0.12	2.75 ± 0.33	10.56 ± 0.46
LH90	2.1	97.4	11.87 ± 0.19	3.02 ± 0.07	2.47 ± 0.04	10.72 ± 0.12
HH30	2.7	91.7	10.07 ± 1.36	2.97 ± 0.05	2.06 ± 0.01	8.32 ± 0.38
HH60	2.5	96.5	10.71 ± 0.19	2.71 ± 0.19	2.48 ± 0.05	9.07 ± 0.42
HH90	2.6	97.4	14.57 ± 0.63	2.29 ± 0.10	2.80 ± 0.06	12.32 ± 0.40
HT	1.6	96.8	8.53 ± 0.57	2.80 ± 0.06	2.57 ± 0.14	6.63 ± 0.37

3.3.4 Drug content uniformity

The relative standard deviation (RSD) measurements of the drug content for binary and tertiary DPI formulations containing micronised and laagered FP are shown in Table 3.3. For all binary DPI formulations, the RSDs were ≤ 2.5 %, indicating homogeneity of the prepared mixtures. In the tertiary DPI formulations, the RSDs for FP were ≤ 3 %, while for SX were ≤5.5 %, which suggested a homogeneous distribution of the two active ingredients in the formulated mixtures.

3.3.5 *In vitro* aerosolization performance of binary DPI formulations

The in vitro APSD characterization of binary DPI formulations containing lactose monohydrate and micronised or laagered FP sample are summarized in Table 3.3. The MMAD and FPM are also plotted as a function of LH and HH laagering conditions in Figure 3.12, together with a plot of their respective FP-lactose CAB values. For the HT FP sample, there was a significant ($p<0.05$) increase in the FPM and MMAD with respect to the Day 0 FP sample. Similarly, there was also a significant ($p<0.05$) increase in MMAD and FPM of the LH FP samples over 60 and 90 days, with respect to the Day 0 and LH30 samples.

These differences in APSD of the HT and LH FP samples did not appear to be directly related to changes in the material physical properties (e.g. particle size and surface area). The CAB measurements, however, suggested that the balance of forces for the LH FP samples shifted from being cohesive at Day 0 and 30 day exposure to being adhesive following laagering for 60 and 90 days. This was also observed from the Day 0 to HT FP sample. Such a shift in the nature of interaction force corresponds with an increase in MMAD of the formulations, which might be related to formation of API/fines agglomerates owing to the higher adhesive affinity of LH60 and LH90 FP samples to lactose monohydrate fines. It should be noted that with the high levels of intrinsic lactose monohydrate fines (< 4.5 µm) present in the ML001 grade of lactose (ca. 10-15 % w/w), a shift in the balance of forces between FP and lactose monohydrate has been previously shown to lead to a greater elutriation and deaggregation efficiency of FP from the coarse carrier surfaces due to stable

agglomerate formation with lactose monohydrate fines (Jones *et al.,* 2008a; Shur *et al.,* 2008). This mechanism of agglomerate formation, suggested by Jones et. al., indicated that a greater adhesive affinity between API and lactose monohydrate led to a significant increase in MMAD and fine particle mass deposited (Jones *et al.,* 2008a).

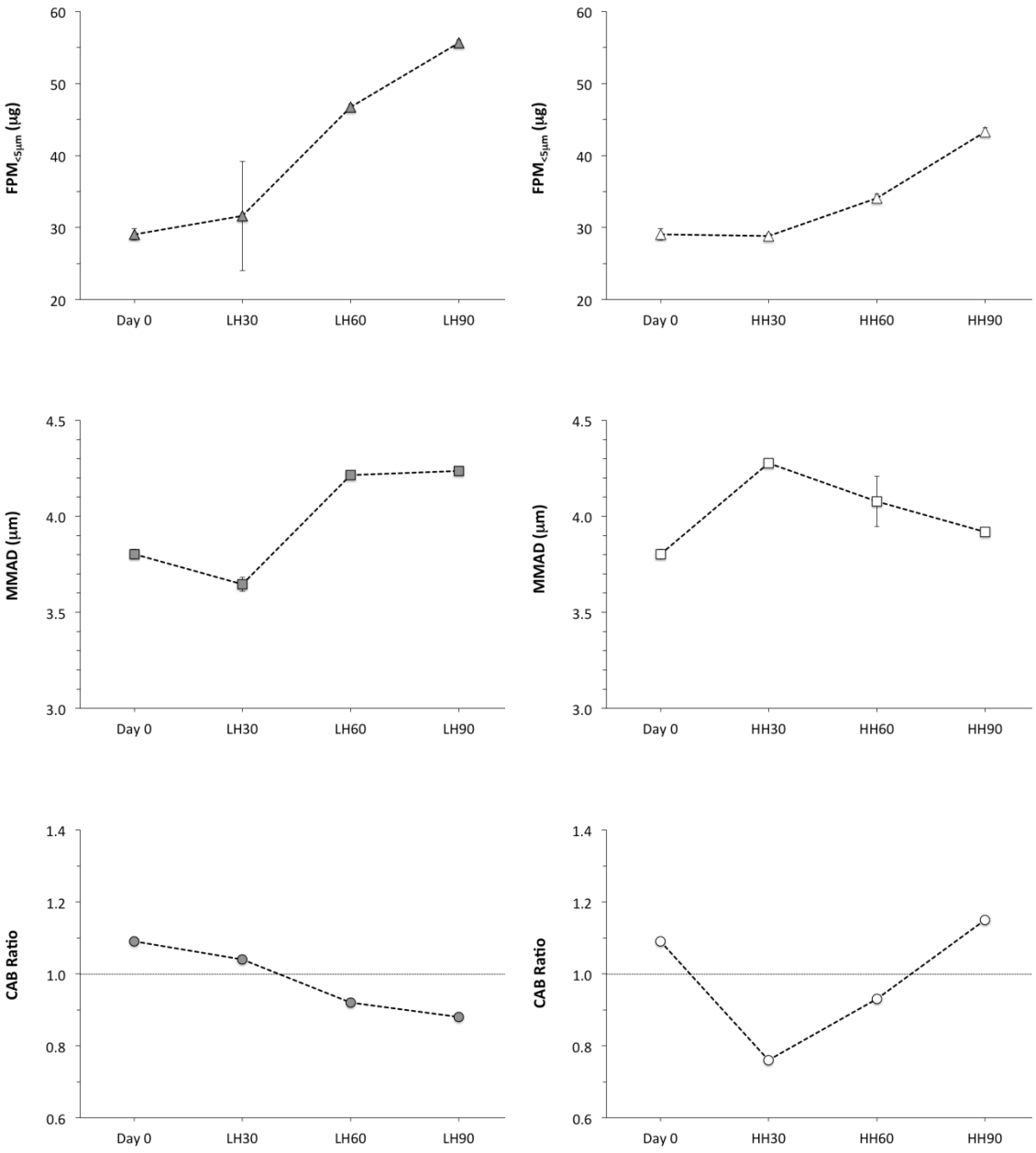

Figure 3.12: In vitro aerosolization performance of FP in binary DPI formulations upon laagering a batch of micronised FP under low and high relative humidity for 30, 60 and 90 days. The corresponding CAB ratios with respect to lactose monohydrate under such conditions are also plotted.

Laagering FP samples under high humidity conditions for 30, 60 and 90 days also had a significant effect on APSD of the carrier-based DPI formulations (Figure 3.12, Table 3.2). Laagering for 30 days under high humidity conditions led to an increase in the MMAD but no significant change in FPM. The increase in MMAD is in agreement with the slight changes in PSD and SSA measurements, and the relative increase in adhesion to the lactose monohydrate, as measured by CAB, which may aid formation of API/lactose monohydrate fines agglomerates (Begat *et al.,* 2004; Jones *et al.,* 2008a). Increasing the period of laagering at the high humidity condition led to an increase in FPM accompanied by a decrease in MMAD (close to but slightly higher than that of the Day 0 FP sample) over 90 days. It was not evident that a single parameter was responsible for or could be used to explain this unique change in formulation performance. Nevertheless, the trends observed here might be related to the combined effect of changes in the physical shape, morphology and interfacial properties of the HH FP particles that may affect the formulation microstructure during processing and formulation performance. Further research is warranted to better understand the fundamental factors and possibly their interactions that influence the performance of binary DPI formulation containing HH30 and HH90 FP samples.

3.3.6 *In vitro* aerosolization performance of tertiary DPI formulations

The in vitro APSD characterization of tertiary DPI formulations containing lactose monohydrate, SX and micronised or laagered FP samples are summarized in Table 3.3. The MMAD and FPM of SX are plotted together with

the FP-SX CAB values in Figure 3.13. As mentioned above, an aged batch of micronised SX (> 12 months) was used. Cohesive-adhesive balance (CAB) measurements indicated that there was no noticeable difference in the interfacial properties of the SX during the duration of the study (The average CAB ratio of SX with respect to lactose monohydrate over the different time points was 1.85 ± 0.13).

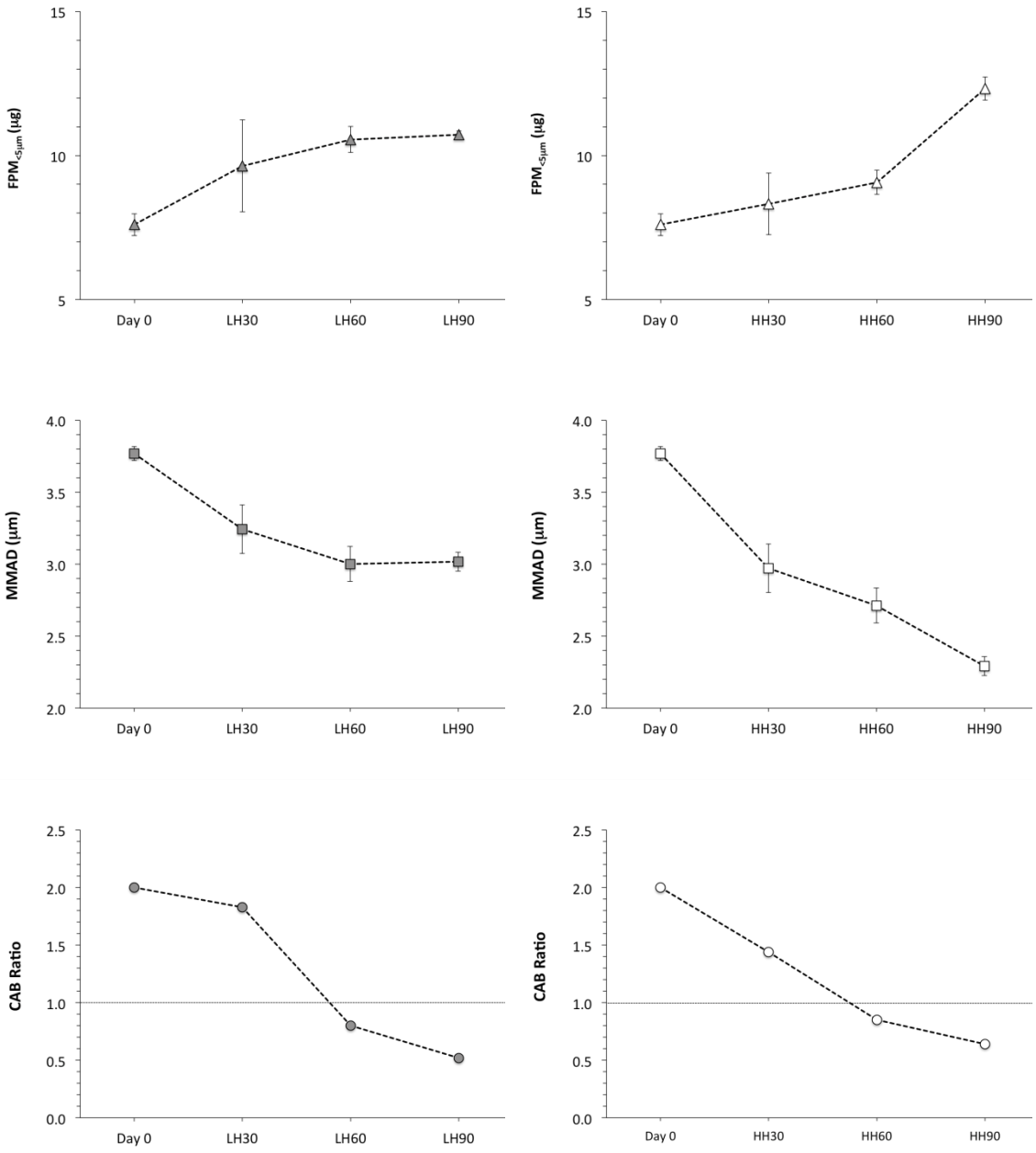

Figure 3.13: In vitro aerosolisation performance of SX in combination with FP in tertiary formulations upon laagering a batch of micronised FP under low and high relative humidity for 30, 60 and 90 days. The corresponding CAB ratios with respect to SX under such conditions are also plotted.

The aerosolization performance of FP were not significantly ($p>0.05$) affected by laagering at low humidity over 60 days. However, extended laagering ($60 < t < 90$ days) led to a significant ($p<0.05$) increase in FPM and a smaller MMAD. Laagering under high humidity, similar to the binary DPI formulations, extended laagering appeared to progressively affect the aerosolization performance of the FP component in the tertiary formulations. However, increasing laagering increased the FPM but decreased the MMAD of the FP component in the presence of SX, whereas for the binary formulation extended laagering showed an initial marked increase followed by a gradual decrease in FP MMAD and a consistent increase in FP FPM. For the SX component, increasing the period of laagering led to an increase in FPM recovery of SX and a decrease in MMAD of the SX component for LH and HH FP samples.

The aerosolization performance of the tertiary DPI formulations (particularly with respect to the SX component) appeared to be sensitive to shift in the balance of forces between FP and SX upon FP laagering. As has been indicated in a number of studies, the greater the adhesive tendency between FP and SX, the more significant is the improvement in aerosolization performance of SX (Kubavat *et al.,* 2012; Jones *et al.,* 2008a; Jones *et al.,* 2008b). These studies proposed that higher deaggregation efficiency of the SX occurred as a result of the greater propensity of FP and SX to form fine particle agglomerates during blending. Similar observations have also been reported for suspension MDI formulations comprising of FP and SX (Rogueda *et al.,* 2011). However, additional studies will be needed to fully understand the

complex relationships between the interfacial properties and aerosolization performance for such tertiary systems.

3.4 CONCLUSIONS

The ability to understand and predict interparticulate forces of secondary processing of APIs in DPI systems is critical in our ability to predict and optimize DPI product performance. The relative magnitudes of the cohesive (drug-drug) and adhesive (drug-excipient, drug 1-drug 2 such as FP-SX) forces and how primary and secondary processing of drug materials may directly impact these interparticulate forces is a major research objective. This study shows that the relative magnitudes of cohesive-to-adhesive forces of secondary processed FP are a direct function of the conditioning environment and duration. While the time to re-equilibrate the FP particles from their unstable amorphous state to the thermodynamically stable crystalline state can be expedited, laagering is an essential parameter requiring controlled conditions of temperature and relative humidity. Unlike high temperature, humidity based conditioning failed to completely eliminate amorphous related disorders and significantly affected the relative balance of the adhesive and cohesive forces during storage. A significant morphological and topographical change was seen following the conditioning of FP under high humidity for 90 days, suggesting a surface reconstruction event. This study clearly shows that the different post-micronisation laagering conditions translated into different interfacial behavior, accompanied by significant changes in product performance characterized by APSD measurements by cascade impaction. However, the fundamental factor(s) and mechanism(s) responsible for the

observed differences in product performance are not fully understood for the complex formulations in DPIs investigated here. Therefore, the present study clearly indicates the critical importance and need for more research in understanding the physical, chemical and interfacial properties of secondary processed materials and their subsequent effect on the product performance.

4 The Stress Relaxation Dynamics of Micronised Salmeterol Xinafoate

4.1 INTRODUCTION

The importance of developing a product with stable critical quality attributes dictates the necessity of having thermodynamically stable active pharmaceutical ingredients. This allows for drug products to not only meet release specifications, but to also remain compliant throughout their shelf-life. This is only possible if post-micronisation kinetics are fully understood as a function of both time and storage conditions. There is a limited amount of published data regarding the influence of relative humidity on the dispersibility of salmeterol xinafoate (SX) powder blends (Das *et al.,* 2009; Adi *et al.,* 2006; Adi *et al.,* 2008). These studies have provided only a limited understanding of the between post-micronisation relaxation kinetics and subsequent aerosolisation performance.

This study investigates the kinetics with which SX reverts back to its more stable crystalline state following micronisation. Conditioning is employed to understand the potential of expediting the stress relaxation profile for micronised SX. This work will look into understanding the physical, chemical and interfacial trends followed during the stress relaxation period, and also relates these trends to *in vitro* aerosolisation performance.

Salmeterol is a long acting β_2 (2)-adrenoceptor agonist (LABA) prescribed for the treatment of asthma and COPD. β_2 (2)-receptor stimulation leads to the relaxation of bronchial smooth muscle, bronchodilation and increased bronchial airflow (Chowdhury and Pan, 2010). SX has a molecular weight of

603.75 and is chemically described as $C_{25}H_{37}NO_4.C_{11}H_8O_3$. It is sparingly soluble in water and has a partition coefficient (logP) of 4.2, reflecting its highly hydrophobic nature. Capillary actions between SX and water are quantified in a contact angle of 67.7°. (Das *et al.,* 2009)

4.2 MATERIALS AND METHODS

4.2.1 MATERIALS

Salmeterol Xinafoate (SX) was purchased from Merck Generics (Potters Bar, UK) and was shipped immediately after being micronised. The sample was packed at low humidity and transported over dry ice. Hydrofluoroalkane 134a (HFA 134a) is an inert gas with a chemical name of 1,1,1,2-Tetrafluoroethane. It has a molecular mass of 102.03 and a molecular formula of CH_2FCF_3. HFA 134a is a non-polar propellant widely used in aerosol products. HFA 134a was purchased from Mexichem, Cheshire, UK (Batch number 003215).

4.2.2 METHODS

4 grams of micronised SX were sampled upon delivery for full physicochemical characterisation. The remaining SX was separated into the four samples of 5 grams each. Three of these samples were put in their respective chambers for environmental conditioning as tabulated in table 4.1. The other sample was conditioned with HFA-134a.

4.2.2.1 Environmental Conditioning

The environmental conditions used for this study were as follows; low humidity at ambient temperature (LH) (25C, 33 % RH), high humidity at ambient temperature (HH) (25C, 75 % RH), and ambient humidity at a high temperature (T) (60°C, 44 %RH). 2 grams were taken from each conditioning chamber at 30 and 60 days for full characterisation and formulation. Samples were sieved through a 500 µm mesh sieve prior to characterisation.

4.2.2.2 *In situ* conditioning

Freshly micronised SX was *in-situ* conditioned in HFA by the addition of 5 grams of SX in 80 grams of HFA 134a in a pressurised vessel (Mexichem Fluor, Cheshire, UK). The HFA was directly inserted into a pressurised vessel and kept under pressure for 21 days. The vessel was then de-pressurised at a rate of 0.1 bar per minute. The conditioned SX was then dried in controlled ambient conditions (25C, 33 % RH) for 12 hours and sieved through a 500 µm mesh sieve prior to characterisation and formulation.

Table 4.1 describes the conditioning and sampling protocol used throughout this study together with their corresponding sample reference.

Conditioning Environment	Conditioning Period	Sample Reference
Freshly Micronised	Day 0	Initial
25°C, 33 %RH	30 Days	LH30
	60 Days	LH60
25°C, 75 %RH	30 Days	HH30
	60 Days	HH60
60°C, 44 % RH	30 Days	T30
	60 Days	T60
HFA	21 Days	HFA

Table 4.1 Summary of SX samples studied throughout this work

4.2.2.3 Particle Size Analysis of SX

The particle size distribution (PSD) for all samples was determined in the wet state using a Sympatec HELOS and CUVETTE (Sympatec GmbH, Clausthal-Zellerfeld, Germany). Each measurement was performed in triplicate and particle size analysis was performed using WINDOX 5.0 software (Sympatec GmbH, Clausthal-Zellerfeld, Germany).

4.2.2.4 Scanning Electron Microscopy of SX samples

The morphology of the SX samples was investigated using scanning electron microscopy (SEM). Sample aliquots were fixed onto sticky carbon tabs (Agar Scientific, Cambridge, UK) followed by removal of excess powder using

pressurised air. Samples were subsequently sputter coated with gold (Edwards Sputter Coater S150B, Edwards High Vacuum, Sussex, UK) to achieve a thickness of approximately 20 nm. Imaging was performed using a scanning electron microscope (JEOL JSM6480LV, Tokyo, Japan) using 15 kV accelerating voltage.

4.2.2.5 X-ray powder diffraction (XRPD) analysis of SX samples

The X-ray powder diffraction (XRPD) patterns of SX samples were analysed on a Bruker Powder Diffractometer (D8; Bruker AXS Inc., Madison, USA) using CuKα radiation (λ=1.54 Å). The data were collected over a single 2θ sweep with range 2θ = 5 - 30° and a step size of 0.025°/step with a step time of 1.5 s.

4.2.2.6 Differential Scanning Calorimetry of SX samples

The thermal properties of all samples were investigated using a differential scanning calorimeter (DSC 2920, TA Instruments, Surrey, UK), calibrated with an indium standard. Approximately 3 mg of sample were accurately weighted into an aluminium pan and crimped with a lid to form a hermetic seal. The sample and reference pan were heated at a rate of 10°C/min from 30°C to 240°C. The calorimeter head was continuously flushed with dry nitrogen gas at 0.2 L/min during all measurements.

4.2.2.7 Specific Surface Area by BET of SX samples

The specific surface area (SSA) of SX samples was measured using a Gemini 2360 surface area analyser (Micromeritics Instrument Corporation, Norcross, USA). A five-point BET nitrogen adsorption analysis was carried out in triplicate after degassing the samples for 24 hours in a FlowPrep 060 degasser (Micromeritics Instrument Corporation, Norcross, USA).

4.2.2.8 Rugosity Calculation

Rugosity (R_a) is the qualitative description of the surface roughness of particles. It is mathematically described in Equation 5.1 (Joshi *et al.,* 2002). It uses the particles' surface volume result obtained from particle size measurement and the specific surface area value achieved from BET analysis. The validity of rugosity values for comparative reasons relies on the lack of change to macroscopic shape.

$$R_a = \frac{\text{Measured BET Surface Area (SSA)}}{\text{Calculated Surface Area from Particle Size Measurements } (S_v)}$$

Equation 5.1

4.2.2.9 Cohesive-Adhesive Balance Measurements

4.2.2.9.1 Crystallisation of substrates

To perform quantitative binary and combination AFM-CAB analysis of secondary processed SX samples, smooth single crystal surfaces of Salmeterol Xinafoate (SX), Fluticasone Propionate (FP) and lactose monohydrate were produced. Briefly, saturated solutions of SX in 2 ml of acetone were prepared and sonicated prior to filtration via a 0.22-µm PTFE membrane filter (Whatman Inc., Clifton, NJ, USA). SX was crystallised using water as the anti-solvent. Briefly, a microscope cover slip (12 mm x 12 mm) was supported on a vertical post in a crystallisation dish that contained the anti-solvent. A droplet of the saturated solution of the API was then placed on the coverslip using a syringe attached to the 0.22-µm-membrane filter. The system was sealed by inverting a glass lid in the crystallisation dish to allow vapour phases of the miscible solvents to come into equilibrium resulting in heterogeneous nucleation and crystal growth within the droplet. The glass cover slip was then attached to a magnetic AFM stub.

Lactose and FP were crystallized upon introduction of saturated droplets between two glass cover slips. Smooth lactose crystals were generated upon preparing a solution of lactose in double-distilled water, which was heated to 100 °C with constant stirring. The heated saturated droplet of the solution was filtered through a 0.2 µm PTFE membrane filter (Whatman Inc., Clifton, NJ, USA) and placed on to the centre of a clean cover slip, which was then sandwiched by placing another cover slip over the droplet. Similarly, a solution of FP (0.75 gm^{-1}) was prepared in methanol following sonication for 30 mins,

following which the solution was filtered through a 0.2 µm PTFE membrane filter and a droplet of this solution was then sandwiched between two coverslips. The resulting crystals of lactose or FP were then isolated upon cleaving the coverslips apart and attaching each coverslip to a magnetic AFM stub.

4.2.2.9.2 Colloidal probe force measurements

Prior to colloidal force measurements, individual particles from each sample of SX were attached onto standard V-shaped tipless cantilevers with pre-defined spring constants (DNP-020, DI, CA, USA) using an epoxy resin glue (Araldite, Cambridge, UK). Five probes were prepared for the as received, LH, HH and T conditioned SX samples at each pre-defined laagering stage. All probes were examined with an optical microscope (magnification 50x) to ensure the integrity of the attached particle, before allowing the thin layer of glue to cure and dry.

Single crystal substrates were loaded onto an AFM scanner stage, which was enclosed in a custom-built environmental chamber, in which the ambient conditions were maintained at a constant temperature of 25 °C (± 1.5 °C) and relative humidity of 35 % RH (± 3 %). The interaction forces were measured by recording the deflection of the AFM cantilever as a function of the substrate displacement (z) by applying Hooke's Law. Individual force curves (n = 1024) were conducted over a 10 µm x 10 µm area at a scan rate of 4 Hz and a compressive load of 40 nN.

A custom-built software was developed to extract data contained within each force-volume dataset. These data was analyzed to ensure normal distribution, indicating uniform contact area between the drug probe and the smooth substrate surfaces. Arithmetic mean and standard deviation were measured to produce CAB plots for the interactions of the different batches of SX with both lactose monohydrate and FP.

4.2.2.10 Preparation of powder formulations

SX binary formulations (0.2 % $^{w}/_{w}$) were manufactured using freshly micronised and conditioned samples of SX (HFA, LH30, HH30, T30, LH60, HH60, T60). Blends were manufactured by the sequential addition of the drug to the milled lactose (ML001) followed by low shear blending using a T2F Turbula® mixer (Wily A Bachofen AG, Basel, Switzerland) for 45 minutes at 46 rpm.

SX/FP combination formulations were also prepared for each sample containing FP (1.0 % $^{w}/_{w}$) (Chemagis Bnei Brak, India) and SX (0.2 % $^{w}/_{w}$).

Each blend was filled into size 3 hydroxypropylmethyl cellulose (HPMC, Shionogi Qualicaps, Madrid, Spain) capsules with a fill weight of 25 ± 1 mg. The loaded dose for the SX binary formulations was 50 µg salmeterol per 25 mg. For the FP/SX combination formulations, the loaded doses were 250 µg of FP and 50 µg of salmeterol per 25 mg fill weight. The capsules were stored at 44 % RH for 24 hours prior to in vitro testing to ensure the dissipation of any electrostatic charges introduced during processing.

4.2.2.11 In vitro aerosolisation studies

Aerosolisation performance of the formulations was tested using a next generation impactor (NGI, Copley Scientific, Nottingham, UK) with pre-separator, which was connected to two vacuum pumps to create sonic flow (GE Motors). The pre-separator contained 15 ml of mobile phase. The NGI cups were coated with 1 % $^{v}/_{v}$ silicone oil in hexane to eliminate any particle bounce. For each experiment, two individual 25 mg capsules of the same blend were discharged into the NGI at 55 L/min for 4.4s, equivalent to a total volume of 4 L, from a Rotahaler® DPI device (Cipla, Mumbai, India). Before each test, the flow rate was verified with a flow meter (DFM 2000, Copley Scientific, Nottingham, UK). The amount of API deposited on each part of the NGI was determined by High Pressure Liquid Chromatography (HPLC). This testing protocol was repeated three times for each blend, following which, the mass median aerodynamic diameter (MMAD) geometric standard deviation (GSD), fine particle mass (FPM) and fine particle fraction (FPF) were determined.

4.2.2.12 HPLC analysis of SX and FP

High Pressure Liquid Chromatography (HPLC) was used to quantify the drug content. For the determination of drug content in SX binary formulations, the HPLC method consisted of a pump coupled to an auto-sampler and multi-wavelength UV detector (Agilent 1200, Wokingham, UK) set at 235 nm. The pump flow rate was set to 1.5 mL/min through a Hypersil ODS-C_{18} column (Fisher Scientific, Loughborough, UK, column length 250 mm, internal

diameter 4.6 mm, and particle size of the packing material 5 μm), which was placed in a column oven (Agilent, Wokingham, UK) set to 40°C. The mobile phase consisted of methanol, acetonitrile and water (45:35:20 % $^{v}/_{v}$). The elution time for the SX peak using this method was 6.7 minutes. For the drug content determination of FP/SX combination formulations, the HPLC method used a flow rate of 1.0 mL/min through a Hypersil BDS-C_{18} column (Fisher Scientific, Loughborough, UK, column length 250 mm, internal diameter 4.0 mm, and particle size of the packing material 5 μm) placed in a column oven set at 40°C. The mobile phase consisted of 75:25 % $^{v}/_{v}$ methanol:0.6 % aqueous ammonium acetate. The elution times were 3.4 and 6.7 for FP and SX respectively.

For both methods, linear regression analysis was used for the assessment of the HPLC calibration. Quantification was carried out by an external standard method, and linearity was verified between 0.05 and 50 μg/mL. The limit of detection was 0.02 μg/mL and 0.03 μg/mL for both FP and SX respectively.

4.2.2.13 Statistical analysis

Linear regression analysis was used for the assessment of HPLC calibration. Statistical analysis between different populations carried out using one-way analysis of variance. Comparison of the mean values was performed by Tukey's multiple comparison. All statistical analyses were performed using GraphPad Prism software (GraphPad Software Inc, California, USA). Error

bars in graphical representations of data show ± standard deviation (s.d.) in all cases.

4.3 RESULTS AND DISCUSSION

A number of physicochemical properties were studied over a period of time to understand the effect of environmental conditioning on the relaxation kinetics of SX following micronisation. Colloid probe investigations through CAB-AFM was used to examine the response of the trended physicochemical properties on the interfacial chemistry between the conditioned SX, FP and inhalation grade lactose monohydrate.

4.3.1 Physicochemical Results for Environmentally Conditioned SX Samples

X-ray powder diffraction (XRPD) scans for micronised SX and SX samples conditioned for 60 days at 33 %RH (LH60), 75 %RH (HH60) and 60°C (T60) are shown in Figure 4.1. The nature of the peaks seen between 10 and 25 angle 2θ° for all samples suggest that environmental conditioning did not alter the polymorphic forms of the conditioned samples. The presence of a broad signal between 5 and 10 angle 2θ° for the initial SX sample, together with more intense responses, maybe probably related to the different packing properties of freshly micronised material.

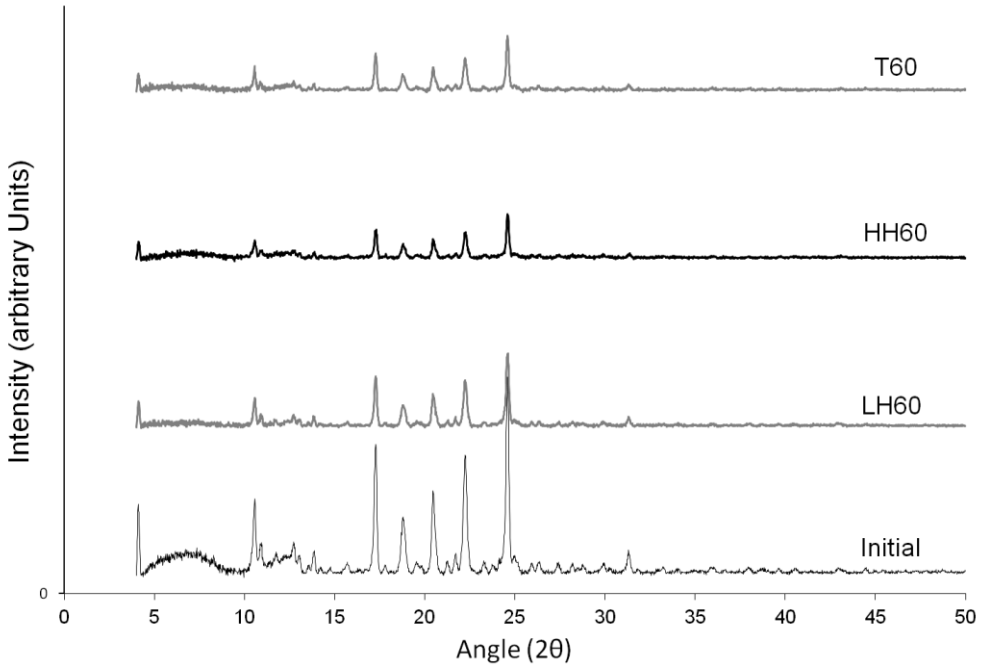

Figure 4.1 X-ray powder diffraction profiles for the Initial, LH60, HH60 and T60 salmeterol xinafoate samples

Differential scanning calorimetry (DSC) thermograms of the SX samples indicated two major endothermic phase changes at approximately 125°C and 140°C, as shown in Figure 4.2. These thermographs correspond to the two polymorphs of salmeterol xinafoate in an enantiotropic system (Tong *et al.,* 2001; Beach *et al.,* 1999). These thermograms further suggested that environmental conditioning had no impact on the polymorphic state of micronised SX.

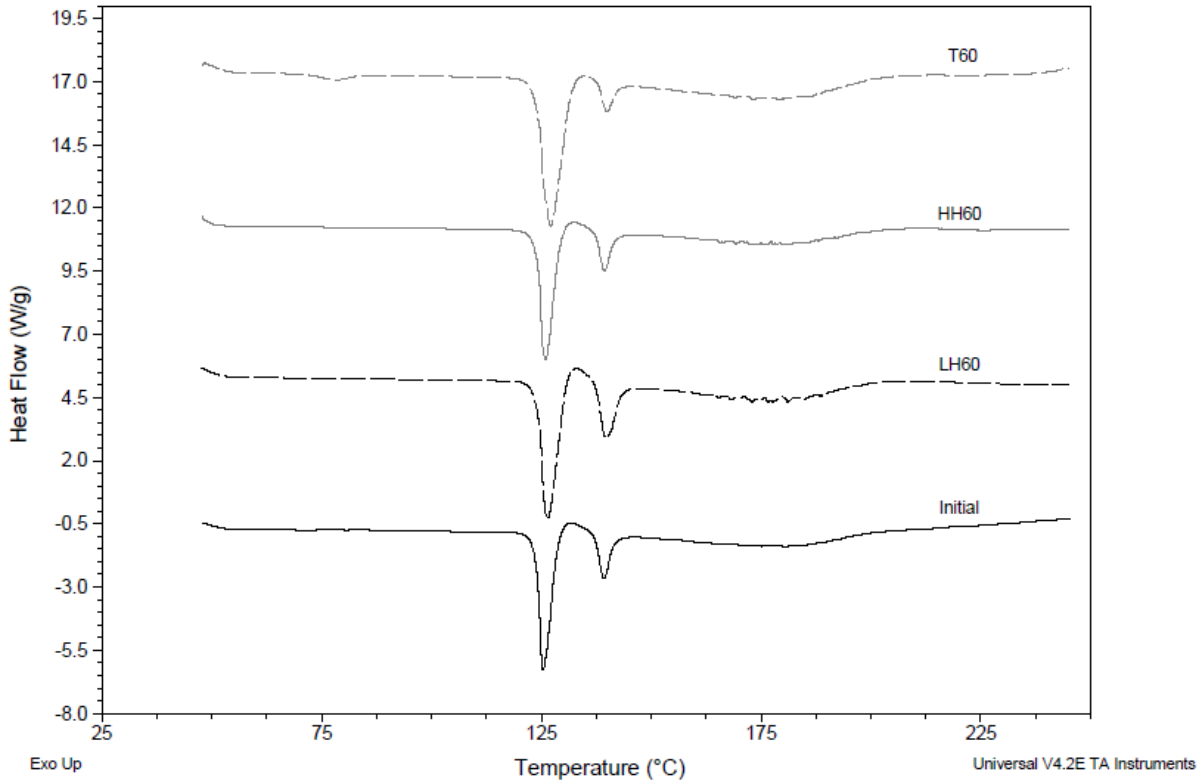

Figure 4.2 Differential Scanning Calorimetry thermographs for the Initial, LH60, HH60 and T60 salmeterol xinafoate samples

The particle size distribution profiles for the freshly micronised and environmentally conditioned SX drug samples are tabulated in Table 4.2. These data show that the distribution for samples conditioned at room temperatures using both low and high humidity remain largely unchanged. This suggests a stable physical system for micronised SX, upon exposure to elevated humidities. Conditioning micronised SX at 60°C, however, led to a significant ($p<0.05$) coarsening in particle size. All percentile (d_{10}, d_{50} and d_{90}) values increased consistently over the conditioning period as shown in Table 4.2. This shift in PSD may directly influence the aerodynamic properties of the

SX and potentially influencing the aerosolisation performance of formulations manufactured using said samples.

		d_{10} (µm)	d_{50} (µm)	d_{90} (µm)
Initial	Day 0	0.91 ±0.03	2.42 ±0.04	5.35 ±0.05
33 % RH	Day 30	0.83 ±0.02	2.25 ±0.06	5.31 ±0.05
	Day 60	0.86 ±0.02	2.35 ±0.01	5.37 ±0.04
75 % RH	Day 30	0.84 ±0.01	2.29 ±0.03	5.29 ±0.03
	Day 60	0.88 ±0.03	2.33 ±0.04	4.95 ±0.05
60°C	Day 30	0.97 ±0.02	2.50 ±0.03	5.40 ±0.05
	Day 60	1.13 ±0.04	2.79 ±0.04	5.83 ±0.05

Table 4.2 Particle Size Distribution of the micronised and subsequently conditioned salmeterol xinafoate determined by laser diffraction

The influence of temperature and humidity conditioning on the specific surface area per unit mass (SSA) of the SX samples is shown in Fig. 5.3. The SSA values together with surface area per unit volume as determined from PSD analysis, and calculated rugosity values for each sample are also tabulated in Table 4.3. Conditioning at low relative humidity appeared to continually reduce the SSA of the SX powder. Exposure to high humidity led to an initial drop in SSA but did not alter significantly upon more exposure. Exposure of SX to high temperature led to the most significant drop in SSA and continued to decrease with extended period of exposure.

Surface rugosity has the potential of influencing the manufacturability and aerosolisation performance of both binary and tertiary formulations through increased or decreased surface interactions based on the physical properties of the surfaces during blending.

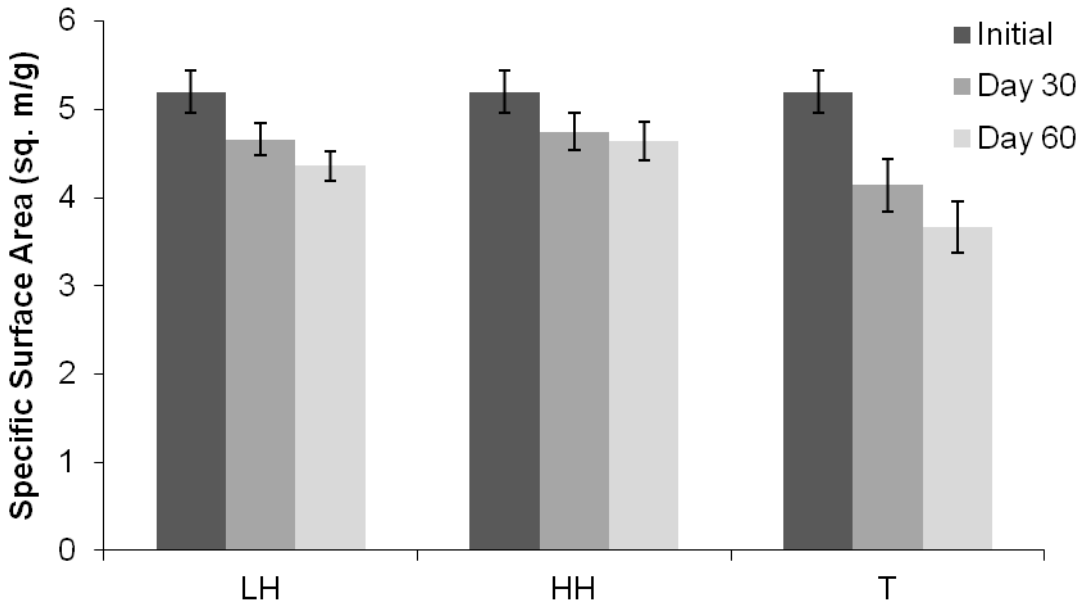

Figure 4.3 Specific Surface Area for salmeterol xinafoate samples determined by BET analysis

		S_v (m^2cm^3)	SSA (m^2/gram)	R_a
Initial	Day 0	3.20	5.20 ±0.24	1.63
33 % RH	Day 30	3.43	4.66 ±0.18	1.27
	Day 60	3.32	4.36 ±0.21	1.40
75 % RH	Day 30	3.39	4.75 ±0.30	1.40
	Day 60	3.32	4.64 ±0.17	1.40
60°C	Day 30	3.08	4.14 ±0.22	1.34
	Day 60	2.75	3.66 ±0.29	1.33

Table 4.3 Surface area per unit volume (S_v), specific surface area per unit mass (SSA), and rugosity values (R_a) for all SX samples

Morphological analysis for the SX samples was performed using SEM imaging as shown in Figure 4.4. The electron micrographs showed how conditioning led to no apparent difference in the bulk morphological properties of the temperature and humidity conditioned samples.

Figure 4.4 Scanning Electron Micrographs for freshly micronised SX (A, B), and for samples conditioned for 60 days at 33%RH (C, D), 75%RH (E, F) and at 60°C (G, H)

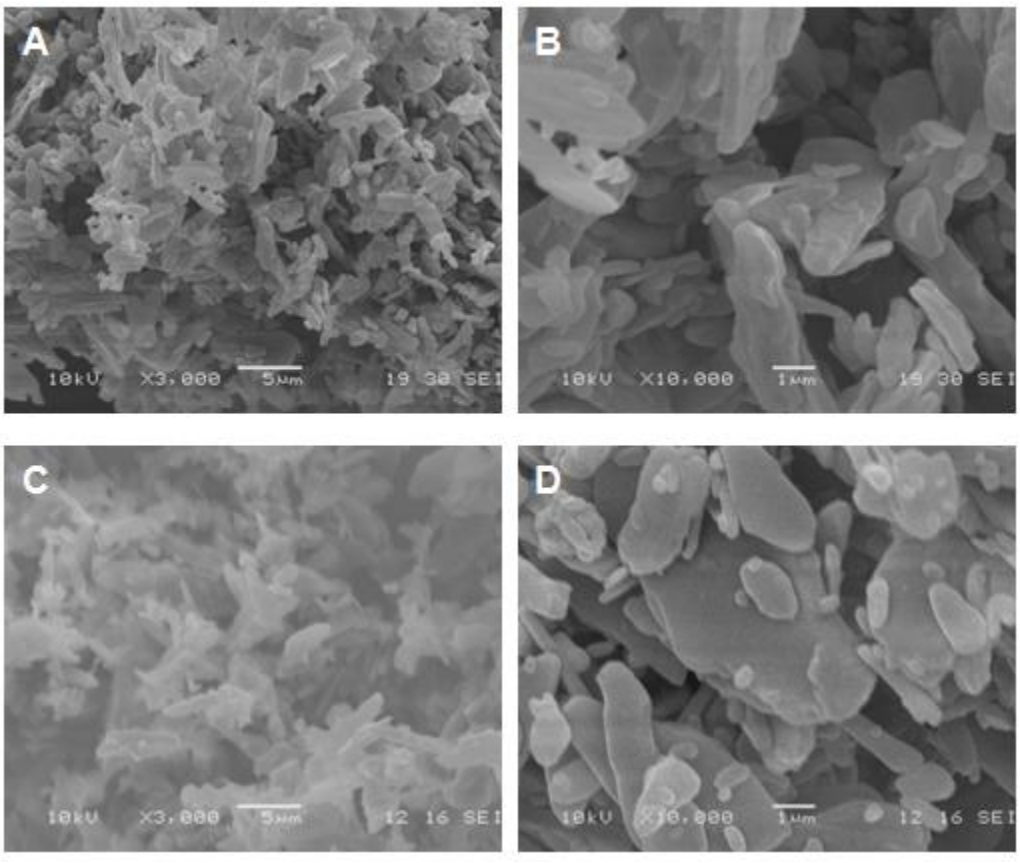

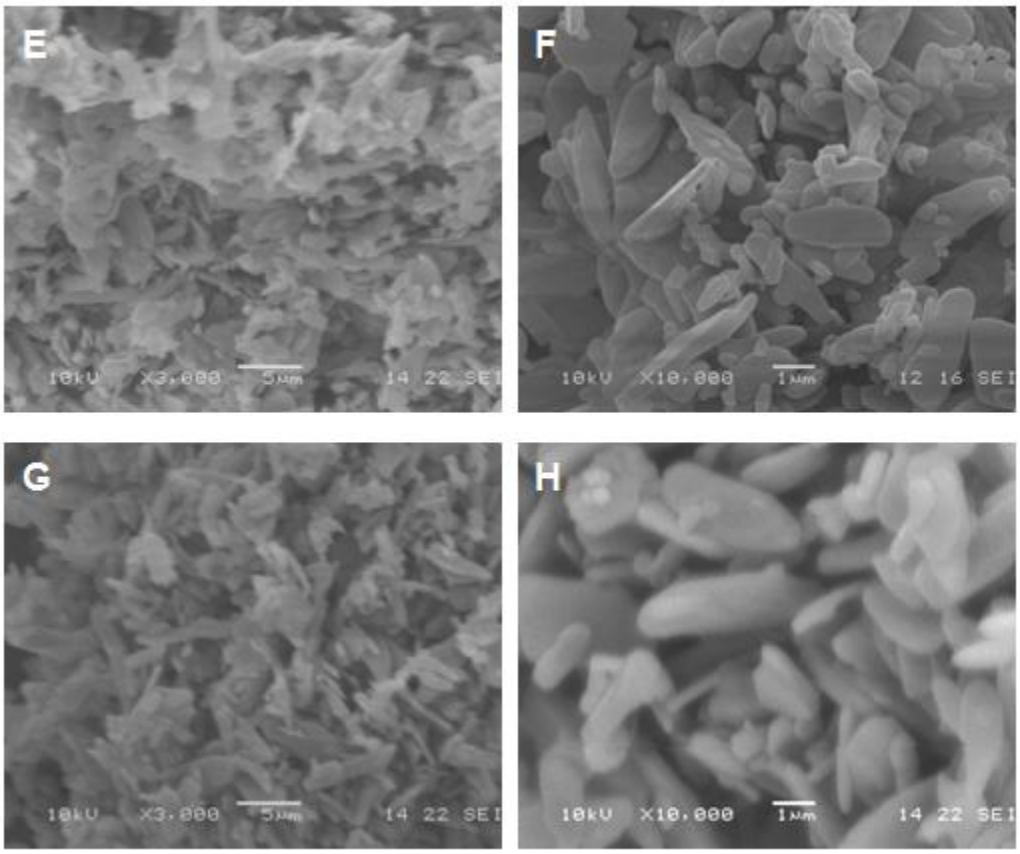

Dynamic vapour sorption (DVS) isotherms for freshly micronised SX and for the samples conditioned for 60 days at 33 %RH (LH60), 75 %RH (HH60) and at 60°C (T60) are shown in Figures 4.5 A-D. The DVS moisture sorption isotherm for the freshly micronised SX sample shows a rapid moisture uptake of ~0.21% w/w between 30% and 90 % RH. The sorption isotherms for the samples conditioned at room temperature (LH60 and HH60) on the other hand only indicated a moisture uptake of ~0.05 % w/w. The representative sorption isotherm for the T60 sample illustrates an even lower moisture uptake of ~0.03 % w/w. This decreased moisture uptake during the moisture sorption cycles of the conditioned samples may suggest a decrease in the level of process

induced structural disorder in the samples. As for the freshly micronised SX samples, the LH60 and HH60 samples retain ~0.05 % w/w of the moisture uptake. The SX sample conditioned at 60°C for 60 days (T60) retains ~0.01 % w/w from the sorption cycle. This seems to suggest that whilst conditioning at room temperature significantly decreases amorphous regions, the application of elevated temperatures in conditioning SX is more effective at minimising surface disorder.

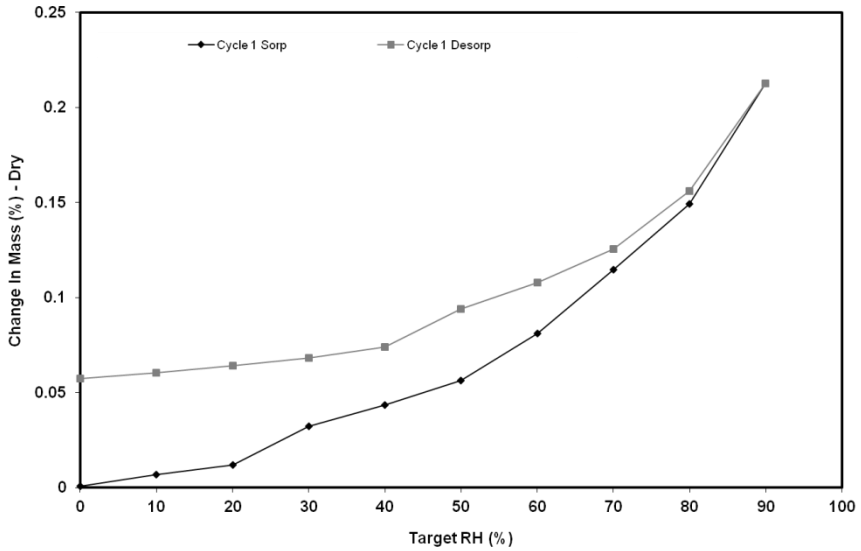

Figure 4.5A Dynamic Vapour Sorption (DVS) isotherm for freshly micronised SX (Initial)

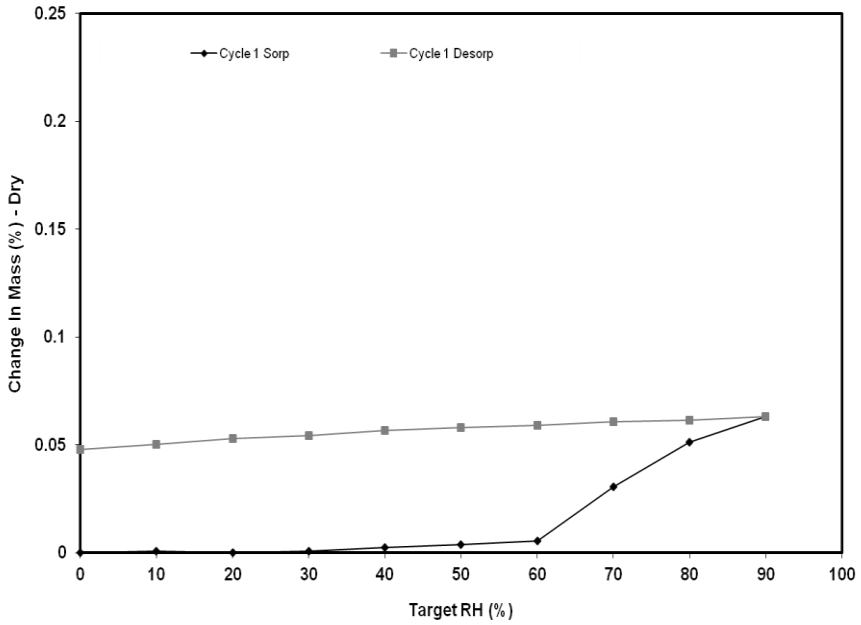

Figure 4.5B Dynamic Vapour Sorption (DVS) isotherm for SX conditioned at 33%RH for 60 days (LH60)

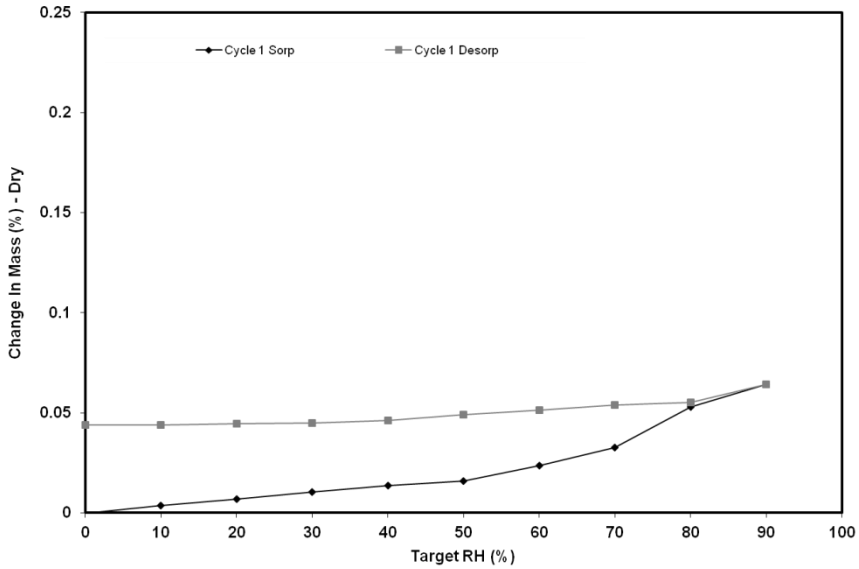

Figure 4.5C Dynamic Vapour Sorption (DVS) isotherm for SX conditioned at 75%RH for 60 days (HH60)

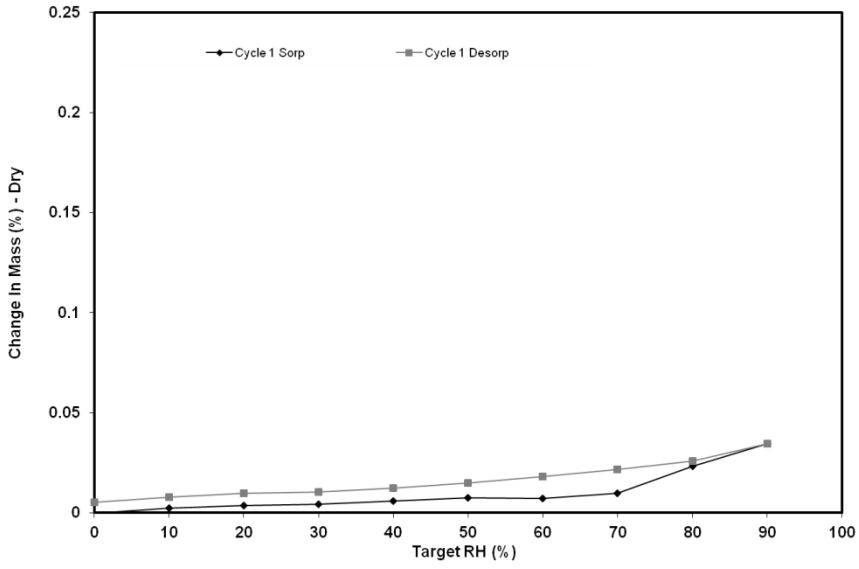

Figure 4.5D Dynamic Vapour Sorption (DVS) isotherm for SX conditioned at 60°C for 60 days (T60)

4.3.2 Cohesive-Adhesive Balance results for environmentally conditioned Salmeterol Xinafoate

CAB values for all SX samples are tabulated in Table 4.4. The CAB plots measures the interfacial chemistry of the SX particles with respect to lactose and FP. Figures 4.6-4.8 show the linear regression analysis of the CAB plots with respect to lactose and to FP.

		CAB wrt Lactose	CAB wrt FP
Initial	Day 0	1.83 ±0.03	1.35 ±0.02
33 % RH	Day 30	2.45 ±0.02	1.74 ±0.01
	Day 60	2.23 ±0.02	1.96 ±0.03
75 % RH	Day 30	2.35 ±0.01	1.84 ±0.03
	Day 60	2.43 ±0.04	2.00 ±0.02
60°C	Day 30	2.37 ±0.03	2.25 ±0.01
	Day 60	2.23 ±0.01	2.08 ±0.03

Table 4.4 Cohesive-Adhesive Balance (CAB) values with respect to Lactose and Fluticasone Propionate for freshly micronised SX and for SX samples conditioned environmentally

CAB ratios show a general and significant trend towards a more cohesive interfacial system, suggesting a higher tendency for SX-SX interactions upon

conditioning. Freshly micronised SX already exhibits a cohesive tendency with respect to lactose monohydrate with a CAB ratio of 1.83, suggesting SX-SX interactions have a surface affinity 1.83 times greater than SX-Lactose interactions. This cohesive tendency is less pronounced with respect to FP, with SX-SX interactions 1.35 times greater than SX-FP interactions. These data suggest a predominant cohesive chemical nature for freshly micronised SX.

Environmental conditioning seemed to drive a cohesive shift for environmentally conditioned SX samples. This shift seems to largely occur within the first 30 days of conditioning, suggesting that interfacial instability for micronised SX is more significant ($p<0.05$) during the first 30 days post-micronisation. Whilst the cohesive shift is observed in all samples, the interfacial chemical nature of SX with respect to FP seems to be more responsive to post-micronisation conditioning. The cohesive shift for conditioned samples with respect to FP varies from 45 to 54 % at the 60 day mark. On the other hand, the cohesive shift with respect to lactose varies between 22 and 32 % for conditioned SX.

Figure 4.6A Cohesive-Adhesive Balance (CAB) plot of the freshly micronised SX sample (Initial) and samples conditioned at low humidity (LH30, LH60) with respect to lactose

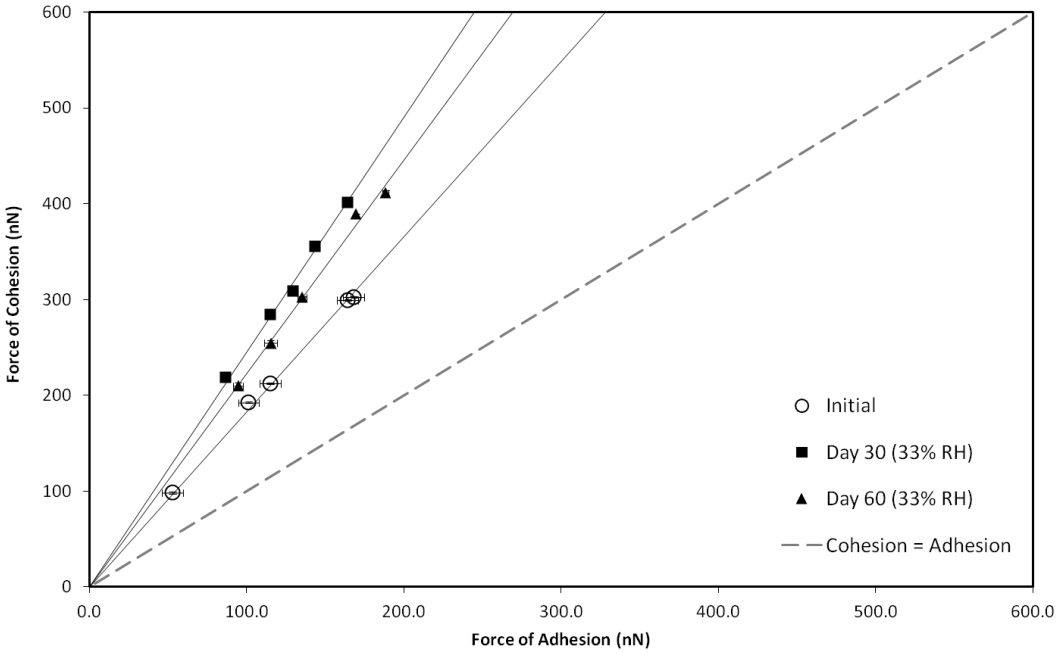

Figure 4.6B Cohesive-Adhesive Balance (CAB) plot of the freshly micronised SX sample (Initial) and samples conditioned at low humidity (LH30, LH60) with respect to FP

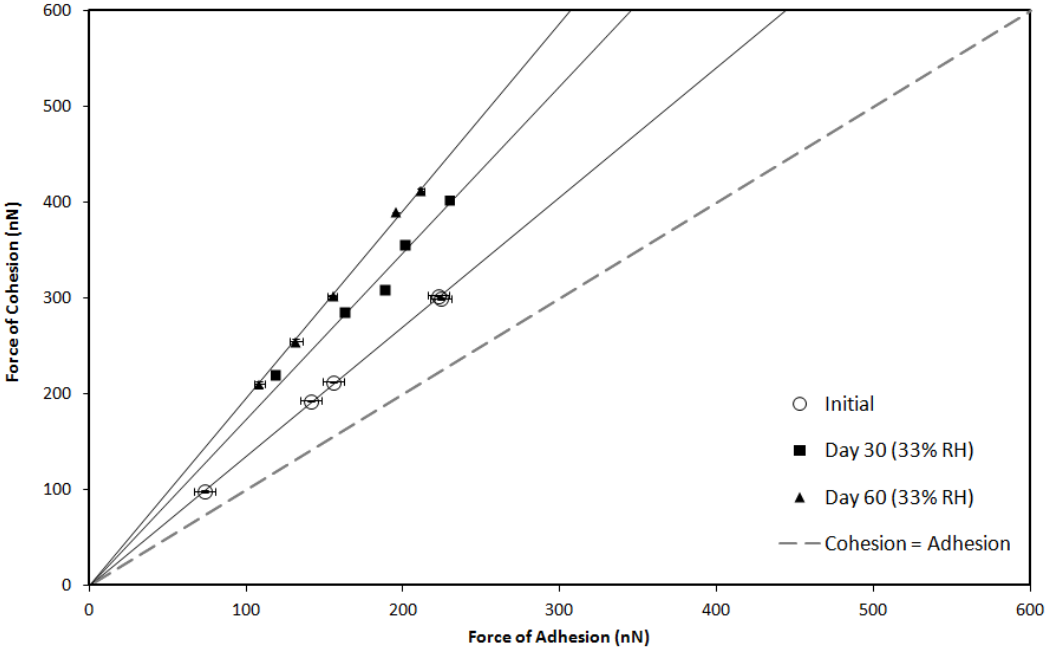

Figure 4.7A Cohesive-Adhesive Balance (CAB) plot of the freshly micronised SX sample (Initial) and samples conditioned at high humidity (HH30, HH60) with respect to lactose

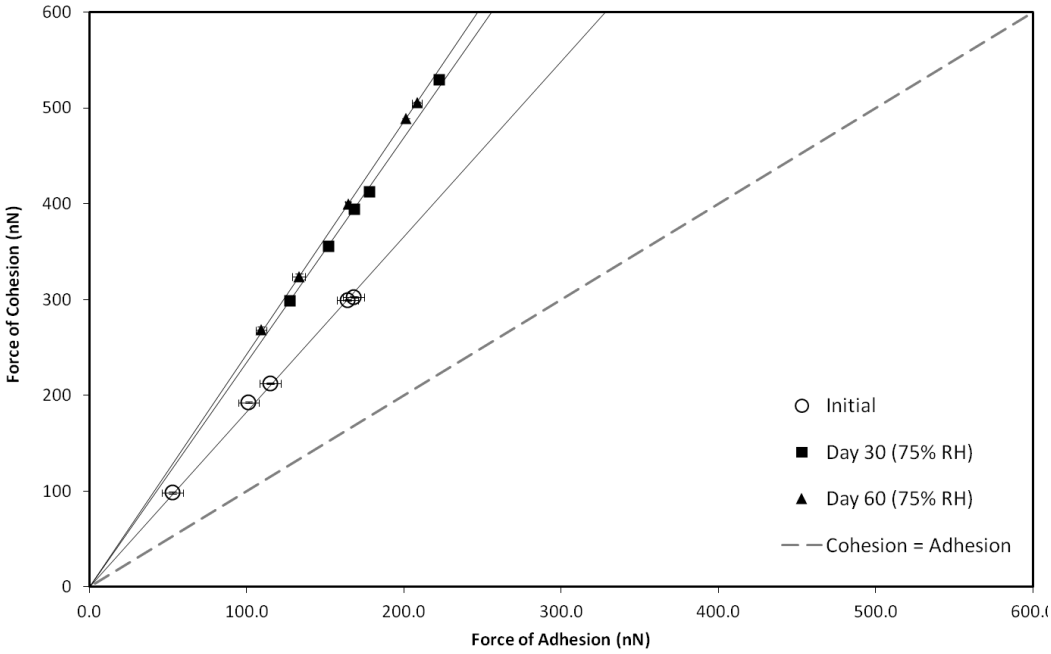

Figure 4.7B Cohesive-Adhesive Balance (CAB) plot of the freshly micronised SX sample (Initial) and samples conditioned at high humidity (HH30, HH60) with respect to FP

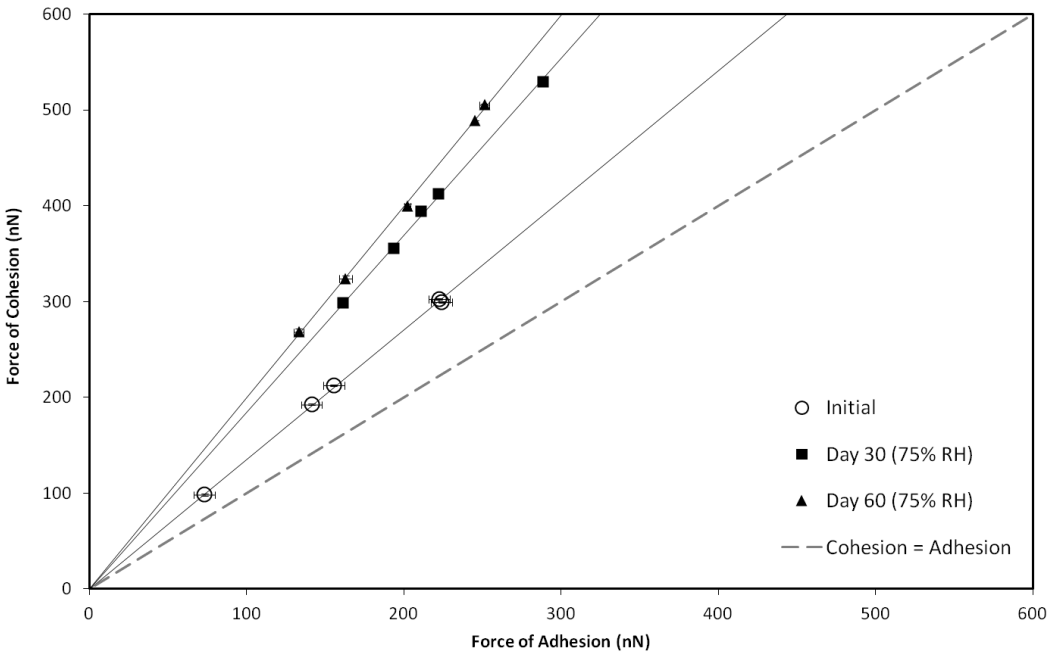

Figure 4.8A Cohesive-Adhesive Balance (CAB) plot of the freshly micronised SX sample (Initial) and samples conditioned at 60°C (T30, T60) with respect to lactose

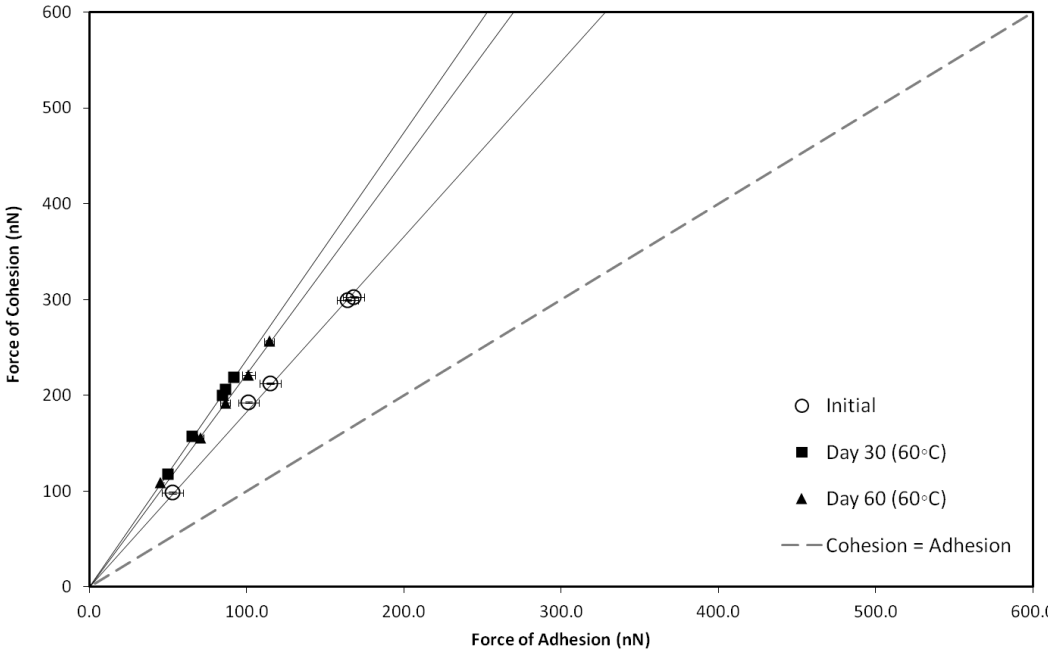

Figure 4.8B Cohesive-Adhesive Balance (CAB) plot of the freshly micronised SX sample (Initial) and samples conditioned at 60°C (T30, T60) with respect to FP

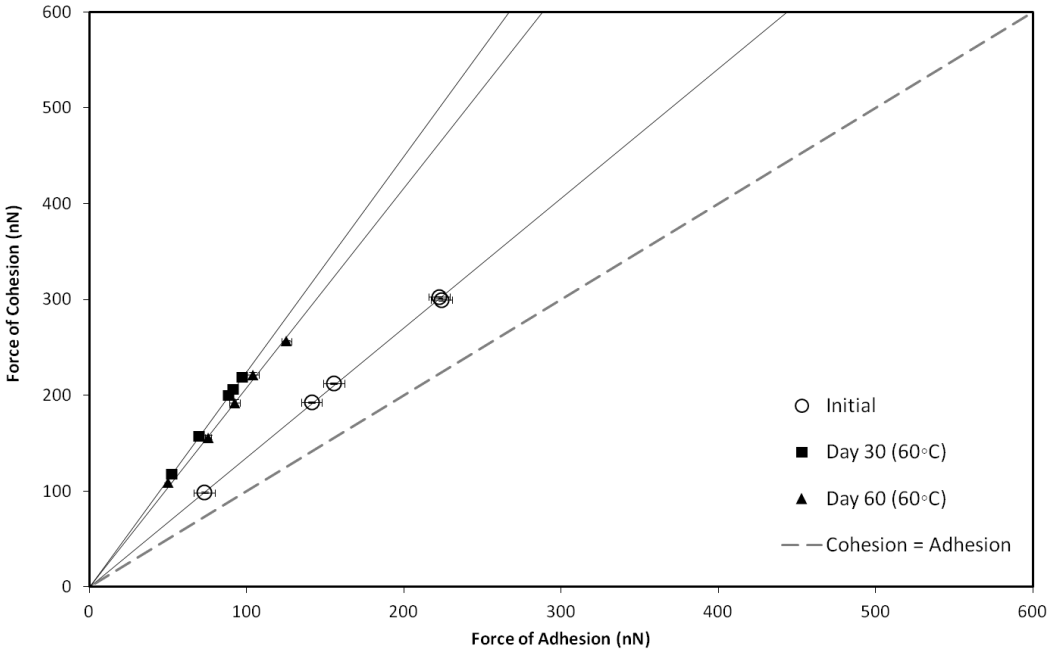

4.3.3 Aerosolisation performance results for environmentally conditioned Salmeterol Xinafoate in binary formulations

The aerosolization performance for binary, carrier-based DPI formulations with freshly micronised and conditioned SX samples are tabulated in Table 4.5. These data support the cohesive shift observed in the CAB analysis. The emitted dose (ED) dropped significantly (p<0.02) for all formulations manufactured using SX samples conditioned for 30 days. Thereafter, the emitted dose seemed to remain stable confirming interfacial instability is largely affected within the first 30 days post-micronisation. This initial drop in ED maybe directly related to the increased cohesive chemical nature of SX particles, leading to increase particle segregation and hindering aerosolisation deaggregation efficiency (Jones *et al.,* 2008). This marked drop in emitted dose leads to a concomitant decrease in fine particle mass (FPM). Furthermore, the mass median aerodynamic diameter (MMAD) results reflect an increased cohesive nature of SX for all three formulations conditioned for 30 and 60 days. These MMAD data are consistent with greater cohesion between SX particles which are unable to deaggregate as efficiently as the freshly micronised particles.

These in vitro data support the increase in cohesive behaviour of SX upon conditioning and that interfacial stability is obtained within the first 30 days of conditioning and translates into aerosolisation performance stability.

	RD (µg)	ED (µg)	FPM (µg)	FPF (%ED)	MMAD (µm)	GSD (µm)
Initial	54.58 ±3.12	32.11 ±2.55	11.69 ±1.01	36.39 ±2.34	1.98 ±0.02	2.71 ±0.02
LH30	49.11 ±2.46	24.02 ±2.04	9.31 ±0.78	38.76 ±2.14	3.04 ±0.03	2.07 ±0.01
LH60	47.66 ±3.01	22.70 ±1.67	8.12 ±0.92	35.78 ±1.97	3.08 ±0.02	2.14 ±0.02
HH30	45.09 ±2.98	27.09 ±3.24	8.87 ±1.44	32.74 ±2.89	3.40 ±0.02	2.03 ±0.01
HH60	43.61 ±3.45	28.69 ±2.01	8.96 ±0.89	31.21 ±2.43	3.66 ±0.02	2.11 ±0.02
T30	47.12 ±4.21	24.57 ±1.78	8.84 ±1.09	35.98 ±1.79	3.46 ±0.04	1.90 ±0.02
T60	47.02 ±4.11	23.55 ±1.12	8.25 ±0.83	35.01 ±2.13	3.94 ±0.03	2.09 ±0.01

Table 4.5 In Vitro aerosolisation performance for SX formulations manufacture with freshly micronised and environmentally conditioned SX. Results are described by the recovered dose (RD), emitted dose (ED), fine particle mass (FPM), fine particle fraction (FPF) expressed as a percentage of the emitted dose, mass median aerodynamic diameter (MMAD) and geometric standard deviation (GSD)

Stage by stage deposition profiles of SX binary formulations manufactured using freshly micronised and environmentally conditioned SX samples are show in Figures 4.9 A-C. Figure 4.9A shows a significant (p<0.02) increase in drug deposition in the device, whilst figures 5.9B and 5.9C show significant decreases in stages 2-4. These deposition profiles are consistent with a cohesive shift in the chemical nature of the formulations.

Figure 4.9A Stage by stage deposition profile expressed as the percentage of emitted dose per stage for SX in binary formulations manufactured using SX conditioned at 33%RH

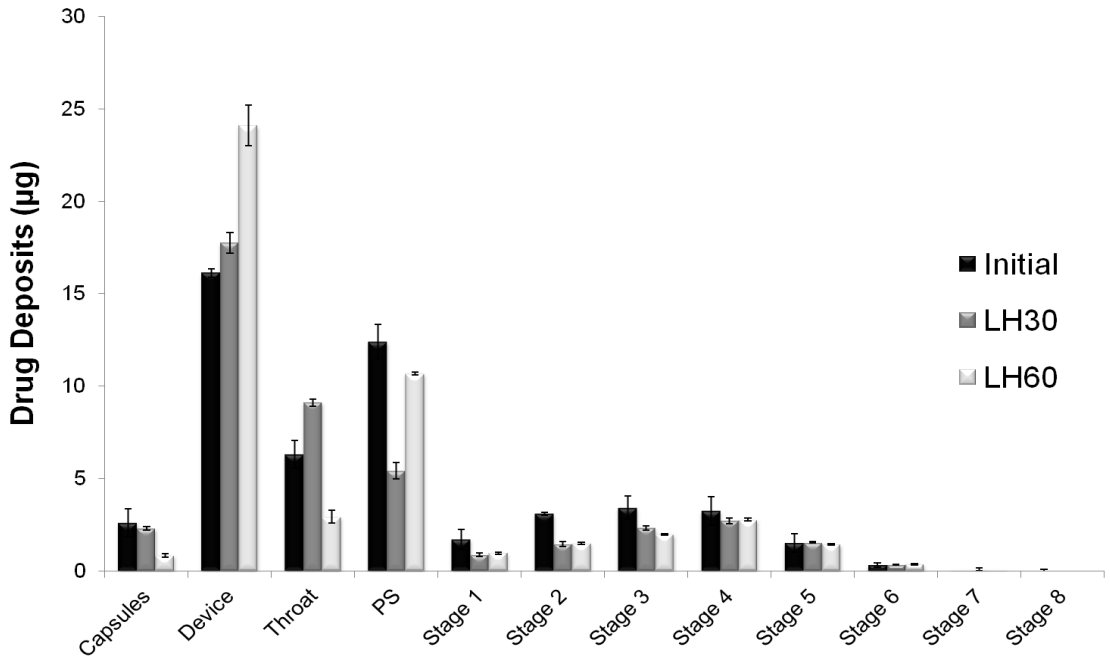

Figure 4.9B Stage by stage deposition profile expressed as the percentage of emitted dose per stage for SX in binary formulations manufactured using SX conditioned at 75%RH

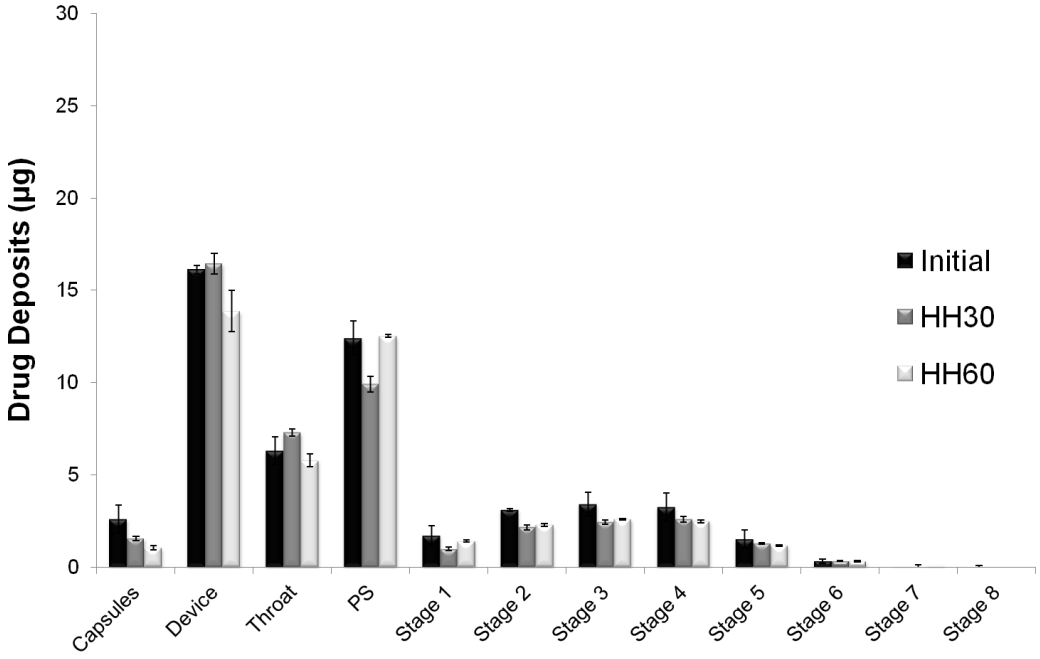

Figure 4.9C Stage by stage deposition profile expressed as the percentage of emitted dose per stage for SX in binary formulations manufactured using SX conditioned at 60°C

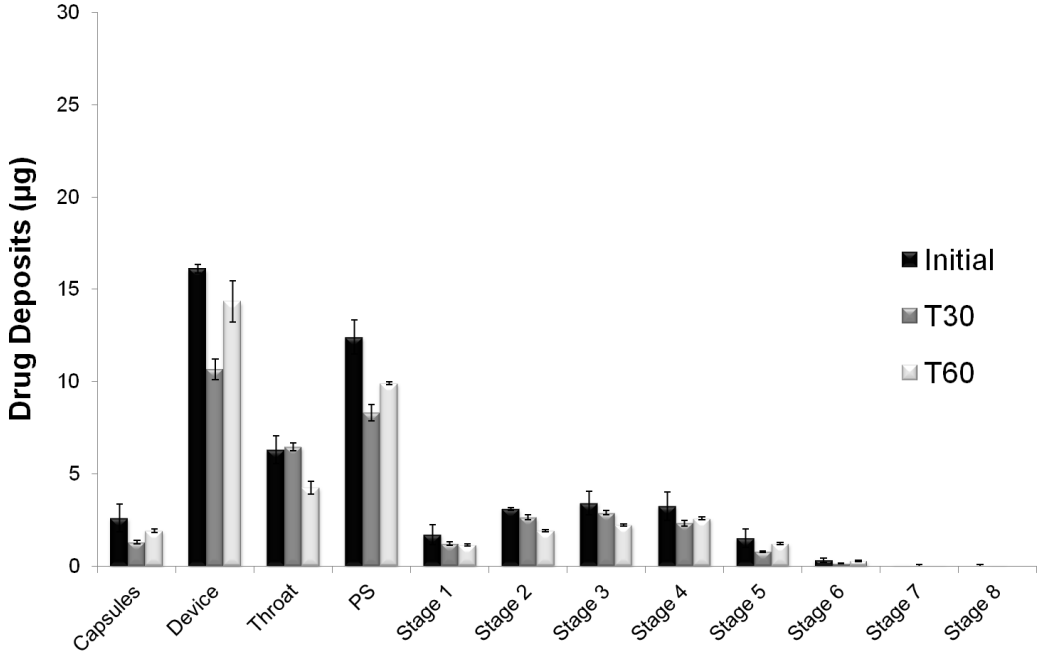

4.3.4 Aerosolisation performance results for environmentally conditioned Salmeterol Xinafoate in ternary formulations

Tables 4.6 and 4.7 tabulate the *in vitro* performance results SX and FP, respectively for freshly micronised and conditioned SX. These results describe the influence of SX post-micronisation relaxation kinetics on ternary formulations with inhalation grade lactose monohydrate and an aged and stable batch of FP. These data seem to be consistent with interfacial shifts towards to more cohesively-led chemical system. Fine Particle Mass (FPM) for SX drops consistently for samples conditioned at room temperatures (LH60, HH60). The formulations manufactured using SX conditioned at 60°C on the other hand seem to stabilise within the first 30 days of conditioning. There seems to be however a significant increase (p<0.02) in the MMAD for T60 sample. This MMAD increase is also observed in the FP data for the T60 sample and together with the cohesive shift in the interfacial properties of the SX, might be consistent with the lower rugosity and SSA values reported for this sample in table 4.3. Data for the aerosolisation performance of FP follow similar trends to SX data and suggest that FP is influenced by the changing properties of freshly micronised SX.

Table 4.6 ***In vitro*** **aerosolisation performance for SX in ternary formulations with FP manufactured with freshly micronised and environmentally conditioned SX. Results are described by the recovered dose (RD), emitted dose (ED), fine particle mass (FPM), fine particle fraction (FPF) expressed as a percentage of the emitted dose, mass median aerodynamic diameter (MMAD) and geometric standard deviation (GSD)**

	RD (µg)	ED (µg)	FPM (µg)	FPF (%ED)	MMAD (µm)	GSD (µm)
Initial	48.75 ±3.57	28.78 ±2.21	11.90 ±1.27	41.35 ±1.36	3.08 ±0.03	2.00 ±0.02
LH30	57.89 ±5.36	30.78 ±3.01	12.63 ±1.83	41.07 ±1.87	3.07 ±0.02	2.00 ±0.02
LH60	45.74 ±4.28	29.33 ±2.48	7.33 ±0.78	24.97 ±1.42	3.17 ±0.02	2.00 ±0.01
HH30	47.98 ±3.48	25.96 ±3.01	9.09 ±0.38	35.02 ±1.37	2.75 ±0.01	1.89 ±0.01
HH60	43.99 ±2.98	26.20 ±2.45	6.90 ±0.46	26.34 ±1.36	3.08 ±0.02	1.96 ±0.01
T30	41.62 ±4.38	21.57 ±1.84	5.13 ±0.67	23.78 ±0.83	3.16 ±0.03	1.84 ±0.02
T60	41.14 ±5.73	23.11 ±2.24	5.21 ±0.83	22.54 ±0.69	3.98 ±0.01	1.94 ±0.02

Table 4.7 ***In vitro*** **aerosolisation performance for FP in ternary formulations with SX manufactured with freshly micronised and environmentally conditioned SX. Results are described by the recovered dose (RD), emitted dose (ED), fine particle mass (FPM), fine particle fraction (FPF) expressed as a percentage of the emitted dose, mass median aerodynamic diameter (MMAD) and geometric standard deviation (GSD)**

	RD (µg)	ED (µg)	FPM (µg)	FPF (%ED)	MMAD (µm)	GSD (µm)
Initial	216.50 ±7.35	139.28 ±4.55	47.26 ±2.45	33.93 ±1.35	3.91 ±0.04	2.00 ±0.02
LH30	231.10 ±8.35	119.34 ±3.98	40.22 ±1.38	33.70 ±1.03	4.01 ±0.03	1.98 ±0.02
LH60	206.11 ±6.98	131.91 ±4.58	23.52 ±2.01	17.83 ±0.85	4.34 ±0.03	1.96 ±0.03
HH30	207.49 ±5.36	111.50 ±6.02	31.40 ±1.48	28.17 ±1.23	3.72 ±0.02	1.96 ±0.01
HH60	195.28 ±9.46	106.53 ±4.36	29.33 ±1.82	27.54 ±1.83	3.40 ±0.04	1.87 ±0.02
T30	202.87 ±6.24	106.25 ±9.11	28.05 ±0.97	26.41 ±1.49	3.40 ±0.03	1.88 ±0.02
T60	220.06 ±8.88	143.45 ±5.45	34.02 ±1.35	23.72 ±0.97	4.56 ±0.02	2.02 ±0.02

4.3.5 Physicochemical Characterisation of Post-Micronised Conditioned SX using HFA-134a

Physicochemical analysis of *in-situ* conditioned SX with HFA-134a was performed to determine any possible influence on material properties.

The XRPD diffractograms for the freshly micronised and HFA conditioned SX are shown in Fig. 5.10. The peaks present between 10 and 40 angle 2θ° suggest there is no change in the polymorphic nature of the two samples. There is a significant decrease in peak intensity for the HFA conditioned sample, however this seems to be consistent with packing differences between freshly micronised and aged material.

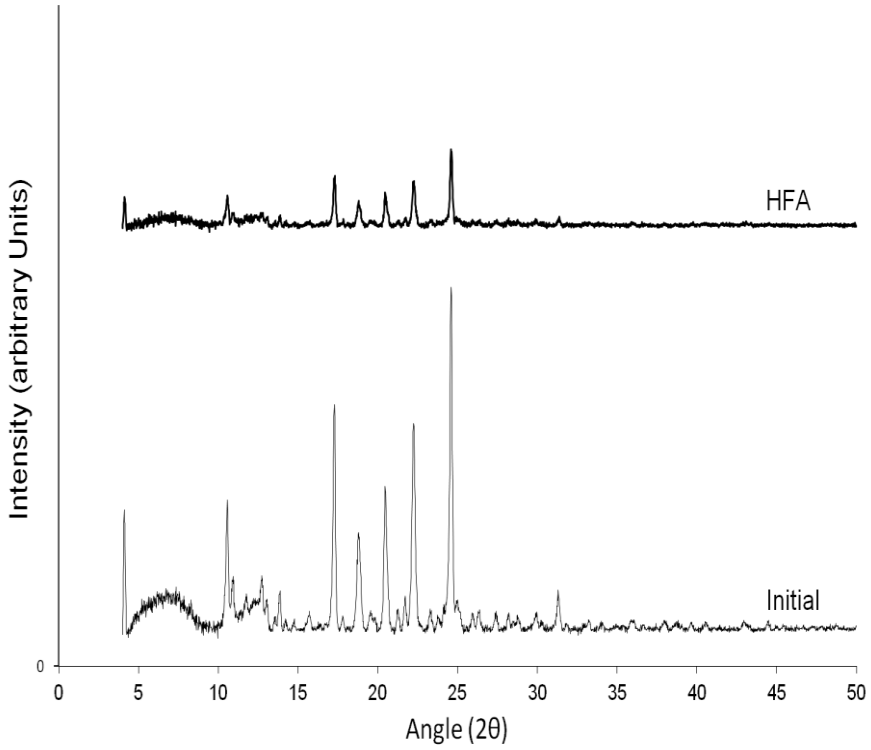

Figure 4.10 X-ray powder diffraction profiles for the Initial and HFA conditioned SX samples

Figure 4.11 shows the DSC thermographs for the unconditioned and HFA conditioned SX. This thermal analysis suggests that HFA conditioning has either led to a complete conversion of form II into form I or possibly the removal of the form II seeds, which may be formed during micronisation of form I of SX. This is consistent with the findings documented in (Tong *et al.,* 2001; Beach *et al.,* 1999) form II is less stable than form I. Fast-cooling crystallisation processes and particle engineering technologies are known to produce salmeterol xinafoate of exclusively form I (Beach *et al.,* 1999).

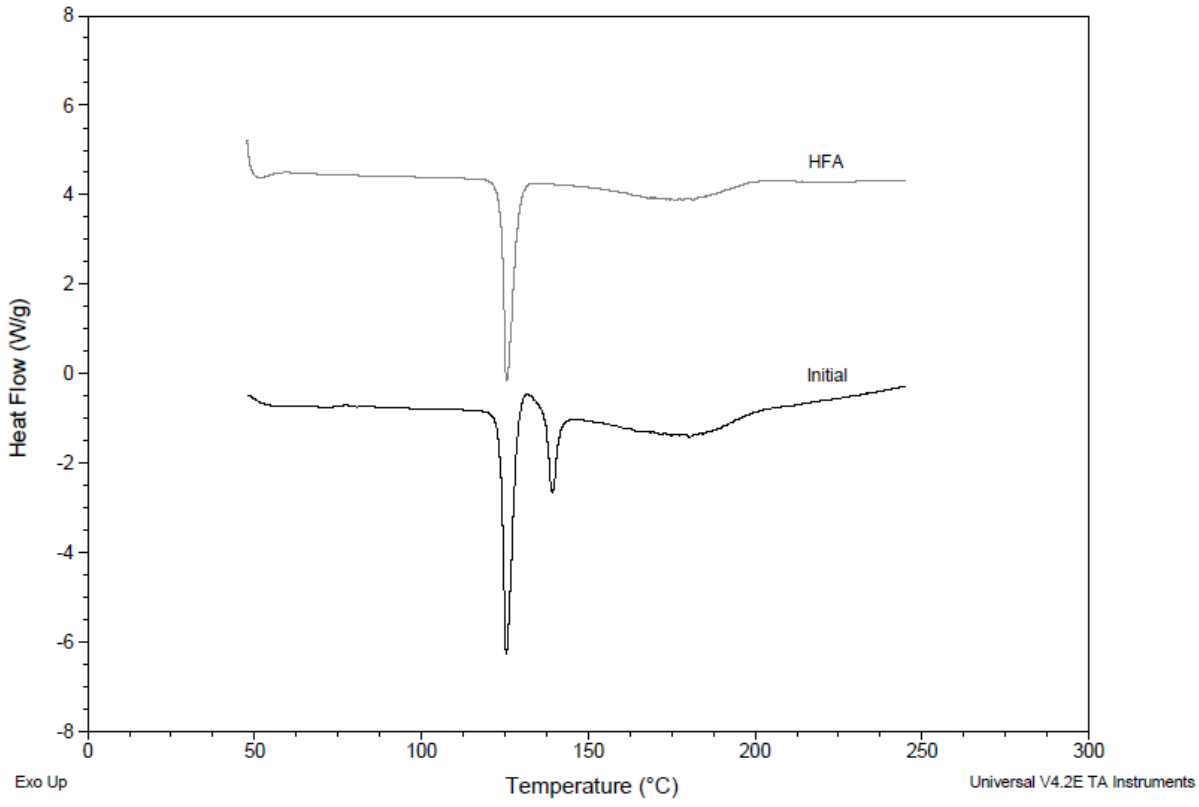

Figure 4.11 Differential Scanning Calorimetry thermographs for the Initial and HFA conditioned SX samples

Particle size distribution data of the initial and HFA conditioned SX is shown in Table 4.8. The d_{10} and d_{50} percentiles indicate that conditioning using HFA has limited influence on the physical size of the micronised SX. There is a slight increase in the d90 values which suggests a small but significant shift towards a coarser distribution. Whilst this shift is consistent with the use of elevated temperatures and the possible influence of Ostwald ripening, the overall particle size distribution remains largely stable.

		d_{10} (µm)	**d_{50} (µm)**	**d_{90} (µm)**
Initial	Day 0	0.91 ±0.03	2.42 ±0.04	5.35 ±0.05
HFA	Day 21	0.90 ±0.03	2.45 ±0.05	5.62 ±0.07

Table 4.8 Particle Size Distribution of the Initial and HFA conditioned SX samples determined by laser diffraction

Figure 4.12 shows a significant drop in specific surface area (SSA) determined by BET analysis consistent with the drop seen for environmentally conditioned (LH60, HH60, T60) SX samples. With similar PSD profiles, the drop in SSA coincides with a significant drop in rugosity from 1.63 for the freshly micronised SX to 1.28 for SX conditioned *in-situ* with HFA. With stable physicochemical properties, a drop in rugosity may prove a significant factor due to the altered mixing pattern smoother particles may undergo. A rugosity value of 1.28 represent the lowest value observed in this conditioning study, suggesting that HFA conditioning produced SX particles with the smoothest surfaces.

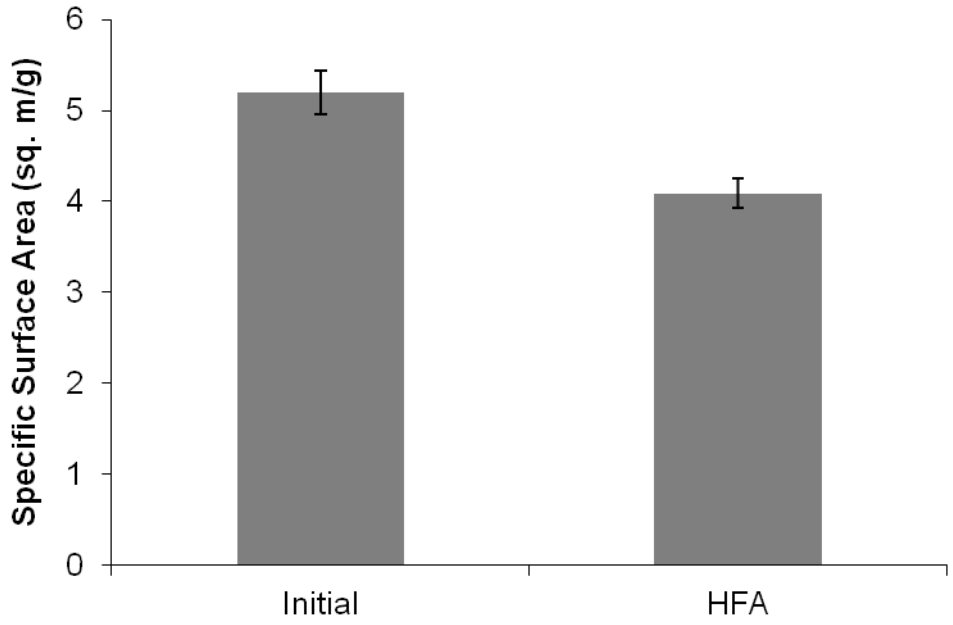

Figure 4.12 Specific Surface Area for Initial and HFA conditioned SX drug samples determined by BET analysis

		S_v (m^2cm^3)	SSA (m^2/gram)	R_a
Initial	Day 0	3.20	5.20 ±0.24	1.63
HFA	Day 21	3.19	4.09 ±0.16	1.28

Table 4.9 Surface area per unit volume (S_v), specific surface area per unit mass (SSA), and rugosity values (R_a) for the Initial and HFA conditioned SX samples

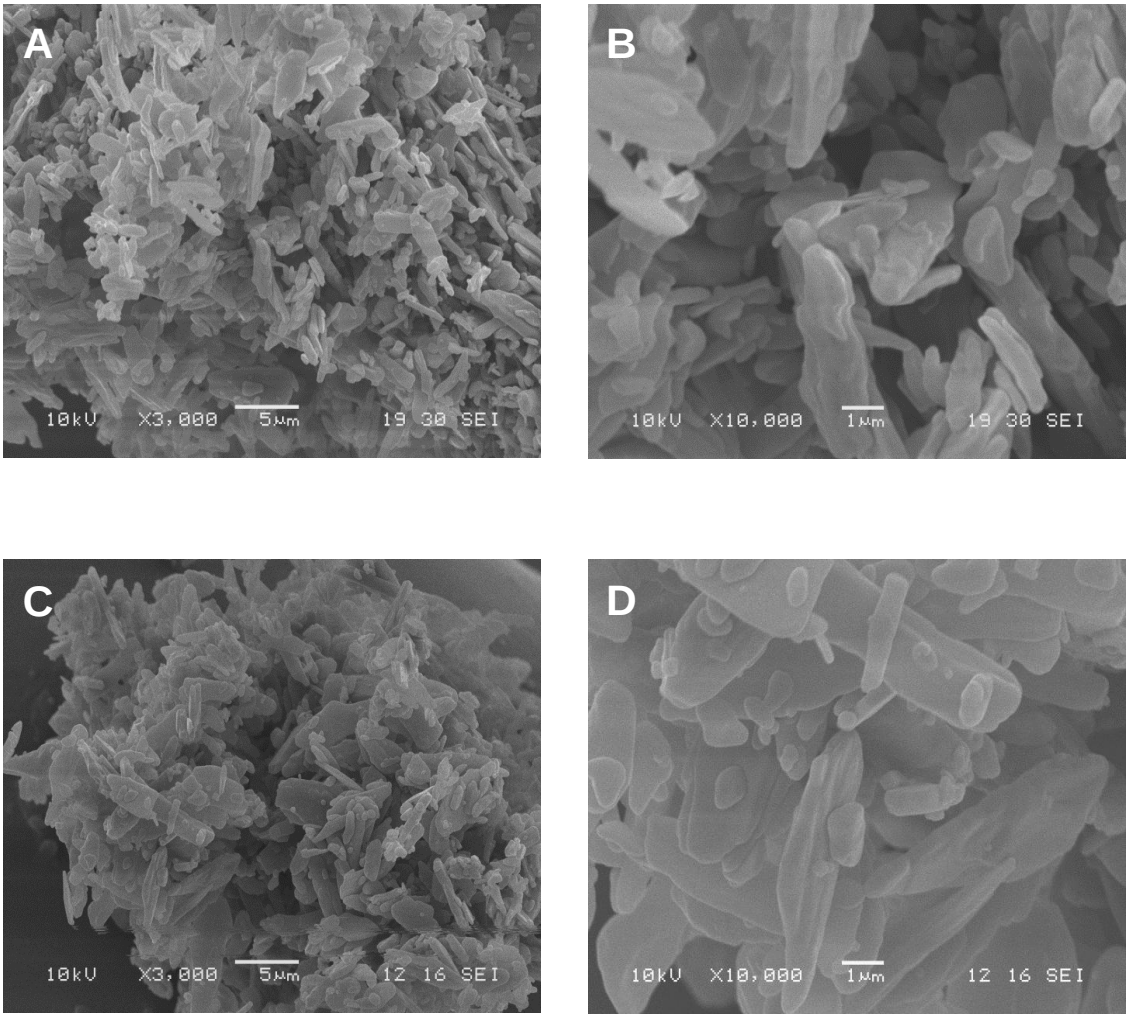

Figure 4.13 Scanning Electron Micrographs for the Initial SX sample (A) and for the HFA conditioned sample (C) at a magnification factor of 3,000, and for the Initial SX sample (B) and the HFA conditioned sample (D) at a magnification factor of 10,000

The morphology of the HFA conditioned sample was studies using SEM imaging. The scans shown in Figure 4.13 do not show any significant differences to the bulk morphologies of the samples. Conditioning micronised SX *in-situ* with HFA had no impact on particle shape.

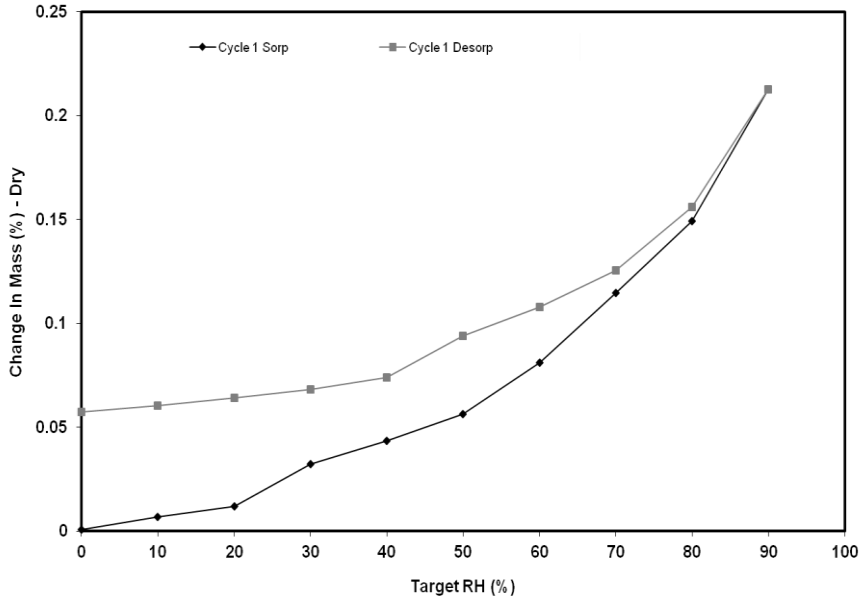

Figure 4.14A Dynamic Vapour Sorption (DVS) isotherms for freshly micronised SX

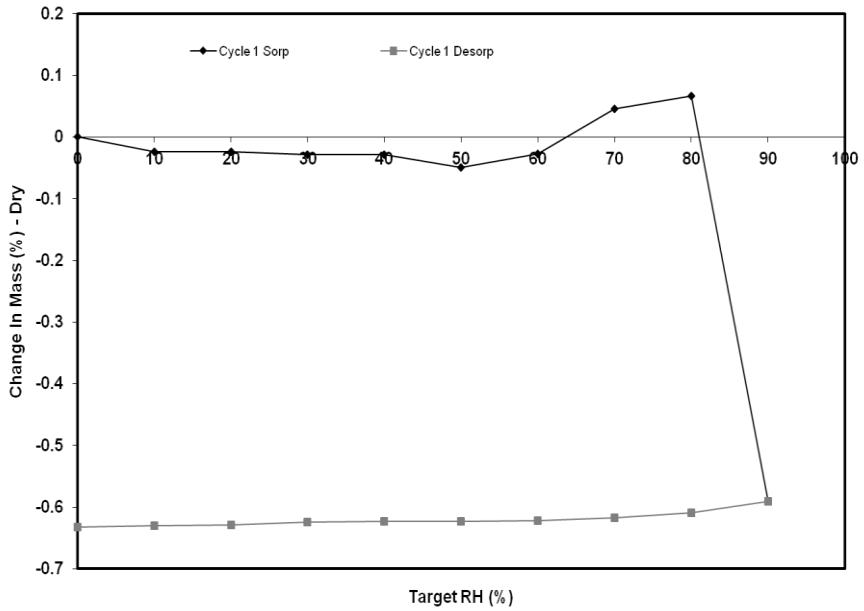

Figure 4.14B Dynamic Vapour Sorption (DVS) isotherms for SX conditioned *in-situ* with HFA for 21 days

Figures 4.14 A-B show the isotherms for freshly micronised and HFA conditioned SX respectively. The DVS moisture sorption isotherm for the freshly micronised SX, described previously, shows a significant moisture uptake (~0.21 % w/w between 30 % and 90 % RH) which is only partially retained following the desorption cycle. The HFA isotherm shows (Figure 4.14B) a negative hysteresis with a net moisture loss of ~0.65 % w/w, possibly suggesting some moisture retention trapped in slightly amorphous regions.

4.3.6 Cohesive-Adhesive Balance and Impaction results for SX conditioned *in-situ* with HFA post-micronisation

The interfacial chemistry and aerosolisation behaviour were examined to further understand the influence of conditioning freshly micronised SX using HFA. The CAB values in Table 4.10 indicated a similar cohesive shift in the interfacial nature of SX as previously observed for the environmentally conditioned SX samples. A significant (p<0.02) cohesive shift is noted for SX particles with respect to both lactose and FP. As previously shown (Table 4.4), the cohesive shift is larger for SX with FP (~45 %) than then it is for SX with respect to lactose (~36 %). The linear regression analysis of the CAB plots are shown in figures 4.15 A-B. The gradient of each plot represents the CAB ratio.

Table 4.10 Cohesive-Adhesive Balance (CAB) values with respect to Lactose and Fluticasone Propionate for freshly micronised SX and for SX samples conditioned *in-situ* with HFA

		CAB wrt Lactose	CAB wrt FP
Initial	Day 0	1.83 ±0.03	1.35 ±0.02
HFA	Day 30	2.48 ±0.04	1.96 ±0.04

Figure 4.15A Cohesive-Adhesive Balance (CAB) plot of the freshly micronised SX sample (Initial) and and SX conditioned *in-situ* with HFA with respect to lactose

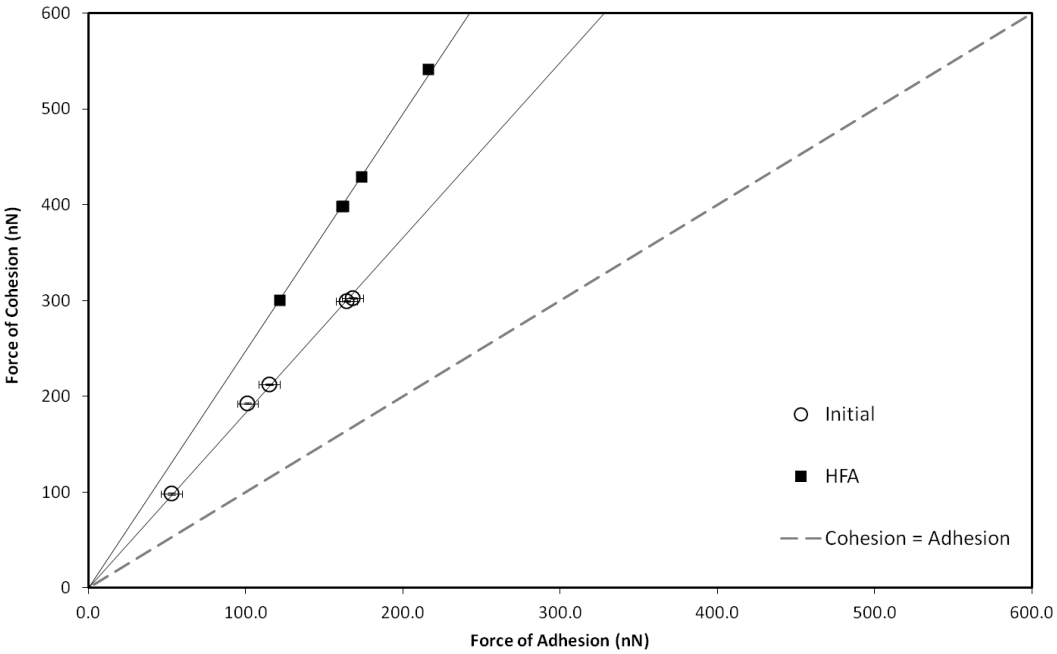

Figure 4.15B Cohesive-Adhesive Balance (CAB) plot of the freshly micronised SX sample (Initial) and SX conditioned *in-situ* with HFA with respect to FP

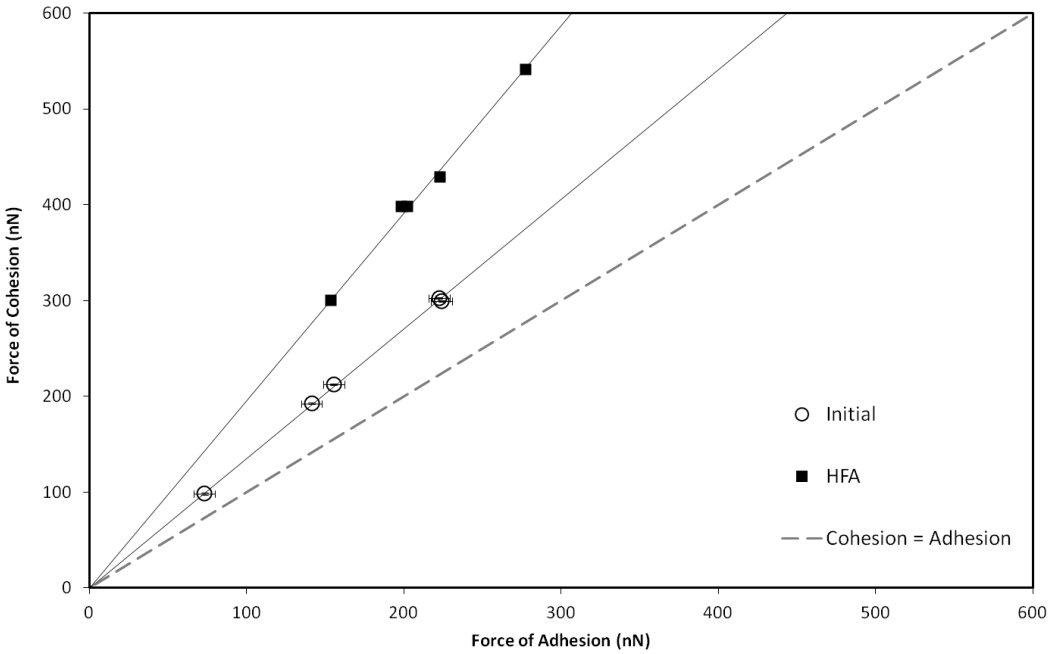

The *in vitro* aerosolisation data for binary and ternary formulations manufactured using freshly micronised and HFA conditioned SX are tabulated in table 4.11. As previously seen with environmentally conditioned SX samples, the cohesive shift observed in the CAB data leads to a decreased aerosolisation performance. Data shown for the binary formulation evidence a significant (p<0.02) increase in MMAD with concurrent significant drops (p<0.02) in ED and FPF. Figure 4.16 reflects this cohesive shift with a significant (p<0.02) increase in drug deposition recorded in the device stage with subsequent significant (p<0.05) decrease in deposition recorded on stages 1-5.

Data shown for the ternary formulation evidence how the larger cohesive shift observed in the SX-FP chemical system leads to a decreased aerosolisation performance for FP too. This is probably due to a reduction in the formation iof stbale FP-SX agglomerates which leads to lower deaggreation efficiency of the APIs and is indicated by the decrease in MMAD of the FP upon SX conditioning in HFA-134a.

Table 4.11 *In vitro* aerosolisation performance data for formulations manufactured using SX conditioned *in-situ* with HFA. Results are described by the recovered dose (RD), emitted dose (ED), fine particle mass (FPM), fine particle fraction (FPF) expressed as a percentage of the emitted dose, mass median aerodynamic diameter (MMAD) and geometric standard deviation (GSD)

	RD (µg)	ED (µg)	FPM (µg)	FPF (%ED)	MMAD (µm)	GSD (µm)
SX Binary						
Initial	54.58 ±3.12	32.11 ±2.55	11.69 ±1.01	36.39 ±2.34	1.98 ±0.02	2.71 ±0.02
HFA	46.54 ±2.38	24.74 ±1.98	6.40 ±0.78	25.87 ±1.31	3.99 ±0.03	2.17 ±0.02
SX in Combination with FP						
Initial	48.75 ±3.57	28.78 ±2.21	11.90 ±1.27	41.35 ±1.36	3.08 ±0.03	2.00 ±0.02
HFA	47.50 ±3.61	24.41 ±2.01	6.38 ±0.69	26.14 ±0.99	3.23 ±0.03	1.92 ±0.02
FP in Combination with SX						
Initial	216.50 ±7.35	139.28 ±4.55	47.26 ±2.45	33.93 ±1.35	3.91 ±0.04	2.00 ±0.02
HFA	209.49 ±6.58	115.07 ±4.07	29.56 ±1.48	25.69 ±1.27	3.73 ±0.03	1.92 ±0.02

Figure 4.16 Stage by stage deposition profile expressed as the percentage of emitted dose per stage for SX in binary formulations manufactured using SX conditioned *in-situ* with HFA

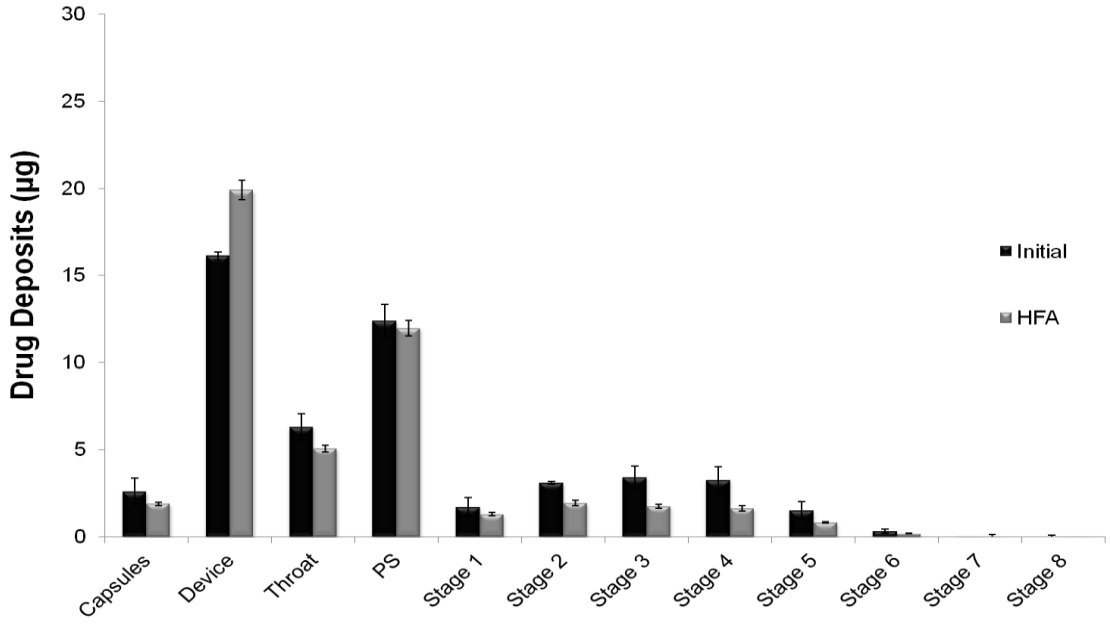

4.4 CONCLUSIONS

The results reported in this study have shown how post-micronisation conditioning can expedite the stress relaxation of micronised SX. Whilst particle size is largely unaffected by conditioning, other key physical properties such as specific surface area and surface roughness are directly influenced when SX particles are exposed to elevated temperature or humidity. These changes also coincide with a cohesive shift in the interfacial chemical system of SX particles. The ability of having a manufacturing process which expedites the thermodynamic stability of the drug properties is critical in being able to formulate a drug product which remains stable throughout the registered shelf-life. Whilst conditioning SX drives a cohesive shift in the chemical nature of the

SX particles, this shift is more pronounced with respect to FP. Results show how conditioning SX has a significant impact on the performance of FP in a ternary formulation. Interfacial and surface area stability seem to be achieved within the first 30 days of conditioning for SX particles using both conditioning methods employing HFA and elevated temperatures of 60°C.

5 The Post-Micronisation Dynamics of Freshly Micronised Glycopyrrolate Bromide

5.1 INTRODUCTION

The use of glycopyrrolate bromide (GLY) as an inhaled dosage form was first approved in 2012 (European Medicines Agency, 2012) as a once-daily maintenance bronchodilator treatment to relieve symptoms in adult patients with chronic obstructive pulmonary disease (COPD). It is administered as a 50µg dose in a capsule based dry powder inhaler. Phase III clinical trial data showed how the use of GLY improved lung function and reduced both shortness of breath and exacerbations (D'Urzo *et al.,* 2011; Beeh *et al.,* 2011). Clinical trials also demonstrated superior bronchodilation effect over tiotropium (Kerwin *et al.,* 2012), another maintenance bronchodilator used for the treatment of COPD.

For drug delivery to the lungs, GLY crystals need to be reduced to a mean particle size of less than 10µm (Jones *et al.,* 2008). This is commonly achieved by highly energetic air-jet micronisation, creating high velocity collisions which lead to size reduction. This process, as discussed previously, creates new surfaces, and may induce mechanical activation which may lead to physical and chemical modifications which can influence flow, adhesion and stability issues (Shur *et al.,* 2008). It has been widely reported, that while unmicronised GLY is stable, the micronisation process appears to lead to instability in terms

of handling, due to irreversible particle agglomeration as the hydrophilic GLY molecules aggressively absorbing water from the atmosphere (Rich, 2007). The tendency to form drug aggregates is synonymous with quaternary ammonium compounds (Pandy *et al.,* 2010) and relates to instability in physical and chemical properties, leading to a high degree of variation in the performance of formulations. It has been reported elsewhere (Morton *et al.,* 2008) that the introduction of a post-micronisation conditioning step can be used to alter the dynamics by which the new surfaces of the drug particles re-equilibrate to the more stable crystalline state. This study therefore aims at assessing the introduction of 2 distinct conditioning steps in such a way as to impede the formation of drug aggregation for post-micronised GLY particles, and thereby yield GLY particles with desirable and stable physicochemical properties.

5.2 MATERIAL & METHODS

5.2.1 Materials

Coarse GLY crystals, batch number 0623003, were bought from Sigma-Aldrich (St. Louis, MO, United States). GLY is a long-acting muscarinic-agonist (LAMA) with a chemical name of 3[(cyclopentylhydroxyphenylacetyl)oxy]-1,1-dimethyl pyrrolidinium bromide. It is a quaternary ammonium salt with a molecular weight of 398.33 and has a chemical formula of $C_{19}H_{28}BrNO_3$. GLY has a highly polar nature with a solubility of 21.66 mg/mL. It's melting point is 192.5°C and has a partition coefficient of 0.304 ($\log_{10}$ P = -1.52) in n-

octanol/water system at ambient temperature. Commercially, GLY is marketed as a once daily bronchodilator treatment for COPD. As an anticholinergic agent, GLY works by blocking the bronchoconstrictor action of acetylcholine on airway smooth muscle cells, consequently dilating the airways. The long duration of action can be partly attributed to the sustained concentrations of the active substance in the lung as reflected by the prolonged terminal elimination half-life of GLY seen in data submitted by the market application holder (European Medicines Agency, 2012).

A milled grade of lactose, ML001, was used throughout this study, supplied by DFE Pharma (Vehgel, Netherlands). All solvents used were of HPLC grade (Fisher Chemicals, Loughborough, UK). Ultra pure water was produced by reverse osmosis (MilliQ, Millipore, Molsheim, France). HFA 134a was supplied by Mexichem Fluor (Cheshire, UK) and had a batch number of 003215.

5.2.2 Methods

5.2.2.1 Micronisation of coarse Glycopyrrolate crystals by air-jet milling

10 grams of glycopyrrolate bromide were micronised by air-jet milling (McOne, Jetpharma, Balerna, Switzerland) under nitrogen using a grinding pressure of 8 bar and an injection pressure of 12 bar. The feed rate used was of approximately 1 gram per minute. These settings yielded just over 6 grams of micronised GLY particles with a d_{90} of 4.20µm which were split into 3 batches of 2 grams for post-micronisation conditioning described in table 5.1.

Conditions	Duration	Sample Reference	Formulations
Ambient (25°C/33 % RH)	7 Days	Ambient	0.4% $^{w}/_{w}$ in ML001
70°C (33 % RH)	7 Days	T70	0.4% $^{w}/_{w}$ in ML001
HFA (*in situ*)	7 Days	HFA	0.4% $^{w}/_{w}$ in ML001

Table 5.1 Summary of GLY post-micronisation conditioning throughout this work

In situ conditioning of the freshly micronised GLY was performed by placing the 2 gram sample in 60 grams of HFA. The HFA was directly inserted into a pressurised vessel and kept under pressure for 7 days. The vessel was then de-pressurised at a rate of 0.1 bar per minute. The HFA conditioned GLY sample was left to dry in controlled ambient conditions (25°C, 33 % RH) for 12 hours.

Following the 7 day laagering period, the 3 conditioned GLY samples, ambient, T70 and HFA were fully characterised for their physicochemical properties, formulated as 0.4 % $^{w}/_{w}$ binary formulations with lactose, and their *in vitro* aerosolization performance measured.

5.2.2.2 Particle Size Analysis

Particle size distributions of all GLY samples were measured in the wet state using a Sympatec HELOS and CUVETTE (Sympatec GmbH, Clausthal-Zellerfeld, Germany) laser diffraction system using an R3 lens (0.5-175 µm).

Approximately 20 mg of GLY particles were suspended in HPLC grade cyclohexane containing 0.5 %w/v lecithin (Acros Organics, Geel, Belgium) and sonicated for 3 minutes and immediately transferred into a 50 mL cuvette to produce an appropriate optical concentration (8-12 %). Each measurement was performed in triplicate and particle size analysis was performed using WINDOX 5.0 software (Sympatec GmbH, Clausthal-Zellerfeld, Germany).

5.2.2.3 Scanning Electron Microscopy

Particle morphology of GLY crystals and the 3 conditioned samples was investigated using scanning electron microscopy (SEM). Imaging was performed using a scanning electron microscope (JEOL JSM6480LV, Tokyo, Japan) using 15 kV accelerating voltage.

5.2.2.4 X-ray powder diffraction (XRPD) analysis

The X-ray powder diffraction (XRPD) patterns of GLY samples were analysed on a Bruker Powder Diffractometer (D8; Bruker AXS Inc., Madison, USA) using CuKα radiation (λ=1.54 Å). The data were collected over a single 2θ sweep with range 2θ = 5 - 30° and a step size of 0.025°/step with a step time of 1.5 s.

5.2.2.5 Differential Scanning Calorimetry

The thermal properties of all samples were investigated using a differential scanning calorimeter (DSC 2920, TA Instruments, Surrey, UK). The sample

and reference pan were heated at a rate of 10˚C/min from 30˚C to 250˚C. The calorimeter head was continuously flushed with dry nitrogen gas at 0.2 L/min during all measurements.

5.2.2.6 Specific Surface Area by BET

The specific surface area of the GLY crystals and all 3 conditioned samples was measured using a Gemini 2360 surface area analyser (Micromeritics Instrument Corporation, Norcross, USA).

5.2.2.7 Rugosity Calculation

Rugosity (R_a) is the qualitative description of the surface roughness of particles. It is mathematically described in Equation 6.1 (Joshi *et al.,* 2002). It uses the particles' surface volume result obtained from particle size measurement and the specific surface area value achieved from BET analysis. The validity of rugosity values for comparative reasons relies on the lack of change to macroscopic shape.

$$R_a = \frac{\text{Measured BET Surface Area (SSA)}}{\text{Calculated Surface Area from Particle Size Measurements } (S_v)}$$

Equation 6.1

5.2.2.8 Methodology of the CAB approach to colloid probe AFM

5.2.2.8.1 Crystallisation of substrates

To perform quantitative binary and combination AFM-CAB analysis of secondary processed GLY samples, smooth single crystal surfaces of GLY and lactose monohydrate were produced. Briefly, saturated solutions of GLY in 2 ml of acetone were prepared and sonicated prior to filtration via a 0.22-µm PTFE membrane filter (Whatman Inc., Clifton, NJ, USA). GLY was crystallised using water as the anti-solvent. Briefly, a microscope cover slip (12 mm x 12 mm) was supported on a vertical post in a crystallisation dish that contained the anti-solvent. A droplet of the saturated solution of the API was then placed on the coverslip using a syringe attached to the 0.22-µm-membrane filter. The system was sealed by inverting a glass lid in the crystallisation dish to allow vapour phases of the miscible solvents to come into equilibrium resulting in heterogeneous nucleation and crystal growth within the droplet. The glass cover slip was then attached to a magnetic AFM stub.

Lactose was crystallized upon introduction of saturated droplets between two glass cover slips. Smooth lactose crystals were generated upon preparing a solution of lactose (1 gm^{-1}) in double-distilled water, which was heated to 100 °C with constant stirring. The heated saturated droplet of the solution was filtered through a 0.2 µm PTFE membrane filter (Whatman Inc., Clifton, NJ, USA) and placed on to the centre of a clean cover slip, which was then sandwiched by placing another cover slip over the droplet. The resulting lactose crystals were then isolated upon cleaving the coverslips apart and attaching each coverslip to a magnetic AFM stub.

5.2.2.8.2 Colloidal probe force measurements

Prior to colloidal force measurements, individual particles from each GLY were attached onto standard V-shaped tipless cantilevers with pre-defined spring constants (DNP-020, DI, CA, USA) using an epoxy resin glue (Araldite, Cambridge, UK). Five probes were prepared for the as received, ambient, T70 and HFA conditioned GLY samples. All probes were examined with an optical microscope (magnification 50x) to ensure the integrity of the attached particle, before allowing the thin layer of glue to cure and dry.

Single crystal substrates were loaded onto an AFM scanner stage, which was enclosed in a custom-built environmental chamber, in which the ambient conditions were maintained at a constant temperature of 25 °C (± 1.5 °C) and relative humidity of 35 % RH (± 3 %). The interaction forces were measured by recording the deflection of the AFM cantilever as a function of the substrate displacement (z) by applying Hooke's Law. Individual force curves (n = 1024) were conducted over a 10 µm x 10 µm area at a scan rate of 4 Hz and a compressive load of 40 nN.

A custom-built software was developed to extract data contained within each force-volume dataset. These data was analyzed to ensure normal distribution, indicating uniform contact area between the drug probe and the smooth substrate surfaces. Arithmetic mean and standard deviation were measured to produce CAB plots for the interactions of the different samples of GLY with lactose monohydrate.

5.2.2.9 Preparation of powder formulations

0.4 % $^{w}/_{w}$ GLY binary formulation blends were manufactured for each of the 3 conditioned GLY samples. All 3 GLY samples were sieved through a mesh size of 200µm prior to formulating. The 4 gram blends were manufactured by the sequential addition of the drug to the milled lactose (ML001) followed by low shear blending using a T2F Turbula® mixer (Wily A Bachofen AG, Basel, Switzerland) for 45 minutes at 46 rpm.

From each blend, 12.5 ± 0.5 mg were hand filled into size 3 hydroxypropylmethyl cellulose (HPMC, Shionogi Qualicaps, Madrid, Spain) capsules. The loaded dose for the GLY binary formulations was 50 µg of GLY per 12.5 mg fill weight. In order to ensure the dissipation of any electrostatic charges induced during processing, the capsules were stored at 44 % RH for 24 hours prior to *in vitro* testing.

5.2.2.10 *In vitro* aerosolisation testing

A next generation impactor (NGI, Copley Scientific, Nottingham, UK) connected to vacuum pumps (GE Motors) was used to test the aersolisation of each formulation. The NGI surfaces were coated with 1 % $^{v}/_{v}$ silicone oil in hexane to eliminate any particle bounce. For each experiment, two individual capsules of the same blend were discharged into the NGI at a flow rate of 60 L/min for 4 seconds, equivalent to a total volume of 4L, from a Rotahaler® DPI device (Cipla, Mumbai, India). A flow meter (DFM 2000, Copley Scientific, Nottingham, UK) was used to verify the air flow prior to each test. The amount of API deposited on each part of the NGI was determined by high pressure liquid chromatography (HPLC) analysis. This testing protocol was repeated

three times for each formulation, following which, the mass median aerodynamic diameter (MMAD) geometric standard deviation (GSD), fine particle mass less than 5.0μm (FPM) and fine particle fraction (FPF) were determined.

5.2.2.10.1 Stability profile assessment for formulations via stress testing

A selection of capsules from each formulation were hermetically sealed in aluminium packaging and put into two distinct stability chambers; one set at 30°C with a relative humidity of 65 %, and the other at 40°C and 75 % RH. The *in vitro* performance of these capsules was tested at the pre-defined time intervals of 1 and 3 months. Testing for *in vitro* aerosolisation performance was conducted as previously described.

5.2.2.11 HPLC Methodology for the quantification of GLY

Detection and quantification of GLY was performed via HPLC analysis. The mobile phase consisted of 10 % acetonitrile (Fisher Chemicals, Loughborough, UK), 40 % 0.02M sodium dihydrogen phosphate monohydrate (Sigma, Gillingham, UK) adjusted to a pH of 6.50 and 50 % methanol (Fisher Chemicals, Loughborough, UK). This was pumped (Jasco PU-980, Tokyo, Japan) at a flow rate of 1.0 mL/min through a 250 mm long hypersil-BDS column of a 4.0 mm inner diameter with silica gel packing with a particle size of 5 μm (Thermo Scientific, Loughborough, UK). The samples were injected using an autosampler (Jasco, Tokyo, Japan) into the column fit into an oven (Jasco CO-965, Tokyo, Japan) kept at 30°C. The eluted drug was detected using a Jasco UV-975 detector (Jasco, Tokyo, Japan) set at a wavelength of

222nm for GLY. The retention time was of approximately 4.75 minutes. A linear regression analysis of GLY standards with known concentrations varying between 0.05 and 50 µg/mL was used to validate the method and quantify the unknown samples. The limit of detection for this method was found to be 0.01 µg/mL and the linearity of the method between the validated concentrations of 0.05 µg/mL and 50 µg/mL had a coefficient of determination of 0.9997.

5.2.2.12 Statistical analysis

Statistical analysis between different populations was carried out using one-way analysis of variance. Comparison of the mean values was performed by Tukey's multiple comparison. Analysis for statistical difference was performed using GraphPad Prism software (GraphPad Software Inc, California, USA). Error bars in graphical representations of data show ± standard deviation (s.d.) in all cases.

5.3 Results and Discussion

5.3.1 Physicochemical characterisation

In order to understand the influence of post-micronisation conditioning on the structural relaxation of GLY, the physicochemical properties of the conditioned samples were studied. The particle size distribution data collected for all the conditioned GLY samples are tabulated in table 5.2.

	d_{10} (µm)	d_{50} (µm)	d_{90} (µm)
Crystals	2.22 ±0.03	36.03 ±0.04	71.54 ±0.29
Post-Micronisation	0.78 ±0.03	2.04 ±0.03	4.20 ±0.11
Ambient (7 Days)	2.11 ±0.02	21.58 ±0.04	66.72 ±0.31
T70 (7 Days)	0.82 ±0.04	2.09 ±0.02	4.35 ±0.17
HFA (7 Days)	0.77 ±0.02	1.90 ±0.03	3.80 ±0.12

Table 5.2 Particle Size Distribution of GLY samples handled during this study as determined by laser diffraction

The particle size data demonstrated a high degree of particle aggregation may occur when freshly micronised GLY is exposed to ambient conditions for 7 days following air-jet micronisation. This particle aggregation process is thought to be caused by the aggressive uptake of water by the hydrophilic GLY particles as reported elsewhere (Rich, 2007). The particle size distribution of this sample exhibited a very significant (p<0.001) increase in the d_{90} value for the ambient GLY sample, suggesting that this sample may not be suitable for delivery to the lungs (Jones *et al.,* 2008a). The T70 and HFA GLY particle size distribution data suggested that post-micronisation conditioning of GLY particles for 7 days using both temperature and *in situ* conditioning may impede the aggregation of the GLY particles. The particle size distributions for both these samples suggest that the GLY particles are suitable for delivery to the lungs (Jones *et al.,* 2008a).

The SEM micrographs for GLY crystals and the three distinct post-micronisation conditioned GLY particles are shown in figure 5.1. These micrographs reaffirm the particle behaviour seen in the particle size distribution results, highlighting how the ambient GLY sample (figure 5.1B) aggregates to form a coarse cluster of micronised particles (figure 5.1A) following ambient storage for 7 days post-micronisation. The GLY particles conditioned as described previously in table 5.1 and referred to as T70 and HFA, produce SEM micrographs (figure 5.1 C-F) show particles suitable for delivery to the lung with no degree of aggregation or agglomeration.

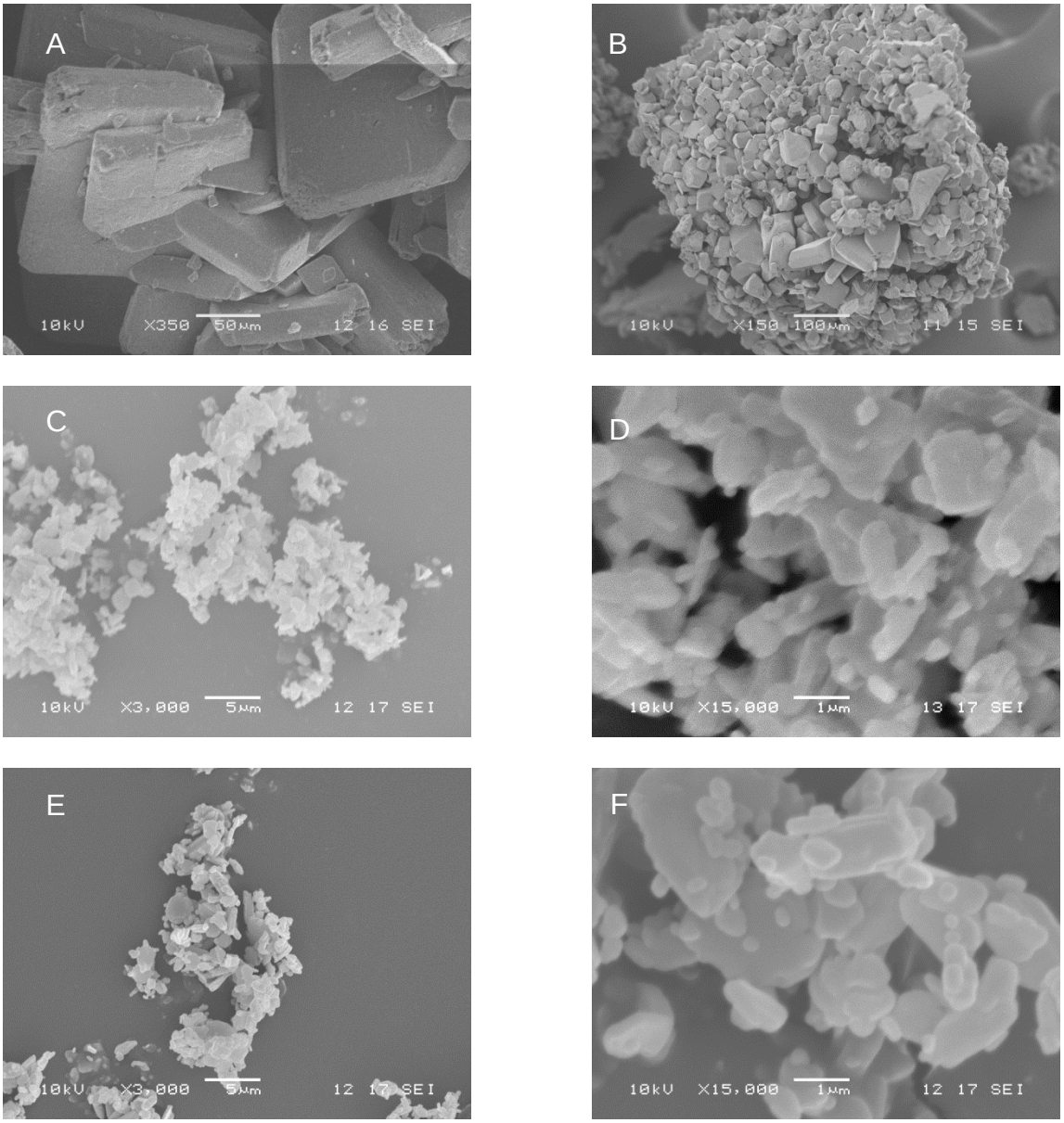

Figure 5.1 Scanning Electron Micrographs for GLY crystals (A), ambient sample (B), T70 sample (C,D) and HFA sample (E,F)

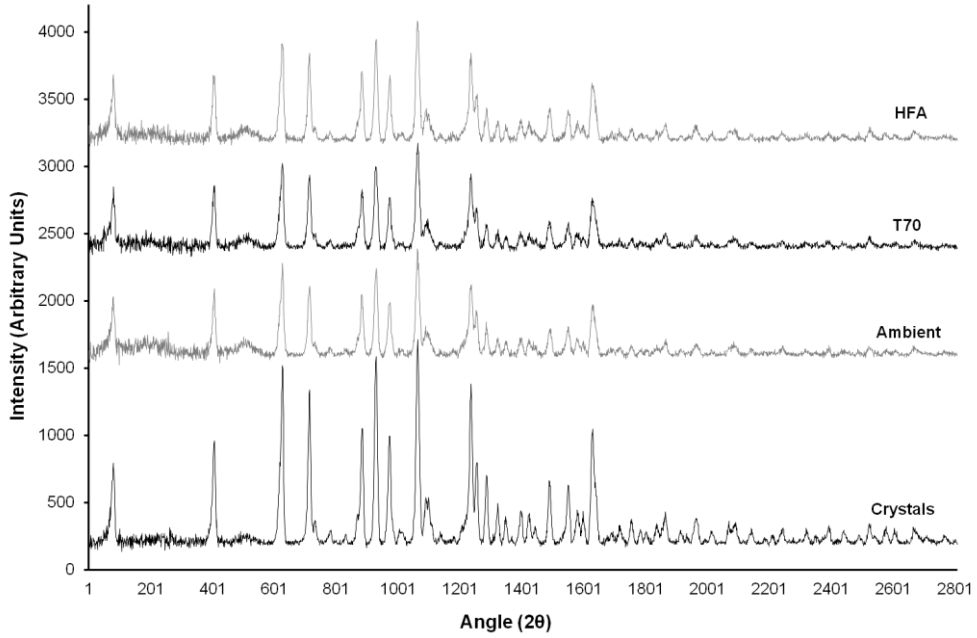

Figure 5.2 X-ray powder diffraction profiles for GLY crystals and the post-micronised conditioned samples

Figure 5.2 shows the XRPD diffractograms for the GLY crystals, ambient, T70 and HFA samples. The sharp peaks observed in the diffractograms for all samples suggest polymorphic stability upon conditioning, although this was expected since only one polymorphic form has been reported for GLY (Baxter, 2011). The XRPD results also suggest that all GLY samples are predominantly crystalline in nature, even though this analytical technique is unable to detect amorphous content levels below 10 % (Saleki-Gerhardt *et al.,* 1994). The decrease in the peak intensities for the conditioned samples maybe caused by the rougher surfaces of the micronised GLY particles, decreasing the efficiency with which X-rays are scattered.

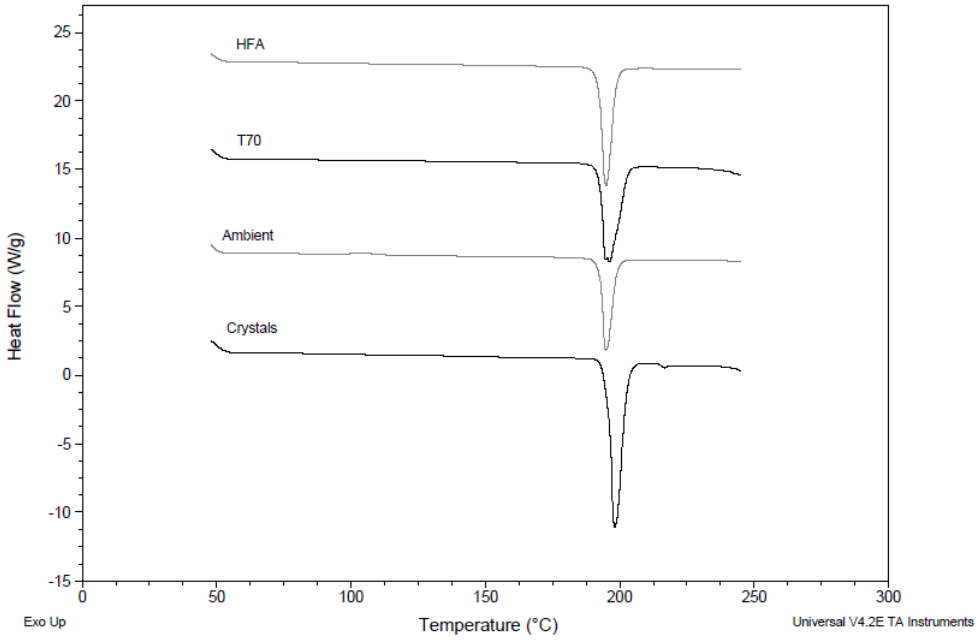

Figure 5.3 Differential Scanning Calorimetry thermographs for the GLY crystals, ambient, T70 and HFA samples

The DSC thermographs are shown in figure 5.3. All thermographs display a melting onset at approximately 193˚C, confirming the purity of the known polymorphic form for GLY which has a reported melting point of 192.5˚C (Baxter, 2011). The glass transition (T_g) from amorphous to crystalline GLY occurs at a temperature of around 65˚C (Baxter, 2011). The absence of any calorimetric activity for all samples at this temperature suggests that all samples have re-crystallised prior to analysis. The particle size distribution and the SEM images suggest that the aggressive intake of water by the GLY particles stored at ambient conditions for 7 days acts as a plasticiser, which may lead to the structural reconstruction of the process induced structural disorder. Whilst this surface-led relaxation process is undesired due to the

physical changes previously discussed rendering the GLY particles unsuitable for inhalation.

One notable difference in the thermographs of the GLY samples is the magnitude of the endotherms upon melting. Table 5.3 tabulates the endothermic enthalpies required in melting the different GLY samples. The GLY crystals required an enthalpy of 384.2 $J.g^{-1}$ for the melting process. This value was relatively high compared to the endothermic response of micronised GLY samples maybe because the molecular arrangements in crystalline regions are generally denser than molecular arrangements found in particles containing amorphous pockets (semi-crystalline), requiring more energy to break down and cause complete melting. The results in table 5.3 show how the energy required for the melting process of the GLY particles stored at ambient conditions for 7 days was significantly (p<0.02) lower than the T70 and HFA samples. The T70 GLY sample also required significantly (p<0.02) more energy in order to melt than the HFA GLY sample. This suggests that post-micronisation conditioning using an elevated temperature of 70˚C for 7 days is more efficient at re-crystallising the disordered, micronised GLY particles.

	Melting Endotherm (J/g)	S_v (m^2/cm^3)	SSA (m^2/gram)	R_a
Crystals	384.20 ±26.51	0.89	0.04 ±0.01	0.04
Ambient	194.95 ±13.69	0.92	4.71 ±0.22	5.11
T70	309.40 ±14.51	3.62	6.41 ±0.08	1.77
HFA	272.33 ±13.49	3.91	4.80 ±0.03	1.23

Table 5.3 Melting endotherm (J/g) from DSC analysis, surface area per unit volume (S_v), specific surface area per unit mass (SSA), and rugosity values (R_a) for GLY crystals and the 3 conditioned micronised samples

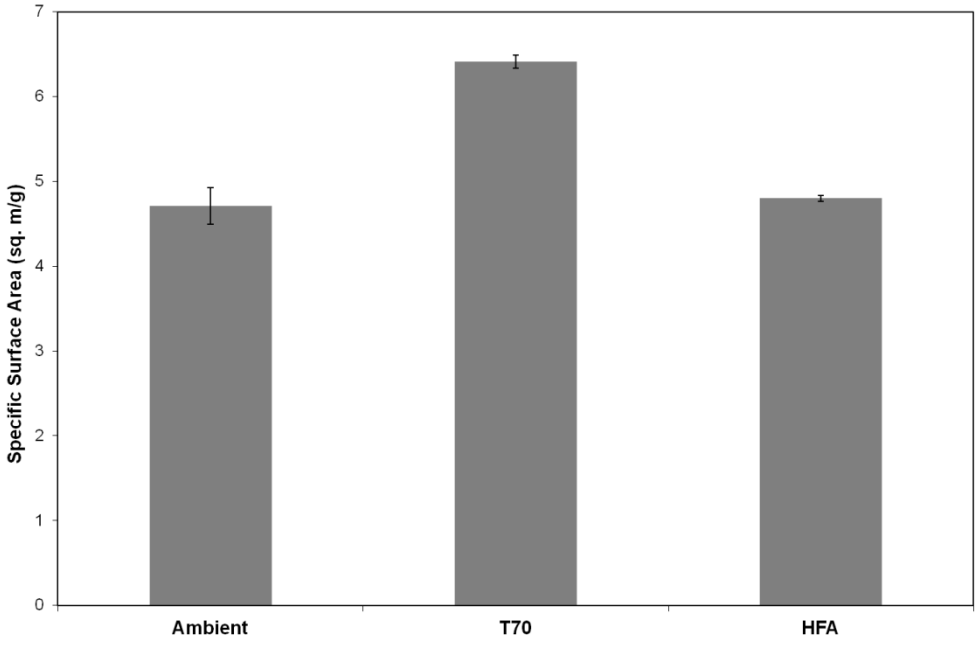

Figure 5.4 Specific Surface Area the conditioned GLY samples determined by BET analysis

Figure 5.4 shows the specific surface area (SSA) for the 3 conditioned GLY samples determined by BET analysis using gas adsorption. This figure shows how the T70 GLY sample had a significantly (p<0.02) higher specific surface

per unit mass than the other 2 conditioned samples. There seemed to be no significant differences between the specific surface area of the ambient and the HFA GLY sample. The SSA results are tabulated in table 5.3 together with the values for the surface area per unit volume obtained from particle size analysis. These 2 surface area measurements are used to determine the rugosity value of the particles. The rugosity values, tabulated in table 5.3, indicate a large difference between the ambient GLY sample and the T70 and HFA samples. This high rugosity value for the ambient sample (Ra = 5.11) is probably due to the nature of the drug aggregates caused by the fusion of GLY particles upon the aggressive uptake of water. The rugosity values also suggest a significant difference in the particle roughness of the T70 and HFA GLY samples, with T70 having a rugosity value of 1.77 as opposed to the 1.23 for the HFA sample.

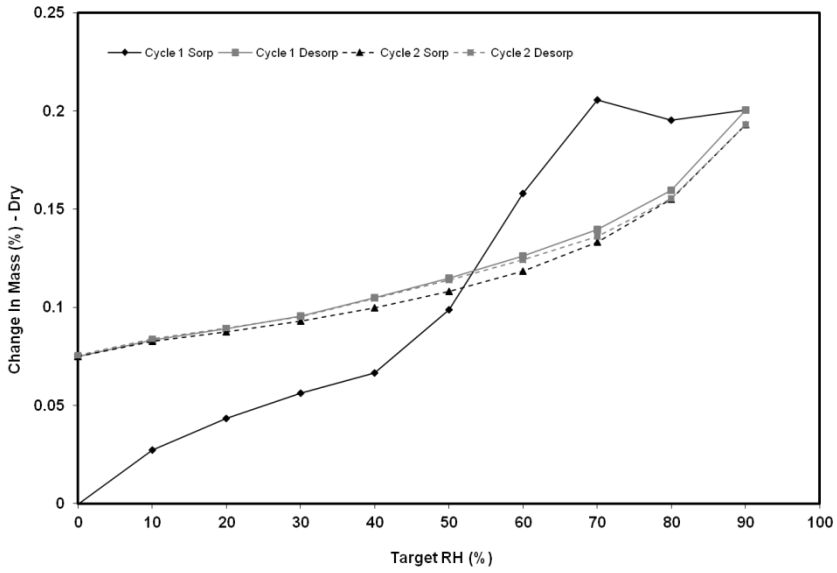

Figure 5.5A Dynamic Vapour Sorption (DVS) isotherm for the ambient GLY conditioned sample

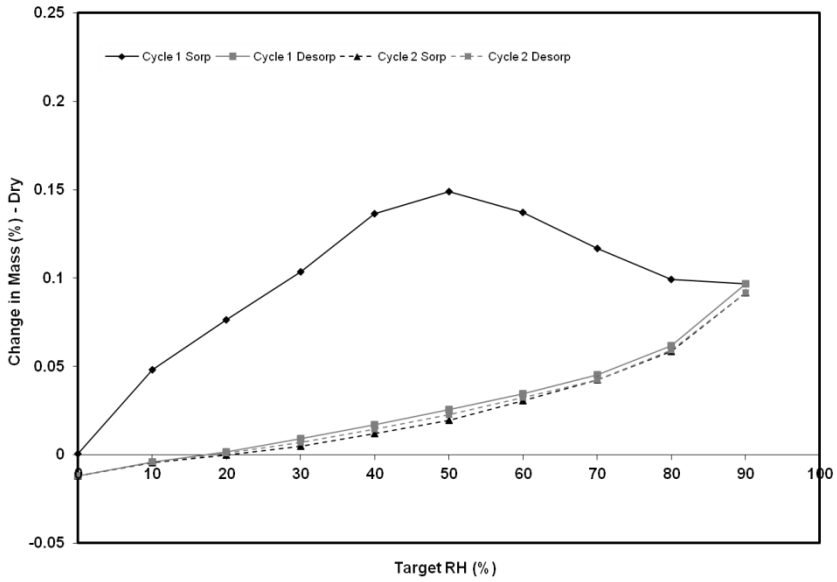

Figure 5.5B Dynamic Vapour Sorption (DVS) isotherm for the T70 GLY conditioned sample

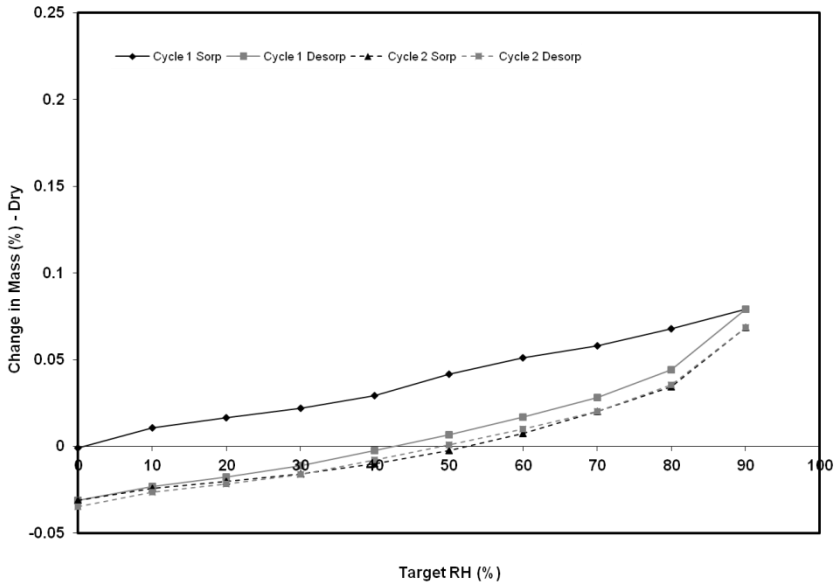

Figure 5.5C Dynamic Vapour Sorption (DVS) isotherm for the HFA GLY conditioned sample

Figures 5.5 (A-C) show the dynamic vapour sorption profiles for the 3 conditioned GLY samples. The isotherm for the ambient GLY sample shown in figure 5.5A seems to show a possible re-crystallisation event occurring between 40% and 70 % RH. The sorption profile accelerates between these 2 humidities suggesting a change is occurring to the molecular arrangement of the GLY particles. Figure 5.5B shows the isotherm for the T70 GLY particles. This profile shows a significant uptake of water between 0 % and 50 % relative humidity. This steep gradient is most probably caused by the rehydration of the GLY particles from the anhydrous to the monohydrate state following dehydration caused by exposing the particles at 70°C for 7 days. Figure 5.5C on the other hand shows no particular isothermic activity suggesting that the GLY particles conditioned *in situ* with HFA have a predominantly crystalline nature. The moisture uptake can be explained in terms of the hydrophilic nature of GLY.

5.3.2 Interfacial Chemistry Results

Table 5.4 tabulates the CAB results for the post-micronised conditioned GLY particles. The results describe the balance between the cohesive and adhesive forces with respect to lactose, determining the interfacial behaviour of the particles.

	CAB w.r.t Lactose
Ambient	0.61 ±0.02
T70	1.19 ±0.03
HFA	0.69 ±0.01

Table 5.4 Cohesive-Adhesive Balance (CAB) values with respect to Lactose for all 3 conditioned GLY samples

The CAB value for the ambient GLY sample describes a powder system which is dominated by adhesive forces. A CAB value of 0.61 suggests that drug-lactose interactions are 1.64 times more frequent than drug-drug interactions, as is the affinity between the 2. This highly adhesive interfacial nature governing the dynamics of the powder system for the ambient GLY sample, suggests that the significant (p<0.02) dominance of the adhesive forces over the cohesive forces may impede the efficient aerosolisation of the drug particles translating to a poor *in vitro* performance. Figure 5.6A shows the linear regression analysis for the cohesive and adhesive forces of the GLY particles conditioned for 7 days at ambient conditions following air-jet micronisation.

The CAB value for the GLY sample conditioned for 7 days at 70˚C shifts from a strongly adhesively-led system to a significant (p<0.02) greater cohesively-led interfacial powder system. This shift suggests that with a CAB value of 1.19, the GLY particles for the T70 sample favour drug-drug interactions over drug-lactose ones. The dominance of the cohesive forces, seen in the linear

regression analysis in figure 5.6B, may suggest that the affinity between drug particles will lead to a degree of drug agglomerates formed during formulation. The aerosolisation efficiency of these drug particles will be very much dependant on the degree cohesiveness governing the formation and coalescence of the drug agglomerates. A CAB value of 1.19 suggests that whilst cohesively-led, the powder system still contains sporadic drug/agglomerates-lactose interactions which enable the drug particles to travel out of the capsules and device using the inertial force gathered by the larger lactose particles, however, said interactions are weak enough to allow the drug agglomerates to detach from on the lactose surface and travel down through the impactor.

The CAB value for the GLY particles following post-micronisation *in situ* conditioning in HFA for 7 days, describes a system dominated by adhesive forces as seen in figure 5.6C. This value, which shows a small but significant ($p<0.05$) difference from the interfacial chemistry describing the ambient sample, suggests the in situ conditioned particles have a greater affinity towards the lactose particles. These preferred drug-lactose interactions may, as discussed previously, hinder the aerosolisation of drug particles from on the lactose carrier particles, negatively impacting the *in vitro* performance of GLY.

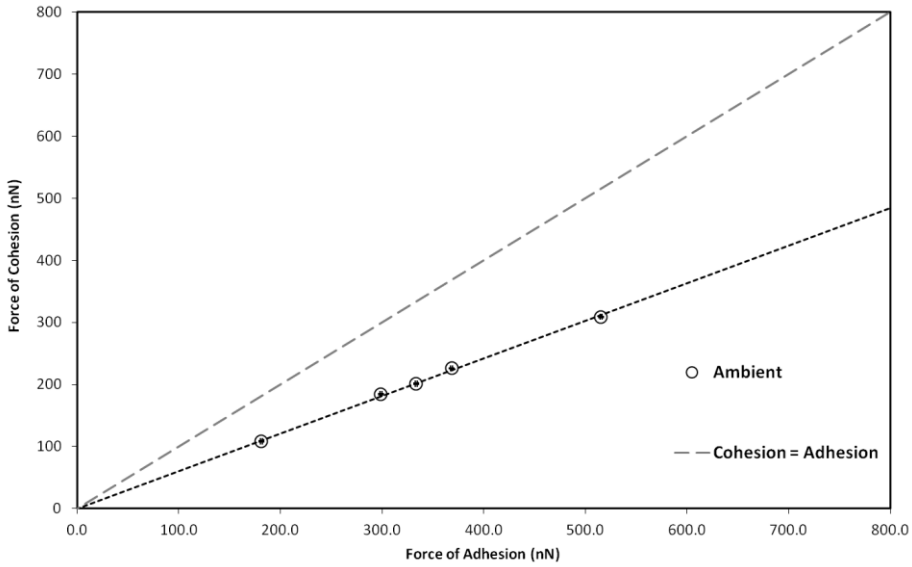

Figure 5.6A Plot for the cohesion and adhesion forces for the ambient GLY particles with respect to lactose

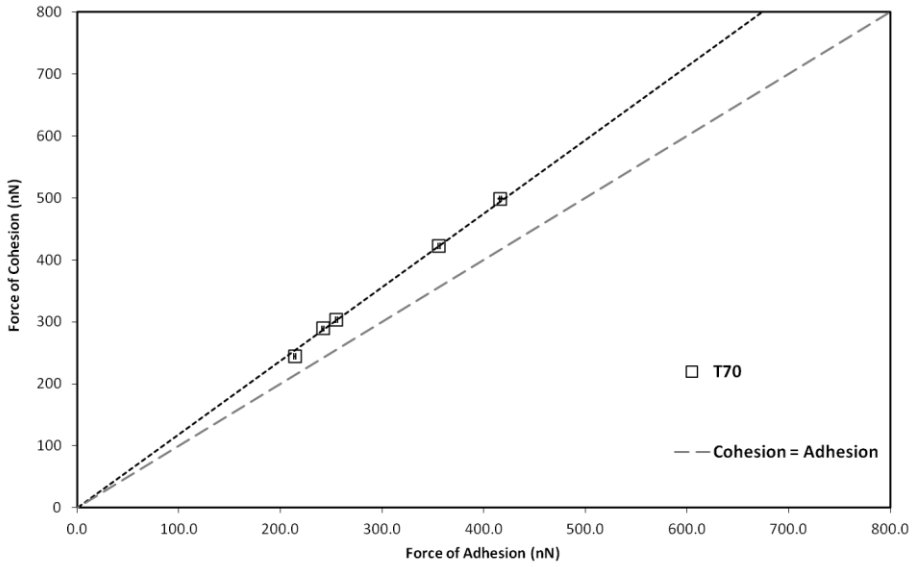

Figure 5.6B Plot for the cohesion and adhesion forces for the T70 GLY particles with respect to lactose

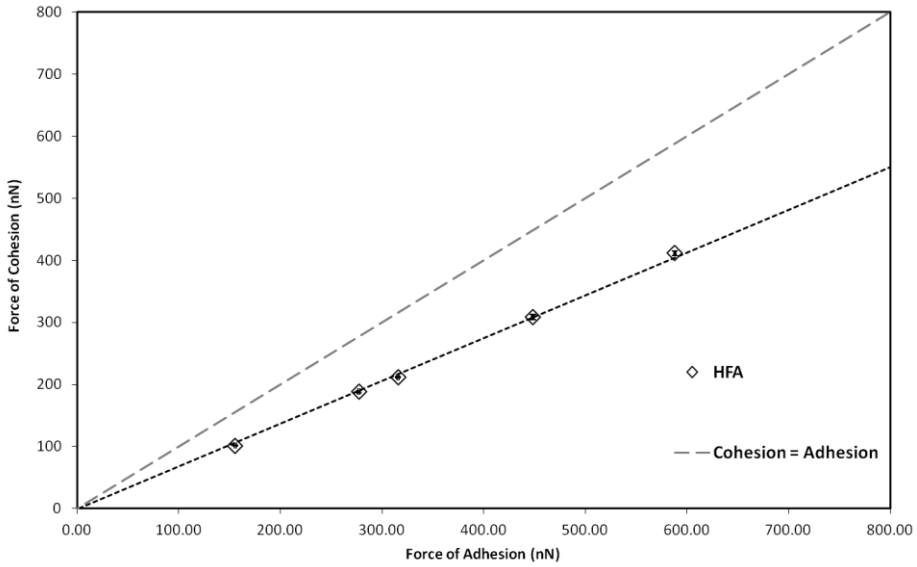

Figure 5.6C Plot for the cohesion and adhesion forces for the HFA GLY particles with respect to lactose

5.3.3 *In vitro* performance

Table 5.5 tabulates the *in vitro* performance data of 3 distinct binary formulations manufactured using the conditioned GLY samples. The results for all 3 formulations are consistent with the CAB results discussed previously.

	RD (µg)	ED (µg)	FPM (µg)	FPF (%ED)	MMAD (µm)	GSD (µm)
Ambient	94.77 ±5.27	70.27 ±3.39	11.07 ±0.91	15.76 ±0.70	2.5 ±0.09	2.14 ±0.04
T70	89.72 ±4.88	69.40 ±2.25	25.58 ±1.71	36.86 ±1.83	3.37 ±0.12	2.33 ±0.04
HFA	89.22 ±4.71	69.72 ±3.12	15.28 ±1.02	21.92 ±1.21	2.68 ±0.04	2.34 ±0.05

Table 5.5 *In vitro* aerosolisation performance for GLY formulations produced using the conditioned GLY samples; ambient, T70 and HFA. Results are described by the recovered dose (RD), emitted dose (ED), fine particle mass (FPM), fine particle fraction (FPF) expressed as a percentage of the emitted dose, mass median aerodynamic diameter (MMAD) and geometric standard deviation (GSD)

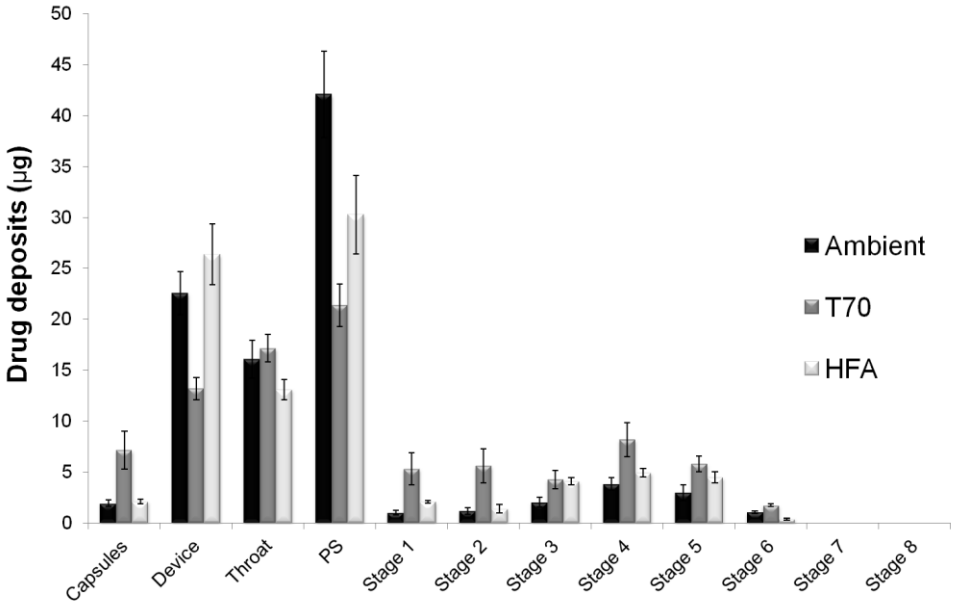

Figure 5.7 Stage by stage deposition profile for the 3 GLY formulations expressed as drug deposits in µg

The FPF for the ambient GLY formulation is relatively low at 15.76 %, a value that may be attributed to the highly adhesive nature of the GLY particles constituting this formulation. As discussed previously, the adhesively-led system leads to the impediment of an efficient drug deagglomeration from of the lactose carrier particles. A clear characteristic of such a powder system can be seen in the stage-by-stage analysis (figure 5.7) where approximately 50 % of the drug particles is deposited in the pre-separator suggesting inefficient deagglomeration from the lactose particle surface.. The relatively low MMAD (MMAD = 2.5 µm) for this formulation is also characteristic of an adhesively-led system, where the particles are more prone to form drug-lactose interactions than form drug agglomerates as shown by the T70 formulation (MMAD=3.37 µm). The FPF for the T70 formulation (36.86 %) is

significantly (p<0.01) higher to the FPF of both the ambient (15.76 %) and the HFA (25.16 %) formulations. Once again, these *in vitro* data are consistent with the CAB results observed for the T70 GLY sample. The T70 drug particles preferentially form drug agglomerates, however, the balance in favour of the cohesive forces over the adhesive ones is not large enough to hinder these drug agglomerates from interacting with the lactose particles, using them as a medium to gaining inertial energy in a way to aerosolise form the capsule and device. On impact, these drug agglomerates detach from on the lactose surface and are free to flow through the impactor. The MMAD for the T70 formulation (3.37µm) suggests the presence of drug agglomerates significantly (p<0.02) larger than those for the ambient (2.5µm) and HFA (2.68) formulations. Figure 5.7 shows the significant drop in drug deposits in the pre-separator discussed previously. There is also a significantly (p<0.05) higher amount of drug deposits in the capsules when compared to the drug deposits of the other 2 formulations. This is highly likely to be due to the presence of some drug agglomerates which failed to have the sufficient inertial energy to aerosolise from the capsules probably as a result of segregation from the coarse lactose particle. The in situ conditioned formulation also shows *in vitro* data in line with its corresponding interfacial properties. The highly adhesive nature of the HFA GLY particles is clearly evidenced in figure 5.7 where the low drug deposits in the capsules together with relatively high values in the throat and pre-separator are a characteristic footprint of highly adhesive systems. Similar to the behaviour of the the ambient formulation, which shares a common adhesively-led nature, the significantly (p<0.05) lower (relative to

T70) drug values seen in the capsules reflect the high affinity between the drug and lactose particles, allowing the drug particles to be effectively entrained from the capsule. The significantly (p<0.05) higher values of drug retention in the device and pre-separator (relative to T70) are also characteristically associated with highly adhesive systems, where the drug particles fail to deagglomerate from on the lactose particles as the latter are too large to travel further down the NGI apparatus. There is a significant (p<0.05) difference in the FPF between the HFA formulation (21.92) and the ambient formulation (15.76). This seems to be mainly accounted for in the pre-separator where the HFA formulation deposits approximately 13 µg (15 %) of drug less than the ambient formulation, and is explained by the slightly more adhesive nature exhibited by the ambient GLY particles.

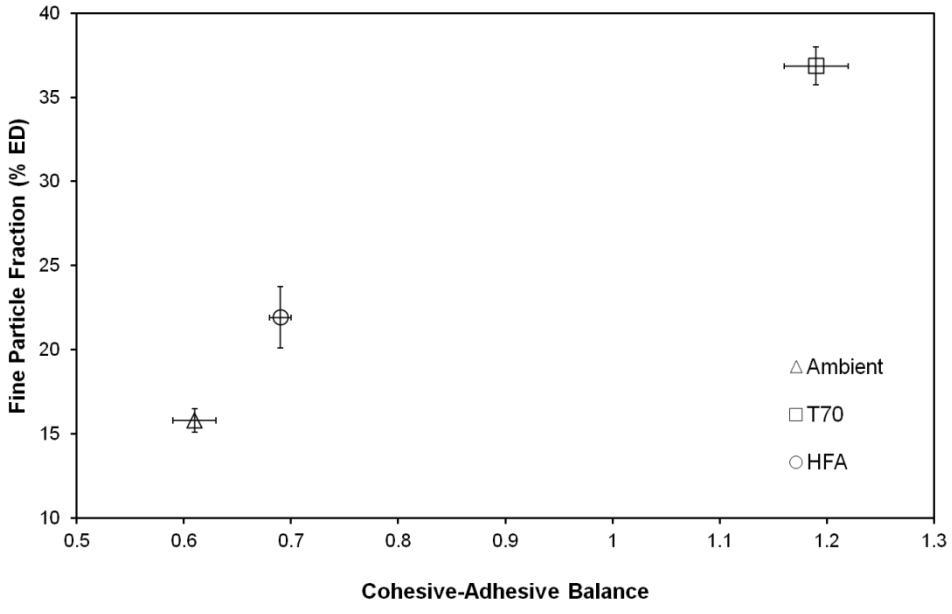

Figure 5.8 Fine particle fraction expressed as a percentage of the emitted dose for each GLY formulation plotted against the respective CAV value of the conditioned GLY particles

Figure 5.8 shows the FPF for each formulation plotted against the respective CAB values of the GLY particles. This figure depicts the close relationship between the interfacial chemistry of the GLY particles and their respective aerosolisation performance. As discussed previously, the slightly cohesive nature governing the GLY particles in the T70 formulation yields a significantly (p<0.01) higher FPF due to the presence of drug agglomerates which maintain a sufficient affinity to lactose to be effectively emitted from the capsules while undergoing sufficient deagglomeration upon aerosolisation. On the other hand, the highly adhesive forces dominating the formulations for the GLY ambient and HFA samples impede the aerosolisation of the GLY particles. Figure 5.8 summarises this rationale, showing the dependence of *in vitro* performance on the interfacial system governing the drug particles.

5.3.4 Stability of Formulation Performance

5.3.4.1 30°C/65 % RH Stability Profile Results

Figure 5.9 shows the *in vitro* performance stability profile for the T70, HFA and ambient formulations stored at 30°C/65 % RH for a period of 3 months. The results show that the aerosolisation performance for the T70 and HFA formulations remain stable throughout the 3 month profile with no significant differences between the different time points. This suggests a high degree of chemical stability for GLY particles conditioned at 70°C and also for those particles conditioned *in situ* with HFA. The statistically similar performances together with the lack of differences in the impactor-sized masses (ISM) shown in Figure 5.10, advocate that the interactions between the GLY particles and the lactose carrier remain unchanged, yielding to a consistent *in vitro*

performance. The ambient formulation, on the other hand, demonstrates a significant (p<0.05) downward trend in the aerosolisation performance over the 3 month period. Whilst there is no statistical significant difference between the performance of month 0 (15.76 %) and month 1 (13.91 %), the FPF of the Ambient formulation at month 3 (11.54 %) is significantly lower than the original timepoint. This downward trend in the FPF for the Ambient formulation over the 3 month 30˚C/65 % RH stability profile study is also reflected in the ISM values shown in Figure 5.10. These values reflect the instability of the adhesive chemical nature of the Ambient GLY particles. The parallel decrease in the ISM and FPF shown by the Ambient formulation over the 3 month study suggest an unstable chemical system for the GLY particles whereas the adhesive nature observed previously changes in magnitude as a function of time and stress conditions, leading to instable performance for the formulation.

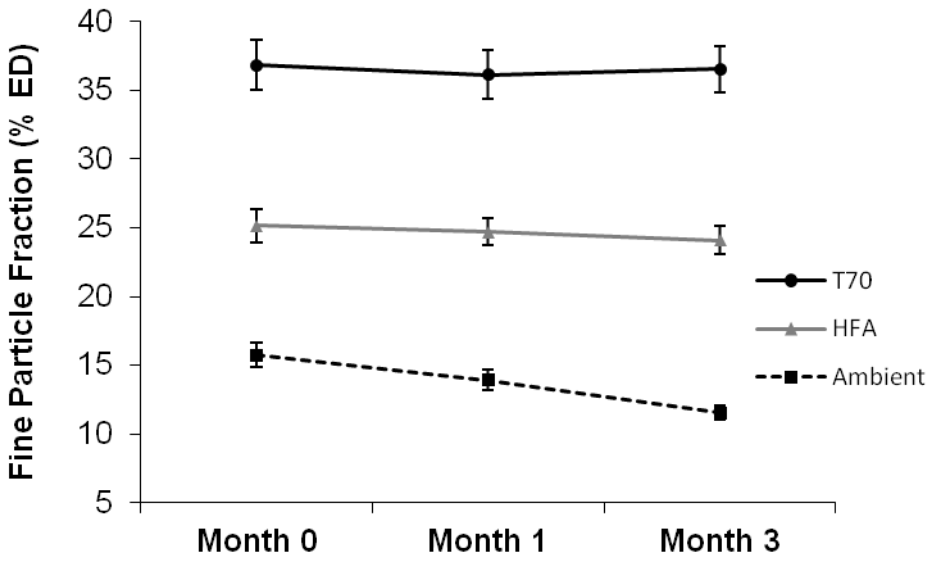

Figure 5.9 FPF (%) of Ambient, T70 and HFA formulations stored at 30˚C/65% relative humidity for a 3 month period

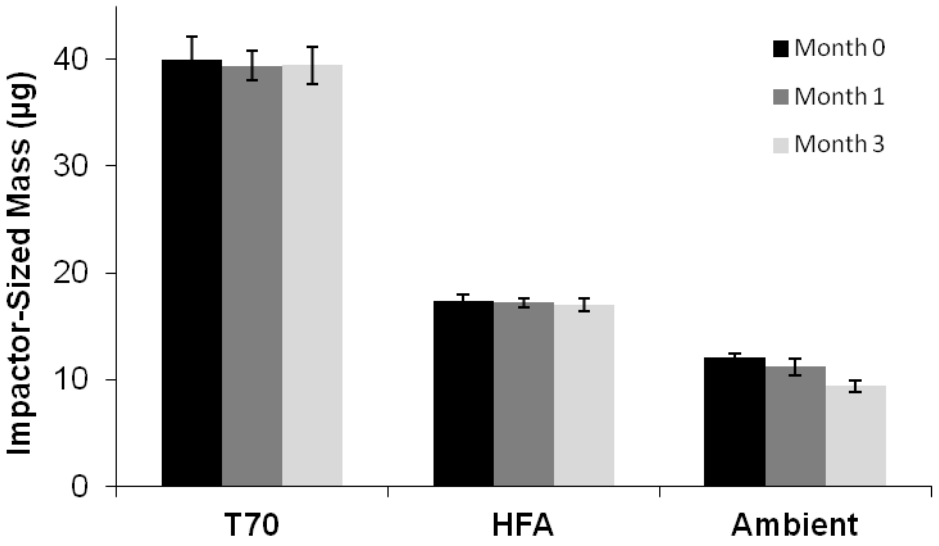

Figure 5.10 The Impactor-Sized Mass (ISM) for the Ambient, T70 and HFA formulations upon testing at the defined stability time intervals following storage at 30°C/65% relative humidity

5.3.4.2 40°C/75% RH Stability Profile Results

The FPF results for the T70, HFA and Ambient formulations following a 40°C/75 % RH stability study are shown in Figure 5.11. Whilst confirming the stability of the T70 and HFA formulations, this stability study provided further evidence of the instability demonstrated by the Ambient GLY formulation. The significant difference ($p<0.05$) between the FPF of month 0 (15.76 %), month 1 (12.17 %) and month 3 (7.92 %) represent a varying chemical stability governing the interactions between the GLY and the lactose particles. The ISM values shown in Figure 5.12 confirm the increasing dominance of the adhesive forces, impeding the GLY particles from aerosolising away from the larger lactose particles and travelling into the impactor.

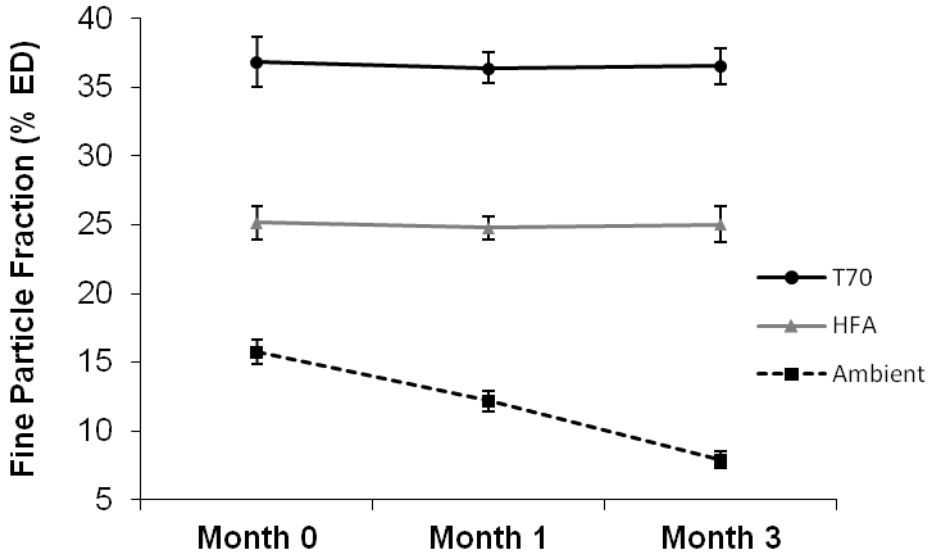

Figure 5.11 FPF (%) of Ambient, T70 and HFA formulations stored at 40°C/75% relative humidity for a 3 month period

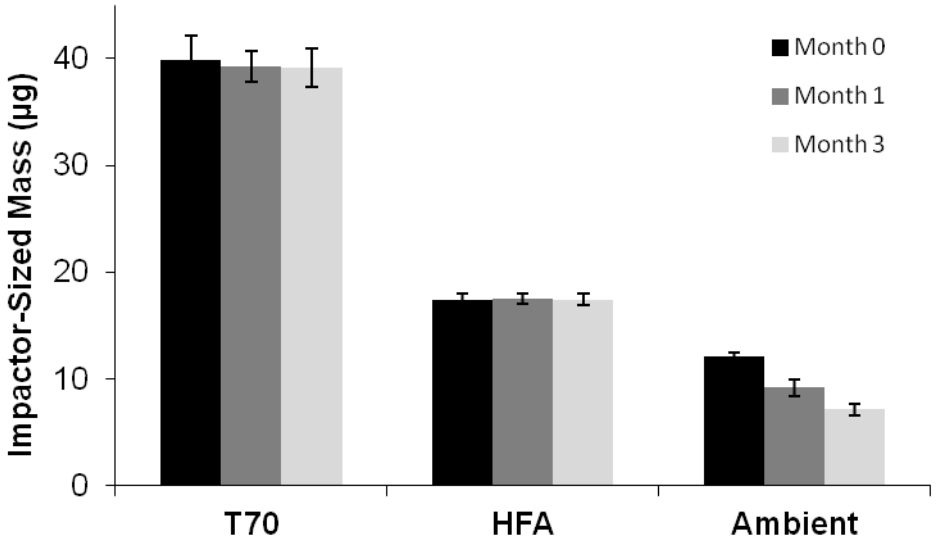

Figure 5.12 The Impactor-Sized Mass (ISM) for the Ambient, T70 and HFA formulations upon testing at the defined stability time intervals following storage at 40°C/75% relative humidity

These data suggest that the T70 and HFA GLY particles possess increased stability translating into stable drug-carrier interactions yielding consistent *in vitro* performances with time and under stress conditions. The unstable nature of the Ambient GLY particles highlight the importance of a post-micronisation conditioning step to expedite the stress relaxation process that enables the attainment of drug particles with a stable chemical properties.

5.4 Conclusions

This study describes the use of a post-micronisation conditioning step to improve the troublesome handling of GLY particles following air-jet micronisation. These data confirmed the possible issues with non-conditioned GLY particles stored under ambient conditions and its influence on physic-chemical properties and in vitro performance and formulation stability. This study further showed how the introduction of a post-micronisation conditioning step may overcome the issues with GLY particles in achieving both physical and chemical stability. Whilst post-micronisation conditioning with both an elevated temperature and *in situ* with HFA for 7 days yielded drug particles which meet particle size requirements for inhalation, the high temperature conditioning appeared to significantly shift the interfacial chemical nature of the GLY particles from a highly adhesive system, to a slightly cohesively-led one. This chemical shift translated into a significantly higher aerosolisation performance, suggesting that the stress relaxation of GLY particles is most sensitive to conditioning using elevate temperatures.

6 General Conclusions

6.1 Introduction

The ever increasing regulatory demands on drug companies for both the development and the lifecycle period of a drug product mean that the understanding of the inhaled dosage form necessitates from a significant increase in published knowledge relating the number of chemical and physical transformations involved in the manufacture of aerosol drug products. The highly empirical approach, which is still adopted in the manufacturing of dry powder inhalers, results in a high failure rate of formulations that are only tested for failure post-processing and packaging of the said products. Furthermore, the impact of environmental conditions and manufacturing cycle-times on product performance remains very poorly understood.

The physicochemical properties of the micronised active pharmaceutical ingredients (API) are key to the performance understanding and stability of this dosage form. The properties of APIs may change considerably during an undefined and unknown period following micronisation. Usage of the API within this period is a main source of drug product variability which impacts both supply ability of a drug product and also the product's quality. This work aimed at enhancing the understanding of the dynamics with which key physicochemical properties change following micronisation, how they related to drug aersolisation performance, and how the introduction of a post-micronisation conditioning step may expedite the stabilising of micronised API properties.

6.2 Summary

In chapters 2 and 3, the post-micronisation dynamics of FP were investigated with respect to both ambient and targeted conditions. Results reported in chapter 2 indicated that whilst the micronised drug remains largely stable in terms of particle size distribution, conditioning over a relatively short period exhibited differing trends in the interfacial chemistry of the FP particles with respect to SX. An adhesive shift was observed for FP samples conditioned using elevated humidity a moderately high temperature over a period of 14 days. On the other hand, drug particles conditioned under ambient relative humidity at an elevated temperature of 70°C for a short period of 72 hours exhibited a cohesive shift with respect to SX particles. The interfacial chemical system with respect to lactose was more stable. *In situ* conditioning with HFA generated conditioned particles which seemed to have stabilised the interfacial properties of freshly micronised FP. The aerosolisation trends observed were consistent with the changes in the interfacial shifts reported for the micronised particles. The same trends were followed by SX particles highlighting the relevance of this work to tertiary formulations. Chapter 3 examines the impact of post-micronisation conditioning on the stress relaxation of micronised FP particles over longer period of times and more specific laagering conditions. Whilst the chemical interfacial system with respect to lactose seems to remain relatively stable once again over a period of 90 days, the chemical system of FP particles conditioned over a period of 90 days experienced a constant adhesive drift with respect to SX particles which seemed to be more sensitive to time rather than laagering conditions. The shift from a highly cohesive to a

highly adhesive chemical system occurred over a period of 90 days. However, approximately 85 % of this shift appears to occur within the first 60 days of conditioning. Conditioning using an elevated related humidity of 75 % at ambient temperature for 90 days produced significant morphological and topographical changes to the FP particles with a significant particle smoothening event being observed. The impaction performance benefitted from the drop in cohesive interactions significantly improving the aerosolisation efficiency of the conditioned FP samples.

Chapter 4 described the kinetics of micronised SX particles upon conditioning. The results indicated an expedited stress relaxation when conditioned at 60°C over a period of 60 days, manifested in a pronounced drop in the specific surface area of the conditioned particles. There was accompanied a generally strong cohesive shift with respect to FP particles, whilst the cohesive drift with respect to lactose whilst significant, was less pronounced. The impactor results were once again consistent with the changing interfacial properties. Conditioning SX particles *in situ* with HFA for 21 days promoted greater physical stability and also expedited the cohesive chemical shift observed in the SX samples conditioned environmentally over a period of 60 days.

Chapter 5 highlights the importance of post-micronisation conditioning for highly hydrophilic drug compounds such as glycopyrrolate bromide (GLY). Whilst storage under ambient conditions producesd particles with physical properties that are not suitable for inhalation, conditioning using an elevated temperature of 70°C generated particles with physical properties within the respirable range and transformed the interfacial chemical system with respect

to lactose from a highly adhesive system to a slightly cohesive system. This translated into a significantly improved aerosolisation performance. *In situ* conditioning with HFA also allowed for optimum physical properties however, failed to influence the highly adhesive interfacial system.

6.3 General Conclusion

This work clearly highlights the importance of secondary processing of APIs intended for use in dry power inhalers in order to assist development of a well understood and stable drug product. Results reported within suggest a clear distinction between the processing requirements of hydrophobic and hydrophilic drug compounds. FP and SX require a laagering period of around 60 days during which the stress relaxation coincides with a general adhesive drift in the interfacial chemistry with respect to each other, whilst the chemical system between the drug compounds and the lactose remains largely unchanged. GLY on the other hand, exhibits relatively rapid kinetics with post-micronisation conditioning that are essential to ensure particles have the required physical properties to be suitable for inhalation. The use of an elevated high temperature imposes a surface chemistry shift from a highly adhesive system to a slightly cohesive one. The use of HFA as a conditioning option seems to promote stable physical properties and generally expedites or stabilises interfacial shifts for hydrophobic compounds. The post-micronisation kinetics of hydrophobic drug particles have been seen to depend highly on time whereas those of hydrophilic compounds are highly reliant on the conditions employed.

6.4 Future Work

Whilst data presented in this work clearly highlight the importance of conditioning drug compounds intended for use in dry power inhaler formulations, the publication of further knowledge is required to add further control to this growing therapeutic branch. Chapter 5 underlined the importance of understating the stability of formulations manufactured using drug particles conditioned following micronisation. Increased knowledge on the stability of DPI formulations is essential in identifying a sustainable secondary processing methodology. Another important aspect meriting investigating is the impurity profile of both the drug compound and formulation as a function of time and conditions following micronisation. The hypothesis would be that secondary processing alters the degradation of the drug compound.

Finally, further work should make use of the progress in vibrational spectroscopy and its application in the assessment of DPIs. This will allow for a better understanding of the chemical composition of the aerosolised drug particles further validating the importance of interfacial chemistry in both binary and ternary powder formulations.

References

Adi, H., Larson, I., Chiou, H., Young, P., Traini, D., & Stewart, P. (2006). Agglomerate strength and dispersion of salmeterol xinafoate from powder mixtures for inhalation. Pharmaceutical research, 23(11), 2556-2565.

Adi, H., Larson, I., Chiou, H., Young, P., Traini, D., & Stewart, P. (2008). Role of agglomeration in the dispersion of salmeterol xinafoate from mixtures for inhalation with differing drug to fine lactose ratios. Journal of pharmaceutical sciences, 97(8), 3140-3152.

Adi, S., Adi, H., Tang, P., Traini, D., Chan, H. K., & Young, P. M. (2008). Micro-particle corrugation, adhesion and inhalation aerosol efficiency. European Journal of Pharmaceutical Sciences, 35(1), 12-18.

Adolfsson,A., Olsson,H., Nystrom,C. (1997). Effect of particle size and compaction load on interparticulate bonding structure for some pharmaceutical materials studied by compaction and strength characterisation in butanol. European Journal of Pharmaceutics and Biopharmaceutics, 44, 243-251.

Ahlneck C, Zografi G. (1990). The Molecular-Basis of Moisture Effects on the Physical and Chemical-Stability of Drugs in the Solid-State. International Journal of Pharmaceutics 62:87-95.

Anagnostou K, Harrison B, Iles R, Nasser S. (2012).Risk factors for childhood asthma deaths from the UK Eastern Region Confidential Enquiry 2001-2006. Prim Care Respir J; 21: 71–77.

Asgharian,B., Anjilvel,S. (1994). Inertial and Gravitational Deposition of Particles in A Square Cross-Section Bifurcating Airway. Aerosol Science and Technology, 20, 177-193.

Asthma Mortality Task Force. (1987) Recommendations of the Asthma Mortality Task Force. J Allergy Clin Immunol; 80 (3 Pt 2): 364–366

Balashazy,I., Hofmann,W. (1993). Particle Deposition in Airway Bifurcations. Inspiratory Flow. Journal of Aerosol Science, 24, 745-772.

Barnes, P. J. (2004). The role of anticholinergics in chronic obstructive pulmonary disease. The American Journal of Medicine Supplements, 117(12), 24-32.

Barnes,P.J. (2002). Scientific rationale for inhaled combination therapy with long-acting beta(2)-agonists and corticosteroids. European Respiratory Journal, 19, 182-191.

Barnes,P.J. (2004). Mediators of chronic obstructive pulmonary disease. Pharmacology Reviews, 56, 515-548.

Barnes,P.J. (2007). Chronic obstructive pulmonary disease: A growing but neglected global epidemic. Plos Medicine, 4, 779-780.

Barnes,P.J. (2008). Immunology of asthma and chronic obstructive pulmonary disease. Nature Reviews Immunology, 8, 183-192.

Barnes,P.J., Chung,K.F., Page,C.P. (1998). Inflammatory mediators of asthma: an update. Pharmacology Reviews, 50, 515-596.

Barnes,P.J., Shapiro,S.D., Pauwels,R.A. (2003). Chronic obstructive pulmonary disease: molecular and cellular mechanisms. European Respiratory Journal, 22, 672-688.

Baxter, A. D. (2011). U.S. Patent No. 7,915,303. Washington, DC: U.S. Patent and Trademark Office.

Beach, S., Latham, D., Sidgwick, C., Hanna, M., & York, P. (1999). Control of the physical form of salmeterol xinafoate. Organic Process Research & Development, 3(5), 370-376.

Beeh, K. M., Singh, D., Di Scala, L., & Drollmann, A. (2012). Once-daily NVA237 improves exercise tolerance from the first dose in patients with COPD: the GLOW3 trial. International journal of chronic obstructive pulmonary disease, 7, 503.

Begat P, Morton DAV, Staniforth JN, Price R. (2004). The cohesive-adhesive balances in dry powder inhaler formulations I: Direct quantification by atomic force microscopy. Pharm. Res.;21:1591–7.

Begat P, Morton DAV, Staniforth JN, Price R. (2004) The cohesive-adhesive balances in dry powder inhaler formulations II: influence on fine particle delivery characteristics. Pharm. Res.;21:1826–33.

Begat P, Morton DAV, Staniforth JN, Price R. (2004). The cohesive-adhesive balances in dry powder inhaler formulations I: Direct quantification

by atomic force microscopy. Pharm. Res.;21:1591–7.

Begat P, Morton DAV, Staniforth JN, Price R. (2004). The cohesive-adhesive balances in dry powder inhaler formulations II: influence on fine particle delivery characteristics. Pharm. Res.;21:1826–33.

Bell,J.H., Hartley,P.S., Cox,J.S.G. (1971). Dry Powder Aerosols .1. New Powder Inhalation Device. Journal of Pharmaceutical Sciences, 60, 1559-1564.

Bender H, Graebner H, Schindler K, Trunk M, Watz M.; Boehringer Ingelheim Pharma Gmbh & Co. (2004). Crystalline micronisate, process for the manufacture thereof and use thereof for the preparation of a medicament. US 20040002510 A1.

Berry,J., Kline,L.C., Hart,J.L., Sequeira,J. (2003). Influence of the storage orientation on the aerodynamic particle size of a suspension metered dose inhaler containing propellant HFA-227. Drug Development and Industrial Pharmacy, 29, 631-639.

Biddiscombe,M.F., Melchor,R., Mak,V.H., Marriot,R.J. (1987). Lung deposition of salbutamol directly labeled with technetium-99m, delivered by pMDI and DPI. International Journal of Pharmaceutics, 91, 111-121.

Binnig, G., Quate, C. F., & Gerber, C. (1986). Atomic force microscope. Physical review letters, 56(9), 930.

Booth, S. W., & Newton, J. M. (1987). Experimental investigation of adhesion between powders and surfaces. Journal of pharmacy and pharmacology, 39(9), 679-684.

Bosquillon, C., Lombry, C., Preat, V., & Vanbever, R. (2001). Influence of formulation excipients and physical characteristics of inhalation dry powders on their aerosolization performance. Journal of controlled release, 70(3), 329-339.

Bragg, W. H., & Bragg, W. L. (1913). The reflection of X-rays by crystals. Proceedings of the Royal Society of London. Series A, 88(605), 428-438.

Briggner L., Buckton G., Bystrom K., and Darcy P. (1994). The use of microcalorimetry in the study of changes in crystallinity induced during the processing of powders. Int. J. Pharm., 105:125-135.

Brittain, H. G., Bogdanowich, S. J., Bugay, D. E., DeVincentis, J., Lewen, G., & Newman, A. W. (1991). Physical characterization of pharmaceutical solids. Pharmaceutical research, 8(8), 963-973.

Brodka-Pfeiffer K, Häusler H, Grass P, Langguth P. (2003b). Conditioning following powder micronisation: influence on particle growth of salbutamol sulfate. Drug Dev Ind Pharm.;29:1077–84.

Brodka-Pfeiffer K, Langguth P, Grass P, Häusler H. (2003a) Influence of mechanical activation on the physical stability of salbutamol sulphate. Eur J Pharm Biopharm.;56:393–400.

Brodka-Pfeiffer K., Grass P., Haeusler H., Thieme H. (2004). Process for providing a stable crystalline form of salbutamol, US 20040052734A1.

Brodka-Pfieffer K., Haeusler H., Graf P., Langguth P. (2003). Conditioning following powder micronisation: Influence on particle growth of salbutamol sulphate. Drug Development and Industrial Pharmacy 29:1077-1084.

Brunauer, S., Emmett, P.H. and Teller, E. (1938). Adsorption of gases in multimolecular layers. Journal of the American Chemical Society, 60, pp. 309-319.

Bucknall CE, Slack R, Godley CC, Mackay TW, Wright SC. (1999). Scottish Confidential Inquiry into Asthma Deaths (SCIAD), 1994-6. Thorax; 54: 978–984.

Buckton G., Choularton A, Beezer A. and Chatman S. (1988). The effect of comminution technique on the surface energy of a powder. Int. J. Pharm., 47:121-128.

Buckton, G. (1997). "Characterisation of small changes in the physical properties of powders of significance for dry powder inhaler formulations." Advanced Drug Delivery Reviews 26(1): 17-27.

Buckton, G. and P. Darcy (1995). "The Use of Gravimetric Studies to Assess the Degree of Crystallinity of Predominantly Crystalline Powders." International Journal of Pharmaceutics 123(2): 265-271.

Buhl, R., & Banerji, D. (2012). Profile of glycopyrronium for once-daily treatment of moderate-to-severe COPD. International journal of chronic

obstructive pulmonary disease, 7, 729.

Byron,P.R., Patton,J.S. (1994). Drug-delivery via the respiratory-tract. Journal of Aerosol Medicine-Deposition Clearance and Effects in the Lung, 7, 49-75.

Byron,P.R., Peart,J., Staniforth,J.N. (1997). Aerosol electrostatics .1. Properties of fine powders before and after aerosolization by dry powder inhalers. Pharmaceutical Research, 14, 698-705.

Calverley,P., Pauwels,R., Vestbo,J., Jones,P., Pride,N., Gulsvik,A., Anderson,J., Maden,C., Tristan,S.G. (2003). Combined salmeterol and fluticasone in the treatment of chronic obstructive pulmonary disease: a randomised controlled trial. Lancet, 361, 449-456.

Campbell,L.M., Szafranski,W. (2002). Budesonide/formoterol in a single inhaler (Symbicort) reduces severe exacerbations in patients with moderate to severe COPD. Thorax, 57.

Castellanos,A. (2005). The relationship between attractive interparticle forces and bulk behaviour in dry and uncharged fine powders. Advances in Physics, 54, 263-376.

Cazzola,M., Ando,F., Santus,P., Ruggeri,P., Di Marco,F., Sanduzzi,A., D'Amato,M. (2007). A pilot study to assess the effects of combining fluticasone propionate/salmeterol and tiotropium on the airflow obstruction of patients with severe-to-very severe COPD. Pulmonary Pharmacology & Therapeutics, 20, 556-561.

Chowdhury, B. A., & Dal Pan, G. (2010). The FDA and safe use of long-acting beta-agonists in the treatment of asthma. New England Journal of Medicine, 362(13), 1169-1171.

Clark,A.R., Egan,M. (1994). Modeling the Deposition of Inhaled Powdered Drug Aerosols. Journal of Aerosol Science, 25, 175-186.

Clarke,A.R. (1995). Medical Aerosol Inhalers: Past, Present and Future. Aerosol Science and Technology, 23, 374-391.

Colombo I, Grassi G, Grassi M. (2009). Drug Mechanochemical Activation. J Pharm Sci.;98:3961–86.

Colton, R., (2004). Nanoscale Measurements and Manipulation. Journal of Vacuum Science and Technogy B. 22, 1609-1635.

Coulomb,A. (1785). Memoires de l'Acadamie Royale des Sciences, 4, 569.

Crowder,T.M., Rosati,J.A., Schroeter,J.D., Hickey,A.J., Martonen,T.B. (2002). Fundamental effects of particle morphology on lung delivery: Predictions of Stokes' law and the particular relevance to dry powder inhaler formulation and development. Pharmaceutical Research, 19, 239-245.

Dalby,R., Spallek,M., Voshaar,T. (2004). A review of the development of Respimat(R) Soft Mist(TM) Inhaler. International Journal of Pharmaceutics, 283, 1-9.

Dalby,R., Suman,J. (2003). Inhalation therapy: technological milestones in asthma treatment. Advanced Drug Delivery Reviews, 55, 779-791.

Das, S., Larson, I., Young, P., & Stewart, P. (2009). Influence of storage relative humidity on the dispersion of salmeterol xinafoate powders for inhalation. Journal of pharmaceutical sciences, 98(3), 1015-1027.

Davies, N. M.; Feddah. (2003). A novel method for assessing dissolution of aerosol inhaler products, M. R. Int. J. Pharm.; 255 (1-2), 175–187.

De Boer, A. H., Hagedoorn, P., Gjaltema, D., Goede, J., & Frijlink, H. W. (2003). Air classifier technology (ACT) in dry powder inhalation: Part 1. Introduction of a novel force distribution concept (FDC) explaining the performance of a basic air classifier on adhesive mixtures. International journal of pharmaceutics, 260(2), 187-200.

de Boer,A.H., Hagedoorn,P., Frijlink,H.W. (2003). The choice of a compressor for the aerosolisation of tobramyicn (TOBI) with the PARI LC PLUS resusable nebuliser. International Journal of Pharmaceutics, 268, 59-69.

Ducker, W. A., Senden, T. J., & Pashley, R. M. (1991). Direct measurement of colloidal forces using an atomic force microscope. nature, 353(6341), 239-241.

Dunbar,C.A., Morgan,B., Van Oort,M., Hickey,A.J. (2000). A comparison of dry powder inhaler dose delivery characteristics using a power criterion.

Journal of Pharmaceutical Science and Technology, 54, 478-484.

D'Urzo, A., Ferguson, G. T., van Noord, J. A., Hirata, K., Martin, C., Horton, R., Overend, T. (2011). Efficacy and safety of once-daily NVA237 in patients with moderate-to-severe COPD: the GLOW1 trial. Respir Res, 12(1), 156.

Edge,S., Muller,S., Price,R., Shur,J. (2008). Factors affecting defining the quality and functionality of excipients used in the manufacture of of dry powder inhaler products. Drug Development and Industrial Pharmacy, 34, 966-973.

European Medicines Agency (2007). European Pharmacopoeia 6.0. Inhalation.

European Medicines Agency, 2012, EMA/CHMP/508029/2012.

Feeley,J.C., York,P., Sumby,B., Dicks,H. (1998). Determination of surface properties and flow characterisation of salbutamol sulphate, before and after micronisation. International Journal of Pharmaceutics, 172, 89-96.

Fletcher HJ, Ibrahim SA, Speight N. (1990). Survey of asthma deaths in the Northern region, 1970-85. Arch Dis Childhood; 65: 163–167.

Florence A., and Salole J. (1976). Changes in crystallinity and solubility on comminution of digoxin and observations on spironolactone and oestradiol. J. Pharm. Pharmac., 28:637-642.

Frijlink H.W., de Boer A.H. (2004). Dry powder inhalers for pulmonary drug delivery, Expert Opinion on Drug Delivery 1; 67–86.

Fuller,K.N.G., Tabor,D. (1975). Effect of Surface-Roughness on Adhesion of Elastic Solids. Proceedings of the Royal Society of London Series A-Mathematical Physical and Engineering Sciences, 345, 327-342.

Ganderton D., Kassem N. M. (1992). Dry powder inhalers, in: D. Ganderton, T. Jones (Eds.), Advances in Pharmaceutical Sciences, Academic Press, London, UK, 1992, pp. 165–191.

Ganderton,D. (1992). The generation of respirable cloud from coarse powder aggregates. Journal of Biopharmaceutical Science, 3, 101-105.

Garcia-Contreras,L., Hickey,A.J. (2003). Aerosol treatment of cystic fibrosis. Critical Reviews in Therapeutic Drug Carrier Systems, 20, 317-356.

Greening,A.P., Ind,P.W., Northfield,M., Shaw,G. (1994). Added Salmeterol Versus Higher-Dose Corticosteroid in Asthma Patients with Symptoms on Existing Inhaled Corticosteroid. Lancet, 344, 219-224.

Guchardi, R., Frei, M., John, E., & Kaerger, J. S. (2008). Influence of fine lactose and magnesium stearate on low dose dry powder inhaler formulations. International journal of pharmaceutics, 348(1), 10-17.

Gurney,J.W. (1991). Cross-Sectional Physiology of the Lung. Radiology, 178, 1-10.

Hamaker,H.C. (1937). London-van der Waals forces attraction between spherical particles. Physica (Utrecht), 4, 1058-1072.

Hannemann,L.A. (1999). What is new in asthma: New dry powder inhalers. Pediatric Health Care, 13, 159-165.

Hansma, H. G., & Pietrasanta, L. (1998). Atomic force microscopy and other scanning probe microscopies. Current opinion in chemical biology, 2(5), 579-584.

Harris,D. (2007). Testing Inhalers. Pharmaceutical Technology Europe, 11, 11.

Harrison B, Stephenson P, Mohan G, Nasser S. (2005). An ongoing confidential enquiry into asthma deaths in the Eastern Region of the UK, 2001-2003. Prim Care Respir J; 14: 303–313.

Heyder,J., Gebhart,J., Rudolf,G., Schiller,C.F., Stahlhofen,W. (1986). Depoistion of particles in the human respiratory tract in the size range 0.005-15mM. Journal of Aerosol Science, 17, 811-825.

Hickey,A.J., Dunbar,C.A. (1997). A new millenium for inhaler technology. Pharmaceutical Technology, 21, 116-125.

Hiestand,E.N. (1966). Powders: Particle-particle interactions. Journal of Pharmaceutical Sciences, 55, 1325-1344.

Hills A, Sommer AR, Adelstein AM. (1982). Death from asthma in two regions of England. Br Med J; 285: 1251–1255.

Hofmann,W., Sturm,R., Winkler-Heil,R., Pawlak,E. (2003). Stochastic model of ultrafine particle deposition and clearance in the human respiratory tract. Radiation Protection Dosimetry, 105, 77-80.

Holgate,S.T. (2008). Pathogenesis of asthma. Clinical and Experimental Allergy, 38, 872-897.

Hooton, J. C., M. D. Jones, et al. (2008). "The Influence of Crystal Habit on the Prediction of Dry Powder Inhalation Formulation Performance Using the Cohesive Adhesive Force Balance Approach." Drug Development and Industrial Pharmacy 34(9): 974 – 983.

Huttenrauch R, Fricke S, Zielke P. (1985). Mechanical Activation of Pharmaceutical Systems. Pharmaceutical Research 302-306.

Huttenrauch R, Fricke S, Zielke P. (1985) Mechanical activation of pharmaceutical systems. Pharm. Res.;2:302–6.

Jakupovic E., Trofast J. (1998). Process for the preparation of respirable particles, EP0820276B1.

Jayasing,S.S., Pilpel,N., Harwood,C.F. (1970). Effect of Temperature and Compression on Cohesive Properties of Particulate Solids. Materials Science and Engineering, 5, 287.

Johnson,K.L. (1996). Continuum mechanics modeling of adhesion and friction. Langmuir, 12, 4510-4513.

Johnson,K.L., Kendall,K., Roberts,A.D. (1971). Surface energy and the contact of elastic solids. Proceedings of the Royal Society of London. Series A, Mathematical and Physical Sciences, 324, 301-313.

Jones MD, Harris H, Hooton JC, Shur J, King GS, Mathoulin CA, et al. (2008a). An investigation into the relationship between carrier-based dry powder inhalation performance and formulation cohesive-adhesive force balances. Eur J Pharm Biopharm.;69:496–507.

Jones MD, Hooton JC, Dawson ML, Ferrie AR, Price R. (2008). An investigation into the dispersion mechanisms of ternary dry powder inhaler formulations by the quantification of interparticulate forces. Pharm. Res.;25:337–48.

Jones MD, Young PM, Traini D, Shur J, Edge S, Price R. (2008). The use of atomic force microscopy to study the conditioning of micronised budesonide. International Journal of Pharmaceutics 357:314-317.

Jones,M.D., Harris,H., Hooton,J.C., Shur,J., King,G.S., Mathoulin,C.A., Nichol,K., Smith,T.L., Dawson,M.L., Ferrie,A.R., Price,R. (2008). An investigation into the relationship between carrier-based dry powder inhalation performance and formulation cohesive-adhesive force balances. European Journal of Pharmaceutics and Biopharmaceutics, 69, 496-507.

Joshi V, Dwivedi S, Ward GH. (2002). Increase in the specific surface area of budesonide during storage postmicronisation. Pharm. Res.;19:7–12.

Kerwin, E., Hébert, J., Gallagher, N., Martin, C., Overend, T., Alagappan, V. K., ... & Banerji, D. (2012). Efficacy and safety of NVA237 versus placebo and tiotropium in patients with COPD: the GLOW2 study. European Respiratory Journal, 40(5), 1106-1114.

Krishnan,S., Busnaina,A.A., Rimai,D.S., Demejo,L.P. (1994). The Adhesion-Induced Deformation and the Removal of Submicrometer Particles. Journal of Adhesion Science and Technology, 8, 1357-1370.

Krupp,H. (1967). Particle adhesion theory and experiment. Advanced Colloid Interface, 1, 111-239.

Kubavat HA, Shur J, Ruecroft G, Hipkiss D, Price R. (2012). Investigation into the influence of primary crystallization conditions on the mechanical properties and secondary processing behaviour of fluticasone propionate for carrier based dry powder inhaler formulations. Pharm. Res.;29:994–1006.

Kulvanich, P. O. J., & Stewart, P. J. (1987). The effect of particle size and concentration on the adhesive characteristics of a model drug-carrier interactive system. Journal of pharmacy and pharmacology, 39(9), 673-678.

Lalor,C.B., Hickey,A.J., (1996). Pharmaceutical aerosols for delivery of drugs to the lungs. In: Collbeck,I. (Ed.), Blackie Academic & Professionals,

London.

Lam, K. K., & Newton, J. M. (1993). The influence of the time of application of contact pressure onparticle adhesion to a substrate surface. Powder technology, 76(2), 149-154.

Lankinen, T. (2003). U.S. Patent No. 6,616,945. Washington, DC: U.S. Patent and Trademark Office.

Li,H.Y., Seville,P.C., Williamson,I.J., Birchall,J.C. (2005). The use of amino acids to enhance the aerosolisation of spray-dried powders for pulmonary gene therapy. Journal of Gene Medicine, 7, 343-353.

Lifshitz,E.M. (1955). Journal of Experimental Theoretical Physics, 29, 94.

Liu J., Rigsbee D.R., Stotz C. And Pikal J. (2002). Dynamics of pharmaceutical amorphous solids: the study of enthalpy relaxation by isothermal microcalorimetry. J. Pharm. Sci, 91(8):1853-1862.

Louey, M. D., P. Mulvaney, et al. (2001). "Characterisation of adhesional properties of lactose carriers using atomic force microscopy." Journal of Pharmaceutical and Biomedical Analysis 25(3-4): 559-567.

Lough, W., Wainer I. (1995). High performance liquid chromatography: Fundamental Principles and Practice. London, CRC Press.

Magee, G. A.; French, J.; Gibbon, B.; Luscombe, C. (2003). Bile salt/lecithin mixed micelles optimized for the solubilisation of a poorly soluble steroid molecule using statistical experimental design, Drug Dev. Ind. Pharm.; 29 (4), 441–450.

Malcolmson R.J., Embleton J.K. (1998). Dry powder formulations for pulmonary delivery. Pharmaceutical Science Technology Today, 1, 394-398.

Malcolmson,R.J., Embleton,J.K. (1998). Dry powder formulations for pulmonary delivery. Pharmaceutical Science Technology Today, 1, 394-398.

Marple, V. A., B. A. Olson, K. Santhanakrishnan, J. P. Mitchell, S. C. Murray and B. L.Hudson-Curtis. (2003). Next Generation Pharmaceutical Impactor (A New Impactor for Pharmaceutical Inhaler Testing). Part II:

Archival Calibration. Journal of Aerosol Medicine 16(3): 301-324

Martonen,T.B., Katz,I. (1993). Deposition Patterns of Polydisperse Aerosols Within Human Lungs. Journal of Aerosol Medicine-Deposition Clearance and Effects in the Lung, 6, 251-274.

Matz,J., Emmett,A., Rickard,K., Kalberg,C. (2001). Addition of salmeterol to low-dose fluticasone versus higher-dose fluticasone: An analysis of asthma exacerbations. Journal of Allergy and Clinical Immunology, 107, 783-789.

McDonald,K.J., Martin,G.P. (2000). Transition to CFC-free metered dose inhalers - into the new millennium. International Journal of Pharmaceutics, 201, 89-107.

McFarlane,J.S., Tabor,D. (1950). Adhesion of solids and the effect of surface films. Proceedings of the Royal Society of London. Series A, Mathematical and Physical Sciences, 202, 224-243.

Mcmurry,P.H., Rader,D.J. (1985). Aerosol Wall Losses in Electrically Charged Chambers. Aerosol Science and Technology, 4, 249-268.

Mie, G. (1908). Articles on the optical characteristics of turbid tubes, especially colloidal metal solutions. Ann. Phys, 25(3), 377-445.

Morrison,F.A. (1974). Inertial impaction in stagnation flow. Journal of Aerosol Science, 5, 241-250.

Morton D., Shott M., Davies R. (2008). Pharmaceutical Compositions, US20080063719A1.

Muhammad, S. A. F. A. S., Langrish, T., Tang, P., Adi, H., Chan, H. K., Kazarian, S. G., & Dehghani, F. (2010). A novel method for the production of crystalline micronised particles. International journal of pharmaceutics, 388(1), 114-122.

Muhrer G, Rasenack N.; Novartis AG. Process for reducing the tendency of a glycopyyronium salt to aggregate during storage. EP2234595 B1. 2012 Nov 28.

Muhrer G, Rasenack N.; Novartis AG. Process for reducing the tendency of a glycopyyronium salt to aggregate during storage. EP2234595 B1. 2012 Nov 28.

Nasr, M. M., D. L. Ross, et al. (1997). "Effect of drug load and plate coating on the particle size distribution of a commercial albuterol metered dose inhaler (MDI) determined using the Andersen and Marple-Miller Cascade Impactors." Pharmaceutical Research 14(10): 1437-1443.

Nelson,H.S., Chapman,K.R., Pyke,S.D., Johnson,M., Pritchard,J.N. (2003). Enhanced synergy between fluticasone propionate and salmeterol inhaled from a single inhaler versus separate inhalers. Journal of Allergy and Clinical Immunology, 112, 29-36.

Newman,S.P., Busse,W.W. (2002). Evolution of dry powder inhaler design, formulation, and performance. Respiratory Medicine, 96, 293-304.

Nowak,N., Kakade,P.P., Annapragada,A.V. (2003). Computational fluid dynamics simulation of airflow and aerosol deposition in human lungs. Annals of Biomedical Engineering, 31, 374-390.

Onsager,L., Samaras,N.T. (1934). The surface tension of Debye-Huckel electrolytes. The Journal of Chemical Physics, 2, 528-536.

Otsuka M. and Kaneniwa N. (1990). Effect of grinding on the crystallinity and chemical stability in the solid state of cephalothin sodium. Int. J. Pharm. 62:65-73.

Pandy, P., Chamarthy, S. P., & Wylie, J. L. (2010). U.S. Patent Application 13/266,067.

Park,S.H., Lee,K.W. (2000). Lognormal size distribution theory for deposition of polydisperse aerosol particles. Nuclear Science and Engineering, 135, 288-295.

Pathak, P., Meziani, M. J., & Sun, Y. P. (2005). Supercritical fluid technology for enhanced drug delivery.

Patton,J.S. (1996). Mechanisms of macromolecule absorption by the lungs. Advanced Drug Delivery Reviews, 19, 3-36.

Pauwels,R., Newman,S., Borgstrom,L. (1997). Airway deposition and airway effects of antiasthma drugs delivered from metered-dose inhalers. European Respiratory Journal, 10, 2127-2138.

Pfeiffer-Brodka K, Haeusler H, Graf P, Langguth P. (2003). Conditioning following powder micronisation: Influence on particle growth of salbutamol sulphate. Drug Development and Industrial Pharmacy 29:1077-1084.

Pitchayajittipong C, Shur J, Price R. (2009). Engineering of crystalline combination inhalation particles of a long-acting beta2-agonist and a corticosteroid. Pharm. Res.;26:2657–66.

Podczeck, F. (1998a). "Adhesion forces in interactive powder mixtures of a micronised drug and carrier particles of various particle size distributions." Journal of Adhesion Science and Technology 12(12): 1323-1339.

Podczeck, F. (1998b). Particle-particle adhesion in pharmaceutical powder handling. London, Imperial College Press.

Podczeck, F., Newton, J. M., & James, M. B. (1997). Influence of relative humidity of storage air on the adhesion and autoadhesion of micronised particles to particulate and compacted powder surfaces. Journal of colloid and interface science, 187(2), 484-491.

Price,R., Young,P.M., Edge,S., Staniforth,J.N. (2002). The influence of relative humidity on particulate interactions in carrier-based dry powder inhaler formulations. International Journal of Pharmaceutics, 246, 47-59.

Prime,D., Atkins,P.J., Slater,A., Sumby,B. (1997). Review of dry powder inhalers. Advanced Drug Delivery Reviews, 26, 51-58.

Pritchard, J.N. (2001). The influence of drug deposition on clinical response. Journal of Aerosol Medicine, 14, 19-26.

Rea HH, Scragg R, Jackson R, Beaglehole R, Fenwick J, Sutherland DC. (1986). A case-control study of deaths from asthma. Thorax; 41: 833–839

Rich, S. A. (2007). U.S. Patent Application 11/935,483.

Richards,J., Hirst,P., Pitcairn,G., Mahashabde,S., Abramowitz,W., Nolting,A., Newman,S.P. (2001). Deposition and pharmacokinetics of flunisolide delivered from pressurized inhalers containing non-CFC and CFC propellants. Journal of Aerosol Medicine-Deposition Clearance and Effects in the Lung, 14, 197-208.

Riebe MT, Dwivedi SK, Li-Bovet L.; Smithkline Beecham Corporation.

Aerosols containing annealed particulate salbutamol and tetrafluoroethane. US6558651 B1. 2003 May 6.

Riebe MT, Dwivedi SK, Li-Bovet L.; Smithkline Beecham Corporation. Aerosols containing annealed particulate salbutamol and tetrafluoroethane. US6558651 B1. 2003 May 6.

Rogueda PGA, Price R, Smith T, Young PM, Traini D. (2011). Particle synergy and aerosol performance in non-aqueous liquid of two combinations metered dose inhalation formulations: an AFM and Raman investigation. J Colloid Interface Sci.;361:649–55.

Royal College of Physicians. Why asthma still kills: the National Review of Asthma Deaths (NRAD) Confidential Enquiry report. Royal College of Physicians: London, 2014.

Saleki-Gerhardt A., Ahlneck C. and Zografi G. (1994). Assessment of disorder in crystalline solids. Int. J. Pharm., 101:237-247.

Sekiguchi K., Shirotani K, Yuasa H., Suzuki E. and Nakagawa F. (1980). Size reducibility of sulfathiazole by heat transition and subsequent ball milling. Chem. Pharm. Bull. 28:3203-3209.

Shekunov, B. Y., Chattopadhyay, P., Tong, H. H. Y. & Chow, A. H. L., (2007). Particle Size Analysis in Pharmaceutics: principles, methods and applications. Pharmaceutical research, 24(2), 203-227.

Shekunov,B.Y., Feeley,J.C., Chow,A.H.L., Tong,H.H.Y., York,P. (2003). Aerosolisation behaviour of micronised and supercritically-processed powders. Journal of Aerosol Science, 34, 553-568.

Shur J, Harris H, Jones MD, Kaerger JS, Price R. (2008). The role of fines in the modification of the fluidization and dispersion mechanism within dry powder inhaler formulations. Pharm. Res.;25:1631–40.

Shur J, Kaerger JS, Price R. Effect of Surface Amorphous Content of Active Pharmaceutical Ingredients on the Performance of Dry Powder Inhaler Formulations. RDD Europe 2007; Dalby RN, Byron PR, Peart J, Suman J, editors, Davis Healthcare, Rover Grove, Illinois, Vol 1, pp. 341–4.

Shur J, Pitchayajittipong C, Rogueda P, Price R. (2013). Effect of

processing history on the surface interfacial properties of budesonide in carrier-based dry-powder inhalers. Ther Deliv.;4:925–37.

Shur, J., Harris, H., Jones, M. D., Kaerger, J. S., & Price, R. (2008). The role of fines in the modification of the fluidization and dispersion mechanism within dry powder inhaler formulations. Pharmaceutical research, 25(7), 1631-1640.

Skoog, D. (1998). Principles of Instrumental Analysis. New York, Harcourt.

Smith,I.J., Parry-Billings,M. (2003). The inhalers of the future? A review of dry powder devices on the market today. Pulm. Pharmacol. Ther., 16, 79-95.

Smyth,H., Hickey,A.J., Brace,G., Barbour,T., Gallion,J., Grove,J. (2006). Spray pattern analysis for metered dose inhalers I: Orifice size, particle size, and droplet motion correlations. Drug Development and Industrial Pharmacy, 32, 1033-1041.

Staniforth,J.N., Rees,J.E. (1982). Electrostatic charge interactions in ordered powder mixes. Journal of Pharmacy and Pharmaceutical Sciences, 34, 69-76.

Stokes,G.G. (1908). Mathematical and physical papers. Astrophysical Journal, 23, 173.

Tabor,D. (1976). Surface forces and surface interactions. Journal of Colloid and Interface Science, 58, 1-13.

Tallon, S. J., & Catchpole, O. J. (2008). Supercritical fluid processing of organic compounds. Chem. New Zealand, 72, 151-154.

Taulbee,D.B., Yu,C.P. (1975). Theory of Aerosol Deposition in Human Respiratory-Tract. Journal of Applied Physiology, 38, 77-85.

Telko,M., Hickey,A.J. (2005). Dry powder inhaler formulations. Respiratory Care, 50, 1209-1227.

Thibert,R., Tawashi,R. (1999). Micronisation of Pharmaceutical Solids. Microspheres, Microcapsules & Liposomes; Ed. Reza Arshady, Vo1: Preparation & Chemical Applications, 327.

Timsina,M.P., Martin,G.P., Marriott,C., Ganderton,D., Yianneskis,M. (1994). Drug-Delivery to the Respiratory-Tract Using Dry Powder Inhalers. International Journal of Pharmaceutics, 101, 1-13.

Tong, H. H., Shekunov, B. Y., York, P., & Chow, A. H. (2001). Characterization of two polymorphs of salmeterol xinafoate crystallized from supercritical fluids. Pharmaceutical research, 18(6), 852-858.

Traini, D., P. Rogueda, et al. (2005). "Surface energy and interparticle forces correlations in model pMDI formulations." Pharmaceutical Research 22(5): 816-825.

Trofast J. (2000). Formulation for Inhalation, US006030604A.

Trofast J., Trofast E., Bystrom K., Jakupovic E. (1992). Process for conditioning of water soluble substances, 92850062.8 ed., Lund: p 1-6.

Tsuda,A., Butler,J.P., Fredberg,J.J. (1994a). Effects of Alveolated Duct Structure on Aerosol Kinetics .1. Diffusional Deposition in the Absence of Gravity. Journal of Applied Physiology, 76, 2497-2509.

Tsuda,A., Butler,J.P., Fredberg,J.J. (1994b). Effects of Alveolated Duct Structure on Aerosol Kinetics .2. Gravitational Sedimentation and Inertial Impaction. Journal of Applied Physiology, 76, 2510-2516.

Tsukada, M., R. Irie, et al. (2004). "Adhesion force measurement of a DPI size pharmaceutical particle by colloid probe atomic force microscopy." Powder Technology 141(3): 262-269.

Valverde,J.M., Ramos,A., Castellanos,A., Watson,P.K. (1998). The tensile strength of cohesive powders and its relationship to consolidation, free volume and cohesivity. Powder Technology, 97, 237-245.

Vervaet, C., & Byron, P. R. (1999). Drug–surfactant–propellant interactions in HFA-formulations. International journal of pharmaceutics, 186(1), 13-30.

Virchow,J.C., Crompton,G.K., Dal Negro,R., Pedersen,S., Magnan,A., Seidenbergf,J., Barnes,P.J. (2008). Importance of inhaler devices in the management of airway disease. Respiratory Medicine, 102, 10-19.

Visser,J. (1995). Particle adhesion and removal: a review. Particulate Science and Technology, 13, 169-196.

Ward GH, Schultz RK. (1995). Process-induced crystallinity changes in albuterol sulfate and its effect on powder physical stability. Pharm. Res.;12:773–9.

Wildfong PLD, Hancock BC, Moore MD, Morri KR. (2006). Towards an understanding of the structurally based potential for mechanically activated disordering of small molecule organic crystals. J Pharm Sci.;95:2645–56.

Yeomans,A.H., Rogers,E.E., Ball,W.H. (1949). Deposition of Aerosol Particles. Journal of Economic Entomology, 42, 591-596.

Yip, C. M. (2001). "Atomic force microscopy of macromolecular interactions." Current Opinion in Structural Biology 11(5): 567-572.

York, P., Hanna, M., Shekunov, B. Y., & Humphreys, G. O. (1998). Microfine particle formation by SEDS (Solution Enhanced Dispersion by Supercritical Fluids): scale up by design. In Proceedings of the 6th International Symposium (p. 169).

Young,P.M., Price,R., Lewis,D., Edge,S., Traini,D. (2003a). Under pressure: predicting pressurized metered dose inhaler interactions using the atomic force microscope. Journal of Colloid and Interface Science, 262, 298-302.

Young,P.M., Price,R., Tobyn,M.J., Buttrum,M., Dey,F. (2003b). Effect of humidity on aerosolization of micronised drugs. Drug Development and Industrial Pharmacy, 29, 959-966.

Zeng, X. M., Martin, G. P., & Marriott, C. (2000). Particulate Interactions in Dry Powder Formulation for Inhalation. Taylor & Francis.

Zetterstrom,O., Buhl,R., Mellem,H., Perpina,M., Hedman,J., O'Neill,S., Ekstrom,T. (2001). Improved asthma control with budesonide/formoterol in a single inhaler, compared with budesonide alone. European Respiratory Journal, 18, 262-268.